

**EXHIBIT D**

RECEIVED

APR 21 2015

DEPARTMENT OF ENVIRONMENTAL QUALITY  
STATE A Q PROGRAM

## P<sub>4</sub> Production, LLC

Soda Springs Plant  
1853 Highway 34  
P.O. Box 816  
Soda Springs, Idaho 83276-0816  
Phone: (208) 547-4300  
Fax: (208) 547-3312

April 17, 2015

VIA CERTIFIED MAIL;  
RETURN RECEIPT REQUESTED – 7013 1710 0000 3213 0942

Mr. Darrin Pampaian  
Air Quality Division  
Department of Environmental Quality  
1410 North Hilton  
Boise, ID 83706

RE: MBACT Tier II Permit Application

Dear Mr. Pampaian:

P4 Production, LLC (“P4”) submitted a Tier II permit application for Mercury BACT (MBACT) to IDEQ on March 5, 2015. On April 7, 2015 we received your email with attached letter stating your determination of incompleteness of the MBACT Tier II permit application. In addition, P4 discussed the MBACT permit application in an April 2, 2015 conference call with IDEQ. This letter presents requested information regarding technical challenges of mercury control technologies reviewed in the MBACT analysis portion of the MBACT permit application.

In 2008 and 2009 P4 initiated a program to identify viable mercury air emission control technologies that could be compatible with the Soda Springs Phosphate Kiln. This was done to support the development of the MBACT based regulation by IDEQ that P4 and ICL petitioned the Department to develop. P4 engaged Monsanto corporate ESH, Technology (R&D), and reputable external environmental engineering resources to identify viable MBACT and permitable emission limits. That evaluation included an extensive survey of existing control technologies for mercury that had been deployed on commercial scale processes and those that were under development in laboratory and pilot scale research systems. The results of this effort are summarized in the P4 MBACT Tier II permit application and supporting documentation. To summarize those findings, all available control technologies have significant incompatibilities and uncertainties associated with their application to the P4 kiln.

P4 operates a unique process, the only elemental phosphorus plant in the US, and to the best of our knowledge the only Phosphate nodulizing kiln in the world. The product from this plant provides the key

intermediate for the manufacture of Roundup® brand herbicide. The raw materials and process conditions simply do not resemble any other industrial process that has technically demonstrated, cost-effective mercury control. One ubiquitous statement in literature on mercury air emission control is ‘there is no universal solution for mercury control, and a case-by-case approach must be taken to establish a compatible method.’ The uniqueness of the phosphate kiln coupled with the uniqueness of mercury control methods make this a scientific challenge that will require significant development to resolve.

An example of this critical challenge surfaced from the results of recent mercury stack tests. The MBACT evaluation utilized a data-driven approach to derive an estimated 35% mercury control efficiency in existing exhaust gas pollution control equipment (spray tower, dust bins, hydrosonics, and SO<sub>2</sub> scrubbing) and a “potential to emit” type permit limit of 746 lb/yr. In 2014 P4 began utilizing ore from a new mine, which was found to contain equal or slightly lower mercury content as the previous mine, however, the apparent mercury control efficiency dropped significantly, compared to the 2002 mercury emission measurement. This indicates that the chemical and physical conditions required for mercury evolution from phosphate ore in the kiln and capture in the existing system are not well understood nor easily predictable. P4 now understands that many of the properties and behaviors of the raw material have not been thoroughly elucidated at high temperature under the conditions of the process. Similarly we have implemented an R&D program to combat an increase of trace metals that have cropped up in the P4 process after transitioning to this new mine. Any generalizations made from coal or precious metal refineries are simply not valid due to the complex chemical composition of phosphate ore. More importantly, it has been found that Hg emissions can change upon switching from one ore body to another, which happens even within the same mine. These attributes together could make it difficult to develop an effective mercury control technology and devise a point source permit limit for mercury from the P4 kiln.

All available mercury control technologies have been developed to exhibit highly efficient mercury capture for industrial processes that have significantly different characteristics than the P4 kiln, including: coal fired power plants, cement kilns, waste incinerators, metal refineries, etc. Consider for a moment that Phosphate kilns do not draw the same visibility as many of these more common industrial mercury emitters. For example, coal fired power plants, cement kilns, etc. have established domestic and global research institutes (i.e., EPRI), contract research laboratories and organizations, and a wide variety research based academic degree programs and university departments focused on collective advancement of these industries that are well known to impact daily lives. This makes sense as there are a much larger number of power plants, cement kilns and waste incinerators than P4 kilns in the world. As a result, the development of control technologies in and for the Phosphorus industry is therefore comparably limited in scope. Therefore, the availability of mercury control technology for the Phosphorus industry is lagging in development and P4 cannot be held to the same standards and timelines as other industries without similar, broad scientific development and support available to the other mercury emitting industries.

The general process chemistry and engineering challenges that P4 faces for mercury control are (i) the large volume of gas, (ii) relative mercury concentration, (iii) limited temperature regime, (iv) short residence time in existing process, (v) and myriad of chemical species present at significantly higher concentration that compete for and inhibit mercury control efficiency. The last attribute (v) is probably the easiest to articulate the impact on MBACT. For example, phosphate rock contains a wide variety of trace metal impurities, including approximately 0.5 ppm total mercury; however it also contains 0.25%

total zinc. Both of these species are known to volatilize to some extent, therefore Zn is four orders of magnitude more abundant in the gas phase than mercury. The leading mercury controls on the market include injection of activated carbon and/or halide oxidants, and because neither is selective for mercury, any estimated cost must account for the capture of other species, such as Zn which has similar gas phase chemical properties as mercury. So for option #1 in the MBACT evaluation a cost estimate of \$8400/lb Hg captured (based on the amount of injected material required just for the Hg content in the gas stream) could, in fact, be as much as four orders of magnitude higher to account for the simultaneous collection of Zn. When taking into account the other species present that would compete for these mercury controls (i.e., SO<sub>2</sub>, Metals, Moisture, etc.) this figure would likely be much higher. The uncertainty and lack of physical data to support the design and evaluation of these technologies for Hg removal in the P4 kiln precludes their inclusion in P4's MBACT, and also precludes the ability of reputable MBACT vendors to provide any relevant estimate on technology applicability.

The table below is pulled from a variety of EPA and other mercury control reports that clearly indicate that the P4 kiln process conditions do not match other processes that have established mercury control with existing methods. For example, the mercury content is much higher than power plants but lower than metal smelters, the flow rates are intermediate, etc.

Flue Gas Parameters	Coal Fired Utility Boiler	Oil Fired Utility Boiler	Municipal Waste Incinerator	Metal Smelters	Cement Kilns	P4 Kiln
Temperature (°C)	121 – 177	121 – 177	177 – 299	550 – 800	163 – 880	68 – 800
Mercury Content (ug/dscm)	1 – 25	0.2 – 2	400 – 1,400	50,000 – 750,000	2 – 23	~300
Halide Content (ug/dscm)	1,000 – 140,000	1,000 – 3,000	200,000 – 400,000	?	?	?
Flow Rate (dscm/min)	11,000 – 4,000,000	10,000 – 2,000,000	80,000 – 200,000	700,000	9,000,000	300,000

Beyond the lack of selectivity, there are numerous other incompatibilities with existing conditions in the P4 kiln. Halide and ACI injection require a few seconds residence time to effectively react with mercury to initiated control. The existing P4 process design and ductwork provides residence times measured at microseconds or milliseconds, which could require orders of magnitude more reagent use for efficient mercury capture. Also, the kiln exhaust gas does not operate in the temperature range required for efficient mercury control. So, additional cost would be required to reheat cooled gas or to cool hot gas. Therefore, implementation would be much more extensive than simply injecting some new material or reagent into the P4 off-gas stream. The installation would require significant corrosion protection and equipment redesign, rebalancing plant water balance to incorporate significant quantities of condensate. The theoretical approach identifies cost prohibitive incompatibility.

Another good example to consider is that phosphate rock injection has been demonstrated in other industries to control and immobilize a number of metal species, including mercury air emissions from some processes. The off-gas in the P4 kiln is loaded with 20 – 35 tons per hour of phosphate rock dust,

but that dust has been shown to contain lower mercury than the native phosphate raw material for the same reasons that ACI and Halide injection are not expected to offer much Hg removal efficiency.

Additional background information can be found in the attached supplemental responses to the original MBACT Tier II permit application, submitted on July 25, 2012, October 10, 2012, November 6, 2012, February 6, 2013 and January 16, 2014.

In accordance with IDAPA 58.01.01.123, I certify based on information and belief formed after reasonable inquiry, that the statements and information in this document are true, accurate, and complete. If you have any questions regarding this submittal, please contact Mr. Jim McCulloch at (208) 547-1233.

Sincerely,



Roger W. Gibson  
Vice President, Operations

enclosures

bcc: ECF: Air -> Tier II Operating Permit  
Aalbers (scanned copy)  
Vaughn (scanned copy)  
Cooper (scanned copy)  
Wilkinson (scanned copy)  
McCulloch (scanned copy)

Supplemental Responses to P4  
Production, LLC original MBACT  
Tier II Permit

# P<sub>4</sub> Production, LLC

Soda Springs Plant  
1853 Highway 34  
P.O. Box 816  
Soda Springs, Idaho 83276-0816  
Phone: (208) 547-4300  
Fax: (208) 547-3312

July 25, 2012

VIA CERTIFIED MAIL;  
RETURN RECEIPT REQUESTED – 7010 2780 0002 0464 3477

Mr. Dan Pitman, P.E.  
Department of Environmental Quality  
1410 North Hilton  
Boise, Idaho 83706

RE: Facility ID No. 029-00001, P4 Production, LLC, Soda Springs  
Tier II Permit Application and Mercury Best Available Control Technology Analysis

Dear Mr. Pitman:

P4 Production, LLC (P4) submitted a Tier II Permit application and Mercury Best Available Control Technology (MBACT) Analysis to IDEQ on April 6, 2012. On May 7, 2012, P4 received an email and attached letter stating that DEQ had determined that the application was incomplete.

P4 offers the following information in response to the letter received on May 7, 2012:

- 1. Application materials indicate that the existing air pollution control system has a mercury control efficiency of 35%. Please provide the mass balance data that supports this determination, including all calculations.**

The stated mercury control efficiency of 35% for the kiln air pollution control system referenced on pages 3 and 6 of the MBACT For Elemental Phosphorus Process evaluation was calculated from a simple material balance that accounts for the primary inputs and outputs from the kiln. The pertinent data and calculations used for the material balance for operating years 2006 through 2011 are shown in the excel file enclosed with this letter in the file titled "Response to Question 1 – Kiln Mercury Material Balance". The concentration of mercury in the primary inputs and outputs from the kiln is based on the same comprehensive analytical data and production figures used for P4's TRI emission estimates, which is enclosed with this letter in the file titled "Response to Question 1 – Northern Analytical Metals Report." Using production data for operating years 2006 through 2011, the approximate average control efficiency is 33%. However, because the control efficiency for 2011 is slightly higher (approximately 39%), P4 estimated the control efficiency to be 35%. This is equal to the calculated control efficiency

using production data from 2006. It is notable that the air emissions calculated by the material balance are comparable to stack test data for total Hg.

2. **Activated carbon injection with halide injection (control option 1) is estimated to have 50% mercury removal efficiency, and bromated activated carbon injection (control option 2) is estimated to have 30% mercury removal efficiency. Please document the basis of these estimates, or how these removal efficiencies were determined.**

Page 18 of the MBACT For Elemental Phosphorus Process evaluation states that mercury control efficiency between 70% and 90% have been achieved on coal-fired power applications using activated carbon injection (ACI) or brominated activated carbon injection (BACI). However, Section 3.4.1 estimates a control efficiency for ACI combined with halide injection of 50%, and Section 3.4.2 estimates a control efficiency for BACI of 30% for the P4 kiln exhaust gas. These comparably lower control efficiencies are due to the significant differences between the properties of P4 kiln exhaust gas and respective air pollution control equipment and those at any coal-fired power plant or other industrial facility utilizing halide injection/ACI or BACI for mercury control. The expected control efficiency for P4 would be significantly reduced due to adsorption of numerous metallic species (i.e., Cd, Zn, etc.) and sulfur containing species present in the ore and the kiln off-gas (see the ore analysis in the file titled "Response to Question 1 – Northern Analytical Metals Report," as well as P4 TRI data) that are not present in coal-fired power plant applications and would compete for halide, ACI, and BACI adsorption since these materials are not selective for mercury removal. Since the control efficiency of ACI and BACI have never been determined on a gas stream with comparable chemical speciation, flow rates, and temperature profile, the respective control efficiencies of 50% and 30% were determined by estimating the effect of the presence of the numerous metallic and sulfur containing species present in the ore and kiln off-gas, based on the fact that the combined average concentration of such species exceeds the average concentration of mercury by orders of magnitude. The control efficiency of ACI with halide injection is estimated to be higher due to the combination of the two control technologies being utilized in tandem.

3. **Baghouse capital cost is estimated based on EPA's Air Pollution Control Technology Fact Sheet (EPA-452/F-03-025). This fact sheet provides a rough estimate of baghouse capital cost that is between \$6 and \$26 per scfm. This document provides a good overview of baghouses and may provide an order-of-magnitude estimate of baghouse control technologies but should not be used to provide a capital cost estimate for a MBACT analysis. EPA's Air Pollution Control Cost Manual (January 2002) is intended to provide comprehensive costing of control equipment and using it would be acceptable for determining the cost of the baghouse, including the cost of the bags. Please provide a more precise cost estimate for the baghouse.**

The capital cost estimate for a five module, pulse-jet baghouse is provided in the Excel file named Appendix B & C (R1).xls. The cost methodology is found in Chapter 1 of the USEPA OAQPS Manual (EPA-452/B-02-001) and adjusted from 1998 dollars using the Engineering News Record Construction Cost Index. The calculations are shown in the attached file Soda

Spring BH est EPA-452-B-02-001.pdf. The revised methodology results in a cost of control of \$24,200 per pound for Option 1 and \$35,500 per pound for Option 2.

4. Annualized cost for each control option and for control equipment should be based on the life of the control equipment, not the duration of the loan for the baghouse. For the baghouse, provide an estimate of the useful life of the baghouse and the corresponding annualized baghouse cost. EPA's Air Pollution Control Cost Manual (January 2002) states that the baghouse lifetime varies from 5 to 40 years, with 20 years being typical. Please provide an updated cost analysis including documenting how the useful lifetime of the baghouse and other equipment was determined.

A baghouse life of 10 years is used in the cost model due to the conceptual level design and uncertainty of the effects of the exhaust gas on major components of the baghouse. The baghouse components that would experience deterioration include major items such as the housing, venturi throats, bag support cages, and dampers. Causes of the deterioration include corrosion of metal components by absorption of water and steam into the fabric filter media. As a result, it is anticipated that a major rebuild of the components or replacement of the baghouse would be necessary after 10 years of service. This is consistent with the life of the existing equipment in the facility's nodulizing process, which similarly deteriorates due to corrosion. Therefore the 10-year life used to calculate the annualized cost of capital is justified for this application and the cost calculation in the MBACT submittal is appropriate.

5. A significant cost component of both control options is attributed to "Steam Reheat", or the cost of energy necessary to raise 300,000 acfm of flue gas from 161 Fahrenheit to 250 Fahrenheit. A critical assumption of the cost analysis is the need to generate 59 klb/hr of steam. Please provide documentation on how this steam demand estimate was derived, and whether other engineering alternatives such as adding heat exchanger in the existing system could be used to reheat the exhaust.

A steam driven heat exchanger is included in the conceptual design and the steam demand is based on a rise of 88°F. The calculation of the steam demand is included in the Excel file provided (Appendix B & C.xls, and Appendix B & C (R1).xls).

A waste heat boiler cannot be operated with an exit temperature less than 700°C because sulfuric acid in the off-gas would condense and corrode pipes and other equipment.

6. Activated carbon injection and the use of a particulate matter control device to remove the activated carbon is a demonstrated control technology for reducing mercury emissions from coal fired utility boilers. Exhaust from coal fired utility boilers and the exhaust from the phosphate ore nodulizing kiln are similar in that both have a large volume of flue gas with low concentrations of mercury present. EPA and DOE estimated that the cost of activated carbon injection to control mercury emissions ranged from \$4,900 to \$70,000 per pound of mercury, with the average estimated cost being \$31,454 per pound of mercury. From the EPA and DOE studies it can be concluded that maximum degree of reduction practically

achievable by activated carbon injection is expensive on a dollar per pound of mercury basis, as are nearly all mercury control options because of the relatively small amount of mercury involved. Please describe why the maximum degree of reduction practically achievable is not justified for the control of mercury emissions from the nodulizing kiln. Simply stating it is too expensive because the cost per pound of mercury removed is not sufficient justification to eliminate the control option, environmental impacts and other impacts to the source must be considered. Environmental impacts should include impacts of mercury emissions.

Activated carbon injection (ACI) coupled with the use of PM control devices was eliminated as a control option for numerous reasons.

First, P4 estimates the control efficiency of halide injection/ACI (control option 1) and BACI (control option 2) to be no greater than 30% and 50%, respectively. In contrast, the average control efficiency of the existing controls is approximately 35% (as stated in Response to Question 1), not an additional 30%. At best, use of ACI and BACI will therefore result in an additional 15% of mercury control efficiency above existing controls. The control efficiencies (and therefore, the expected emission rate and expected emissions reduction) of ACI and BACI thus are not considerably greater than the control efficiency of existing controls.

Second, the economic impacts resulting from the control efficiency that are estimated to result from control options 1 and 2 are considerable relative to the small incremental control efficiency increase. The properties of exhaust gas from coal-fired power plants differ greatly from P4 kiln exhaust gas, and thus the cost effectiveness of the use of these technologies for mercury control in coal fired power plants cannot be directly generalized to the P4 process. The concentration of total mercury in coal-fired power plant exhaust gas is on the order of <25 µg/dscfm. In contrast, the total mercury concentration in P4's kiln off-gas has been quantified by kiln stack test sampling and analysis to be ~300 µg/dscfm, more than an order of magnitude higher than the concentration found in coal-fired power plant exhaust gas. In addition, the phosphate ore raw material contains numerous metals at significantly higher concentrations than coal (refer to Response to Question #2), and many of these species are present in the exhaust gas stream. Therefore, it is likely that additional halide and/or ACI or BACI utilization would be needed at an estimated cost near \$70,000 per pound of mercury and an annual operating cost of \$26.4M or \$48.4M, respectively, for the theoretical control efficiencies mentioned above. Significantly, the cost of handling, disposing of, and/or regenerating the captured activated carbon containing mercury and other species has not been included in these cost schemes.

In addition, the environmental impact associated with the incremental increase in control efficiency is negligible. Any reduction in the mercury air emissions would not result in a decrease in mercury discharged to the environment, as any mercury reduced from the air emissions would essentially be transferred to land emissions in the form of solid waste discharges due to handling and management of mercury containing activated carbon material.

In fact, any dramatic shift in operating costs similar to those estimated above might reduce the competitive position of the sole domestic source of elemental phosphorus and result in the need to import greater quantities of elemental phosphorus manufactured in countries that offer little if any environmental controls, including mercury, and it has been well established that mercury air emissions are a global concern. Models suggest that greater than 80% of mercury atmospheric deposition in Idaho originates from the global atmospheric pool. In addition, the trends in patterns of measured mercury in fish tissue from Idaho reservoirs and streams do not demonstrate any clear, direct relation to industrial activities in Idaho. (See the report enclosed with this letter in the file titled "Response to Question 6")

These combined factors would result in significant added cost to P4's elemental phosphorus production with little certainty for improvement in total environmental impact.

7. It is unclear if halogen and activated carbon injection prior to the venturi scrubbers (without the addition of baghouse) was determined to be technically feasible. It is stated that there are challenges to employing this technology, though it is not made clear whether an engineering evaluation was completed to determine whether such an option is technically feasible or not. Please provide details on whether this option is technically feasible or not. If it is determined to be technically feasible, please include it as a control option and perform a cost effectiveness analysis. In addition, it appears that only  $\text{CaBr}_2$  was evaluated for use in the halide injection control option. Please support why other mercury oxidizing and/or complexing agents were not considered. In addition, were gaseous oxidants (such as HCl injection) considered in combination with the existing dual-alkali scrubber (or with wet flue gas desulfurization) as control option(s)?

Control by halide injection and activated carbon injection prior to the venturi scrubbers was deemed technically infeasible for mercury control. Calcium bromide ( $\text{CaBr}_2$ ) was evaluated because it is the most common source of halide and because P4's supporting search of RBLC and other literature did not identify other commercially available halides in use for mercury control.

First, calcium bromide injection is technically infeasible for use in P4's operations because halide injection requires elevated temperatures and prolonged contact time to promote the oxidative conversion of elemental mercury into divalent mercury for subsequent capture in aqueous scrubbers or activated carbon. A solution of calcium bromide would presumably be injected into the kiln, or sprayed onto the ore feed. The kiln sustains sufficiently high temperatures to disassociate the calcium bromide (which requires 1,300° F or higher). Oxidation of the  $\text{Hg}_0$  would begin at gas temperatures below 1,000° F and would continue until the gas drops below 300° F. The gas should remain within this temperature range for at least two or three seconds to provide sufficient contacting time to oxidize the gaseous elemental mercury. But, as described in the MBACT For Elemental Phosphorus Process evaluation, the kiln off-gas temperature drops suddenly in the spray tower from 1,100° F to 160° F, bypassing the working temperature range needed for the bromide anion to oxidize the mercury. In other words, water soluble gas phase bromide species would be scrubbed in the spray tower before having the opportunity to oxidize

any significant portion of the metallic mercury in the lower temperature region beyond the spray tower.

Calcium bromide injection is also technically infeasible for use in P4's operations because there is potential for accelerated corrosion of ductwork and expensive process equipment. While bromide is considered to be less corrosive and more reactive towards mercury than other halides that have been injected into coal-fired boilers such as chloride, the long-term performance and equipment corrosion data for all the components that come into contact with the gas stream is not available.

In addition to the options for mercury control reported in the MBACT for Elemental Phosphorus Process evaluation, P4 also considered injection of sodium hypochlorite solution into the kiln exhaust stream. This technique was specifically developed and proposed by the EPA ORD for P4 during an ICR related to a MACT evaluation in 2010. P4's understanding is that the EPA Region X and ORD collaborators determined this control, along with other commercially available mercury control technologies, to be technically infeasible because P4's existing equipment does not offer either the temperature or contact time required for mercury oxidation, and the soluble halide type species injected would be scrubbed and neutralized by the spray tower and/or venturi scrubbers prior to having any impact on mercury control. In addition, the resulting chloride would result in the rapid corrosion of gas and water handling equipment. Also, it is notable that the management of the process water treatment facility at P4 is dependent on the accumulation of dissolved chlorides to mitigate corrosion and prevent the loss of equipment, and any increase in chlorides or other halides would have a significant impact on the plant water balance. For these reasons, EPA ORD has not pursued its proposal to test this control. Mercury oxidation by HCl injection was not evaluated because it was not identified as a commercially utilized mercury control reagent, and because it would have a similar negligible impact on mercury control and induce corrosion.

Halide injection in combination with the existing dual alkali (wet flue gas desulfurization scrubbers) was determined to be technically infeasible because stack tests suggest that the conversion of  $\text{SO}_2$  into  $\text{SO}_3^-$  and  $\text{SO}_4^{2-}$  byproducts by the scrubbers may create a reducing environment for the re-emission of  $\text{Hg}^0$ . While chemical binding and complexing agents are available to prevent oxidation of divalent mercury and re-emission as gaseous elemental mercury, P4 is not aware of any testing with respect to their compatibility with complex dual alkali aqueous chemistries that would support their use for the capture of elemental mercury.

8. **Please address if it would be technically feasible to inject activated carbon and a halogen as proposed in Option 1, but then use the existing spray tower to cool the exhaust gas to 250 F then add the baghouse downstream of the existing spray tower prior the existing venturi scrubbers. If it is determined to be technically feasible please include it as a control option and perform a cost effectiveness analysis.**

Injecting activated carbon and a halogen as proposed in Option 1, then using the existing spray tower to cool the exhaust gas and adding a baghouse downstream was determined to be

technically infeasible for a variety of reasons, including poor mercury control and negative impacts on the existing kiln off-gas and emissions control processes. The spray tower was designed and installed to quench and scrub the exhaust stream of the kiln nodulizing process. Specifically, the kiln is designed to agglomerate calcium fluorapatite ore ( $\text{Ca}_{10}(\text{PO}_4)_6\text{F}_2$ ) by a thermal process that brings it to a state of incipient fusion (the point at which it starts to melt) while evolving fluorine, sulfur and carbonaceous gases, and vaporizing light-boiling metals and blowing out in the gas stream tens of tons per hour of fine ore. All of these solid, gaseous, and vaporous materials that exit the kiln are removed, primarily, by the spray tower deluging them with a large excess of scrubbing water. If the spray tower were used to only cool the stream, all (or at least, most) of these materials would move through the spray tower to the activated carbon and halogen injection point and then enter the proposed baghouse downstream. These materials, which may enter the baghouses in amounts as great as 40 tons per hour, along with the added water vapor from the partial cooling process, would overwhelm any filter media used in that baghouse, as baghouses are designed to be used to remove relatively low concentrations of solids and are easily blinded with moisture. Solid materials are generally removed from the baghouse filter media by pneumatic pulsing, and blinding with moisture would interfere with this removal process. Additionally, the wet-dry interface in the spray tower would quickly result in scaling and spalling of the concrete inside the spray tower, which would foul and shut down the equipment. Also, the activated carbon and halide would preferentially adsorb the large quantity of dust, gas and vapor relative to the low concentration of gaseous mercury, which would overwhelm the adsorption kinetics necessary for effective mercury control.

9. **The mercuric chloride scrubbing technology (Boliden-Norzink process) was stated to be eliminated from consideration due to technical concerns. Though the application seems to indicate the technology was eliminated due to the scale of equipment required (implying that the technology would be too costly). Again please make clear whether this option is technically feasible or not. If a technology is technically feasible it must be eliminated considering energy, economic and environmental impacts.**

The mercuric chloride ( $\text{HgCl}_2$ ) scrubber, a technology not identified in the RBLC, was determined to be technically infeasible because it was designed for use and has been demonstrated on exhaust gas streams from metal roasters with a flow rate of ~12000 dscfm and an elemental Hg content of 300 mg/dscfm. In contrast, P4's air pollution control system has a flow rate of 300,000 dscfm and an elemental Hg content of approximately 300  $\mu\text{g}$ /dscfm. To the best of P4's knowledge, mercuric chloride scrubbing technology has not been demonstrated in conditions that resemble P4's process conditions. Therefore, the reference to the scale of the equipment does not imply that the equipment itself would be too costly, but rather that the scale required for P4's air pollution control system is beyond the designed and demonstrated feasible capacity of the commercially available mercuric chloride scrubbing technology.

The use of a mercuric chloride scrubber would be infeasible due to differences between demonstrated conditions and P4's operations, and due to potential effects on P4's operations. In order to maximize the scrubber's efficiency, P4's off-gas would require cooling to ~100°F. This would result in a large quantity of condensed process water, the management of which would be a

challenge to incorporate into the existing plant water balance. In addition, the captured mercury in the form of calomel ( $\text{Hg}_2\text{Cl}_2$ ) would either need to be purged from the system for disposal, sale, or reprocessing via chloride regeneration, from which liquid metallic mercury would be produced for disposal or sale. The market of both calomel and liquid metallic mercury of the quality produced from these processes are uncertain. In addition, the added effects of low levels of species present in kiln exhaust are unknown, but it is likely that there would be some interference with mercury capture coupled with issues in regenerating the scrubber fluid.

**10. Please provide an electronic copy of the spreadsheet that was used to estimate costs.**

An electronic copy of the spreadsheet that was used to estimate costs is enclosed with this letter in the file titled "Response to Question 10."

In accordance with IDAPA 58.01.01.123, I certify based on information and belief formed after reasonable inquiry, that the statements and information in this document are true, accurate, and complete. If you have any questions regarding this submittal, please contact Mr. Jim McCulloch at (208) 547-1233.

Sincerely,



Sheldon Alver  
Plant Manager

enclosures

## P<sub>4</sub> Production, LLC

Soda Springs Plant  
1853 Highway 34  
P.O. Box 816  
Soda Springs, Idaho 83276-0816  
Phone: (208) 547-4300  
Fax: (208) 547-3312

October 10, 2012

VIA CERTIFIED MAIL;  
RETURN RECEIPT REQUESTED – 7010 2780 0002 0464 3101

Mr. Dan Pitman, P.E.  
Department of Environmental Quality  
1410 North Hilton  
Boise, Idaho 83706

RE: Facility ID No. 029-00001, P4 Production, LLC, Soda Springs  
Tier II Permit Application and Mercury Best Available Control Technology Analysis

Dear Mr. Pitman:

On September 10, 2012, P4 Production, LLC (“P4”) received your email and attached letter stating that the Idaho Department of Environmental Quality (“IDEQ”) has determined that P4’s Tier II Permit application and Mercury Best Available Control Technology (“MBACT”) Analysis is incomplete. P4 offers the following information in response to your letter:

- 1. The capital equipment costs for control Option 1 (CaBr<sub>2</sub> + ACI) includes \$980,000<sup>1</sup> capital cost for control Option 2 (BACI system). It appears that this cost may actually be for either a BACI or an ACI system. If this correct please update the capital cost spreadsheet to indicate that the capital cost is for either BACI system or ACI system.**

The \$980,000 capital cost stated in the application is the cost of equipment associated with the activated carbon injection system (including storage, conveyance, and injection of a powdered sorbent material into the kiln exhaust stream), and could be applied to ACI and/or BACI. Additional costs are associated with Control Option 1, including the cost of equipment associated with the oxidant injection system (including storage and injection of calcium bromide and a liner in the ductwork to the hydrosonic scrubbers). The capital cost spreadsheet has been updated to reflect this (refer to the “Capital Cost App B&C” spreadsheet in the title and at rows 10, 18, 26-30).

- 2. The economic analysis spreadsheet includes a baghouse cost of \$7,800,000 instead of the updated cost of \$2,100,000 that was provided on August 16, 2012. The updated cost was**

<sup>1</sup> BACI System – Storage and conveyance \$900,000; Injectors \$80,000.

reflected in P4's response to question #3 but the spreadsheet was not updated. Please update the spreadsheet to include the updated baghouse cost.

The economic analysis spreadsheet has been updated as requested (refer to the "Capital Cost App B&C" spreadsheet at row 22).

3. The economic analysis that has been provided is based on control Option 1 providing a 50% control for mercury above what is currently controlled by the existing system<sup>2</sup>, and on control Option 2 providing a 30% control above what is currently provided by the existing system. However, in P4's response to question #6 it is stated that at best the two options will provide no more than 15% mercury control above the existing controls. Please clarify these discrepancies and if necessary update the economic analysis to reflect the estimated control efficiencies.

The economic analysis that has been provided is not based on control Option 1 providing a 50% control option for mercury above what is currently controlled by the existing system, nor on control Option 2 providing a 30% control above what is currently provided by the existing system. Rather, the estimated control efficiencies are for overall or total mercury control. The cost estimates in appendices B and C have been updated to more accurately reflect these control efficiencies (refer to the spreadsheet titled "Option 1 App B (101012)" at rows 106 and 107, and the spreadsheet titled "Option 2 App C (101012)" at rows 102 and 103).

Note that estimated mercury emissions from the current system are 753 lb/yr (not 735 lb/yr, as stated in your letter), which reflects a 35% control efficiency resulting in the removal of 405 lb/yr of mercury. The existing control is generated by the combination of kiln thermal and atmospheric conditions, dust collection devices, spray tower, and hydrosonic/LCDA scrubbing equipment. The estimate of approximately 35% control efficiency in the existing equipment is based on mass balance and supported by stack test results (refer to P4's response dated July 23, 2012 at response #1 and section 1.2 of the MBACT report) which ranges between 31 and 39% control between 2006 and 2011. It is noteworthy that the material balance was constructed using the best available data from process inputs and material analysis. Because the P4 kiln process is non-stoichiometric, the raw materials are processed in hundreds of thousands to million of tons on an annual basis and are highly heterogeneous, and the exact input measurements are based on average material quantities transported and loaded by heavy vehicular equipment. The actual control efficiency could therefore vary by as much as  $\pm 5 - 10\%$ .

Estimated mercury emissions with control Option 1 in place are 579 lb/yr, which reflects a 50% control efficiency resulting in the removal of 579 lb/yr of mercury. Estimated mercury emissions with control Option 2 in place are 811 lb/yr, which reflects an approximate 30% control efficiency resulting in the removal of 347 lb/yr of mercury. This should be noted as a correction to the mercury control efficiencies for control Option 1 and control Option 2 stated on pages 27 and 28 of the MBACT analysis.

---

<sup>2</sup> Estimated mercury emissions from the current system is 735 lb/yr., total estimated emissions after the addition of Control Option 1 is 376.5 lb/yr.

A detailed explanation for the basis of these estimated control efficiencies are given in P4's response #2 and #6 dated July 23, 2012. To reiterate these key points, no mercury control technology has been demonstrated at any scale on any industrial process exhaust gas with chemical speciation, flow rates, residence time, and temperature profile comparable to the P4 nodulizing kiln exhaust gas stream. The expected control efficiency for either control Option 1 or control Option #2 as applied to P4's process would be significantly impacted by numerous gaseous and particulate phase metallic species (i.e., Cd, Zn, etc.), sulfur-containing species, and moisture present in the kiln off-gas. These species are present at a combined average concentration that exceeds the average concentration of mercury in other industries by orders of magnitude and would compete for injected halide and ACI (control Option 1) or BACI (control Option 2) adsorption since these control materials are not selective for mercury removal. Together, these effects would result in a significant increase in operating cost because excessive quantities of halide and/or ACI/BACI would be required. Control Option 1 may provide a 15% increase in mercury control over the existing equipment at an annual cost of \$9.2M, for an incremental increase of 174 lb/yr of mercury (\$53,000/lb), whereas control option 2 is estimated to provide no increased control at an annual cost of \$7.9M. In fact, the installation of a halide injection system in control Option #1 could have a negative impact on the mercury control efficiency estimated for the existing equipment. Since these technologies have not been demonstrated under comparable conditions, there are significant uncertainties associated with any cost estimate. In addition, the cost for either control option is likely to be much higher than those seen for other industrial processes (refer to response #5 below), and the concentration of mercury and other metallic species in spent activated carbon would impact the technical and economic ability to handle and dispose of or regenerate these materials (refer to response #4 below).

It is notable that EPA Region X and EPA Office of Research and Development (ORD) collaborators determined that commercially available mercury control technologies are technically infeasible because P4's existing equipment does not offer either the temperature or contact time required for mercury capture (refer to P4's July 23, 2012 response #7).

- 4. In response to question #6 P4 states that it is significant that the cost of handling, disposing of, and/or regenerating activated carbon is not included in the economic analysis. However, the economic analysis that has been provided does include carbon costs and disposal costs. Please address this apparent discrepancy and if necessary update the carbon and disposal costs that have been provided in the economic analysis. The economic analysis should include estimates for any significant costs.**

You are correct that the MBACT evaluation does quantify carbon disposal costs. Response #6 should state that "Significantly, only the cost of handling and disposal of the spent ACI disposal has been incorporated in the cost estimate; the cost of regenerating the captured activated carbon containing mercury has not been included." This economic analysis therefore does not reflect the full economic impact of transferring mercury from air emissions to land discharges.

- 5. In response to question #3 P4 provides that the cost of mercury control, as reflected by the updated baghouse cost analysis, is \$24,000 per pound for Option 1 and \$35,000 per pound for Option 2. In response to question #6 P4 states the estimated cost to achieve the**

**theoretical control efficiencies is likely \$70,000 per pound of mercury. Please addresses these discrepancies and update the economic analysis spreadsheet that has been provided.**

Note that the cost estimates in appendices B and C have been updated to more accurately reflect these control efficiencies (refer to the spreadsheet titled "Option 1 App B (101012)" at rows 106 and 107, and the spreadsheet titled "Option 2 App C (101012)" at rows 102 and 103). The response to #6 does not state that the cost of ACI or BACI would be \$70,000, but rather implies that there are a myriad of uncertainties in the application of any available control technology proposed for controlling mercury emissions from the P4 kiln stacks and that the operating costs would be closer to the upper end of the EPA/DOE published cost estimates for coal fired power plants or other industrial processes. These technologies have not been successfully tested nor demonstrated at any scale on any industrial process under conditions comparable to those in P4's kiln. The cost estimate provided in P4's July 23, 2012 response to question #3 is unable to account for the unknown costs of operating a control system in a process with a total mercury concentration more than an order of magnitude higher than the concentration found in coal-fired power plant exhaust gas, and with a raw material input containing numerous metals and other species at significantly higher concentrations than coal. Therefore, P4 anticipates that there will be substantial additional cost for the significant volume of ACI or BACI powdered sorbent control materials that would be required, but that cost cannot be quantified at this time.

In accordance with IDAPA 58.01.01.123, I certify based on information and belief formed after reasonable inquiry, that the statements and information in this document are true, accurate, and complete. If you have any questions regarding this submittal, please contact Mr. Jim McCulloch at (208) 547-1292.

Sincerely,



Sheldon Alver  
Plant Manager

Enclosures

**Alternate Appendix B**  
**P4 Production, L.L.C. - Hq BACT Analysis**  
**Conceptual Control Option 1**  
**[Includes oxidant injection (CaBr<sub>2</sub>) and ACI]**  
**Nodulizing Kiln**

Control Efficiency (%)	50.0
------------------------	------

**Facility Input Data**

Item	Value
Operating Schedule	
Shifts per day	3
Hours per day	24
Days per week	7
Total Hours per year	8760
Economic Life, years	10
Interest Rate (%)	7
Source(s) Controlled	Nodulizer Kiln
Total Flowrate (acfm)	300,000
Hg from Kiln Operation (lb/hr)	0.132
Hg from Kiln Operation (lb/yr)	1,158
Site Specific Electricity Cost (\$/kWh)	0.043
Site Specific Operating Labor Cost (\$/hr)	\$45.00
Site Specific Maint. Labor Cost (\$/hr)	\$45.00

**Capital Costs**

	Value	Basis
<b>Direct Costs</b>		
1.) Purchased Equipment Cost		
a.) Equipment cost + auxiliaries	\$5,599,000	See Capital Cost Estimate, A
b.) Instrumentation	\$0	Included
c.) Sales taxes	\$0	Included
d.) Freight	\$279,950	0.05 X A
Total Purchased equipment cost, (PEC)	\$5,878,950	B
2.) Direct Installation costs		
a.) Foundations and supports	\$293,900	0.10 x B
b.) Handling and erection	\$1,175,800	0.20 x B
c.) Electrical	\$58,800	0.01 x B
d.) Piping	\$58,800	0.01 x B
e.) Insulation for ductwork & painting	\$58,800	0.01 x B
f.) Stack modification	\$117,600	0.02 x B
Total direct installation cost	\$1,763,685	0.30 x B
3.) Site preparation	\$200,000	As Required, SP
4.) Buildings	NA	As Required, Bldg.
<b>Total Direct Cost, DC</b>	\$7,842,600	1.30B + SP + Bldg.
<b>Indirect Costs (Installation)</b>		
5.) Engineering	\$117,600	0.02 x B
6.) Construction and field expenses	\$293,900	0.05 x B
7.) Contractor fees	\$587,900	0.10 x B
8.) Start-up	\$117,600	0.02 x B
9.) Performance test	\$58,800	0.01 x B
10.) Contingencies	\$881,800	0.15 x B
<b>Total Indirect Cost, IC</b>	\$2,057,600	0.35 x B + Other
<b>Total Capital Investment (TCI) = DC + IC</b>	<b>\$9,900,200</b>	<b>1.61B + SP + Bldg. + Other</b>

**Alternate Appendix B**  
**P4 Production, L.L.C. - Hq BACT Analysis**  
**Conceptual Control Option 1**  
**[Includes oxidant injection (CaBr<sub>2</sub>) and ACI]**  
**Nodulizing Kiln**

Control Efficiency (%)	50.0
------------------------	------

**Annual Costs**

Item	Value	Basis	Source
<b>1) Electricity</b>			
Fan Power Requirement (kW)	1,648		
Electric Power Cost (\$/kWh)	0.043		Estimate
Cost (\$/yr)	\$620,769		
<b>2) Operating Costs</b>			
Operating Labor Requirement (hr/shift)	1	1 hour per shift	
Unit Cost (\$/hr)	\$40.00	Facility Data	Estimate
Labor Cost (\$/yr)	\$43,680		
<b>3) CaBr<sub>2</sub> Cost (\$/gal)</b>	9.00		
Hourly Requirement (gal/hour)	14	Based on CaBr <sub>2</sub> :ACI ratio of 0.15	
Annual requirement (gal/year)	118,260		Estimate
Total NaOCl Costs (\$/year)	\$1,064,340		
<b>4) Steam Reheat</b>			
Temperature rise (°F)	88		
Steam requirement (klb/hr)	59		Estimate
Steam cost (\$/klb)	\$9.0	Estimated	
Total Cost	\$4,851,560		
<b>5) AC Cost (\$/lb)</b>	\$1		
Hourly Requirement (Lbs/hour)	90	5 lb/MMacfm	
Annual requirement (Lbs/year)	788,400		Estimate
Total BAC Costs (\$/year)	\$788,400		
<b>6) Residual Disposal</b>			
Annual Quantity (TPY)	434		
Cost (\$/T)	\$200	Special Waste Assumed	Estimate
Total Disposal Cost (\$/year)	\$86,724		
<b>Total Operating Costs</b>	<b>\$7,255,473</b>		
<b>7) Supervisory Labor</b>			
Cost (\$/yr)	\$6,550	15% Operating Labor	OAQPS
<b>8) Maintenance</b>			
Maintenance Labor Req. (hr/year)	876.0	10% Operating Hours	Estimate
Unit Cost (\$/hr)	\$45.00	Facility Data	Estimate
Labor Cost (\$/yr)	\$39,420		
Material Cost (\$/yr)	\$39,420	100% of Maintenance Labor	OAQPS
Total Cost (\$/yr)	\$78,840		
<b>9) Indirect Annual Costs</b>			
Overhead	\$77,440	60% of O&M Costs	OAQPS
Administration	\$198,000	2% of Total Capital Investment	OAQPS
Property Tax	\$99,000	1% of Total Capital Investment	OAQPS
Insurance	\$99,000	1% of Total Capital Investment	OAQPS
Capital Recovery	\$1,409,570	10 yr life; 7% Interest	OAQPS
Total Indirect (\$/yr)	\$1,883,010		
<b>Total Annualized Cost (\$/yr)</b>	<b>\$9,223,900</b>		
<b>Total Controlled (lb/yr)</b>	<b>579.0</b>		
<b>Cost Effectiveness (\$/lb)</b>	<b>\$15,900</b>		

**Alternate Appendix C**  
**P4 Production, L.L.C. - Hg BACT Analysis**  
**Conceptual Control Option 2**  
**[Does not include oxidant injection (CaBr<sub>2</sub>); BACI only]**  
**Nodulizing Kiln**

Control Efficiency (%)	30.0
------------------------	------

**Facility Input Data**

Item	Value
Operating Schedule	
Shifts per day	3
Hours per day	24
Days per week	7
Total Hours per year	8760
Economic Life, years	10
Interest Rate (%)	7
Source(s) Controlled	Nodulizer Kiln
Total Flowrate (acfm)	300,000
Hg from Kiln Operation (lb/hr)	0.132
Hg from Kiln Operation (lb/yr)	1,158
Site Specific Electricity Cost (\$/kWh)	0.043
Site Specific Operating Labor Cost (\$/hr)	\$45.00
Site Specific Maint. Labor Cost (\$/hr)	\$45.00

**Capital Costs**

	Value	Basis
<b>Direct Costs</b>		
1.) Purchased Equipment Cost		
a.) Equipment cost + auxiliaries	\$5,181,000	See Capital Cost Estimate, A
b.) Instrumentation	\$0	Included
c.) Sales taxes	\$0	Included
d.) Freight	\$259,050	0.05 X A
Total Purchased equipment cost, (PEC)	\$5,440,050	B
2.) Direct installation costs		
a.) Foundations and supports	\$272,000	0.10 x B
b.) Handling and erection	\$1,088,000	0.20 x B
c.) Electrical	\$54,400	0.01 x B
d.) Piping	\$54,400	0.01 x B
e.) Insulation for ductwork & painting	\$54,400	0.01 x B
f.) Stack modification	\$108,800	0.02 x B
Total direct Installation cost	\$1,632,015	0.30 x B
3.) Site preparation	\$200,000	As Required, SP
4.) Buildings	NA	As Required, Bldg.
Total Direct Cost, DC	\$7,272,100	1.30B + SP + Bldg.
<b>Indirect Costs (Installation)</b>		
5.) Engineering	\$108,800	0.02 x B
6.) Construction and field expenses	\$272,000	0.05 x B
7.) Contractor fees	\$544,000	0.10 x B
8.) Start-up	\$108,800	0.02 x B
9.) Performance test	\$54,400	0.01 x B
10.) Contingencies	\$816,000	0.15 x B
Total Indirect Cost, IC	\$1,904,000	0.35 x B + Other
<b>Total Capital Investment (TCI) = DC + IC</b>	<b>\$9,176,100</b>	<b>1.61B + SP + Bldg. + Other</b>

**Alternate Appendix C**  
**P4 Production, L.L.C. - Hg BACT Analysis**  
**Conceptual Control Option 2**  
**[Does not include oxidant injection (CaBr<sub>2</sub>); BACI only]**  
**Nodulizing Kiln**

Control Efficiency (%)	30.0
------------------------	------

**Annual Costs**

Item	Value	Basis	Source
<b>1) Electricity</b>			
Fan Power Requirement (kW)	1,648		Estimate
Electric Power Cost (\$/kWh)	0.043		
Cost (\$/yr)	\$620,769		
<b>2) Operating Costs</b>			
Operating Labor Requirement (hr/shift)	1	1 hour per shift Facility Data	Estimate
Unit Cost (\$/hr)	\$40.00		
Labor Cost (\$/yr)	\$43,680		
<b>3) Steam Reheat</b>			
Temperature rise (°F)	88	Estimated	Estimate
Steam requirement (klb/hr)	59		
Steam cost (\$/klb)	\$9.0		
Total Cost	\$4,651,560		
<b>4) BAC Cost (\$/lb)</b>			
Hourly Requirement (Lbs/hour)	\$1	5 lb/MMacfm	Estimate
Annual requirement (Lbs/year)	90		
Total BAC Costs (\$/year)	788,400		
	\$788,400		
<b>5) Residual Disposal</b>			
Annual Quantity (TPY)	434	Special Waste Assumed	Estimate
Cost (\$/T)	\$200		
Total Disposal Cost (\$/year)	\$86,724		
<b>Total Operating Costs</b>			
	<b>\$6,191,133</b>		
<b>6) Supervisory Labor</b>			
Cost (\$/yr)	\$6,550	15% Operating Labor	OAQPS
<b>7) Maintenance</b>			
Maintenance Labor Req. (hr/year)	438.0	5% Operating Hours Facility Data	Estimate
Unit Cost (\$/hr)	\$45.00		
Labor Cost (\$/yr)	\$19,710		
Material Cost (\$/yr)	\$19,710	100% of Maintenance Labor	OAQPS
Total Cost (\$/yr)	\$39,420		
<b>8) Indirect Annual Costs</b>			
Overhead	\$53,790	60% of O&M Costs	OAQPS
Administration	\$183,520	2% of Total Capital Investment	OAQPS
Property Tax	\$91,760	1% of Total Capital Investment	OAQPS
Insurance	\$91,760	1% of Total Capital Investment	OAQPS
Capital Recovery	\$1,306,470	10 yr life; 7% interest	OAQPS
Total Indirect (\$/yr)	\$1,727,300		
<b>Total Annualized Cost (\$/yr)</b>			
	<b>\$7,964,400</b>		
<b>Total Controlled (lb/yr)</b>			
	<b>347.0</b>		
<b>Cost Effectiveness (\$/lb)</b>			
	<b>\$23,000</b>		

**Alternate Appendix B & C**  
**P4 Production, L.L.C - Hg BACT Analysis**  
**Equipment Capital Cost Estimate**  
**for Conceptual Control Options 1 & 2**

Item	Cost Estimate	Basis
Activated Carbon Injection System		
Storage and conveyance	\$900,000	United Conveyor price list
Injectors	\$80,000	Estimate
Oxidant Injection (CaBr <sub>2</sub> )		(Included for Conceptual Control Option 1 only)
Storage (CaBr <sub>2</sub> )	\$100,000	Tank cost estimate RS Means
Injection system	\$80,000	Estimate
Steam Reheat		
Housing	\$100,000	RS Means
Steam Line	\$100,000	RS Means
Heat Exchanger	\$1,000,000	AB&CO - TT Boilers (316 SS)
Ductwork, Dampers, & Fans		
FRP Liner to hydrosolic scrubbers	\$200,000	Est. (Included for Conceptual Control Option 1 only)
Dampers	\$60,000	Estimate
Fans	\$250,000	RS Means
Baghouse		
Baghouse	\$2,100,000	EPA-452/B-02-001 (escalation used based on ENR)
Hopper	\$60,000	Estimate
Residual Storage	\$60,000	Estimate
Controls		
Integrated Control System (Option 1)	\$509,000	10% of equipment cost
Integrated Control System (Option 2)	\$471,000	10% of equipment cost
Capital Cost Total		
Integrated Control System (Option 1)	\$5,599,000	10% of equipment cost
Integrated Control System (Option 2)	\$5,181,000	10% of equipment cost



# P<sub>4</sub> Production, LLC

Soda Springs Plant  
1853 Highway 34  
P.O. Box 816  
Soda Springs, Idaho 83276-0818  
Phone: (208) 547-4300  
Fax: (208) 547-3312

November 6, 2012

VIA CERTIFIED MAIL;  
RETURN RECEIPT REQUESTED – 7010 2780 0002 0464 3132

Mr. Dan Pitman, P.E.  
Department of Environmental Quality  
1410 North Hilton  
Boise, Idaho 83706

RE: Facility ID No. 029-00001, P<sub>4</sub> Production, LLC, Soda Springs  
Tier II Permit Application and Mercury Best Available Control Technology Analysis

Dear Mr. Pitman:

On October 19, 2012, you called P<sub>4</sub> Production, LLC (“P<sub>4</sub>”) to discuss two questions regarding P<sub>4</sub>’s Tier II Permit application and Mercury Best Available Control Technology (“MBACT”) Analysis. P<sub>4</sub> offers the following information in response to your call:

1. P<sub>4</sub>’s spreadsheets submitted on October 10, 2012, show a cost effectiveness (\$/lb) based on the overall or total mercury control (including existing controls), while P<sub>4</sub>’s response letter submitted on that date states the cost effectiveness based on the incremental mercury control (above existing controls). Please update the spreadsheets so both approaches to cost effectiveness are addressed.

The enclosed spreadsheets have been updated per your request.

2. P<sub>4</sub>’s Response #3 in its letter submitted October 10, 2012, states that control Option 2 will provide no increase in mercury control. Please explain why installing additional control technology (in sequence with, rather than in place of, existing control equipment) will not provide any increased controls.

Based on material balance data and stack testing, the total mercury control efficiency of the existing control equipment is estimated to be between 31 and 35%. This is comparable to the estimated total 30% control efficiency that may be achieved by installing control Option 2 downstream from the existing hydrosonic scrubbers and SO<sub>2</sub> control processes. In other

words, the installation of control Option 2 will provide essentially no increase in mercury control above the existing air pollution control equipment.

P4 has determined control Option 2 will provide no additional increase in mercury control due to the conditions unique to P4's process, including the mercury speciation, the low mercury concentration and residence time, the high exhaust gas moisture content, flow rate and temperature, and the presence of a myriad of chemical species present at much higher concentrations than mercury that will compete for BACI. Control option 2 has never been demonstrated at any scale on any gas stream with comparable conditions. The numerous challenges and resulting uncertainty to effectively using control Option 2 are detailed at page 22 of the MBACT Analysis and in P4's correspondences dated July 23, 2012, and October 10, 2012.

For the sake of calculating a cost effectiveness for control Option 2, P4 has estimated an increase in mercury control of one pound.

In contrast, control Option 1 may achieve an additional control efficiency of up to 15%. This is because control Option 1 would use both an ACI injection system, similar to the BACI proposed for control Option 2, and a halide injection system, which would inject halides upstream of the existing controls. The potential incremental increase in mercury control might result from the presence of the halides in the system.

In accordance with IDAPA 58.01.01.123, I certify based on information and belief formed after reasonable inquiry, that the statements and information in this document are true, accurate, and complete. If you have any questions regarding this submittal, please contact Mr. Jim McCulloch at (208) 547-1233.

Sincerely,



Sheldon Alver  
Plant Manager

Enclosures

**Appendix B & C**  
**P4 Production, L.L.C - Hg BACT Analysis**  
**Equipment Capital Cost Estimate**  
**for Conceptual Control Options 1 & 2**

Item	Cost Estimate	Basis
Activated Carbon Injection System		
Storage and conveyance	\$900,000	United Conveyor price list
Injectors	\$80,000	Estimate
Oxidant Injection (CaBr <sub>2</sub> )		(Included for Conceptual Control Option 1 only)
Storage (CaBr <sub>2</sub> )	\$100,000	Tank cost estimate RS Means
Injection system	\$80,000	Estimate
Steam Reheat		
Housing	\$100,000	RS Means
Steam Line	\$100,000	RS Means
Heat Exchanger	\$1,000,000	AB&CO - TT Boilers (316 SS)
Ductwork, Dampers, & Fans		
FRP Liner to hydrosolic scrubbers	\$200,000	Est. (Included for Conceptual Control Option 1 only)
Dampers	\$60,000	Estimate
Fans	\$250,000	RS Means
Baghouse		
Baghouse	\$2,100,000	EPA-452/B-02-001 (escalation used based on ENR)
Hopper	\$60,000	Estimate
Residual Storage	\$60,000	Estimate
Controls		
Integrated Control System (Option 1)	\$509,000	10% of equipment cost
Integrated Control System (Option 2)	\$471,000	10% of equipment cost
Capital Cost Total		
Integrated Control System (Option 1)	\$5,599,000	10% of equipment cost
Integrated Control System (Option 2)	\$5,181,000	10% of equipment cost

**Appendix B - Total Control**  
**P4 Production, L.L.C. - Hg BACT Analysis**  
**Conceptual Control Option 1**  
**[Includes oxidant injection (CaBr<sub>2</sub>) and ACI]**  
**Nodulizing Kiln**

Control Efficiency (%)	50.0
------------------------	------

**Facility Input Data**

Item	Value
<b>Operating Schedule</b>	
Shifts per day	3
Hours per day	24
Days per week	7
Total Hours per year	8760
Economic Life, years	10
Interest Rate (%)	7
<b>Source(s) Controlled</b>	Nodulizer Kiln
Total Flowrate (acfm)	300,000
Hg from Kiln Operation (lb/hr)	0.132
Hg from Kiln Operation (lb/yr)	1,158
Site Specific Electricity Cost (\$/KWh)	0.043
Site Specific Operating Labor Cost (\$/hr)	\$45.00
Site Specific Maint. Labor Cost (\$/hr)	\$45.00

**Capital Costs**

	Value	Basic
<b>Direct Costs</b>		
1.) Purchased Equipment Cost		
a.) Equipment cost + auxiliaries	\$5,599,000	See Capital Cost Estimate, A
b.) Instrumentation	\$0	Included
c.) Sales taxes	\$0	Included
d.) Freight	\$279,950	0.05 X A
Total Purchased equipment cost, (PEC)	\$5,878,950	B
2.) Direct installation costs		
a.) Foundations and supports	\$293,900	0.10 x B
b.) Handling and erection	\$1,175,800	0.20 x B
c.) Electrical	\$58,800	0.01 x B
d.) Piping	\$58,800	0.01 x B
e.) Insulation for ductwork & painting	\$58,800	0.01 x B
f.) Stack modification	\$117,600	0.02 x B
Total direct installation cost	\$1,763,685	0.30 x B
3.) Site preparation	\$200,000	As Required, SP
4.) Buildings	NA	As Required, Bldg.
Total Direct Cost, DC	\$7,842,600	1.30B + SP + Bldg.
<b>Indirect Costs (Installation)</b>		
5.) Engineering	\$117,600	0.02 x B
6.) Construction and field expenses	\$293,900	0.05 x B
7.) Contractor fees	\$587,900	0.10 x B
8.) Start-up	\$117,600	0.02 x B
9.) Performance test	\$58,800	0.01 x B
10.) Contingencies	\$881,800	0.15 x B
Total Indirect Cost, IC	\$2,057,600	0.35 x B + Other
<b>Total Capital Investment (TCI) = DC + IC</b>	<b>\$9,900,200</b>	<b>1.61B + SP + Bldg. + Other</b>

**Appendix B - Total Control  
P4 Production, L.L.C. - Hg BACT Analysis  
Conceptual Control Option 1  
[Includes oxidant Injection (CaBr<sub>2</sub>) and ACI]  
Nodulizing Kiln**

Control Efficiency (%)	50.0
------------------------	------

**Annual Costs**

Item	Value	Basis	Source
<b>1) Electricity</b>			
Fan Power Requirement (kW)	1,648		Estimate
Electric Power Cost (\$/kWh)	0.043		
Cost (\$/yr)	\$620,769		
<b>2) Operating Costs</b>			
Operating Labor Requirement (hr/shift)	1	1 hour per shift Facility Data	Estimate
Unit Cost (\$/hr)	\$40.00		
Labor Cost (\$/yr)	\$43,880		
<b>3) CaBr<sub>2</sub> Cost (\$/gal)</b>	9.00	Based on CaBr <sub>2</sub> :ACI ratio of 0.15	Estimate
Hourly Requirement (gal/hour)	14		
Annual requirement (gal/year)	118,280		
Total NaOCl Costs (\$/year)	\$1,064,340		
<b>4) Steam Reheat</b>			
Temperature rise (°F)	88	Estimated	Estimate
Steam requirement (klb/hr)	59		
Steam cost (\$/klb)	\$9.0		
Total Cost	\$4,651,560		
<b>5) AC Cost (\$/lb)</b>	\$1	5 lb/MMacfm	Estimate
Hourly Requirement (Lbs/hour)	90		
Annual requirement (Lbs/year)	788,400		
Total BAC Costs (\$/year)	\$788,400		
<b>6) Residual Disposal</b>			
Annual Quantity (TPY)	434	Special Waste Assumed	Estimate
Cost (\$/T)	\$200		
Total Disposal Cost (\$/year)	\$86,724		
<b>Total Operating Costs</b>	<b>\$7,255,473</b>		
<b>7) Supervisory Labor</b>			
Cost (\$/yr)	\$6,550	15% Operating Labor	OAQPS
<b>8) Maintenance</b>			
Maintenance Labor Req. (hr/year)	876.0	10% Operating Hours Facility Data	Estimate
Unit Cost (\$/hr)	\$45.00		
Labor Cost (\$/yr)	\$39,420	100% of Maintenance Labor	OAQPS
Material Cost (\$/yr)	\$39,420		
Total Cost (\$/yr)	\$78,840		
<b>9) Indirect Annual Costs</b>			
Overhead	\$77,440	60% of O&M Costs	OAQPS
Administration	\$198,000	2% of Total Capital Investment	OAQPS
Property Tax	\$99,000	1% of Total Capital Investment	OAQPS
Insurance	\$99,000	1% of Total Capital Investment	OAQPS
Capital Recovery	\$1,409,570	10 yr life; 7% interest	OAQPS
Total Indirect (\$/yr)	\$1,883,010		
<b>Total Annualized Cost (\$/yr)</b>	<b>\$9,223,900</b>		
<b>Total Controlled (lb/yr), including current controls</b>	<b>579.0</b>		
<b>Cost Effectiveness (\$/lb)</b>	<b>\$15,900</b>		

**Appendix C - Total Control**  
**P4 Production, L.L.C. - Hg BACT Analysis**  
**Conceptual Control Option 2**  
**[Does not include oxidant injection (CaBr<sub>2</sub>); BACI only]**  
**Nodulizing Kiln**

Control Efficiency (%)	30.0
------------------------	------

**Facility Input Data**

Item	Value
<b>Operating Schedule</b>	
Shifts per day	3
Hours per day	24
Days per week	7
Total Hours per year	8760
Economic Life, years	10
Interest Rate (%)	7
Source(s) Controlled	Nodulizer Kiln
Total Flowrate (acfm)	300,000
Hg from Kiln Operation (lb/hr)	0.132
Hg from Kiln Operation (lb/yr)	1,158
Site Specific Electricity Cost (\$/kWh)	0.043
Site Specific Operating Labor Cost (\$/hr)	\$45.00
Site Specific Maint. Labor Cost (\$/hr)	\$45.00

**Capital Costs**

	Value	Notes
<b>Direct Costs</b>		
1.) Purchased Equipment Cost		
a.) Equipment cost + auxiliaries	\$5,181,000	See Capital Cost Estimate, A
b.) Instrumentation	\$0	Included
c.) Sales taxes	\$0	Included
d.) Freight	\$259,050	0.05 X A
Total Purchased equipment cost, (PEC)	\$5,440,050	B
2.) Direct Installation costs		
a.) Foundations and supports	\$272,000	0.10 x B
b.) Handling and erection	\$1,088,000	0.20 x B
c.) Electrical	\$54,400	0.01 x B
d.) Piping	\$54,400	0.01 x B
e.) Insulation for ductwork & painting	\$54,400	0.01 x B
f.) Stack modification	\$108,800	0.02 x B
Total direct installation cost	\$1,632,015	0.30 x B
3.) Site preparation	\$200,000	As Required, SP
4.) Buildings	NA	As Required, Bldg.
Total Direct Cost, DC	\$7,272,100	1.30B + SP + Bldg.
<b>Indirect Costs (Installation)</b>		
5.) Engineering	\$108,800	0.02 x B
6.) Construction and field expenses	\$272,000	0.05 x B
7.) Contractor fees	\$544,000	0.10 x B
8.) Start-up	\$108,800	0.02 x B
9.) Performance test	\$54,400	0.01 x B
10.) Contingencies	\$816,000	0.15 x B
Total Indirect Cost, IC	\$1,904,000	0.35 x B + Other
Total Capital Investment (TCI) = DC + IC	\$9,176,100	1.61B + SP + Bldg. + Other

**Appendix C - Total Control**  
**P4 Production, L.L.C. - Hg BACT Analysis**  
**Conceptual Control Option 2**  
**[Does not include oxidant injection (CaBr<sub>2</sub>); BACl only]**  
**Nodulizing Kiln**

Control Efficiency (%)	30.0
------------------------	------

**Annual Costs**

Item	Value	Basis	Source
<b>1) Electricity</b>			
Fan Power Requirement (kW)	1,648		
Electric Power Cost (\$/kWh)	0.043		Estimate
Cost (\$/yr)	\$620,769		
<b>2) Operating Costs</b>			
Operating Labor Requirement (hr/shift)	1	1 hour per shift	
Unit Cost (\$/hr)	\$40.00	Facility Data	Estimate
Labor Cost (\$/yr)	\$43,680		
<b>3) Steam Reheat</b>			
Temperature rise (°F)	88		
Steam requirement (klb/hr)	59		Estimate
Steam cost (\$/klb)	\$9.0	Estimated	
Total Cost	\$4,651,560		
<b>4) BAC Cost (\$/lb)</b>	\$1		
Hourly Requirement (Lbs/hour)	90	5 lb/MMacfm	
Annual requirement (Lbs/year)	788,400		Estimate
Total BAC Costs (\$/year)	\$788,400		
<b>5) Residual Disposal</b>			
Annual Quantity (TPY)	434		
Cost (\$/T)	\$200	Special Waste Assumed	Estimate
Total Disposal Cost (\$/year)	\$86,724		
<b>Total Operating Costs</b>	<b>\$6,191,133</b>		
<b>6) Supervisory Labor</b>			
Cost (\$/yr)	\$6,550	15% Operating Labor	OAQPS
<b>7) Maintenance</b>			
Maintenance Labor Req. (hr/year)	438.0		
Unit Cost (\$/hr)	\$45.00	5% Operating Hours	Estimate
Labor Cost (\$/yr)	\$19,710	Facility Data	Estimate
Material Cost (\$/yr)	\$19,710	100% of Maintenance Labor	OAQPS
Total Cost (\$/yr)	\$39,420		
<b>8) Indirect Annual Costs</b>			
Overhead	\$53,790	60% of O&M Costs	OAQPS
Administration	\$183,520	2% of Total Capital Investment	OAQPS
Property Tax	\$91,760	1% of Total Capital Investment	OAQPS
Insurance	\$91,760	1% of Total Capital Investment	OAQPS
Capital Recovery	\$1,306,470	10 yr life; 7% interest	OAQPS
Total Indirect (\$/yr)	\$1,727,300		
<b>Total Annualized Cost (\$/yr)</b>	<b>\$7,964,400</b>		
<b>Total Controlled (lb/yr), including current controls</b>	<b>347.0</b>		
<b>Cost Effectiveness (\$/lb)</b>	<b>\$23,000</b>		

**Appendix B - Incremental Control**  
**P4 Production, L.L.C. - Hg BACT Analysis**  
**Conceptual Control Option 1**  
**[Includes oxidant injection (CaBr<sub>2</sub>) and ACI]**  
**Nodulizing Kiln**

Control Efficiency (%)	50.0
------------------------	------

**Facility Input Data**

Item	Value
Operating Schedule	
Shifts per day	3
Hours per day	24
Days per week	7
Total Hours per year	8760
Economic Life, years	10
Interest Rate (%)	7
Source(s) Controlled	Nodulizer Kiln
Total Flowrate (acfm)	300,000
Hg from Kiln Operatlon (lb/hr)	0.132
Hg from Kiln Operation (lb/yr)	1,158
Site Specific Electricity Cost (\$/kWh)	0.043
Site Specific Operating Labor Cost (\$/hr)	\$45.00
Site Specific Maint. Labor Cost (\$/hr)	\$45.00

**Capital Costs**

	Value	Basis
<b>Direct Costs</b>		
1.) Purchased Equipment Cost		
a.) Equipment cost + auxiliaries	\$5,599,000	See Capital Cost Estimate, A
b.) Instrumentation	\$0	Included
c.) Sales taxes	\$0	Included
d.) Freight	\$279,950	0.05 X A
Total Purchased equipment cost, (PEC)	\$5,878,950	B
2.) Direct installation costs		
a.) Foundations and supports	\$293,900	0.10 x B
b.) Handling and erection	\$1,175,800	0.20 x B
c.) Electrical	\$58,800	0.01 x B
d.) Piping	\$58,800	0.01 x B
e.) Insulation for ductwork & painting	\$58,800	0.01 x B
f.) Slack modification	\$117,600	0.02 x B
Total direct installation cost	\$1,763,685	0.30 x B
3.) Site preparation	\$200,000	As Required, SP
4.) Buildings	NA	As Required, Bldg.
Total Direct Cost, DC	\$7,842,600	1.30B + SP + Bldg.
<b>Indirect Costs (Installation)</b>		
5.) Engineering	\$117,600	0.02 x B
6.) Construction and field expenses	\$293,900	0.05 x B
7.) Contractor fees	\$587,900	0.10 x B
8.) Start-up	\$117,600	0.02 x B
9.) Performance test	\$58,800	0.01 x B
10.) Contingencies	\$881,800	0.15 x B
Total Indirect Cost, IC	\$2,057,600	0.35 x B + Other
<b>Total Capital Investment (TCI) = DC + IC</b>	<b>\$9,900,200</b>	<b>1.61B + SP + Bldg. + Other</b>

**Annual Costs**

Item	Value	Basis	Source
<b>1) Electricity</b>			
Fan Power Requirement (kW)	1,648		
Electric Power Cost (\$/kWh)	0.043		Estimate
Cost (\$/yr)	\$620,769		
<b>2) Operating Costs</b>			
Operating Labor Requirement (hr/shift)	1	1 hour per shift	
Unit Cost (\$/hr)	\$40.00	Facility Data	Estimate
Labor Cost (\$/yr)	\$43,680		
<b>3) CaBr<sub>2</sub> Cost (\$/gal)</b>	9.00		
Hourly Requirement (gal/hour)	14	Based on CaBr <sub>2</sub> :ACI ratio of 0.15	
Annual requirement (gal/year)	118,260		Estimate
Total NaOCl Costs (\$/year)	\$1,064,340		
<b>4) Steam Reheat</b>			
Temperature rise (°F)	88		
Steam requirement (klb/hr)	59		Estimate
Steam cost (\$/klb)	\$9.0	Estimated	
Total Cost	\$4,651,560		
<b>5) AC Cost (\$/lb)</b>	\$1		
Hourly Requirement (Lbs/hour)	90	5 lb/MMacfm	
Annual requirement (Lbs/year)	788,400		Estimate
Total BAC Costs (\$/year)	\$788,400		
<b>6) Residual Disposal</b>			
Annual Quantity (TPY)	434		
Cost (\$/T)	\$200	Special Waste Assumed	Estimate
Total Disposal Cost (\$/year)	\$86,724		
<b>Total Operating Costs</b>	<b>\$7,255,473</b>		
<b>7) Supervisory Labor</b>			
Cost (\$/yr)	\$6,550	15% Operating Labor	OAQPS
<b>8) Maintenance</b>			
Maintenance Labor Req. (hr/year)	876.0	10% Operating Hours	Estimate
Unit Cost (\$/hr)	\$45.00	Facility Data	Estimate
Labor Cost (\$/yr)	\$39,420		
Material Cost (\$/yr)	\$39,420	100% of Maintenance Labor	OAQPS
Total Cost (\$/yr)	\$78,840		
<b>9) Indirect Annual Costs</b>			
Overhead	\$77,440	60% of O&M Costs	OAQPS
Administration	\$198,000	2% of Total Capital Investment	OAQPS
Property Tax	\$99,000	1% of Total Capital Investment	OAQPS
Insurance	\$99,000	1% of Total Capital Investment	OAQPS
Capital Recovery	\$1,409,570	10 yr life; 7% interest	OAQPS
Total Indirect (\$/yr)	\$1,883,010		
<b>Total Annualized Cost (\$/yr)</b>	<b>\$9,223,900</b>		
<b>Total Controlled (lb/yr), above current controls</b>	<b>174.0</b>		
<b>Cost Effectiveness (\$/lb)</b>	<b>\$53,000</b>		

**Appendix C - Incremental Control**  
**P4 Production, L.L.C. - Hg BACT Analysis**  
**Conceptual Control Option 2**  
**[Does not Include oxidant injection (CaBr<sub>2</sub>); BACI only]**  
**Nodulizing Kiln**

Control Efficiency (%)	30.0
------------------------	------

**Facility Input Data**

Item	Value
<b>Operating Schedule</b>	
Shifts per day	3
Hours per day	24
Days per week	7
Total Hours per year	8760
Economic Life, years	10
Interest Rate (%)	7
<b>Source(s) Controlled</b>	
Total Flowrate (acfm)	300,000
Hg from Kiln Operation (lb/hr)	0.132
Hg from Kiln Operation (lb/yr)	1,158
Site Specific Electricity Cost (\$/kWh)	0.043
Site Specific Operating Labor Cost (\$/hr)	\$45.00
Site Specific Maint. Labor Cost (\$/hr)	\$45.00

**Capital Costs**

	Value	Basis
<b>Direct Costs</b>		
1.) Purchased Equipment Cost		
a.) Equipment cost + auxiliaries	\$5,181,000	See Capital Cost Estimate, A
b.) Instrumentation	\$0	Included
c.) Sales taxes	\$0	Included
d.) Freight	\$259,050	0.05 X A
Total Purchased equipment cost, (PEC)	\$5,440,050	B
2.) Direct Installation costs		
a.) Foundations and supports	\$272,000	0.10 x B
b.) Handling and erection	\$1,088,000	0.20 x B
c.) Electrical	\$54,400	0.01 x B
d.) Piping	\$54,400	0.01 x B
e.) Insulation for ductwork & painting	\$54,400	0.01 x B
f.) Stack modification	\$108,800	0.02 x B
Total direct installation cost	\$1,632,015	0.30 x B
3.) Site preparation	\$200,000	As Required, SP
4.) Buildings	NA	As Required, Bldg.
Total Direct Cost, DC	\$7,272,100	1.30B + SP + Bldg.
<b>Indirect Costs (installation)</b>		
5.) Engineering	\$108,800	0.02 x B
6.) Construction and field expenses	\$272,000	0.05 x B
7.) Contractor fees	\$544,000	0.10 x B
8.) Start-up	\$108,800	0.02 x B
9.) Performance test	\$54,400	0.01 x B
10.) Contingencies	\$816,000	0.15 x B
Total Indirect Cost, IC	\$1,904,000	0.95 x B + Other
<b>Total Capital Investment (TCI) = DC + IC</b>	<b>\$9,176,100</b>	<b>1.61B + SP + Bldg. + Other</b>

**Annual Costs**

Item	Value	Basis	Source
<b>1) Electricity</b>			
Fan Power Requirement (kW)	1,648		Estimate
Electric Power Cost (\$/kWh)	0.043		
Cost (\$/yr)	\$620,769		
<b>2) Operating Costs</b>			
Operating Labor Requirement (hr/shift)	1	1 hour per shift	Estimate
Unit Cost (\$/hr)	\$40.00	Facility Data	
Labor Cost (\$/yr)	\$43,680		
<b>3) Steam Reheat</b>			
Temperature rise (°F)	88		Estimate
Steam requirement (klb/hr)	59		
Steam cost (\$/klb)	\$9.0	Estimated	
Total Cost	\$4,651,560		
<b>4) BAC Cost (\$/lb)</b>			
Hourly Requirement (Lbs/hour)	90	5 lb/MMacfm	Estimate
Annual requirement (Lbs/year)	788,400		
Total BAC Costs (\$/year)	\$788,400		
<b>5) Residual Disposal</b>			
Annual Quantity (TPY)	434		Estimate
Cost (\$/T)	\$200	Special Waste Assumed	
Total Disposal Cost (\$/year)	\$86,724		
<b>Total Operating Costs</b>	<b>\$6,191,133</b>		
<b>6) Supervisory Labor</b>			
Cost (\$/yr)	\$6,550	15% Operating Labor	OAQPS
<b>7) Maintenance</b>			
Maintenance Labor Req. (hr/year)	438.0	5% Operating Hours	Estimate
Unit Cost (\$/hr)	\$45.00	Facility Data	Estimate
Labor Cost (\$/yr)	\$19,710		
Material Cost (\$/yr)	\$19,710	100% of Maintenance Labor	OAQPS
Total Cost (\$/yr)	\$39,420		
<b>8) Indirect Annual Costs</b>			
Overhead	\$53,790	60% of O&M Costs	OAQPS
Administration	\$183,520	2% of Total Capital Investment	OAQPS
Property Tax	\$91,760	1% of Total Capital Investment	OAQPS
Insurance	\$91,760	1% of Total Capital Investment	OAQPS
Capital Recovery	\$1,306,470	10 yr life; 7% interest	OAQPS
Total Indirect (\$/yr)	\$1,727,300		
<b>Total Annualized Cost (\$/yr)</b>	<b>\$7,964,400</b>		
<b>Total Controlled (lb/yr), above current controls</b>	<b>1.0</b>		
<b>Cost Effectiveness (\$/lb)</b>	<b>\$7,964,400</b>		



# P<sub>4</sub> Production, LLC

Soda Springs Plant  
1853 Highway 34  
P.O. Box 816  
Soda Springs, Idaho 83276-0816  
Phone: (208) 547-4300  
Fax: (208) 547-3312

February 6, 2013

VIA CERTIFIED MAIL;  
RETURN RECEIPT REQUESTED – 7010 2780 0002 0464 3279

Mr. Dan Pitman, P.E.  
Department of Environmental Quality  
1410 North Hilton  
Boise, Idaho 83706

RE: Facility ID No. 029-00001, P<sub>4</sub> Production, LLC, Soda Springs  
Tier II Permit Application and Mercury Best Available Control Technology Analysis

Dear Mr. Pitman:

On December 17, 2012, you emailed P<sub>4</sub> Production, LLC (“P<sub>4</sub>”) a list of questions regarding P<sub>4</sub>’s Tier II Permit application and Mercury Best Available Control Technology (“MBACT”) Analysis. P<sub>4</sub> offers the following information in response to your inquiry:

1. **An MBACT analysis was not provided for the nodule crushing and screening operation because emissions are two orders of magnitude greater from the kiln. MBACT is triggered for all sources that emit mercury (IDAPA 58.01.01.401.02.a.ii). Since close to 3 pounds per year of mercury is estimated to be emitted from the crushing and screening operation an MBACT assessment will need to be provided for this source.**

Table 2 to the Facility Wide Potential To Emit Emission Inventory identifies all 37 point sources at the facility that, together with fugitive sources, have the potential to emit 757.07 pounds of mercury each year. The MBACT For Elemental Phosphorus Process final report (the “MBACT Analysis”) prepared by Environmental Resources Management (“ERM”) evaluates MBACT for the kiln hydrosonics, which has the potential to emit 753 lb/yr, or 99.46% of mercury emitted from the facility. In contrast, the nodule crushing and screening scrubber stack has the estimated potential to emit only 2.72 lb/yr, or 0.36% of mercury emitted from the facility, and all other sources together have the potential to emit only 1.28 lb/yr, or 0.17% of mercury emitted from the facility. If controls were installed to effectively remove 100% of all Hg air emissions from all P<sub>4</sub> emission sources except the kiln hydrosonic stacks, the total environmental impact would be negligible, the cost would be significant, and emissions from the kiln hydrosonics stacks would still exceed the 62 lb/yr threshold.

The mercury emitted from the nodule crushing and screening scrubber stack is characterized only as Hg(PM). (P4 has not collected data for gaseous Hg air emissions since P4 does not expect the process conditions to result in any mercury chemical transformation or volatilization during nodule crushing and screening.) In all cases, stack test results for the nodule crushing and screening source for Hg(PM) were below the analytical detection, so P4 conservatively estimated the emissions by using half the detection limit according to SARA guidance (refer to lines 14-18, column F, "TRI Calculations," of the enclosed emissions calculations). If P4 were to use a less conservative mass balance approach using more accurate analytical data to calculate Hg emissions from this point source, such as multiplying the total PM emissions per year from the source by the mercury concentration in nodules of 5e-8 lb Hg/lb, the potential Hg(PM) emissions would be approximately 0.0020 lb/yr, which is over three orders of magnitude lower than that used by P4 for the PTE in the MBACT Analysis. Furthermore, the trace levels of mercury contained in nodule particulate matter emitted from the nodule crushing and screening scrubber stack are not expected to pose as significant a threat to the environment as gas-phase mercury that contributes to the "global pool" and has the likelihood for deposition and uptake in flora and fauna (refer to the "Response to Question 6" submitted with P4's response dated July 23, 2012).

Considering these combined factors, P4 respectfully suggests that the contribution of mercury by emission sources other than the kiln hydrosonics is insignificant and that a MBACT evaluation for those sources, including the nodule crushing and screening scrubber stack, is unnecessary. P4 notes, however, that Table 2 does not identify emissions from the Thermal Oxidizer or flares. The Thermal Oxidizer did not come online until October 1, 2012, after the initial permit application was submitted. P4 cannot estimate with any accuracy the Hg emissions from these sources due to the limited data available. However, operation of the TO should not result in a net increase in emissions of Hg across the plant. P4 has existing plans to prepare estimates of mercury emissions from the Thermal Oxidizer in 2013 and will submit them to IDEQ as soon as they are available.

Considering these combined factors, P4 respectfully suggests that the contribution of mercury by emission sources other than the kiln hydrosonics is insignificant and that a MBACT evaluation for those sources, including the nodule crushing and screening scrubber stack, is unnecessary.

- 2. ACI and calcium bromide injection was evaluated as a technically feasible option. Additional mercury was estimated to be removed at a cost of \$53,000 per pound, including the cost of corrosion prevention measures. In addressing the conceptual control option of injecting calcium bromide prior to the existing scrubbers to increase mercury capture in the scrubbers P4 states the use of calcium bromide is technically infeasible due to temperature and corrosion issues. Please address these apparently contradictory assertions regarding the technical feasibility of injecting calcium bromide to enhance mercury oxidation.**

Control options #1 and #2 are the leading technologies on the market used to effectively remove 70 – 90% of gaseous mercury in elemental or divalent species from exhaust gas from a variety of industrial sources. In the MBACT Analysis, P4 identified certain challenges to installation of an ACI and calcium bromide injection system (control Option #1) upstream of the hydrosonics LCDA scrubbers, including mercury speciation, short residence times, the presence of compounds and ions that compete for activated carbon sites, process temperatures out of range for ACI adsorption, and the particulate recovery efficiency in the wet scrubbers. However, the MBACT Analysis also notes that "[a]n ACI or BACI system could be designed

downstream of the venturi scrubbers that would include ACI or BACI, reheating the flue gas to the target temperature and above the saturation temperature, and a baghouse or other pm removal device for carbon removal. For this reason, ACI and BACI are retained for further evaluation." These options could be installed and applied to P4's process without any need for a complete redesign of the existing kiln process, but would only offer marginal Hg control as described in detail in the MBACT evaluation and follow-up incompleteness responses dated July 27, 2012 and October 10, 2012.

To reiterate, there are no off-the-shelf mercury control technologies that are universally applicable to all industrial sources, and even with significant modification and process development P4 does not estimate that these technologies would offer efficient Hg control for the P4 kiln.

3. It is stated that the oxidation of mercury by calcium bromide injection begins to occur at 1,000 F, and continues until the gas drops below 300 F. Please provide the reference documentation for these reaction temperatures. From the process flow diagram that was provided the kiln off gas temperature drops into this range sometime after the dust bin, possibly in the boiler, and presumptively remains in this range until the spray tower. Please provide the residence time of the off gas in the temperature range of 1,000 °F to 300 °F. Please provide an estimate of the additional oxidation of mercury that would occur from adding bromine during this residence time, even if not at the optimum temperature, and provide an estimate of the increase in mercury control that would occur in the scrubbers due to the additional mercury having been oxidized. Also, since additional control is apparently achievable by oxidizing the mercury prior to the scrubbers please provide the incremental cost for this control in dollars per pound of mercury removed.

Numerous experimental and theoretical works debate the exact temperature range in which oxidation of mercury by calcium bromide occurs. For example, Chapter 5 of EPA-600/R-01-109 (see attached) provides a comprehensive summary of gas-phase oxidation of mercury species in coal fired power plant exhaust gas-and that summary states that oxidation begins to occur at 538 °C (1,000 °F). In contrast, the attached research report "Investigation of Mercury Transformation by HBr addition in a Slipstream Facility with Real Flue Gas Atmospheres of Bituminous Coal and PRB Coal," 21 Energy Fuels, 2719-2730 (2007), suggests that mercury oxidation by HBr formed from the injection of brominated species into flue gas occurs in the range between 300 °C and 700 °C. This document generally agrees with numerous reports available in peer-reviewed technical literature on the same topic. In addition, these temperature ranges were confirmed during personal communications with mercury control technology vendors (1) Gary Tonnemacher, Nalco Mobotec: November 23 and November 30, 2009 and (2) Mike Phillips, Alstom Power: December 1, 2009.

The-process flow diagram in figure 1 of the MBACT Analysis clearly indicates that the kiln off-gas temperature is in the range 450 °C (842°F) – 800 °C (1472 °F). The low end of this range corresponds to low kiln production, whereas the high end of this range corresponds to bypass of the waste heat boiler. The residence time of the gas in the temperature range where mercury oxidation occurs (up to 538 °C (1000 °F)) is estimated to be approximately 2 seconds due to the large volume of exhaust gas passing through ductwork between the kiln exit and the spray tower. The temperature of the gas in this region, typically near 600 °C (1112 °F), is not consistently below 1000 °F, and depends on steam generation for the plant since a waste heat boiler is installed in parallel to the dust bins. Even if the waste heat boiler could extract enough heat to lower the temperature to 1000 °F, the estimated residence time

between the waste heat boiler and spray tower on the order of 30 milliseconds would not allow sufficient time for bromide to contact gas phase elemental mercury and oxidize prior to the soluble halide being scrubbed in the kiln spray tower.

Since alkali halide species are not in fact chemical oxidants, some fraction of the residence time is needed for the injected halide conversion at high temperature into the corresponding halogen which then in turn must contact Hg(0) in the appropriate temperature range to drive the oxidation of Hg(0). It has been estimated that this multistep mechanism takes several seconds to occur, and longer residence times typically result in greater Hg oxidation by reducing these kinetic limitations (refer to attached document, Zhengyang, Yan Cao, et. Al., Impacts of Halogen Additions on mercury Oxidation, in a Slipstream Selective Catalyst Reduction (SCR) Reactor When Burning Sub-Bituminous Coal, Environ. Sci. Technol., 2008, 42, 256 – 261). There is also an estimated 30 to 40 tons per hour of dust in this gas stream, with numerous other gas phase species that would contribute to ineffective control by the calcium bromide injection.

The remaining issues are already addressed in the MBACT Analysis and in P4's follow-up incompleteness responses. First, control Option #2 (BACI alone) is estimated to have a total control efficiency of 30%, comparable to existing controls, while Control Option #1 (injection of calcium bromide and ACI) is estimated to have a total control efficiency of 50%, representing an increase of approximately 15% over existing controls. P4's response dated November 6, 2012, states that the potential increase in mercury control for control option #1 "might result from the presence of the halides in the system." This 15% represents the estimate of the increase in mercury control that may occur in the scrubbers due to the addition of the two control technologies in combination. Also, control Option #2 (BACI alone) is estimated to have a cost effectiveness of \$7,964,400 per pound of mercury controlled, while control Option #1 (injection of calcium bromide and ACI) is estimated to have a cost effectiveness of \$53,000 per pound of mercury controlled. This \$53,000 represents the incremental cost of this control.

- 4. Halide injection, in particular Br and Cl, in combination with the existing dual alkali scrubbers was stated to be technically infeasible, in part because a reducing environment might exist in the scrubber and cause the re-emission of elemental mercury. It was stated the chemical agents are available to prevent the re-emission of mercury but their use in the dual alkali scrubbers has not been demonstrated. Please provide the technical differences between the flue gas desulfurization (FGD) systems the additives have been demonstrated on and the FGD system that P4 utilizes which supports the elimination of the use of the additives. Were the suppliers of the chemical agents solicited regarding their use in the dual alkali system?**

Characteristic mercury re-emission across P4's hydrosonic-LCDA scrubber was identified both before and after the hydrosonic scrubbers during 2006 stack test for mercury speciation using the Ontario-Hydro method (ASTM D6784). The estimated total Hg emission rate was equivalent for both sampling points, as shown in Table 1; however, the amount of divalent Hg is lower and the amount of elemental Hg is comparably higher after the hydrosonic scrubbers.

Table 1. Results from Mercury Speciation testing Pre- and Post-Hydrosonic Scrubbers

		9 ft Diameter Duct (6.77% O <sub>2</sub> Basis)	Hydro Stack #2 (9.17% O <sub>2</sub> Basis)
Hg(PM)	Concentration (µg/M <sup>3</sup> )	62	19.4
	Emission Rate (lb/hr)	0.028	0.0019
	%	21.2	5.9
Hg(II)	Concentration (µg/M <sup>3</sup> )	47	4.8
	Emission Rate (lb/hr)	0.021	0.00047
	%	15.9	1.5
Hg(0)	Concentration (µg/M <sup>3</sup> )	184	305
	Emission Rate (lb/hr)	0.083	0.0298
	%	62.9	92.6
Total	Concentration (µg/M <sup>3</sup> )	293	329
	Emission Rate (lb/hr)	0.132	0.032

Note that there are four hydrosonic stacks, and emissions from hydrosonic stack #2 are generally considered representative of emissions from each stack. Divalent mercury reduction from Hg(II) to Hg(0) is common for wet FGD processes. In P4's process, P4 believes that Hg(II) is reduced and re-emitted as gaseous Hg(0) as it passes through the concentrated dual alkali scrubbing liquor in the hydrosonic scrubbers. Approximately 165 lb/yr Hg(II) is converted into Hg(0) as it passes through the hydrosonic scrubbers.

A paucity of information is available regarding the demonstration of FGD additives to reduce Hg(0) re-emission at lab, pilot, or full scale. Available reports provide little information regarding the type of FGD system, and references to Hg concentrations in the salable Gypsum produced indicate that FGD has not been demonstrated on LCDA-type systems because such systems produce a calcium sulfate/sulfite mixture. The FGD systems discussed in the reports are likely used for basic wet limestone scrubbing processes, which are used most widely for SO<sub>2</sub> emission control at coal-fired electric utility boilers. In general, dual alkali systems are used by a very small percentage of the total number of FGD systems due to the high cost of caustic usage. For more information on additives to reduce Hg re-emission across FGD, refer to the attached report (Gary Blythe, URS Corporation, Field Testing of an FGD Additive for Enhanced Mercury Control; Steven A. Benson et al., Large-Scale Mercury Control Technology Testing for Lignite-Fired Utilities – Oxidation Systems for Wet FGD).

Monsanto cannot accurately provide any comprehensive information on the types of FGD systems available because the mercury re-emission controls that have been installed are proprietary confidential business information between the actual process vendors, engineering firms, and process owners, and the request seeks information well outside of the scope of P4's business and this MBACT application. However, for a general description of the types of FGD systems, refer to chapter 15 of "Air Pollution Control: A Design Approach," David A. Cooper (Waveland Press Inc., 2002).

P4 has contacted both Nalco and B&W to discuss the use of FGD additives to prevent Hg re-emission with the existing dual alkali scrubbers. P4 has not yet received a response from either supplier.

- Application materials state that the nodulizing process does not offer the temperature or contact time required for sodium hypochlorite injection to oxidize mercury. Please

provide documentation on the necessary reaction temperature range. If the nodulizing kiln off gas is within this temperature range please provide an estimate of: the residence time at these temperatures; the additional oxidation of mercury that would occur from the addition of sodium hypochlorite (even if not at the optimum temperature); and an estimate of the increase in mercury control that would occur in the scrubbers due to the additional mercury having been oxidized. Also, if additional control is achievable provide the incremental cost for this control in dollars per pound of mercury removed.

The reaction temperature range for sodium hypochlorite injection to oxidize mercury is 95 – 100 °C, as reported in the attached EPA report. (See Nick D. Hutson & John C.S. Chang, Pilot-Scale Study of a Wet Scrubber System for Control of SO<sub>2</sub>, NO<sub>x</sub>, and Hg in Coal Combustion Flue Gas, Paper #47, page 8.) The nodulizing kiln off gas is not within this temperature range, as described in response #3.

Also, the injection of sodium hypochlorite is not an available mercury control technology, and to the best of P4's knowledge it has not been demonstrated at any scale or process conditions comparable to the P4 kiln beyond the laboratory ideal exhaust gas conditions. For this reason, P4 contends that this technology is outside the scope of the MBACT evaluation. To reiterate, the assessment of this technology provided by P4 in the response dated October 10, 2012, the residence time required for oxidation by sodium hypochlorite would be analogous to that needed for mercury oxidation by halide injection, and the limiting factor in the P4 kiln exhaust would be the thermodynamics and kinetics of mercury oxidation. The appropriate physical and chemical conditions simply do not exist to allow hypochlorite or any other halogenated species to oxidize mercury.

No cost estimate has been prepared by P4 for this technology since it does not fit the definition for MBACT. P4 mentioned the use of sodium hypochlorite because this control was proposed by the EPA Office of Research and Development on February 10, 2011 (EPA attendees: Susan Fairchild, Nick Hutson, Mike Thrift, Peter Westlin, Barrett Parker) in discussions that resulted in the EPA agreeing that there are no available mercury control technologies, whether fully developed or not, that offer compatibility with the P4 kiln process. Refer to P4's July 23, 2012 response #2 and October 10, 2012 response #3.

6. The ability of ACI and BACI to control mercury emissions is stated to be adversely affected by the presence of constituents (Cd, Zn, SO<sub>3</sub>, etc.) that occur at concentrations much greater than mercury. This is stated to be the case whether carbon is injected before or after the scrubbers. Please provide the concentrations of these constituents that compete for AC and BAC in the exhaust gas before and after the scrubbers. Please document how these concentrations were determined. Also provide the documentation that AC and BAC have an affinity for these constituents that is equal to or greater than that of mercury. Do these concentrations, before and after the scrubber, alone preclude the use of ACI and BACI?

Activated carbon ("AC") is a universal sorbent with many forms available for the removal of a myriad of impurities in water and flue gas streams. According to the provided documentation, AC has an affinity for the absorption of moisture, Cd, As, Cr, other heavy metals and common species present in flue gas streams (i.e., SO<sub>2</sub>, NO<sub>x</sub>, PM, dioxins, VOCs, etc.). (Anthony A. Lizzio, Joseph A. DeBarr, and Carl W. Kruse, Production of Activated Char from Illinois Coal for Flue Gas Cleanup, 11 Energy & Fuels 250-259 (1997), p. 250; Zhen Shu Liu, Control of Heavy Metals During Incineration Using Activated Carbon Fibers (2006), p. 506 - 511; Jacobi Carbons, Activated Carbon for Flue Gas Purification; APTI 415:

Control of Gaseous Emission, Chapter 4: Adsorption, p. 4-3, 4-30.) Any AC manufacturer can be contacted to confirm this.

The relative quantities of these constituents before and after the scrubbers are shown in Table 1. There is no direct measurement of species in the stream before the scrubbers, so material balances were used to estimate the relative quantities of these species. It is notable that the estimated quantities of these species present in the process before the scrubbers are four orders of magnitude larger than the kiln's potential to emit Hg.

High levels of SO<sub>2</sub> are known to significantly inhibit Hg capture by ACI and BACI in utility boilers, as referred to in the attached report (Presto, Alberta A., Impact of Sulfur Oxides on Mercury Capture by Activated Carbon, Environ. Sci. Technol., 41, 6579 – 6584 (2007)). Prior to the spray tower and LCDA system it has been estimated that SO<sub>2</sub> is present in excess of 2800 lb/hr (~22M lb/yr), which would contribute to the interference with Hg capture.

The gas stream before and after the scrubbers also contains elevated levels of moisture that has been documented in the attached report to inhibit mercury removal from gas (Li, Y. H., et. al., The effect of Activated Carbon Surface Moisture on Low Temperature Mercury Adsorption, Carbon, 40, 2002, p 65 – 72). Kiln CFD modeling indicates 12% moisture in the gas stream at the exit of the kiln, and stack test results after the spray tower and at the hydrosonic stack are saturated with 35% moisture at 154 °F (i.e., upstream and downstream from the hydrosonics). These high concentrations of moisture relative to Hg would render the ACI inefficient in Hg removal.

**Table 1. Annual Metal Quantities Estimated Before and After Scrubbers in lb/yr.**

	Cd	Zn	As	Cu	Pb	Se	Ni	Sb	Cr
<b>Before Scrubbers (lb/yr)</b>	627,276	7,417,188	111,056	239,359	89,124	127,591	30,3258	30,122	1,377,707
<b>After Scrubbers (lb/yr)</b>	7640	2.54	519	70.6	343	2630	585	186	573

Therefore, the quantities of competing constituents before and after the scrubbers support the elimination of ACI or BACI since neither control option has been demonstrated under P4's process conditions. The Hg removal efficiency and the cost estimates provided for the use of these control options in P4's MBACT Analysis was likely extremely conservative considering the excessive quantity of ACI or BACI that would be required to capture low levels of mercury in the midst of high levels of these other species. P4 is not able to assess the preferential selective adsorption of any of these species based on information available.

Also, note that another critical factor in ACI or BACI adsorption is the large quantity of moisture in the gas streams before and after the scrubbers that will compete with active sites for mercury adsorption or oxidation/adsorption, respectively.

- 7. If the concentration of exhaust gas constituents that exist before the scrubbers does not completely eliminate the use of ACI or BACI prior to the scrubbers please address the following -In asserting that carbon injection prior to the scrubbers is technically infeasible it is stated that it is unclear whether the existing venturi scrubbers can handle**

the additional loading of ACI or BACI. Please provide an estimate of the current particulate matter loading to the scrubbers and an estimate of the additional loading that would occur from the addition of ACI or BACI. Also please provide an estimate of the particle size of ACI and BACI and an engineering estimate of the removal efficiency of these particles in the venturi scrubbers.

It is also stated that the carbon particles would add an abrasive particle to the venturi throat and cause erosion of the throat. Please provide the current particle loading rate and the estimate of the incremental increase of loading provided by ACI or BACI. Also, please provide an estimate of the increase of the rate of the corrosion of the venturi throats due to the addition of ACI or BACI.

The excessively high concentration of exhaust gas constituents before the scrubbers that would interfere with relatively low levels of mercury adsorption as detailed in response #6, coupled with the exceedingly short residence time between the spray tower and hydrosonic scrubbers, make the utilization of ACI or BACI prior to the scrubbers technically infeasible for P4's purposes.

8. If the concentration of exhaust gas constituents that exist before the scrubbers does not completely eliminate the use of ACI or BACI prior to the scrubbers please address the following -It is stated that ACI or BACI prior to the scrubbers would be out of the optimum temperature range (200 °F – 400 °F) for capturing mercury. Please provide the documentation for this temperature range. Also, please provide a technical argument why a marginally lower exhaust gas temperature (~160 F) warrants supporting the elimination of ACI or BACI as infeasible.

As stated in responses #6 and #7, the concentration of exhaust gas constituents coupled with the short residence time before the scrubbers does completely eliminate the use of ACI or BACI prior to the scrubbers.

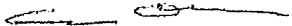
9. All control technologies evaluated are technology transfers that have not been demonstrated on off gases from nodulizing kilns. It is stated no vendor, engineer, or contractor would offer a guarantee of performance for these systems. To provide more support to the application please provide a listing of the sources that were solicited for a guarantee.

This statement is based on ERM's extensive experience in the evaluation, installation, and operation of mercury control technologies. Mercury control systems are designed based on on-site pre-engineering and pilot-scale studies, and there is no "off-the-shelf" technology for mercury control for industrial scale systems. Pre-engineering studies provide the designer information necessary to provide a performance guarantee and OEM costs, and this information is unavailable here because no pilot-scale study or formal pre-engineering study for mercury control has been completed for any phosphate kiln.

However, P4 did contact several vendors to discuss MBACT controls for P4's key process conditions. Alstom representatives would not speculate on the suitability of their Mer-Cure technology for this application (Jeff Edwards, Alstom Power: October 23, 2009). Also, a representative of Novinda speculated that control technology using amended silicates might still be effective at 160° F, although it has only been tested around 300° F. He also expressed concern that the increase in gas viscosity resulting from sorbent injection could impair the function of the venturi scrubbers (Bill Byers, Novinda Corporation: 2/15/2010).

In accordance with IDAPA 58.01.01.123, I certify based on information and belief formed after reasonable inquiry, that the statements and information in this document are true, accurate, and complete. If you have any questions regarding this submittal, please contact Mr. Jim McCulloch at (208) 547-1233.

Sincerely,



Sheldon Alver  
Vice President, Operations

Enclosures



## Chapter 5

### Mercury Speciation and Capture

#### 5.1 Introduction

The source of Hg emissions from coal-fired electric utility boilers is the Hg that naturally exists in coal and is released during the combustion process. As discussed in Chapter 2, the Hg content of a coal varies by coal type and where it is mined. When the coal is burned in an electric utility boiler, most of the Hg bound in the coal is released into the combustion product gases. This chapter provides an introduction to Hg chemistry and behavior of Hg as it leaves the combustion zone of the furnace and passes in the flue gas through the downstream boiler sections, air heater, and air pollution control devices. Recent research on Hg chemistry in coal-fired electric utility boiler flue gas is summarized.

#### 5.2 General Behavior of Mercury in Coal-fired Electric Utility Boilers

The majority of Hg in coal exists as sulfur-bound compounds and compounds associated with the organic fraction in coal. Small amounts of elemental Hg may also be present in the coal. Figure 5-1 presents a simplified schematic of the coal combustion process. The primary products of coal combustion are carbon dioxide (CO<sub>2</sub>) and water (H<sub>2</sub>O). In addition, as discussed in Chapter 3, significant quantities of the pollutants sulfur dioxide (SO<sub>2</sub>) and nitrogen oxides (NO<sub>x</sub>) are also formed. When the coal is burned in an electric utility boiler, the resulting high combustion temperatures in the vicinity of 1,500 °C (2,700 °F) vaporize the Hg in the coal to form gaseous elemental Hg. Subsequent cooling of the combustion gases and interaction of the gaseous elemental Hg with other combustion products result in a portion of the Hg being converted to other forms.

There are three basic forms of Hg in the flue gas from a coal-fired electric utility boiler: (1) elemental Hg (represented by the symbol Hg<sup>0</sup> in this report); (2) compounds of oxidized Hg (collectively represented by the symbol Hg<sup>2+</sup> in this report); and (3) particle-bound mercury (represented by the symbol Hg<sub>p</sub> in this report). Oxidized mercury compounds in the flue gas from a coal-fired electric utility boiler may include mercury chloride (HgCl<sub>2</sub>), mercury oxide (HgO), and mercury sulfate (HgSO<sub>4</sub>). Some researchers refer to oxidized mercury compounds collectively as *ionic mercury*. This is because, while oxidized mercury compounds may not exist as mercuric ions in the boiler flue gas, these compounds are measured as ionic mercury by the

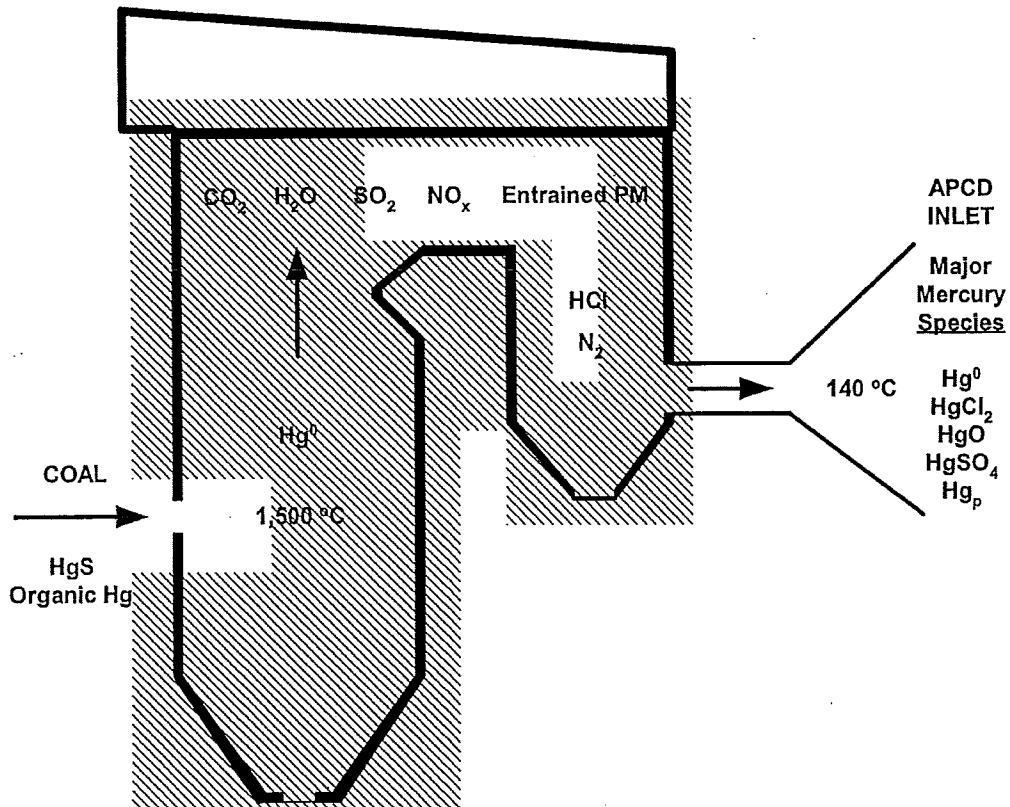


Figure 5-1. Mercury species distribution in coal-fired electric utility boiler flue gas.

speciation test method used to measure oxidized Hg (discussed in Chapter 4). Similarly, particle-bound Hg is referred to as *particulate mercury* by some researchers. The term *particle-bound mercury* is the preferred and is used in this report to emphasize that the mercury is bound to a solid particle.

The term *speciation* is used to denote the relative amounts of these three forms of Hg in the flue gas of the boiler. At present, speciation of Hg in the flue gas from a coal-fired electric utility is not well understood. A number of laboratory and field studies have been conducted, or are ongoing, to improve the understanding of the transformation of  $\text{Hg}^0$  to the other Hg forms in the flue gas downstream of the boiler furnace. Data obtained to date indicate that combinations of site-specific factors affect the speciation of Hg in the flue gas. These factors include:

- Type and properties of the coal burned.
- Combustion conditions in the boiler furnace.
- Boiler flue gas temperature profile.
- Boiler flue gas composition.
- Boiler fly ash properties.
- Post-combustion flue gas cleaning technologies used.

The current understanding of the mechanisms by which  $\text{Hg}^0$  transforms to  $\text{Hg}^{2+}$  and  $\text{Hg}_p$  in the flue gas from coal-fired electric utility boilers is discussed in subsequent sections of this chapter. It is important to understand how Hg speciates in the boiler flue gas because the overall effectiveness of different control strategies for capturing Hg often depends on the concentrations of the different forms of Hg present in the boiler flue gas. This topic will be discussed in detail in Chapters 6 and 7.

### 5.3 Speciation of Mercury

As mentioned above, high temperatures generated by combustion in the boiler furnace vaporize Hg in the coal. The resulting gaseous  $\text{Hg}^0$  exiting the furnace combustion zone can undergo subsequent oxidation in the flue gas by several mechanisms. The predominant oxidized Hg species in boiler flue gases is believed to be  $\text{HgCl}_2$ . Other possible oxidized species may include  $\text{HgO}$ ,  $\text{HgSO}_4$ , and mercuric nitrate monohydrate  $\text{Hg}(\text{NO}_3)_2 \cdot \text{H}_2\text{O}$ . The potential mechanisms for oxidation of  $\text{Hg}^0$  in the boiler flue gas include:

- Gas-phase oxidation.
- Fly ash mediated oxidation.
- Oxidation by post-combustion  $\text{NO}_x$  controls.

Each of these oxidation mechanisms is discussed in the following sections.

### 5.3.1 Gas-phase Oxidation

As mentioned above, Hg in coal is believed to completely vaporize and convert into gaseous  $\text{Hg}^0$  in the combustion zone of a boiler system. As gaseous  $\text{Hg}^0$  travels with the flue gas in the boiler, it can undergo gas-phase oxidation to form gaseous  $\text{Hg}^{2+}$ , most of which is believed to be  $\text{HgCl}_2$ . Recent research<sup>1</sup> has speculated that the major gas-phase reaction pathway to form gaseous  $\text{HgCl}_2$  is the reaction of gaseous  $\text{Hg}^0$  with gaseous atomic chlorine (Cl). The latter is formed when chlorine in coal vaporizes during combustion.

At the furnace exit, the temperature of the flue gas is typically in the vicinity of 1400 °C (2552 °F). The flue gas cools as it passes through the heat exchanging equipment in the post-combustion region. At the outlet of the air heater (the last section of heat exchanging equipment), the temperature of the flue gas ranges from 127 to 327 °C (261 to 621°F). Chemical equilibrium calculations predict that gas-phase oxidation of  $\text{Hg}^0$  to  $\text{Hg}^{2+}$  starts at about 677 °C (1251 °F) and is essentially complete by 427 °C (801 °F). Based on these results, Hg should exist entirely as  $\text{Hg}^{2+}$  downstream of the air heater. However, flue-gas measurements of Hg at air heater outlets indicate that gaseous  $\text{Hg}^0$  is still present at this location, and that  $\text{Hg}^{2+}$  ranges from 5 to 95 percent of the gas-phase Hg. These data suggest that, due to kinetic limitations, the oxidation of  $\text{Hg}^0$  does not reach completion.

As mentioned previously, gas-phase oxidation of  $\text{Hg}^0$  is believed to take place via reaction with gaseous Cl. At furnace flame temperatures, a major portion of the chlorine in the coal exists as gaseous chlorine atoms, but as gas cools in post-combustion, the chlorine atoms combine to form primarily hydrogen chloride (HCl) and minor amounts of molecular chlorine ( $\text{Cl}_2$ ). The rapid decrease in Cl concentration results in "quenched"  $\text{Hg}^{2+}$  concentrations corresponding to equilibrium values around 527 °C (981 °F).

Figures 5-2 and 5-3 show predicted distributions of Hg species in coal-fired electric utility flue gas as a function of flue gas temperature. The predicted distributions are based on equilibrium calculations of gas-phase oxidation of  $\text{Hg}^0$  in flue gas from the combustion of a bituminous coal<sup>1</sup> and a subbituminous coal<sup>2</sup>, respectively. Figure 5-2 shows that 80 percent of gaseous  $\text{Hg}^0$  is oxidized to  $\text{HgCl}_2$  by 527 °C (981°F). Figure 5-3 indicates no oxidation of  $\text{Hg}^0$  at or above 527 °C (981°F). As mentioned above, the gas-phase oxidation of  $\text{Hg}^0$  is believed to be kinetically limited, proceeding only to equilibrium levels around 527 °C (981 °F).

The difference in the equilibrium oxidation levels at 527 °C (800 K) in Figures 5-2 and 5-3 is attributed to the different chlorine levels in the model coals used in the calculations. The calculated data in Figure 5-2 are based on a bituminous coal with a relatively high chlorine concentration of several hundred parts per million by weight (ppmw). In contrast, the calculated data in Figure 5-3 are based on a typical western subbituminous coal with a relatively low chlorine content of 26 ppmw. Research indicates that coals with relatively high chlorine contents tend to produce more  $\text{Hg}^{2+}$  than coals with relatively low chlorine contents.<sup>3</sup>

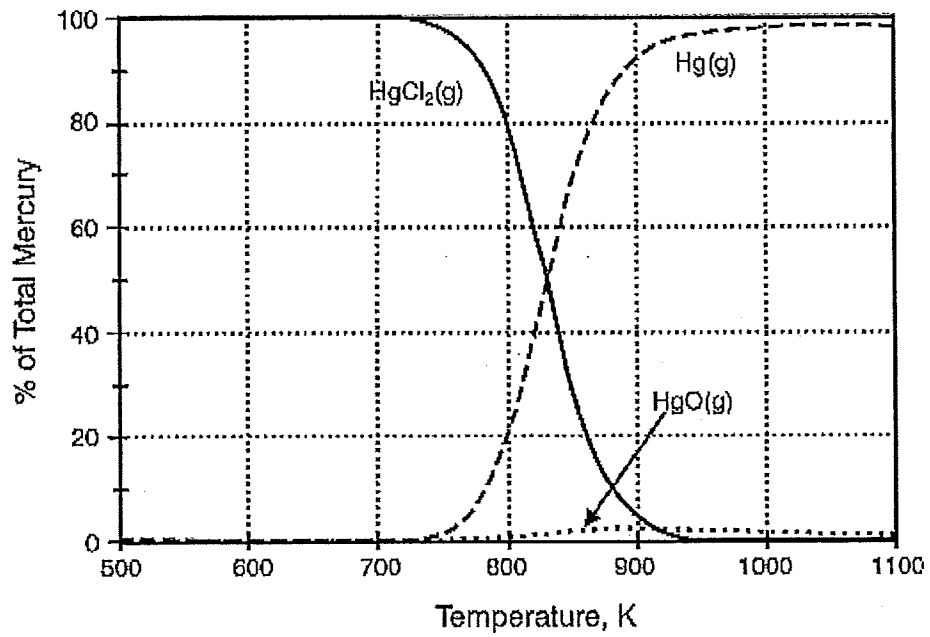


Figure 5-2. Predicted distribution of Hg species at equilibrium, as a function of temperature for a starting composition corresponding to combustion of a bituminous coal (Pittsburgh) in air at a stoichiometric ratio of 1.2 (source: Reference 2).

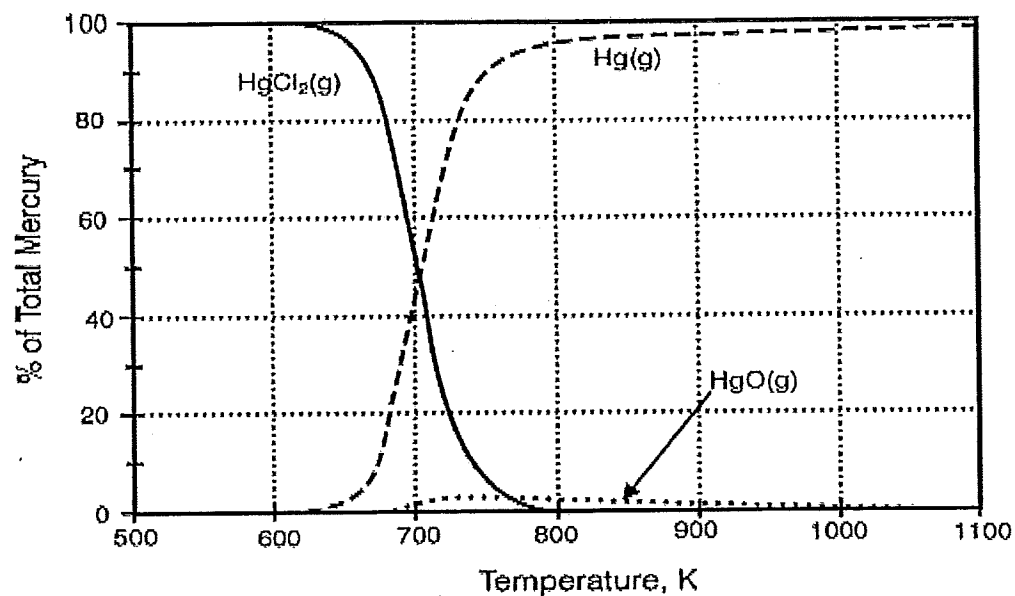


Figure 5-3. Predicted distribution of Hg species at equilibrium, as a function of temperature for a starting composition corresponding to combustion of a subbituminous coal (Powder River Basin) in air at a stoichiometric ratio of 1.2 (source: Reference 2).

In addition to being kinetically limited by Cl concentration, recent research conducted at EPA has found that gas-phase oxidation of  $\text{Hg}^0$  is also inhibited by the presence of  $\text{SO}_2$  and water vapor.<sup>4</sup> As shown in Figure 5-1,  $\text{SO}_2$  and water vapor are constituents in the flue gas from coal-fired electric utility boilers. Figure 5-4 shows results from bench-scale experiments examining the effects of  $\text{SO}_2$  and water vapor on the oxidation of gaseous  $\text{Hg}^0$ . These experiments were carried out using a simulated flue gas containing a base composition of 40 parts per million by volume (ppmv)  $\text{Hg}^0$ , 5 mole % carbon dioxide ( $\text{CO}_2$ ), 2 mole % oxygen ( $\text{O}_2$ ), and a balance of nitrogen ( $\text{N}_2$ ); the temperature of the flue gas was 754 °C (1,389 °F). The effects of  $\text{SO}_2$ , water vapor, and HCl were studied by adding these constituents to the base flue gas. HCl was added to the simulated flue gas at three concentrations typical of coal combustion flue gas (50, 100, and 200 ppmv);  $\text{SO}_2$  and water vapor were added with the HCl at 500 ppmv and 1.7 mole %, respectively.

As shown in Figure 5-4, the oxidation of  $\text{Hg}^0$  was inhibited by the presence of  $\text{SO}_2$  and water vapor. HCl is not believed to react directly with  $\text{Hg}^0$  to cause its oxidation (a chlorinating agent such as atomic chlorine or  $\text{Cl}_2$  is needed). HCl may produce trace quantities of the chlorinating agent in the flue gas. It is speculated that  $\text{SO}_2$  and water vapor may inhibit gas-phase oxidation of  $\text{Hg}^0$  by scavenging the chlorinating agent.

In addition to experimental studies, research has also been reported on the development of a kinetic model that is used to better understand the reaction mechanism involved in gas-phase Hg oxidation. A detailed chemical kinetics model using a chemical mechanism consisting of 60 reactions and 21 chemical species was developed recently to predict Hg speciation in combustion flue gas.<sup>5</sup> The speciation model accounts for the chlorination and oxidation of key flue gas components, including  $\text{Hg}^0$ . The performance of the model is very sensitive to temperature. For low reaction temperatures (< 630 °C), the model produced only trace amounts of Cl and  $\text{Cl}_2$  from HCl, leading to a drastic under-prediction of Hg chlorination compared with experimental data. For higher reaction temperatures, model predictions were in good accord with experimental data. For conditions that produce an excess of Cl and  $\text{Cl}_2$  relative to Hg, chlorination of Hg is determined by the competing influences of the initiation step,  $\text{Hg} + \text{Cl} \rightarrow \text{HgCl}$ , and the recombination reaction,  $2\text{Cl} \rightarrow \text{Cl}_2$ . If the Cl recombination is faster, Hg chlorination will eventually be determined by the slower pathway  $\text{Hg} + \text{Cl}_2 \rightarrow \text{HgCl}_2$ .

Another attempt has been made to formulate an elementary reaction mechanism for gas-phase Hg oxidation.<sup>6</sup> The proposed eight-step Hg oxidation mechanism quantitatively describes the reported extents of Hg oxidation for broad ranges of HCl and temperature. In the proposed mechanism, Hg is oxidized by a Cl atom recycle process, and, therefore, the concentrations of both Cl and  $\text{Cl}_2$  are important. Once a pool of Cl atoms is established,  $\text{Hg}^0$  is first oxidized by Cl into  $\text{HgCl}$ , which, in turn, is oxidized by  $\text{Cl}_2$  into  $\text{HgCl}_2$ . The second step regenerates Cl atoms. Since the concentrations of Hg species are small in coal combustion flue gases, independent reactions establish and sustain the pool of Cl atoms. The pool is governed by the chemistries of moist CO oxidation, Cl species transformations, and nitrogen oxide (NO) production. The model predictions show that  $\text{O}_2$  weakly promotes homogeneous Hg oxidation, whereas moisture is a strong inhibitor as it inhibits the decomposition of HCl to  $\text{Cl}_2$ . NO was identified as an effective inhibitor for  $\text{Hg}^0$  oxidation through its effect on reducing the concentration of hydroxyl (OH)

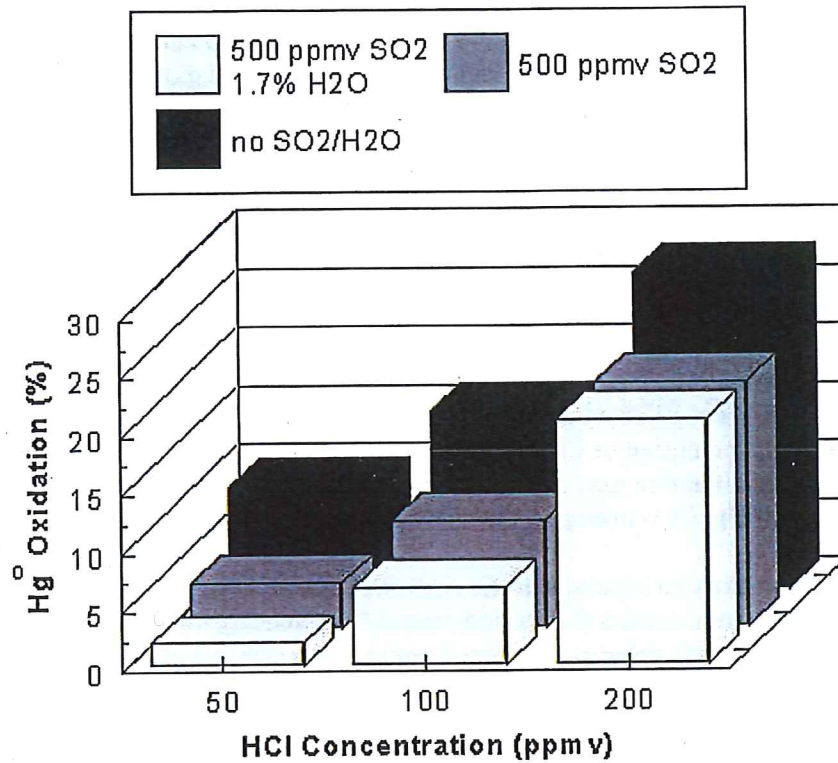


Figure 5-4. Effects of SO<sub>2</sub> and water vapor on the gas-phase oxidation of Hg<sup>0</sup> at 754 °C and at three different HCl concentrations.

in the flue gas. The formation of HOCl from OH and Cl is essential for the oxidation of Hg, which oxidizes HgCl into HgCl<sub>2</sub> and OH. The elimination of OH via OH+NO+M = HONO+M is believed to inhibit Hg<sup>0</sup> oxidation.

### 5.3.2 Fly Ash Mediated Oxidation

In fabric filtration, flue gas penetrates a layer of fly ash as it passes through the filtering unit. The intimate contact between the flue gas and the fly ash on the filter provides an opportunity for the latter to oxidize some of the incoming gaseous Hg<sup>0</sup>. However, this phenomenon does not occur across ESPs because the flue gas does not pass through a collected layer of fly ash (see Chapter 3 for a description of the operation of FFs and ESPs).

Certain fly ashes have been shown to promote oxidation of Hg<sup>0</sup> across a FF more actively than others. For example, fly ashes from bituminous coals tend to oxidize Hg<sup>0</sup> at higher rates than fly ashes from subbituminous coals and lignite. Differences in oxidation appear to be attributable to the composition of the fly ash, the presence of certain flue gas constituents, and the operating conditions of FFs.

Bench-scale tests were conducted at EPA to investigate the effects of fly ash composition and flue gas parameters on the oxidation of gaseous Hg<sup>0</sup>.<sup>4,7</sup> In these experiments, a simulated flue gas containing Hg<sup>0</sup> (and other species) was passed through a fixed bed of simulated or actual coal fly ash, and oxidation of Hg<sup>0</sup> was measured across the reactor. Experimental results indicated two possible reaction pathways for fly-ash-mediated oxidation of Hg<sup>0</sup>. One possible pathway is the oxidation of gaseous Hg<sup>0</sup> by fly ash in the presence of HCl, and the other is the oxidation of gaseous Hg<sup>0</sup> by fly ash in the presence of NO<sub>x</sub>. The research also reflected that the iron content of the ash appeared to play a key role in oxidation of Hg<sup>0</sup>. This EPA research is described in the ensuing paragraphs.

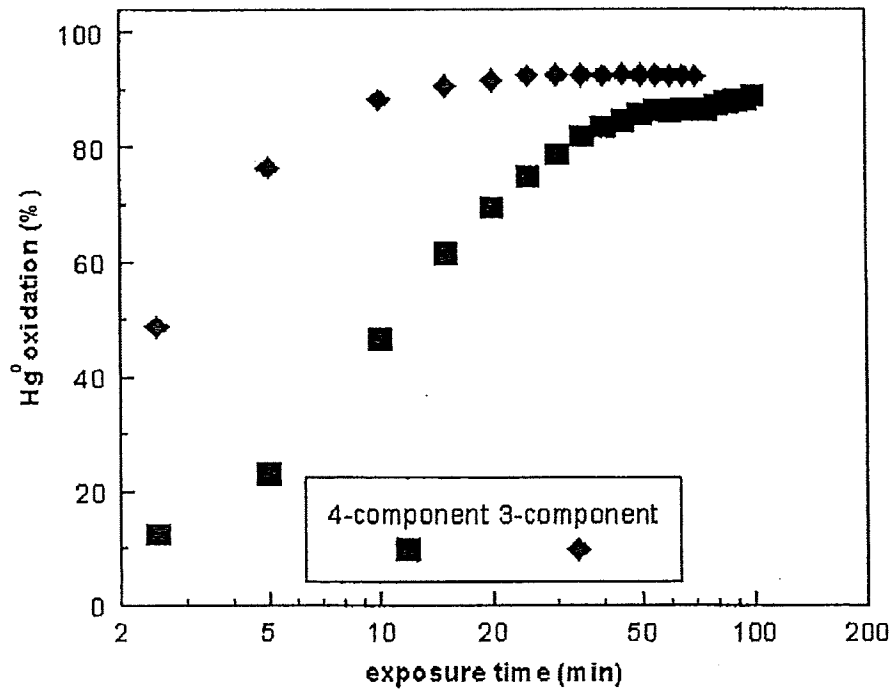
Coal fly ash is a mixture of metal oxides found in both crystalline and amorphous forms. Glasses are common ash constituents, composed primarily of the oxides of silicon and aluminum (known as aluminosilicate glasses) that can contain a significant amount of cations such as iron, sodium, potassium, calcium, and magnesium. Iron oxide (in the form of magnetite or hematite) is also as commonly found in ash as calcium oxide and calcium sulfate. In the presence of sufficiently high flue-gas concentrations of HCl or Cl<sub>2</sub>, metallic oxides in fly ash may be converted to metal chlorides such as cuprous chloride (CuCl). Three-component model fly ashes were prepared by adding Fe<sub>2</sub>O<sub>3</sub> or CuO at various weights to a base mixture of Al<sub>2</sub>O<sub>3</sub> and SiO<sub>2</sub>. An additional three-component fly ash was prepared by adding CuCl to a base mixture of Al<sub>2</sub>O<sub>3</sub> and SiO<sub>2</sub>. Municipal waste combustion fly ashes contain significant amounts of copper compared to coal combustion fly ashes that contain only trace levels of copper. Model fly ashes were prepared and tested in order to understand the effect of differences in copper content on the oxidation of Hg<sup>0</sup>. Four-component fly ashes were prepared by adding various weights of CaO, and Fe<sub>2</sub>O<sub>3</sub> or CuO to a base mixture of Al<sub>2</sub>O<sub>3</sub> and SiO<sub>2</sub>. Actual coal fly ashes were obtained from the combustion of three different coals (two subbituminous and one bituminous) from a pilot-size, pulverized-coal-fired furnace.

Model flue gas compositions were simulated to represent the temperature and composition of coal-fired electric utility flue gas as it enters a FF. The temperature of coal combustion flue gas as it enters a FF typically ranges from 150 °C (302 °F) to 250 °C (482 °F). Potentially important flue gas species (in terms of Hg<sup>0</sup> oxidation) include chlorine (primarily in the form of HCl at FF temperatures), NO<sub>x</sub> (primarily in the form of NO at FF temperatures), SO<sub>2</sub>, and water vapor. The base flue gas consisted of 40 ppbv Hg<sup>0</sup>, 2 mole % O<sub>2</sub>, 5 mole % CO<sub>2</sub>, and the balance N<sub>2</sub> at a temperature of 250 °C (482 °F). HCl (50 ppmv), NO (200 ppmv), SO<sub>2</sub> (500 ppmv), and/or water vapor (1.7 mole %) were added to the base gas to determine their effect on oxidation. About 10 percent of NO<sub>2</sub> (10 ppmv) was measured when 200 ppmv of NO was added to the base flue gas which contains 2 mole % of O<sub>2</sub>. The mixture of NO and NO<sub>2</sub> in flue gas is referred to collectively as NO<sub>x</sub>. Table 5-1 shows the simulated and actual fly ashes and simulated flue gas tested.

*Oxidation Behavior of Model Fly Ashes.* HCl and NO<sub>x</sub> were identified as the active components in flue gases for the oxidation of Hg<sup>0</sup>. NO<sub>x</sub> were more active than HCl. Cupric oxide (CuO) and ferric oxide (Fe<sub>2</sub>O<sub>3</sub>) were identified as the active components in model fly ashes for Hg<sup>0</sup> oxidation. In the presence of NO<sub>x</sub>, inert components of model fly ashes such as alumina (Al<sub>2</sub>O<sub>3</sub>) and silica (SiO<sub>2</sub>) appeared to become active in oxidation of Hg<sup>0</sup>. Steady-state oxidation of Hg<sup>0</sup> promoted by the four-component model fly ashes (containing calcium oxide, CaO) was reached at much slower rates compared to those obtained using the three-component model fly ashes that contained no CaO (Figures 5-5 and 5-6). The partial removal of gas-phase HCl by CaO in the CaO-containing model fly ashes may have reduced the available chlorinating agent and resulted in slower oxidation of Hg<sup>0</sup>.

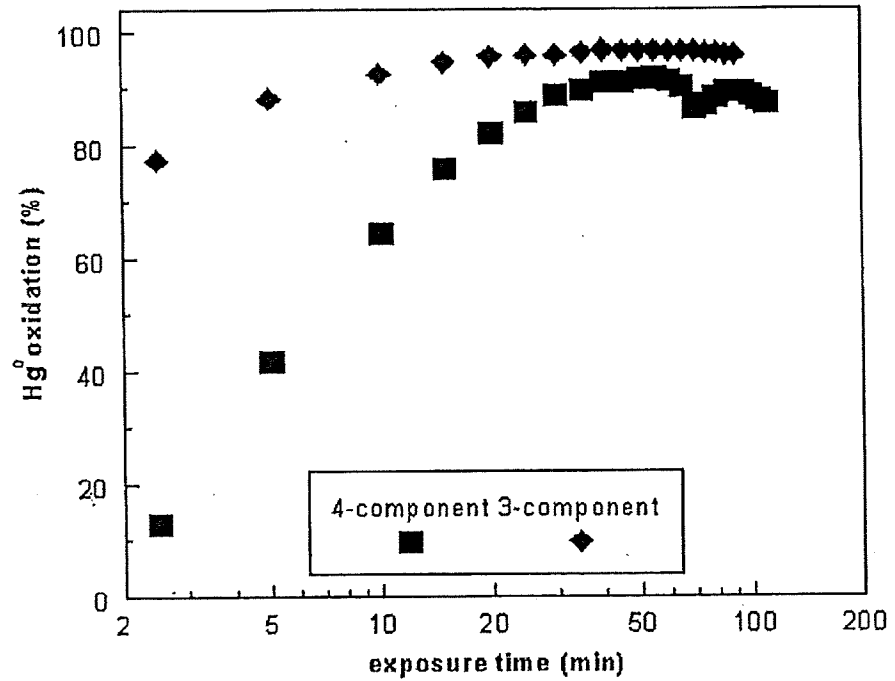
*Oxidation Behavior of Actual Coal Fly Ashes.* As shown in Table 5-1, the Blacksville fly ash (derived from a bituminous coal) completely oxidized Hg<sup>0</sup> in the presence of NO (base + NO), but showed little oxidation in the presence of HCl (base + HCl).<sup>7</sup> The Comanche fly ash (derived from a subbituminous coal) did not oxidize Hg<sup>0</sup> in the presence of NO or HCl. The Absaloka coal (derived from a subbituminous coal) showed 30 to 35 percent oxidation of Hg<sup>0</sup> in the presence of NO, but no oxidation in the presence of HCl. It is believed that the high reactivity of the Blacksville coal in NO is related to its relatively high Fe<sub>2</sub>O<sub>3</sub> concentration (22 percent); this observation is in agreement to that seen for the high iron (approximately 14 percent) three- and four-component model fly ashes.

More tests were conducted recently at EPA on actual fly ash samples with different coal ranks and iron contents in order to get a better understanding of the effects of iron in coal fly ashes on speciation of Hg.<sup>8</sup> It was observed that one subbituminous (3.7 percent iron) and three lignite coal fly ash (1.5 to 5.0 percent iron) samples tested with low iron content did not oxidize Hg<sup>0</sup> in the presence of NO and HCl. However, a bituminous coal fly ash sample (Valmont Station) with a low iron content (2.3 percent iron) completely oxidized Hg<sup>0</sup> in the presence of NO and HCl. It was also found that, upon adding Fe<sub>2</sub>O<sub>3</sub> to the low iron content subbituminous and lignite fly ash samples to reach an iron content similar to that of the Blacksville sample, significant Hg<sup>0</sup> oxidation reactivity was measured (33 to 40 percent oxidation of Hg<sup>0</sup>) for these iron-doped samples.



3-Component: silica/alumina (3.5/1) and 14 wt% Fe<sub>2</sub>O<sub>3</sub>  
 4-Component: silica/alumina (3.5/1), 13 wt% Fe<sub>2</sub>O<sub>3</sub>, and 6 wt% CaO

Figure 5-5. Hg<sup>0</sup> oxidation in the presence of the three- and four-component model fly ashes containing iron at a bed temperature of 250 °C (source: Reference 4).



3-Component: silica/alumina (3.5/1) and 1 wt% CuO  
 4-Component: silica/alumina (3.5/1), 1 wt% CuO, and 6 wt% CaO

Figure 5-6. Hg<sup>0</sup> oxidation in the presence of the three- and four-component model fly ashes containing copper at a bed temperature of 250 °C (source: Reference 4).

**Table 5-1. Percent oxidation of Hg<sup>0</sup> by simulated and actual coal-fired electric utility boiler fly ash (source: Reference 4).**

Fly Ash Composition (by weight percentages)	% Oxidation of Hg <sup>0</sup> by fly ash					
	Base <sup>a</sup>	Base + HCl	Base + HCl, SO <sub>2</sub>	Base + HCl, SO <sub>2</sub> , H <sub>2</sub> O	Base + NO	Base + NO, SO <sub>2</sub>
<b>2-Component Model Fly Ash</b>						
22% Al <sub>2</sub> O <sub>3</sub> + 78% SiO <sub>2</sub>	b	0			39	4
<b>5-Component Model Fly Ashes</b>						
19% Al <sub>2</sub> O <sub>3</sub> , + 67% SiO <sub>2</sub> + 14% Fe <sub>2</sub> O <sub>3</sub>	0	92	88	54	93	80
22% Al <sub>2</sub> O <sub>3</sub> + 77% SiO <sub>2</sub> + 1% Fe <sub>2</sub> O <sub>3</sub>		67	43	37	48	26
22% Al <sub>2</sub> O <sub>3</sub> + 78% SiO <sub>2</sub> + 0.1% Fe <sub>2</sub> O <sub>3</sub>		15			11	3
22% Al <sub>2</sub> O <sub>3</sub> + 77% SiO <sub>2</sub> + 1% CuO		93	89	84	70	16
22% Al <sub>2</sub> O <sub>3</sub> + 78% SiO <sub>2</sub> + 0.1% CuO		92	86	63	35	3
22% Al <sub>2</sub> O <sub>3</sub> + 72% SiO <sub>2</sub> + 7% CaO	0	0	13	14	0.86	13
22% Al <sub>2</sub> O <sub>3</sub> + 78% SiO <sub>2</sub> + 0.1% CuCl	87	77		23		
<b>4-Component Model Fly Ashes</b>						
21% Al <sub>2</sub> O <sub>3</sub> + 71% SiO <sub>2</sub> , + 1% CuO + 7% CaO		91	82	43		
18% Al <sub>2</sub> O <sub>3</sub> , + 63% SiO <sub>2</sub> + 13% Fe <sub>2</sub> O <sub>3</sub> + 6% CaO		87	93	49		
<b>Actual Fly Ash Samples</b>						
Blacksville coal fly ash (bituminous) 22% Fe <sub>2</sub> O <sub>3</sub> , 6% CaO		6			100	
Comanche coal fly ash (subbituminous) 5% Fe <sub>2</sub> O <sub>3</sub> , 32% CaO		0			0	
Absaloka coal fly ash (subbituminous) 4% Fe <sub>2</sub> O <sub>3</sub> , 24% CaO					30-35	

- (a) Base gas consisted of 40 ppbv Hg<sup>0</sup>, 2 mole% O<sub>2</sub>, 5 mole% CO<sub>2</sub>, and balance N<sub>2</sub> at a temperature of 523 K. HCl, NO, SO<sub>2</sub>, and water vapor were added to the base gas in the following concentrations 50 ppmv, 200 ppmv, 200 ppmv, and 1.7 mole%, respectively.
- (b) Blank cells mean test not conducted.

The physical, chemical, and carbon properties of the Blacksville and Valmont samples were also characterized. It was found that the two fly ash samples have different unburned carbon contents (3.4 percent for Valmont and 16.8 percent for Blacksville). Based on this finding, it appears that iron content may not be the only ash-related factor that affects the  $\text{Hg}^0$  oxidation reactivity of bituminous coal fly ashes. The effect of physical properties, such as surface area, and the effects of chemical properties, such as sodium content and alkalinity, in the fly ash may also determine the propensity of different fly ashes to oxidize Hg in flue gas.

Research for obtaining a better understanding of the roles of  $\text{NO}_x$  and  $\text{Fe}_2\text{O}_3$  in the heterogeneous oxidation of  $\text{Hg}^0$  was reported recently by UND/EERC.<sup>9</sup> In UND/EERC's reported research, the effects of  $\text{NO}_x$  and hematite ( $\alpha\text{-Fe}_2\text{O}_3$ ) on Hg transformations were studied by injecting them into actual coal combustion flue gases produced from burning bituminous (Blacksville), subbituminous (Absaloka), and lignite (Falkirk) coals in a 7-kW combustion system. It was found that the Blacksville fly ash has high  $\text{Fe}_2\text{O}_3$  content (12.1 percent), and the Absaloka and Falkirk fly ashes have significantly lower  $\text{Fe}_2\text{O}_3$  contents (4.5 and 7.9 percent, respectively). Portions of the  $\text{Fe}_2\text{O}_3$  in Blacksville and Falkirk fly ashes are present as maghemite ( $\gamma\text{-Fe}_2\text{O}_3$ ), and a portion of the  $\text{Fe}_2\text{O}_3$  in Absaloka fly ash is present as hematite ( $\alpha\text{-Fe}_2\text{O}_3$ ). The flue gas generated from the combustion of Blacksville coal contained  $\text{Hg}^{2+}$  as the predominant Hg species (77 percent), whereas Absaloka and Falkirk flue gases contained predominantly  $\text{Hg}^0$  (84 and 78 percent, respectively). Injections of  $\text{NO}_2$  (80 to 190 ppm) at 440 to 880 °C and  $\alpha\text{-Fe}_2\text{O}_3$  (6 and 15 percent) at 450 °C into Absaloka and Falkirk coal combustion flue gases did not change Hg speciation. The UND/EERC researchers suggested that the lack of transformation from  $\text{Hg}^0$  to  $\text{Hg}^{2+}$  in the 7-kW combustion system was possibly due to components of either Absaloka and Falkirk coal combustion flue gases, or their fly ashes, inhibiting the  $\alpha\text{-Fe}_2\text{O}_3$  catalyzed heterogeneous oxidation of  $\text{Hg}^0$  by  $\text{NO}_x$ . The researchers also believed that an abundance of  $\text{Hg}^{2+}$  in Blacksville coal combustion flue gas and  $\gamma\text{-Fe}_2\text{O}_3$  in the corresponding fly ash, and the inertness of injected  $\alpha\text{-Fe}_2\text{O}_3$  with respect to heterogeneous  $\text{Hg}^0$  oxidation in Absaloka and Falkirk flue gases, are indications that  $\gamma\text{-Fe}_2\text{O}_3$  rather than  $\alpha\text{-Fe}_2\text{O}_3$  catalyzes  $\text{Hg}^{2+}$  formation.

A study of the role of fly ash in the speciation of Hg in coal combustion flue gases was reported by Iowa State University.<sup>10</sup> In this study, bench-scale laboratory tests were performed in a simulated flue gas stream using two fly ash samples obtained from the ESPs of two full-scale coal-fired electric utility boilers. One fly ash was derived from burning a western subbituminous coal (Powder River Basin) while the other was derived from an eastern bituminous coal (Blacksville). Each of the two samples was separated into three subsamples with particle sizes greater than 10, 3, and 1  $\mu\text{m}$  using three cyclones. The amount of sample collected in these three size ranges was 85 to 90 percent, 10 to 15 percent, and 1 percent of the total ash, respectively. Only the two largest sized subsamples were tested for  $\text{Hg}^0$  oxidation reactivity. The Blacksville sample was also separated into strongly magnetic (20 percent), weakly magnetic (34 percent), and nonmagnetic (46 percent) fractions using a hand magnet for testing  $\text{Hg}^0$  oxidation reactivity of the individual fractions. Since magnetism of the fly ash samples is contributed mainly by iron oxides in the samples, the iron oxide content of the magnetically separated samples is in the following order: strongly magnetic > weakly magnetic > nonmagnetic. The low iron content PRB fly ash is nonmagnetic and was not magnetically

separated for testing. Scanning electron microscopy with energy-dispersive x-ray analysis (SEM-EDX) was used to examine the surface morphology and chemical composition of the fly ash samples. X-ray diffraction (XRD) was also used to examine the mineralogical composition of the whole and fractionated fly ash samples. XRD identifies only crystalline components of the samples. This is important since coal combustion fly ashes typically contain a considerably amount of glassy, amorphous material.

It was observed that, although the fly ashes tested were chemically and mineralogically different, there were no large differences in the catalytic potential for oxidizing  $\text{Hg}^0$ .<sup>10</sup> The Blacksville fly ash tended to show somewhat more catalytic reactivity (16 to 19 percent  $\text{Hg}^0$  oxidation) than the PRB fly ash (4 to 10 percent  $\text{Hg}^0$  oxidation). The researchers of this project suggested that the difference in reactivity could be due largely to the larger surface area ( $3.4 \text{ m}^2/\text{g}$ ) of the Blacksville fly ash compared to that ( $1.5 \text{ m}^2/\text{g}$ ) of the PRB fly ash. It was found from the SEM-EDX analyses that the iron-rich (highly magnetic) phases in the greater than  $10 \text{ }\mu\text{m}$  size fraction of the Blacksville sample contained about 25 percent (atomic) Fe, 10 percent each of Al and Si, 2 percent Ca, and lesser amounts of Na, S, K, and Ti. The nonmagnetic Blacksville fly ash fraction in the greater than  $10 \text{ }\mu\text{m}$  size range contained only 4 percent Fe, 10 percent Al, 20 percent Si, and lesser amounts of Na, S, K, and Ti. For the PRB fly ash (all nonmagnetic), both the greater than  $10 \text{ }\mu\text{m}$  and greater than  $3 \text{ }\mu\text{m}$  fractions contained about 3 percent Fe, 10- 20 percent Al and Si, about 10 percent Ca, and 2 percent or less of Mg, S, K, and Ti. The XRD results showed that the whole Blacksville ash contained primarily quartz ( $\text{SiO}_2$ ), mullite ( $3\text{Al}_2\text{O}_3 \cdot 2\text{SiO}_2$ ), magnetite ( $\text{Fe}_3\text{O}_4$ ), hematite ( $\text{Fe}_2\text{O}_3$ ), and a trace of lime ( $\text{CaO}$ ). The PRB fly ash contained mostly quartz and lesser amounts of lime, periclase ( $\text{MgO}$ ), and calcium aluminum oxide ( $\text{Ca}_3\text{Al}_2\text{O}_6$ ). No magnetite or hematite was found in this ash. It is interesting to note that the nonmagnetic fractions actually showed substantially higher amounts of oxidized Hg than the magnetic fractions. The reported test results of this study indicated that the nonmagnetic fraction resulted in 24 percent of the Hg being oxidized, while 3 percent of the Hg oxidized when using the magnetic ash. It has been suspected that the magnetic (iron-rich) fraction in fly ash would be more catalytic than the nonmagnetic (aluminosilicate-rich) fraction because of its mineralogy (predominantly iron oxides), and possibly because the magnetic phase tends to be enriched in transition metals that could also serve as  $\text{Hg}^0$  oxidation catalysts. However, under the experimental conditions employed in this study, the test results do not support this. It was found that the surface area of the nonmagnetic fraction is about four times that of the magnetic fraction. From this study it appears that surface area is a dominant factor in determining the ash's  $\text{Hg}^0$  oxidation reactivity.

Because major differences were not observed with the two fly ashes, a set of tests involving a full factorial design was conducted using only the Blacksville fly ash in order to apply statistical techniques for identifying the important factors in determining  $\text{Hg}^0$  oxidation.<sup>10</sup> The statistical analysis results indicated that the composition of the simulated flue gas used in the tests and whether or not ash was present in the gas stream were the two most important factors. The presence of HCl, NO,  $\text{NO}_2$ , and  $\text{SO}_2$  and all two-way gas interactions of the four gases listed above were found statistically significant for  $\text{Hg}^0$  oxidation. The HCl,  $\text{NO}_2$ , and  $\text{SO}_2$  appeared to contribute to  $\text{Hg}^0$  oxidation, while the presence of NO appeared to suppress  $\text{Hg}^0$  oxidation.  $\text{NO}_2$  was found to be the most important of the four reactive gases tested; next were HCl and NO.

However, the effect of NO depended on whether NO<sub>2</sub> was present. Although the presence of NO<sub>2</sub> was statistically significant as a main factor, it was found more important in its interactions with other gas components. Based on the statistical analysis results, the researchers of this project concluded that the interactions of flue gases with fly ash to cause Hg<sup>0</sup> oxidation are extremely complex, and the difficulty in understanding the Hg chemistry in coal combustion flue gases is not surprising. It is noted that the EPA study showed significant Hg oxidation reactivity of the Blacksville ash, while studies at UND/EERC and Iowa State University show little Hg oxidation reactivity of Blacksville ash. Since the ash samples used in the above studies were generated at three different plant operating conditions, these conditions may play an important role in contributing to the reactivity of the ashes.

### *5.3.3 Oxidation by Post-combustion NO<sub>x</sub> Controls*

There are indications that post-combustion NO<sub>x</sub> controls SCR and SNCR may oxidize some of the Hg<sup>0</sup> in the flue gas of a coal-fired electric utility boiler. The research on this issue is ongoing. For current understanding of this subject, the reader is referred to Chapter 6.

### *5.3.4 Potential Role of Deposits, Fly Ash, and Sorbents on Mercury Speciation*

Gaseous Hg (both Hg<sup>0</sup> and Hg<sup>2+</sup>) can be adsorbed by the solid particles in the coal-fired electric utility boiler flue gas. Adsorption is the phenomenon where a vapor molecule in a gas stream contacts the surface of a solid particle and is held there by attractive forces between the vapor molecule and the solid. Solid particles are present in all coal-fired electric utility boiler flue gas as a result of the ash that is generated during combustion of the coal. Ash that exits the furnace with the flue gas is called fly ash. Other types of solid particles may be introduced into the flue gas stream (e.g., lime, powdered activated carbon) for pollutant emission control. Both types of particles may adsorb gaseous Hg in the boiler flue gas. This section addresses the adsorption of gaseous Hg by fly ash. Adsorption of Hg by sorbent particles introduced into the flue gas stream and subsequently captured in a downstream PM control device is discussed in Chapter 6 as related to specific control technologies that may be implemented to increase overall Hg removal from the boiler flue gas.

Gaseous Hg can be adsorbed by fly ash in the flue gas (sometimes called "in-flight" adsorption). In-flight adsorption of gaseous Hg by fly ash occurs in the post-combustion region where the flue gas contains its highest concentration of fly ash (i.e., prior to the first PM control device). The type of coal from which a fly ash originates appears to strongly influence its ability to adsorb Hg. Pilot-scale<sup>11</sup> and field data<sup>12</sup> have indicated that fly ashes from subbituminous coals (specifically, those from the Powder River Basin in Wyoming) adsorb more gaseous Hg than fly ash from lignite and bituminous coals. Test data show 30 percent in-flight adsorption of gaseous Hg by fly ashes from boilers burning these subbituminous coals compared to 10 to 20 percent adsorption by the fly ashes from boilers burning lignite or bituminous coals. It has been suggested that the measured removals of Hg by fly ash can be inflated based on the sampling method, but in most cases are below 15 percent. General trends indicate that in-flight field capture of Hg from combustion of subbituminous coals is higher than from combustion of bituminous coals.<sup>13</sup>

The carbon content of fly ash is another parameter that may influence adsorption of gaseous Hg (the carbon in fly ash is unburned coal). Conditions that result in increased amounts of carbon in fly ash tend to increase the amount and subsequent capture of particle-bound Hg. Hg has been found to concentrate in the carbon-rich fraction of fly ash.<sup>14,15</sup> For similar coals, both laboratory<sup>16</sup> and pilot- and large-scale data<sup>11</sup> have shown a positive correlation between adsorption of gas-phase Hg and carbon content in fly ash. A research project conducted at full-scale coal-fired electric utility boilers in Colorado indicates that certain fly ashes adsorb significant levels of Hg from flue gas. Chapter 7 describes the methodology and results of this study in detail. Many of these fly ashes have carbon content greater than 7 percent, but one low-carbon content fly ash has also been identified. This research project and the possibility of using fly ash re-injection for Hg control is discussed in Chapter 6.

Gaseous Hg also can be adsorbed by fly ash collected on the surface of a FF. In a FF, there is contact of gaseous Hg in the flue gas with the collected layer of fly ash on the FF bags as the gases flow through the FF. Pilot-scale tests of a low-carbon fly ash (less than 0.5 percent carbon) showed that the fly ash adsorbed 65 percent of the gaseous Hg<sup>0</sup> entering a FF; the data indicate that fly ash properties other than just carbon content may affect adsorption. The tested fly ash was produced from the combustion of a subbituminous coal from the Powder River Basin in Wyoming. Western subbituminous coals generally contain high concentrations of CaO and tend to adsorb high levels of Hg<sup>0</sup>. At this time, the mechanisms by which these Western coals adsorb Hg<sup>0</sup> are not known; however, the CaO content may be a factor. It has been shown in a pilot-scale study that combustion of western coals tends to produce relatively high particle-bound Hg emissions.<sup>17</sup>

## 5.4 Capture of Mercury by Sorbent Injection

Mercury can be captured and removed from a flue gas stream by injection of a sorbent into the exhaust stream with subsequent collection in a PM control device such as an electrostatic precipitator or a fabric filter. The implementation of this type of Hg control strategy requires the development, characterization, and evaluation of low-cost and efficient Hg sorbents. Experimental methods for characterization and evaluation are presented below. Further, efforts to develop better sorbents, with greater capacity and lower cost, are also discussed.

### 5.4.1 Sorbent Characterization

Sorbents are characterized by their physical and chemical properties. The most common physical characterization is surface area. The interior of a sorbent particle is highly porous. The surface area of sorbents is determined using the Brunauer, Emmett, and Teller (BET) method of N<sub>2</sub> adsorption.<sup>18</sup> Nitrogen is adsorbed at the normal boiling point of -195.8 °C and the surface area is determined based on mono-molecular coverage. Surface areas of sorbents range from 5 m<sup>2</sup>/g for Ca-based sorbents to over 2000 m<sup>2</sup>/g for highly porous activated carbons. Mercury capture often increases with increasing surface area of the sorbent. However, recent research<sup>19</sup> has suggested that pore surface area in the micropores is more important than the total surface area for the removal of part per billion concentrations of Hg from coal combustion flue gases.

Particle size distribution is another physical characteristic that is used to describe sorbents. Activated carbons that are used for Hg control are powdered with a size on the order of 44  $\mu\text{m}$  or less. Particle size is measured using sieves or a scanning electron microscope (SEM). Generally, the smaller the particle size of an activated carbon, the better the access to the surface area and the faster the rate of adsorption kinetics. Careful consideration of particle size distribution can provide significant operating benefits, both in fabric filter applications, where pressure drop must be considered, and in ESP (or duct injection) applications, where mass transfer limitations in the short residence time mean that adsorption is a function of sorbent particle size.

Determination of the pore size distribution of an activated carbon is an extremely useful way of understanding the performance characteristics of the material. Pore sizes are based on the diameter of the pore and are categorized using the following IUPAC conventions: micropores <2 nm, mesopores 2-50 nm, and macropores >50 nm. Micropore volume can be estimated from  $\text{CO}_2$  adsorption at 273 K using the Dubinin-Radushkevich (DR) equation. Total pore volume can be determined using  $\text{N}_2$  adsorption.

Some of the chemical properties of activated carbons that influence Hg capture include sulfur content, iodine content, chlorine content, and water content. Functional groups of a sorbent have been shown to play an important role in adsorption behavior. Many carbon-oxygen functional groups have been identified in activated carbon including carbonyl, carboxyl, quinone, lactones, and phenol groups. Many methods have been used to study the functional groups present in carbonaceous materials including neutralization of bases, direct analysis of the oxide layer by chemical reaction, infrared spectroscopy, and x-ray photoelectron spectroscopy. For example, specific surface oxygen functional groups can be estimated by using the data measured from the base titration based on the following assumptions:  $\text{NaHCO}_3$  titrates carboxyl groups;  $\text{NaOH}$  titrates carboxyl, lactone, and phenol groups;  $\text{CO}_2$  is a decomposition product of carboxyl and lactone groups; and  $\text{CO}$  is a decomposition product of phenol and carbonyl groups.<sup>20</sup> The  $\text{NaOH}$  and  $\text{HCl}$  titration values can estimate the acidity and basicity of a carbon, respectively.

#### *5.4.2 Experimental Methods Used in Sorbent Evaluation*

In order to evaluate the performance of a specific Hg sorbent, several types of experimental reactors are used. The first step is testing in a bench-scale reactor system, which may be a fixed-bed, entrained-flow, or a fluidized-bed system. Sorbents that perform well in bench-scale tests are then tested in a pilot-scale system and may eventually be tested in a full-scale system. These systems are discussed below.

##### *5.4.2.1 Bench-scale Reactors*

Bench-scale reactors are the smallest category of reactors, hence the term “bench-scale.” There are several types of bench-scale reactors that are used to evaluate Hg sorbents. The first type that will be discussed is a fixed-bed or packed-bed system. This type of reactor simulates  $\text{Hg}^0$  capture that would occur in a FF. Another type of bench-scale reactor is an entrained-flow

reactor, which simulates in-flight capture of  $\text{Hg}^0$  upstream of an ESP. It is important to highlight the major differences between these two reactors as shown in Table 5-2.

*Fixed-bed Reactor.* A schematic of the experimental apparatus used by EPA to study the capture of  $\text{Hg}^0$  and  $\text{HgCl}_2$  is shown in Figure 5-7. A detailed description of the apparatus can be found elsewhere.<sup>21</sup> In this system the Hg vapor generated is carried into a manifold by a nitrogen stream where it is mixed with  $\text{SO}_2$ , HCl,  $\text{CO}_2$ ,  $\text{O}_2$ , and water vapor (as required by each particular experiment). The sorbent to be studied (approximately 0.02 g diluted with 2 g inert glass beads; bed length of approximately 2 cm) is placed in the reactor and maintained at the desired bed temperature by a temperature controller. A furnace kept at 850 °C is placed downstream of the reactor to convert any  $\text{Hg}^{2+}$  (as in  $\text{HgCl}_2$ ) to  $\text{Hg}^0$ . According to thermodynamic predictions, the only Hg species that exists at this temperature is  $\text{Hg}^0$ .<sup>22</sup> Quality control experiments, in the absence of HCl in the simulated flue gas, also showed that all the  $\text{HgCl}_2$  could be recovered as  $\text{Hg}^0$  across this furnace. The presence of the furnace enables detection of non-adsorbed  $\text{HgCl}_2$  as  $\text{Hg}^0$  by the on-line ultraviolet (UV)  $\text{Hg}^0$  analyzer, thus providing actual, continuous  $\text{Hg}^0$  or  $\text{HgCl}_2$  capture data by the fixed bed of sorbent. The UV  $\text{Hg}^0$  analyzer used in this system responds to  $\text{SO}_2$  as well as  $\text{Hg}^0$ . Signal effects due to  $\text{SO}_2$  are corrected by placing an on-line  $\text{SO}_2$  analyzer (UV) downstream of the  $\text{Hg}^0$  analyzer and subtracting the measured  $\text{SO}_2$  signal from the total response of the Hg analyzer; the  $\text{SO}_2$  analyzer is incapable of responding to Hg in the concentration range generally used.

In each test, the fixed bed is exposed to the Hg-laden gas for 7 hours or until 100 percent breakthrough (saturation) is achieved (whichever comes first). During this period the exit concentration of Hg is continuously monitored. The instantaneous removal of  $\text{Hg}^0$  or  $\text{HgCl}_2$  at any time (t) is obtained as follows:

$$\text{Instantaneous removal at time } t \text{ (\%)} = 100 * [(\text{mercury})_{in} - (\text{mercury})_{out}] / (\text{mercury})_{in}$$

The specific amount of Hg uptake (q, cumulative removal up to time t; weight Hg species/weight sorbent) is determined by integrating and evaluating the area under the removal curves. Selected experiments conducted using this experimental setup have been run in duplicate and indicated a range of  $\pm 10\%$  about the mean in the experimental results. It was found that differences in equilibrium  $\text{Hg}^0/\text{HgCl}_2$  capacities, at 200-300  $\text{mg}/\text{Nm}^3$  inlet concentration, are statistically significant if the  $\text{Hg}^0/\text{HgCl}_2$  capacities are at least  $\pm 10$  percent different from one another.

*Entrained-flow Reactor.* An example of a bench-scale entrained-flow reactor<sup>23</sup> is shown in Figure 5-8. This EPA reactor is constructed of quartz and is 310.5 cm long with an inside diameter of 4 cm. Three gas-sampling ports are located along the length of the reactor and are labeled SP1, SP2, and SP3. The reactor is heated with three Lindberg, 3-zone electric furnaces in series. The baseline  $\text{Hg}^0$  concentration is measured in the absence of activated carbon using an ultraviolet (UV) analyzer (Buck Scientific, model 400A). Once the baseline is established, activated carbon is fed into the top of the reactor using a fluidized-bed feeder (0.2-0.5 std. L/min). The gas-phase  $\text{Hg}^0$  concentration is then measured at one of the sample ports by pulling a gas sample (0.5 std. L/min) through a 1  $\mu\text{m}$  filter to remove any particles, then through a

**Table 5-2. Comparison of bench-scale fixed-bed with entrained-flow reactors.**

Test Condition	Fixed-Bed Reactor	Entrained-Flow Reactor
Simulation of capture in	Fabric filter	Upstream of an ESP
Sorbent exposure	Minutes/Hours/Days	Less than 4 seconds
Sorbent evaluation based on	Breakthrough or uptake capacity	Reactivity

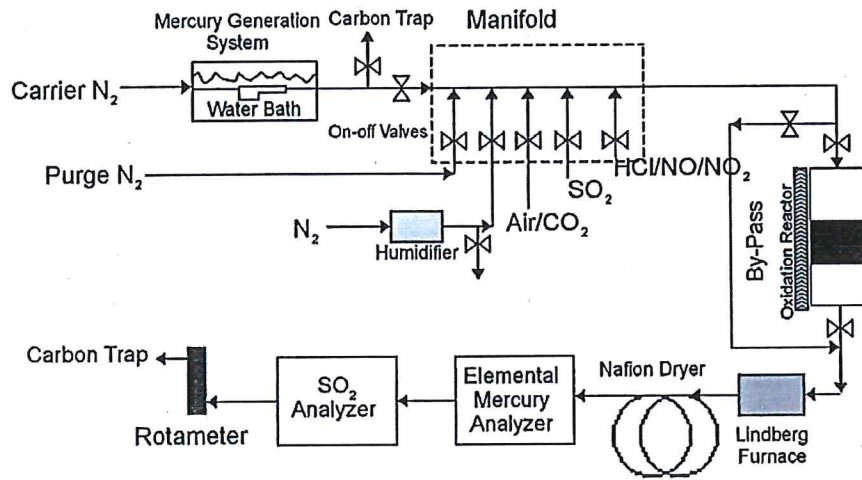


Figure 5-7. Schematic of bench-scale fixed-bed reactor (source: Reference 21).

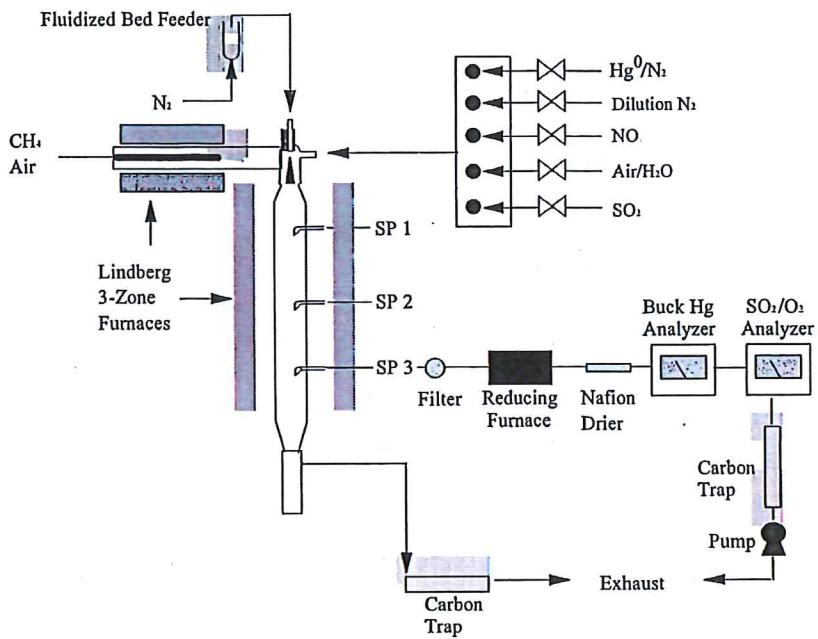


Figure 5-8. Schematic of bench-scale flow reactor with methane burner (source: Reference 23).

reducing furnace to convert any oxidized Hg to Hg<sup>0</sup>. The reduction method is described elsewhere.<sup>21</sup> After the reducing furnace, the gas is dried using a Nafion<sup>®</sup> gas sample dryer (Perma Pure, Inc.) and is finally sent to a Buck analyzer.

Initial tests are conducted using nitrogen (N<sub>2</sub>) as the carrier gas with later tests performed in a flue gas from a methane flame. In the N<sub>2</sub> carrier gas tests, industrial grade N<sub>2</sub> (1 std. L/min) flows over a Hg<sup>0</sup> permeation tube that is housed in a permeation oven (VICI Medtronic's, model 190) to generate a Hg<sup>0</sup>-laden gas stream. The N<sub>2</sub>/Hg<sup>0</sup> stream is diluted with a second N<sub>2</sub> stream (12 std. L/min) to the desired concentration before entering the top of the reactor. Other gases (SO<sub>2</sub>, NO<sub>x</sub>, O<sub>2</sub>, water vapor) can be blended into the N<sub>2</sub> carrier gas in the mixing manifold.

A fluidized-bed feeder is used to inject sorbent into the reactor. An inlet line of N<sub>2</sub> is used to fluidize and carry the activated carbon to the reactor. The carbon feed rate is adjusted by varying the amount of N<sub>2</sub> (0.2 to 0.5 std. L/min) entering the feeder.

Because the UV analyzer used to detect Hg<sup>0</sup> is sensitive to particles, a filter is used to remove any carbon that may have been carried with the gas. Tests have been conducted to determine if carbon particles accumulate on the filter, as this would act like a packed bed and the reactor's removal of Hg<sup>0</sup> would be a combination of in-flight and filter (packed-bed) capture. In these tests, activated carbon was injected in the absence of Hg<sup>0</sup>, and a gas sample was pulled through the filter. After 1 minute, Hg<sup>0</sup> was added to the gas stream to see if there was a lag in the time it takes for the baseline to return. The results were the same as for a blank filter, suggesting that the filter does not have an effect on the results.

The total flow through the reactor is typically 13 std. L/min, which gives residence times of 5.2, 11.5, and 17.7 s at ports SP1, SP2, and SP3, respectively. The velocity of the particles through the reactor is assumed to be the same as that of the gas flow since the terminal velocity of the particles is smaller than the velocity of the gas through the reactor by a factor of 3.

*Fluidized-bed Reactor.* Another type of bench-scale reactor that is used to evaluate sorbents is a fluidized-bed reactor,<sup>24</sup> shown in Figure 5-9. The advantage of this type of reactor is the extended contact time between the sorbent and the Hg-laden gas. Bench-scale Hg removal tests can be performed on a fluidized-bed reactor apparatus. In a typical experiment, an Hg/NO/SO<sub>2</sub> mixture, nitrogen, and dry air are metered through rotameters to produce 12 scfh of a dry simulated flue gas of 300 ppmv NO<sub>x</sub>, 600 ppmv SO<sub>2</sub>, 8 percent O<sub>2</sub>, and varying Hg concentrations. This gas is preheated to reaction temperature (80 °C) and humidified with vaporized water to an average 10.5 mol % water. The resulting wet simulated flue gas is then passed through a vertical reactor loaded with fluidized sorbent and sand, and then passed through a filter to remove any entrained particulate to protect the downstream equipment. The reactor and filter assembly are housed in an oven maintained at 80 °C. The test stand is equipped with a bypass of the reactor and filter assembly to allow for bias checks. Sorbent is exposed to simulated flue gas for 30 minutes. Water is removed from the spent flue gas with a NAFION<sup>™</sup> Dryer. Dry gas is then serially analyzed with Hg, SO<sub>2</sub>, and NO<sub>x</sub> continuous emission monitors (CEMs).

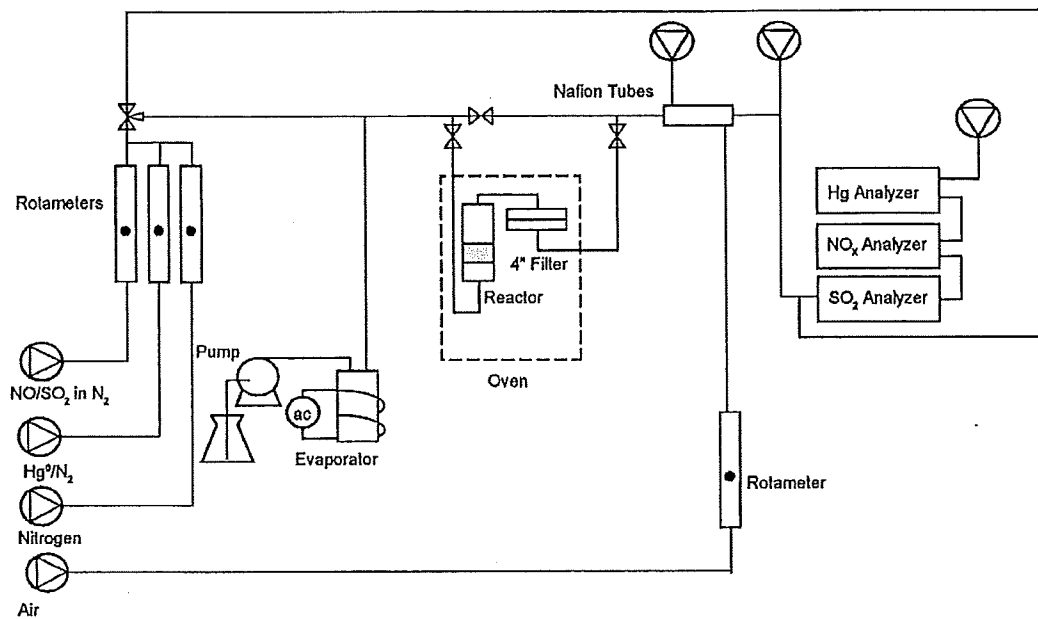


Figure 5-9. Schematic of bench-scale fluidized-bed reactor system (source: Reference 24).

#### 5.4.2.2 Pilot-scale Systems

Initial design and testing is done in bench-scale reactors. Once the fundamentals of Hg capture have been tested in a bench-scale system, the next step is to move up to a larger or pilot-scale system. The main difference between bench- and pilot-scale systems involves testing sorbents in a more realistic situation involving coal combustion flue gas. This gas is generated in a pilot-scale combustor that contains a FF or ESP for particulate control. An example of this is the pilot-scale combustor operated by DOE (see Figure 7-3). This system burns coal at a rate of 500 lb/hr and is equipped with a FF. Sorbents, such as activated carbon, are injected upstream of the PM control device. Mercury removal is determined by gas-phase sampling upstream of the sorbent injection point and downstream of the PM control device.

Pilot-scale Hg removal can also be examined using a flue gas slipstream from a full-scale unit. An ESP or FF is attached to the slipstream and tested. A portable FF was developed by EPRI and called a COHPAC (COmpact Hybrid PARTICulate Collector) unit.<sup>26</sup> This unit was tested for Hg removal using activated carbon. The URS Corporation (formerly Radian International) also developed a reactor system that uses a slipstream of actual flue gas withdrawn from a power plant to evaluate sorbents or catalysts in a fixed bed.<sup>27</sup> It should be noted that the slipstream reactor, which uses actual coal combustion flue gas, does not always produce the same Hg capture behavior of a sorbent that a similar laboratory system does using simulated flue gas.<sup>28</sup> It is important to perform pilot-scale tests prior to conducting full-scale tests to eliminate uncertainties and costly redesign of a process. With the data collected in the pilot-scale studies, full-scale tests can be initiated.

#### 5.4.2.3 Full-scale Tests

Most of work to date in Hg control has been done in bench- or pilot-scale systems. These reduced-scale systems provide insight into many issues, but cannot fully account for the impacts that additional control technologies have on plant-wide equipment. Therefore, it is necessary to scale up and perform full-scale tests to document actual performance in a full-scale boiler. These tests are based on the results obtained in bench- and pilot-scale tests. Screening tests in bench- and pilot-scale systems identify sorbents that are effective in capturing Hg. These sorbents are then tested in a full-scale coal-fired electric utility power plant to determine full-scale performance.

Each full-scale unit is unique in terms of the pollution control equipment that is present as well as the operating conditions. Some of the factors that are evaluated include:

- Type of particulate control equipment that is used (ESP or FF),
- Impact of cake thickness and cleaning frequency in a FF, and
- Removal of Hg by the fly ash in the system. Subbituminous coal ashes have been shown to be effective in capturing Hg.

### 5.4.3 Research on Sorbent Evaluation

#### 5.4.3.1 Sorbent Evaluation Using Enhanced-flow Reactors

A flow reactor was designed to simulate  $\text{Hg}^0$  capture through a duct or ESP and to obtain kinetic rate constants for the adsorption of  $\text{Hg}^0$  onto sorbents. Several researchers have predicted that, under certain conditions, dispersed-phase capture would be limited by mass transfer.<sup>29,30</sup> Calculations were performed to determine the required operating conditions to minimize external mass transfer effects in the flow reactor, and experimental tests were performed to verify these calculations.<sup>23,31,32</sup> The first test involved changing the diffusion coefficient by changing the gas in the system from  $\text{N}_2$  to helium (He) and to argon (Ar) while holding all other parameters constant (particle size, residence time, temperature, and  $\text{Hg}^0$  concentration). The diffusion coefficient increased by an order of magnitude by changing the gas from  $\text{N}_2$  to He. Using a lignite-based commercially available carbon (Norit FGD) at 100 °C and a  $\text{Hg}^0$  concentration of 86 ppb,  $\text{Hg}^0$  removal was 6 percent at a carbon to Hg ratio (C:Hg) of 1,500:1 and increased to 30 percent at a C:Hg of 8,000:1. Experimental results were similar when He was used as compared to  $\text{N}_2$ . If external mass transfer were controlling, then a higher  $\text{Hg}^0$  removal would have been obtained using He, since the mass transfer coefficient increased.

A second test involved using two commercially available activated carbons, Norit FGD and Calgon WPL at 100 °C and 124 ppb  $\text{Hg}^0$  in dry  $\text{N}_2$ . Removal for the FGD carbon ranged from 9 percent (C:Hg=2200:1) to 23 percent (C:Hg=6400:1). Removal for the WPL carbon ranged from 11 percent (C:Hg=340) to 94 percent (C:Hg=5000:1). If dispersed-phase capture in the flow reactor were film-mass-transfer limited, the two activated carbons would have removed similar amounts of  $\text{Hg}^0$  at a given C:Hg, assuming each carbon had sufficient  $\text{Hg}^0$  capacity.

The flow reactor has been used to examine the effect of temperature, particle size, residence time, carbon type, and gas composition on  $\text{Hg}^0$  removal.<sup>31-33</sup> The effect of particle size on  $\text{Hg}^0$  removal for Darco FGD at 100 °C and a  $\text{Hg}^0$  concentration of 86 ppb is shown in Figure 5-10. Several particle sizes (4-8, >8-16, >16-24, and >24-44  $\mu\text{m}$ ) were injected into the flow reactor at C:Hg ratios ranging from 2000 to 11,000:1. The gas was sampled at SP2, resulting in a gas contact time of 8.4 s. Figure 5-11 shows that greater  $\text{Hg}^0$  removal is achieved by increasing the feed rate and by decreasing the particle size. At a C:Hg of 5000:1, a 5 percent reduction was obtained with the >24-44  $\mu\text{m}$  size fraction as compared to a 20 percent reduction with the 4-8  $\mu\text{m}$  fraction. Thus by using a smaller particle a higher removal can be obtained at a given C:Hg. Both external and internal mass transfers are dependent on particle size: the effect of mass transfer increases with an increase in particle size.

#### 5.4.3.2 Sorbent Evaluation Using Packed-bed Reactors

Recent bench-scale studies at the University of North Dakota's Energy and Environmental Research Center (UND/EERC) have focused on the interactions of gaseous flue gas constituents on the adsorption capacity of activated carbon for  $\text{Hg}$ .<sup>34</sup> Bench-scale studies were performed using a fixed bed of carbon. The tested carbon was a commercially available lignite-based activated carbon (LAC) commercially known as Darco FGD<sup>TM</sup> from Norit

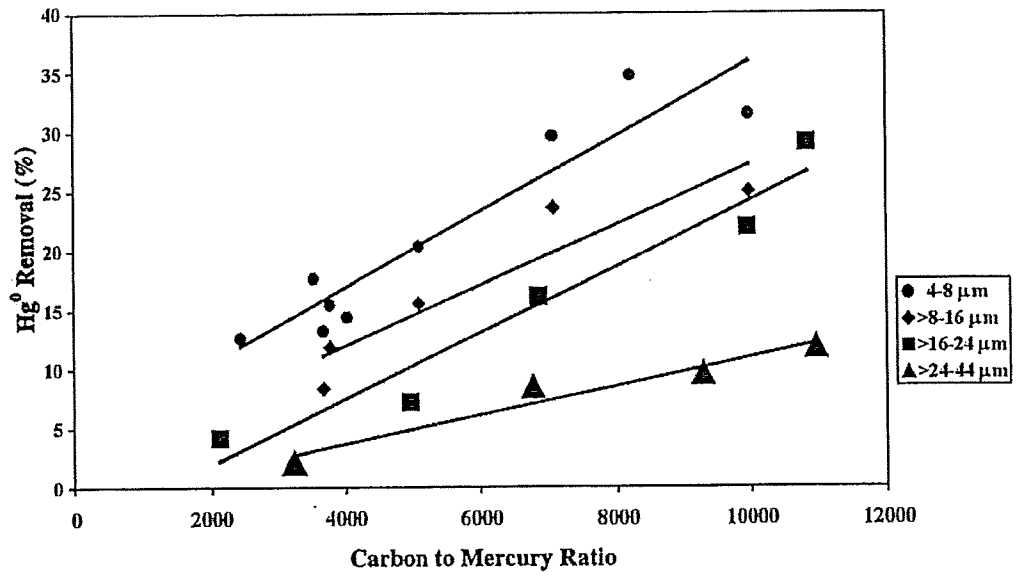


Figure 5-10. Effect of particle size on adsorption for Darco FGD at 100 °C, 86 ppb Hg<sup>0</sup> concentration, and 8.4 s contact time (source: Reference 31).

Americas, Inc. A simulated flue gas containing a nominal concentration of  $15 \mu\text{g}/\text{Nm}^3$  of gaseous  $\text{Hg}^0$  was passed through the fixed bed of carbon. In addition to  $\text{Hg}$ , the baseline test gas contained 6 percent  $\text{O}_2$ , 12 percent  $\text{CO}_2$ , 8 percent  $\text{H}_2\text{O}$ , and the balance  $\text{N}_2$ . Various flue gas constituents ( $\text{SO}_2$ ,  $\text{HCl}$ ,  $\text{NO}$ , and  $\text{NO}_2$ ) were added individually and in combination to the baseline test gas to determine the effects of flue gas constituents on  $\text{Hg}$  adsorption. Temperature effects were also examined. Table 5-3 shows the various compositions of gas tested.

For each adsorption test, a  $\text{Hg}$  CEM was used to monitor total or elemental  $\text{Hg}$ . Measurements were alternated between the inlet and outlet locations of the test bed. For a given test, measurements took place primarily at the outlet location; however, occasionally the inlet location was tested to confirm that a constant concentration of gaseous  $\text{Hg}^0$  was entering the test bed. For each test, the analyzer was set to measure total gaseous  $\text{Hg}$  at the outlet; however, occasionally the analyzer was set to measure only gaseous  $\text{Hg}^0$  at the outlet. The purpose of measuring only gaseous  $\text{Hg}^0$  at the outlet was to determine if any incoming gaseous  $\text{Hg}^0$  was being oxidized by carbon in the bed (evident if the concentration of gaseous  $\text{Hg}^0$  in the outlet gas was less than the concentration of total gaseous  $\text{Hg}$  in the outlet gas).

For adsorption to take place (assuming attractive forces exist between a particular gaseous specie and sorbent), the adsorbing specie must have sufficient time to reach the surface of a sorbent and diffuse into its pores (where most adsorption takes place). If any of the adsorbing specie in a gas stream passing through a fixed bed of sorbent cannot reach the surface of the sorbent (mainly its pore surfaces), the specie will pass through the bed unadsorbed. Researchers conducted preliminary tests to show that the gaseous  $\text{Hg}$  in the test gas had sufficient time (under the conditions tested) to contact the sorbent and to diffuse into its pores. Proving this point was important since some of the adsorption tests showed immediate breakthrough of  $\text{Hg}$  in the outlet gas. In these cases, immediate breakthrough was not due to insufficient contact time but rather the carbon's inability to adsorb all of the gaseous mercury.

Figure 5-11 shows an example of the sampling and measurements taken during testing of the baseline test gas with  $\text{HCl}$ ,  $\text{NO}_2$ , and  $\text{SO}_2$  (as noted in the graph,  $\text{SO}_2$  was added to the baseline test gas 2.5 hours after the start of the test). Except where noted, the  $\text{Hg}$  concentrations in Figure 5-11 are those in the outlet test gas and represent concentrations of total gaseous  $\text{Hg}$ . Mercury concentrations in the graph are quantified as a percentage of the inlet concentration of gaseous  $\text{Hg}^0$ . The percentage of  $\text{Hg}$  in the outlet test gas is called percent breakthrough. Figure 5-11 indicates that the analyzer sampled and measured total gaseous  $\text{Hg}$  in the outlet gas at all times during testing except at approximately 5.2 hours, at which time the analyzer sampled and measured  $\text{Hg}$  in the inlet gas. At approximately 5.15 hours the analyzer measured gaseous  $\text{Hg}^0$  instead of total gaseous  $\text{Hg}$  in the outlet test gas; the drop in the concentration curve at this time from approximately 150 percent to zero percent indicates that  $\text{Hg}$  in the outlet test gas consisted entirely of gaseous  $\text{Hg}^{2+}$ . Thus, while only gaseous  $\text{Hg}^0$  was in the test gas entering the carbon bed, the  $\text{Hg}^0$  was oxidized to  $\text{Hg}^{2+}$  as it passed through the bed. (Why some of the outlet concentrations of total gaseous  $\text{Hg}$  exceeded 100 percent of the inlet  $\text{Hg}$  concentration for this run is explained further on in this section.)

**Table 5-3. Composition of test gases to simulate coal combustion flue gas used for UND/EERC bench-scale study (source: Reference 34).**

SO <sub>2</sub> ppmv	HCl ppmv	NO ppmv	NO <sub>2</sub> ppmv
Baseline test gas <sup>a</sup>			
0	0	0	0
Baseline test gas plus 1 additional gas			
1600	0	0	0
0	50	0	0
0	0	300	0
0	0	0	20
Baseline test gas plus 2 additional gases			
1,600	50	0	0
1,600	0	300	0
1,600	0	0	20
0	50	0	20
0	50	300	0
0	0	300	20
Baseline test gas plus 3 additional gases			
1,600	50	300	0
1,600	50	0	20
1,600	0	300	20
0	50	300	20
Baseline test gas plus 4 additional gases			
1600	50	300	20

(a) Prior to adding SO<sub>2</sub>, HCl, NO, and/or NO<sub>2</sub>, the baseline test gas contained 15 µg/nm<sup>3</sup> of gaseous Hg<sup>0</sup>; 6 percent O<sub>2</sub>; 12 percent CO<sub>2</sub>; 8 percent H<sub>2</sub>O; and the balance N<sub>2</sub>.

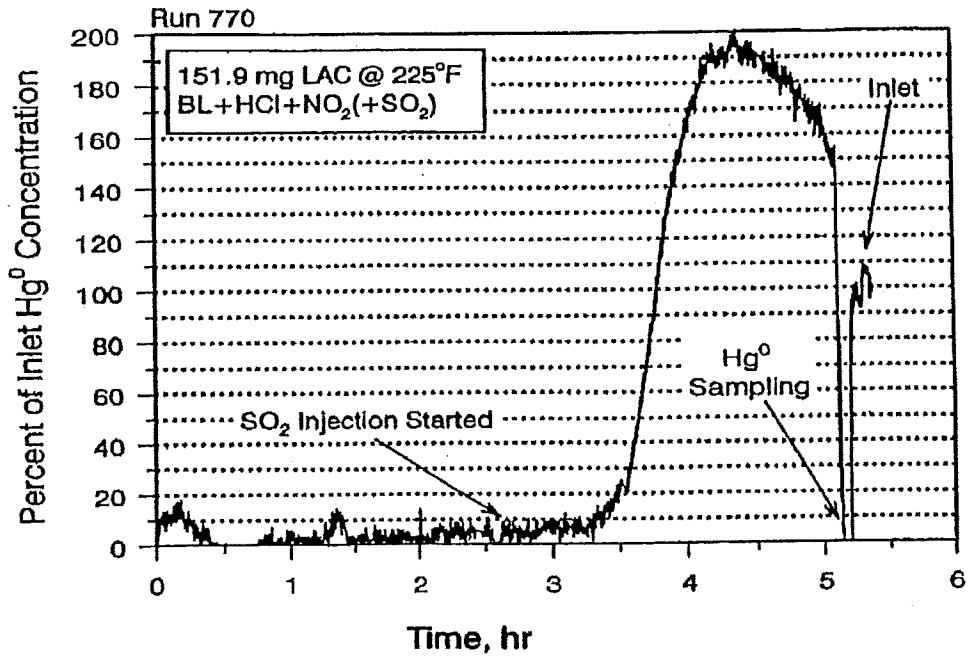


Figure 5-11. Example of the sampling and measurements taken during testing of the baseline test gas with HCl, NO<sub>2</sub>, and SO<sub>2</sub>. (source: Reference 34).

Graphs of the adsorption tests with the 15 remaining gases in Table 5-3 can be found elsewhere;<sup>13</sup> the cited graphs are similar to Figure 5-11 in that Hg concentrations (primarily outlet concentrations of total gaseous Hg) are plotted versus the time of the adsorption test.

The following summarizes the detailed test results:

- When the sorbent was exposed to the baseline gas only, the sorbent initially captured 10 to 20 percent of the incoming gaseous Hg<sup>0</sup>; the rest of the Hg passed through the bed (i.e., was not adsorbed).
- When the sorbent was exposed to SO<sub>2</sub> in addition to the baseline gas, Hg capture improved slightly.
- Under exposure of the sorbent to HCl, NO, or NO<sub>2</sub> added one at a time to the baseline gas, the Hg capture of the sorbent improved to 90 to 100 percent.
- An apparently significant interaction between SO<sub>2</sub> and NO<sub>2</sub> gases and the sorbent caused a rapid breakthrough of Hg as well as conversion of the Hg to its volatile oxidized form. This effect occurred at both 107 and 163 °C (225 and 325 °F) and with or without the presence of HCl and NO.
- In the presence of all four acid gases (SO<sub>2</sub>, HCl, NO, and NO<sub>2</sub>), rapid breakthrough and oxidation of the Hg occurred at both 107 and 163 °C (225 and 325 °F). This suggests that the interactions between the sorbent and NO<sub>2</sub> and SO<sub>2</sub> gases produced poor sorbent performance, which may be a major effect. This may be likely to occur over a variety of conditions typical of coal-fired electric utility boilers, and represents a hurdle that must be overcome to achieve effective Hg control by carbon adsorption.

The UND/EERC is continuing to investigate the interactions of gaseous flue gas constituents on the adsorption capacity of activated carbon for Hg. In addition, other types of sorbents are being developed and investigated under similar simulated flue gas conditions. Other gaseous flue gas constituents are also being examined to assess their impact on the adsorption of Hg.

#### 5.4.3.3 Sorbent Evaluation Using Fluidized-bed Reactors

Under DOE's Small Business Innovative Research (SBIR) Program, Environmental Elements Corporation (EEC) has been developing a circulating fluidized bed (CFB)<sup>24</sup> to promote agglomeration of fine PM, allowing for its capture in an ESP. In addition, a single injection of iodide-impregnated activated carbon was added to the fluidized bed to adsorb gaseous Hg. High residence time, as a result of particle recirculation, allows for effective utilization of the carbon and high collection of the fine particles. Laboratory tests with heated air indicate that, with a high density of fly ash at a 4-second residence time within the bed, fine particle emissions are reduced by an order of magnitude.

Results from the laboratory-scale testing indicate that spiked gaseous  $\text{Hg}^0$  was significantly reduced when passed through the fluidized bed of fly ash (50 percent Hg removed) with a further reduction to essentially zero, when activated carbon was injected into the bed ( $25 \mu\text{g}/\text{m}^3$  to zero) at  $110^\circ\text{C}$  ( $230^\circ\text{F}$ ). The iodide-impregnated activated carbon was fully utilized after greater than 2 hours within the bed. An adsorption capacity was calculated to be  $770 \mu\text{g}/\text{g}$  for the carbon and  $480 \mu\text{g}/\text{g}$  for the bed of ash. Other field tests were conducted at Public Service Electric and Gas- Mercer Station with similar results.<sup>24</sup>

## 5.5 Sorbent Development

The implementation of an effective and efficient Hg control strategy using sorbent injection requires the development of low-cost and efficient Hg sorbents. Of the known Hg sorbents, activated carbon and calcium-based sorbents have been the most actively studied. However, improved versions of these sorbents and new classes of Hg sorbents can be expected, as this is still a very active field.

### 5.5.1 Powdered Activated Carbons

Activated carbons have been extensively studied for their Hg capture capability. Activated carbon is the reference sorbent for Hg control in municipal waste combustors. Many factors may affect the adsorptive capability of the activated carbon sorbent. These include the temperature and composition of the flue gas, the concentration of Hg in the exhaust stream, and the physical and chemical characteristics of the activated carbon (or functionalized/impregnated carbon). Some specific efforts at understanding these effects are given below.

#### 5.5.1.1 Effects of Temperature, Mercury Concentration, and Acid Gases

The effects of bed temperature, Hg concentration, presence of acid gases ( $\text{HCl}$  and  $\text{SO}_2$ ), and presence of water vapor on the capture of  $\text{Hg}^0$  and  $\text{HgCl}_2$  by thermally activated carbons (FGD and PC-100) and Ca-based sorbents [ $\text{Ca}(\text{OH})_2$  and a mixture of  $\text{Ca}(\text{OH})_2$  and fly ash] were examined in a fixed-bed, bench-scale system.<sup>21</sup> Sorption studies indicated an abundance of  $\text{HgCl}_2$  adsorption sites in calcium-based sorbents. Increasing the  $\text{HgCl}_2$  concentration increased its uptake, and increasing the bed temperature decreased its uptake. Gas-phase  $\text{HgCl}_2$  concentration had a very strong effect on its adsorption, while bed temperature had a small influence on adsorption. The observed temperature and concentration trends suggest that the process is adsorption-controlled and that the rate of  $\text{HgCl}_2$  capture is determined by how fast molecules in the vicinity of the active sites are being adsorbed. Mixtures of  $\text{Ca}(\text{OH})_2$  and fly ash with 7 times higher surface area than  $\text{Ca}(\text{OH})_2$  and a totally different pore size distribution exhibited identical  $\text{HgCl}_2$  capture to that of  $\text{Ca}(\text{OH})_2$ . The presence of acid gases (1000 ppm  $\text{SO}_2$  and 50 ppm  $\text{HCl}$ ) drastically decreased the uptake of  $\text{HgCl}_2$  by  $\text{Ca}(\text{OH})_2$ . The inhibition effect of  $\text{SO}_2$  was more drastic than  $\text{HCl}$ , and essentially controlled the  $\text{HgCl}_2$  uptake. It was hypothesized that the inhibition effect is due to competition between these acid gases and  $\text{HgCl}_2$  for the available alkaline sites.

Sorption studies further indicated that the available active sites for capturing  $\text{Hg}^0$  in the activated carbons are limited, suggesting that it is more difficult to control  $\text{Hg}^0$  emissions than  $\text{HgCl}_2$  emissions. Increasing the  $\text{Hg}^0$  inlet concentration and decreasing the bed temperature increased the saturation capacities of the activated carbons, the time needed to reach this capacity, and the initial rate of  $\text{Hg}^0$  uptake. Unlike  $\text{HgCl}_2$  capture by  $\text{Ca}(\text{OH})_2$ , bed temperature had a very strong effect on the  $\text{Hg}^0$  adsorption by the activated carbons, and gas-phase  $\text{Hg}^0$  concentration had a small influence on such adsorption. PC-100, with twice the surface area of FGD, consistently exhibited higher saturation capacities (3-4 times higher) than FGD. The presence of acid gases had a positive effect on the capture of  $\text{Hg}^0$  by a lignite-coal-based activated carbon (FGD) and had no influence on  $\text{Hg}^0$  capture by a bituminous-coal-based activated carbon (PC-100). This difference was related to a higher concentration of Ca (acid gas sorbent) in FGD. It appears that adsorption of these acid gases by FGD creates active S and Cl sites, which are instrumental in capturing  $\text{Hg}^0$ , through formation of S-Hg and Cl-Hg bonds in the solid phase (chemisorption). These results indicate that the optimum region for the control of  $\text{Hg}^0$  by injection of activated carbon is upstream of the acid gas removal system.

#### 5.5.1.2 Role of Surface Functional Groups

The content of oxygenated acidic and alkaline surface functional groups (SFGs) on the surface of two activated carbons was manipulated to investigate their role in  $\text{Hg}^0$  and  $\text{HgCl}_2$  capture.<sup>35</sup> Acidic SFGs on the surface of activated carbons were neutralized by a variety of alkaline washes. The alkaline-treated activated carbon showed no enhancement in  $\text{Hg}^0$  and  $\text{HgCl}_2$  capture, thus indicating that acidic SFGs play no role in capturing Hg species. The alkaline SFGs content was increased by a thermal treatment process. The thermally treated activated carbons did not exhibit any improvement with regard to their  $\text{Hg}^0$  and  $\text{HgCl}_2$  capture capabilities as compared to the untreated ones. The activated carbons were then treated with a very dilute HCl solution to decrease their alkaline SFGs content. The HCl-treated activated carbon showed a very significant improvement in its  $\text{Hg}^0$  and  $\text{HgCl}_2$  capture capabilities. This observation was contrary to the initial hypothesis that alkaline sites are needed to capture acidic  $\text{HgCl}_2$  from the flue gas. It was then hypothesized that HCl treatment increases the number of active surface chlorine sites, which subsequently enhance  $\text{Hg}^0$  and  $\text{HgCl}_2$  capture. An analytical technique, Energy-Dispersive X-ray Spectroscopy (EDXS), was used to quantify surface Cl sites. A strong correlation between the increased amount of surface Cl and  $\text{Hg}^0/\text{HgCl}_2$  uptake enhancement was observed. The role of SFGs containing Cl atoms in providing  $\text{Hg}^0/\text{HgCl}_2$  active sites was established. Future investigation using SEM/EDXS and Fourier Transform Infrared (FTIR) will focus on understanding the nature of Cl bonds on the surface of carbon, so that more effective Hg species sorbents can be manufactured.

#### 5.5.1.3 In-flight Capture of Mercury by a Chlorine-impregnated Activated Carbon

Activated carbon duct injection seems to be the most promising Hg control technology for coal-fired electric utility boilers equipped with ESPs. In this technology, the injected activated carbon removes Hg only while contacting the flue gas during very limited sorbent/gas contact time (<3 seconds). Prior investigations have shown that very high, and rather costly, carbon-to-Hg weight ratios (>50,000) are needed to achieve adequate Hg removal. In order to

reduce the operating cost of the carbon injection process, either a more efficient sorbent that can operate at a lower carbon-to-Hg weight ratio or a lower-cost activated carbon (or possibly both) are required. In this study<sup>33</sup>, a cost-effective Cl-impregnation process was successfully implemented on an inexpensive virgin activated carbon. The Cl-impregnated carbon was produced in a 5 pound large batch, and its in-flight Hg<sup>0</sup> removal efficiency was evaluated in a flow reactor (as previously discussed in Section 5.4.2.1) with gas/solid contact times of 3 to 4 seconds. The Hg<sup>0</sup> removal efficiency of more than 80 percent was obtained in a flue gas containing the effluent of natural gas combustion doped with coal combustion levels of NO<sub>x</sub> and SO<sub>2</sub> at carbon-to-Hg weight ratios of about 3000. Hg<sup>0</sup> removal was rather insensitive to the adsorption temperature in the range of 100-200 °C. Cost analysis showed that this Cl-impregnation process can produce a very active and cost-effective activated carbon that can be used as a practical sorbent in a duct injection control technology in ESP-equipped coal-fired electric utility boilers. Preliminary cost estimates indicated that approximately 53 percent reduction of the total annual cost of Hg control could be possible when using Cl-impregnated FGD in lieu of virgin activated carbon. Future investigations would be focused on evaluating the Cl-impregnated activated carbon in a pilot-scale, 21-kW (90,000-Btu/hr) refractory-lined, furnace fired with pulverized coal.<sup>33</sup>

### 5.5.2 Calcium-based Sorbents

Work conducted by EPA and ARCADIS Geraghty & Miller, Inc. [funded by the Illinois Clean Coal Institute (ICCI)] indicates that the injection of calcium-based sorbents into flue gas can result in significant removal of Hg.<sup>36,37</sup> Researchers examined the high-temperature/short-gas-phase residence time removal of Hg using injection of lime while burning an Illinois #6 coal in a pilot-scale combustor. The lime was injected as a slurry at a calcium-to-sulfur (Ca:S) ratio of 2.0 mol/mol at 968 °C (1775 °F). Under these conditions, 77 percent of the total Hg was removed from the flue gas (Table 5-4). Based on these results, they concluded, "injection of lime in the high temperature regions of coal-fired processes upstream of air pollution control systems can efficiently transfer Hg from the gas to the solid phase." Summaries of work follow.

#### 5.5.2.1 Capture of Low Concentrations of Mercury Using Calcium-based Sorbents

The capture of Hg<sup>0</sup> and mercuric chloride (HgCl<sub>2</sub>), the Hg species identified in coal flue gas, by three types of calcium-based sorbents differing in their internal structure, was examined in a packed-bed, bench-scale study under simulated flue gas conditions for coal-fired electric utility boilers.<sup>38</sup> The results obtained were compared with Hg<sup>0</sup> and HgCl<sub>2</sub> capture by an activated carbon (FGD) under identical conditions. Tests were conducted with and without SO<sub>2</sub> to evaluate the effect of SO<sub>2</sub> on Hg<sup>0</sup> and HgCl<sub>2</sub> control by each of the sorbents.

The Ca-based sorbents showed insignificant removal of Hg<sup>0</sup> in the absence of SO<sub>2</sub>. However, in the presence of SO<sub>2</sub>, Hg<sup>0</sup> capture was enhanced for the three Ca-based sorbents. It was postulated that the reaction of hydrated lime with SO<sub>2</sub> would result in pore mouth closure as evidenced by the sharp drop in the SO<sub>2</sub> removal rate after the initial 10 minutes of exposure. Despite the loss of internal surface area, the relatively high uptake of Hg<sup>0</sup>, observed for these sorbents in the presence of SO<sub>2</sub>, suggests that Hg<sup>0</sup> and SO<sub>2</sub> do not compete for the same active

**Table 5-4. Mercury removal by lime sorbent injection as measured by EPA bench-scale tests (source: Reference 36).**

Test	Total Hg Concentration, µg/dscm	Total Gaseous Hg, percent	Total Particle-bound Hg, percent
Baseline	5.7	100	0
Lime sorbent injection	8.0	23	77

sites, and that the sites for  $\text{Hg}^0$  capture are influenced positively by the presence of  $\text{SO}_2$ . Moreover, the capture of  $\text{Hg}^0$  in the presence of  $\text{SO}_2$  increased with sorbent surface area and internal pore structure.

Conversely, the three Ca-based sorbents showed decreased removal of  $\text{HgCl}_2$  in the presence of  $\text{SO}_2$ . In the absence of  $\text{SO}_2$ , roughly 25 percent of the incoming  $\text{HgCl}_2$  was captured. The alkaline sites in the Ca-based sorbents were postulated to be instrumental in the capture of acidic  $\text{HgCl}_2$ .  $\text{SO}_2$  not only competed for these alkaline sites but also, as mentioned, likely closed pores with subsequent reduction in accessibility of the interior of the Ca-based sorbent particles to the  $\text{HgCl}_2$  molecules.

It was hypothesized that the capture of  $\text{Hg}^0$  in the presence of  $\text{SO}_2$  may occur through a chemisorption mechanism, while the nature of the adsorption of  $\text{HgCl}_2$  molecules may be explained through a physisorption mechanism. The effect of temperature studies further supported this hypothesis. Increasing the system temperature caused an increase in  $\text{Hg}^0$  uptake by the sorbents in the presence of  $\text{SO}_2$ . However, the increase in temperature resulted in a significant decrease in the  $\text{HgCl}_2$  uptake in the absence or presence of  $\text{SO}_2$ . Increased sorbent surface area and internal pore structure had no observable effect on  $\text{HgCl}_2$  capture in the presence of  $\text{SO}_2$ .

With the relatively large quantities of Ca needed for  $\text{SO}_2$  control at coal-fired electric utility boilers, the above results suggest that Ca-based sorbents, modified by reaction with fly ash, can be used to control total Hg emissions and  $\text{SO}_2$  cost effectively. The most effective calcium-based sorbents are those with significant surface area (for  $\text{SO}_2$  and  $\text{HgCl}_2$  capture) and pore volume (for  $\text{Hg}^0$  capture).

#### 5.5.2.2 Simultaneous Control of $\text{Hg}^0$ , $\text{SO}_2$ , and $\text{NO}_x$ by Oxidized-calcium-based Sorbents

Multipollutant sorbents have been developed that can remove both  $\text{Hg}^0$  and  $\text{Hg}^{+2}$  as effectively as FGD activated carbon in fixed-bed simulations of coal-fired electric utility boiler flue gas at 80 °C.<sup>39</sup> Oxidant-enriched, calcium-based sorbents proved far superior to activated carbon with respect to  $\text{SO}_2$  uptake on the same fixed-bed simulations. These oxidant-enriched, calcium-based sorbents also performed better with respect to  $\text{NO}_x$  and  $\text{SO}_2$  uptake than baseline lime hydrates for fixed- and fluid-bed simulations at 80 °C.

Preliminary economic analyses suggest that silicate sorbents with oxidants are 20 percent of the cost of activated carbon for Hg removal, while oxidant-enriched lime hydrates offer reduced, but significant savings. Credits for  $\text{SO}_2$  and  $\text{NO}_x$  increase the savings for multipollutant sorbents over activated carbon.

The apparent superiority of multipollutant lime and silicate hydrates enhanced with oxidants has been confirmed at conditions typical of gas-cooled, semi-dry adsorption processes on boilers; performance of sorbents at higher-temperature conditions of duct sorbent injection technologies remains to be evaluated. Planned field evaluations of both semi-dry adsorption and

duct sorbent injection will allow better economic and performance comparisons of activated carbon sorbents to that of oxidant-enriched lime and silicate hydrates.

A technology for the efficient capture of Hg through in furnace injection of a calcium-based sorbent has been developed by McDermott Technologies recently. A discussion of the full-scale tests of the technology is presented in Chapter 7.

### *5.5.3 Development of Low-cost Sorbents*

Since 1995, EPRI has supported a sorbent development program for removal of Hg emissions from coal-fired electric utility power plants at several research organizations including Illinois State Geological Survey (ISGS), University of Illinois (UI), and URS Corporation. The development of effective Hg sorbents that can be produced at lower costs than existing commercial activated carbons is the main objective of the program. The development efforts were documented in three EPRI Reports.<sup>40-42</sup> A significant number of sorbents were derived from a variety of precursor materials, including coal, biomass, waste tire, activated carbon fibers, fly ash, and zeolite, through this work. Different preparation methods were used to determine the effects of sorbent properties, such as pore size distribution, pore volume, surface area, particle size, and sulfur content, on the ability to remove Hg. The effects of different processing methods, including steam activation, grinding, size-fractionation, and sulfur-impregnation, on sorbent performance were also investigated in laboratory tests. Promising low-cost sorbents were further evaluated in actual flue gas at several full-scale coal-fired electric utility power plants.

Results of the EPRI sorbent development work showed that effective sorbents can be prepared from inexpensive precursor materials using simple activation steps. One notable example is that a char produced from corn fiber, a by-product from a corn-to-ethanol production process, showed a Hg<sup>0</sup> adsorption capacity over twice that of the commercial FGD carbon sorbent, after the char was activated in CO<sub>2</sub> at 865 °C for 3.5 hours.<sup>40</sup> Inactivated corn char had no capacity for HgCl<sub>2</sub>, and only a low capacity for Hg<sup>0</sup>. It appears that the composition of the flue gas has a significant effect on the Hg adsorption capacities of the coal-derived activated carbons.<sup>41</sup> The EPRI-funded study found that the presence of acid gases (SO<sub>2</sub> and HCl) inhibits Hg<sup>0</sup> and HgCl<sub>2</sub> adsorption for both lignite- and bituminous-coal-derived activated carbons. However, research conducted by EPA showed that the presence of acid gases enhanced the capture of Hg<sup>0</sup> by a lignite activated carbon and had no influence on the adsorption by a bituminous-coal-derived activated carbon.<sup>21</sup> In a later more extensive follow-up study funded by EPRI and ICCI, the effects of acid gases on the HgCl<sub>2</sub> and Hg<sup>0</sup> adsorption capacities of activated carbons were found to vary, depending on the precursor materials and characteristics of the carbons.<sup>43</sup> For example, carbons derived from tire and corn fiber had much higher HgCl<sub>2</sub> and Hg<sup>0</sup> adsorption capacities when they were tested in a high-SO<sub>2</sub> concentration flue gas simulating the combustion of Eastern bituminous coals compared to those when they were tested in the low-SO<sub>2</sub> concentration flue gas simulating Western subbituminous coal combustion. Complex interactions occurring between the characteristics of the carbons and the acid gases may lead to the observed varying effects of the acid gases on Hg adsorption behaviors of the carbon sorbents.

More fundamental research is needed to understand and predict the effects of acid gases on the performance of sorbents derived from different precursor materials.

The most effective sorbents were obtained by the sulfur-impregnation of activated carbons derived from waste material and carbon fibers.<sup>40</sup> Researchers at the University of Pittsburgh demonstrated that impregnation of heteroatoms such as sulfur<sup>44</sup> and chloride<sup>45</sup> is an effective method to improve the vapor-phase Hg adsorption capacities of activated carbons. It has been suggested that sorbent-impregnation studies should focus on highly microporous sorbents since the presence of active surface functional groups, sulfur as an example, in the micropores through impregnation is likely to provide the most reactive sites for Hg adsorption from coal combustion flue gas.<sup>19</sup> They stressed that the micropore surface area of sorbent is an important physical property for vapor-phase Hg adsorption. Most of the commercial activated carbons are used for liquid-phase applications and contain a large mesopore surface area, in addition to micropores, that are less effective for adsorption of ppb levels of Hg from coal combustion flue gases. EPA researchers<sup>46</sup> have observed the importance of active functional groups in the micropores for vapor-phase Hg adsorption. After treating an activated carbon with an aqueous sulfuric solution, they found that most of the mesopores of the carbon are filled with water due to the presence of the hygroscopic sulfuric acid, and the carbon becomes a highly microporous sorbent. The Hg<sup>0</sup> adsorption capacity of the sulfuric-acid-treated carbon is much higher than that of the as-received carbon due to the presence of the active sulfuric acid functional groups in the micropores of the treated carbon.

The most recent research conducted by ISGS, UI, and URS Corporation showed that relatively low surface area microporous biomass-based carbon sorbents, such as those derived from pistachio nut shells and from corn fiber, are as effective as the commercial FGD carbon sorbent for Hg adsorption.<sup>43</sup> They found that the Hg adsorption capacities of the biomass-based carbon sorbents, which contained negligible (0.09 percent) sulfur, are comparable to those of the coal- and tire-derived carbons that have substantial sulfur contents (0.98 to 2.1 percent). The biomass-based carbon sorbents also have very little chlorine functional groups. It appears that more oxygen, another heteroatom, remained in the biomass-based carbon sorbents after the pyrolysis of the oxygen-rich biomass from the carbon-making process contributing to the significant Hg adsorption capacities of such sorbents. It has been suggested recently by EPA researchers<sup>47</sup> that the Hg<sup>0</sup> adsorption capacity of an activated carbon is correlated to the concentrations of the oxygen functional groups of the carbon. They changed the oxygen functional group concentrations of a carbon by heating the carbon sample to 900 °C in an inert atmosphere to remove the functional groups. Also, more oxygen functional groups were introduced to the carbon sample by oxidizing the carbon sample in an aqueous nitric acid solution. They suggested that lactone and carbonyl groups introduced during the oxidation of the carbon by nitric acid treatment might be the active sites for Hg<sup>0</sup> adsorption.

#### *5.5.4 Modeling of Sorbent Performance*

The Hg adsorption data produced from bench-scale tests provide a relative indication of performance for different sorbents; however, the actual Hg removal performance of the sorbents in full-scale systems cannot be predicted based on bench-scale results alone. To predict Hg

removal in full-scale systems, mass transfer considerations have to be combined with laboratory data. Such an approach was applied by by EPRI recently to develop a model for predicting sorbent performance in full-scale systems.<sup>48</sup> The model is also capable of determining when mass transfer limits Hg removal and when it is limited by sorbent capacity. By incorporating the appropriate mass transfer expressions, the model relates the adsorption characteristic data for a given sorbent tested under a given set of flue gas conditions in the laboratory to the expected Hg removal performance across a FF or an ESP.

Results of the sorbent performance predicted by the model agree reasonably well with data of the same sorbent measured by pilot-scale tests for both ESP and FF applications. The pilot-scale facilities used for the tests consisted of an ESP with a 160-acfm wire-tube ESP, and a FF with a 4000-acfm transportable pulse-jet FF operating in the COHPAC configuration. Results of the pilot-scale tests and modeling both showed that a carbon sorbent with 15  $\mu\text{m}$  diameter and 1000  $\mu\text{g/g}$  Hg adsorption capacity achieved about 80 percent Hg removal in a FF operated at about 140 °C (280 °F) with 3 lb/Macf sorbent injection rate and cleaning cycle of 45 min. However, test and modeling results both showed that Hg removal decreases to less than 20 percent when the same sorbent was injected upstream of an ESP under conditions similar to the above.

Laboratory tests which have been conducted to evaluate the adsorption characteristics of potential sorbents for Hg removal seem to suggest that reactivity of the sorbent might be more important than its equilibrium adsorption capacity for sorbent injection. Currently, an ESP is more widely used than a FF as a PM control device for coal-fired electric utility boilers in the United States. Sorbent reactivity is the important parameter determining Hg removal when injecting a powdered sorbent upstream of an ESP, where adsorption of Hg occurs mainly in-flight with short residence times (about 2 seconds). When injecting sorbent upstream of a FF, additional Hg removal can occur due to the presence of accumulated sorbent in the filter cake, resulting in improved mass transfer and sorbent utilization. Sorbent capacity becomes a more important parameter than reactivity in such cases.

## 5.6 Capture of Mercury in Wet FGD Scrubbers

### 5.6.1 *Wet Scrubbing*

Mercuric chloride is readily soluble in water. Thus, the oxidized fraction of Hg vapors in flue gas is efficiently removed when a power plant is operated with a wet scrubber for removing  $\text{SO}_2$ . The elemental fraction, on the other hand, is insoluble and is not removed to any significant degree. A DOE-funded study<sup>49</sup> conducted by CONSOL, Inc. showed that the nominal Hg removal for wet FGD systems on units firing bituminous coals is approximately 55 percent, with the removal of  $\text{Hg}^{2+}$  between 80 and 95 percent. Studies conducted by McDermott Technologies, Inc. at its 10-MWe research facility suggested a possible conversion of the  $\text{Hg}^{2+}$  captured in the scrubbing media and reemissions as  $\text{Hg}^0$ .<sup>50</sup> McDermott Technologies performed follow up tests to investigate the use of additives to prevent the conversion of adsorbed  $\text{Hg}^{2+}$  to gaseous  $\text{Hg}^0$ .<sup>51</sup> These tests are described in more detail in Chapter 7.

### 5.6.2 Oxidation

The challenge to Hg removal in wet scrubbers for SO<sub>2</sub> is to find some way to oxidize the elemental Hg vapor before it reaches the scrubber or to modify the liquid-phase of the scrubber to cause oxidation to occur there.

URS Radian International has conducted various laboratory and field-test studies to investigate adsorption and catalytic oxidation of gaseous Hg<sup>0</sup> in coal-fired electric utility flue gas. The results of the bench-scale testing are discussed below. The additional pilot- and full-scale testing conducted by URS Radian International are discussed in Chapter 7.

Different compositions of catalysts and fly ashes were tested in a bench-scale, fixed-bed configuration to identify materials that adsorb and/or oxidize gaseous Hg<sup>0</sup>.<sup>52</sup> Mixing sand with a particular catalyst or fly ash created fixed beds of sorbents. A simulated coal-fired electric utility boiler flue gas containing gaseous Hg<sup>0</sup> was then passed through the bed. The flue gas was tested at the inlet and outlet of each sorbent bed to determine Hg adsorption and/or oxidation across the bed. Table 5-5 lists the simulated flue gas conditions and the most active catalysts and fly ashes identified during testing for oxidation of gaseous Hg<sup>0</sup>.

Figure 5-12 is an example of the adsorption/oxidation of gaseous Hg<sup>0</sup> with time by one of the iron catalysts in Table 5-5. In this figure, the oxidation of gaseous Hg<sup>0</sup> increases as the breakthrough of Hg from the catalyst bed increases (breakthrough is quantified as a percentage of the incoming Hg). At 100 percent breakthrough when the catalyst is no longer adsorbing any of the incoming Hg (i.e., the catalyst has reached its equilibrium adsorption capacity for the incoming Hg<sup>0</sup>), all of the Hg<sup>0</sup> passing through the bed is being oxidized to Hg<sup>2+</sup>.

Figure 5-13 shows adsorption/oxidation results for all of the catalysts in Table 5-5. Adsorption and oxidation of gaseous Hg<sup>0</sup> was greater at 149 °C (300 °F) than at the higher temperature of 371 °C (700 °F). The adsorption and oxidation activity of the activated carbon was considered the highest among the materials tested because a lower mass was utilized during the tests compared to the other materials.

Figure 5-14 shows the adsorption/oxidation results for the fly ashes from Table 5-5. Like the catalysts, the fly ashes showed higher adsorption and oxidation of gaseous Hg<sup>0</sup> at 149 °C (300 °F) than at 371 °C (700 °F); for this reason, only the lower temperature results are shown in Figure 5-14. The subbituminous and bituminous coal fly ashes generally showed higher oxidation rates than the lignite coal fly ashes. As seen, the #2 bituminous coal fly ash had varying adsorption and oxidation rates depending upon where the fly ash samples were collected. Samples collected from the hoppers of the first field of the ESP indicated lower oxidation of gaseous Hg<sup>0</sup> but a higher adsorption of Hg compared to the finer fly ash collected in the fifth and final field of the ESP. Although not shown, fly ash captured by a cyclone in the Hg speciation sampling train indicated a higher adsorption but no oxidation of the gaseous Hg<sup>0</sup>. Fly ash from the fifth field of the ESP indicated the highest rate of oxidation and the lowest size-fractionated particles. This may be associated with the size differences of the fly ash and/or the surface

**Table 5-5. Simulated flue gas conditions with the most active catalysts and fly ashes indicated for oxidation of gaseous Hg<sup>0</sup> to gaseous Hg<sup>2+</sup> (source: Reference 52)**

Parameter	Baseline Conditions	Most Active Catalysts	Most Active Fly Ashes
Fixed-bed Temperature	300 and 700 °F	Fe #1 (1000 mg)	Subbituminous #1
Hg <sup>0</sup> Injection	45 to 60 µg/Nm <sup>3</sup>	Pd #1 (1000 mg)	Subbituminous #2
Oxygen	7 percent	Fe #2 (200 mg)	Bituminous #1
Carbon Dioxide	12 percent	Fe #3 (200 mg)	Bituminous #2-Field 1 <sup>a</sup>
Moisture	7 percent	NO <sub>x</sub> Catalysts (1000 mg)	Bituminous #2-Field 5 <sup>a</sup>
Sulfur Dioxide	1600 ppmv	Fe #4 (1000 mg)	Bituminous #3
HCl	50 ppmv	Pd #2 (1000 mg)	Lignite #1
Gas Flow Rate	1 L/min	Carbon (20 mg)	Oil-Fired #1

(a) Fly ash collected at the first and fifth field of the ESP at the EPRI ECTC.

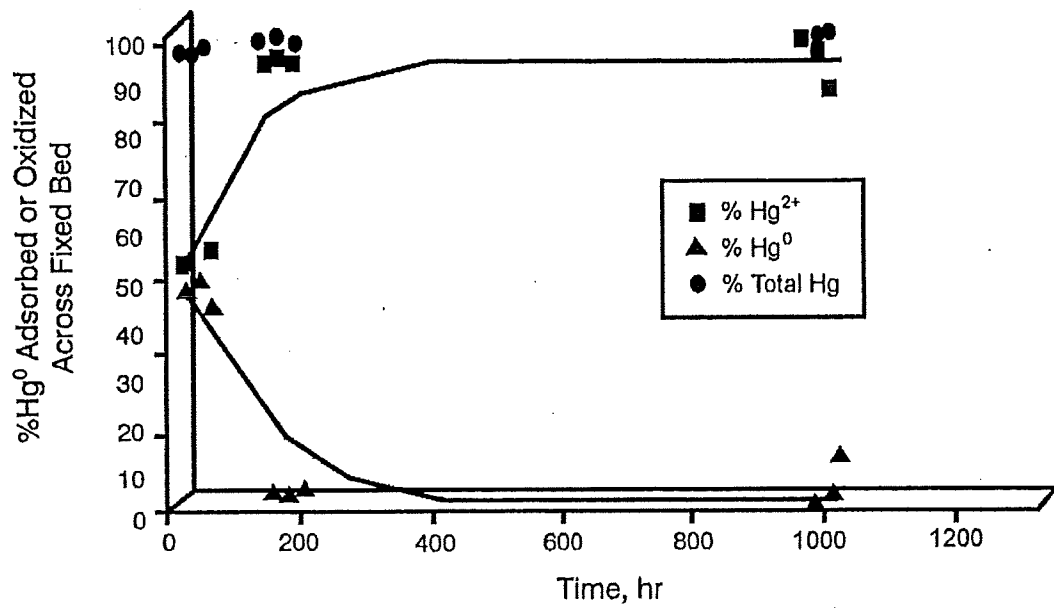


Figure 5-12. Adsorption and subsequent oxidation of gaseous Hg<sup>0</sup> in a simulated flue gas at 149°C (300 °F) (source: Reference 52).

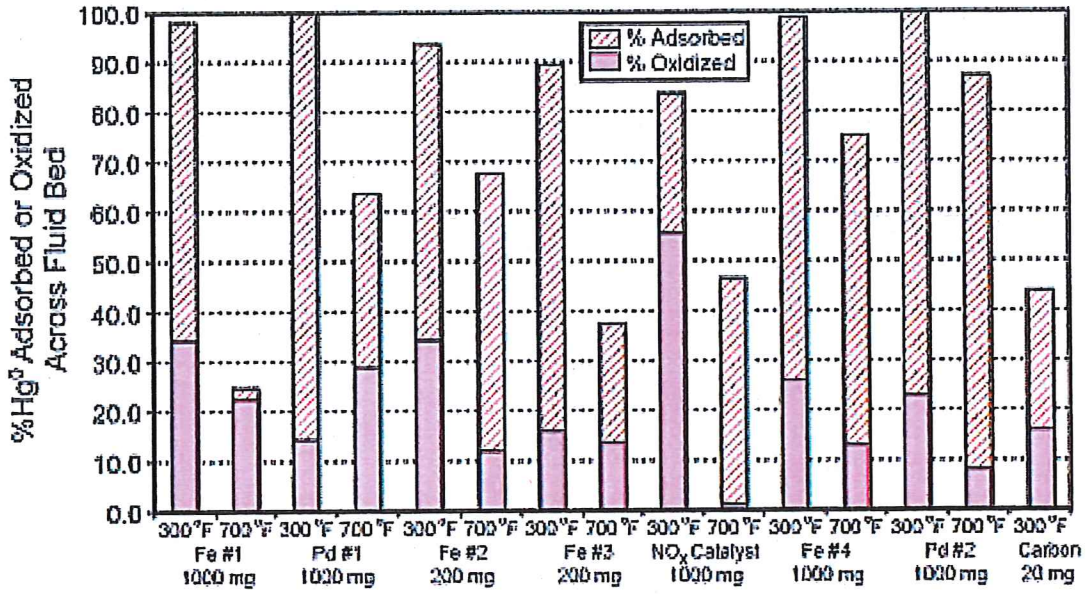


Figure 5-13. Adsorption and oxidation of gaseous Hg<sup>0</sup> by various catalysts at 149 °C (300 °F) and 371 °C (700 °F) (source: Reference 52).

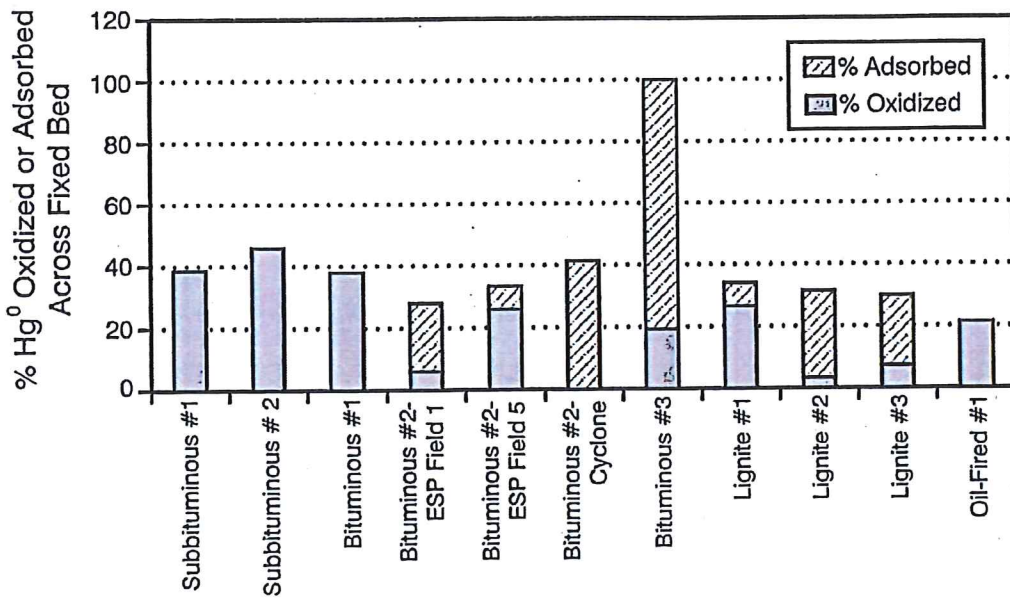


Figure 5-14. Adsorption and oxidation of gaseous  $Hg^0$  by various coal fly ashes at 149 °C (300 °F) and 371 °C (700 °F) (source: Reference 52).

chemistry of the finer fly ash being enriched in trace metals or other condensed or adsorbed compounds from the flue gas during the combustion of the bituminous coal.

### 5.6.3 Gas and Liquid Oxidation Reagents

Argonne National Laboratory has been investigating the use of oxidizing agents that could potentially convert gaseous  $\text{Hg}^0$  into more soluble species that would be absorbed in wet FGD systems.<sup>53</sup> Current research is focused on a process concept that involves introduction of an oxidizing agent into the flue gas upstream of the scrubber. The oxidizing agent employed is NOXSORBI, which is a commercial product containing chloric acid and sodium chlorate. When a dilute solution of this agent was introduced into a gas stream containing gaseous  $\text{Hg}^0$  and other typical flue-gas species at 300 °F (149 °C), it was found that nearly 100 percent of the gaseous  $\text{Hg}^0$  was removed from the gaseous phase and recovered in process liquids. A significant added benefit was that approximately 80 percent of the NO was removed at the same time. Thus, the potential exists for a process that combines removal of  $\text{SO}_2$ , NO,  $\text{Hg}^0$ , and, perhaps, PM.

Continuing laboratory research efforts are acquiring the data needed to establish a mass balance for the process. In addition, the effects of such process parameters as reagent concentration,  $\text{SO}_2$  concentration, NO concentration, and reaction time (residence time) are being studied. For example,  $\text{SO}_2$  has been found to decrease slightly the amount of gaseous  $\text{Hg}^0$  oxidized while appearing to increase the removal of NO from the gaseous phase. Preliminary economic projections, based on the results to date, indicate that the chemical cost for NO oxidation could be less than \$5,000/ton NO removed; while for gaseous  $\text{Hg}^0$  oxidation, it would be about \$20,000/lb  $\text{Hg}^0$  removed. These results will be refined as additional experimental results are obtained.

## 5.7 Observations and Conclusions

When coal is burned in an electric utility boiler, the resulting high combustion temperatures in the vicinity of 1500 °C (2700 °F) vaporize the Hg in the coal to form gaseous  $\text{Hg}^0$ . Subsequent cooling of the combustion gases and interaction of the gaseous  $\text{Hg}^0$  with other combustion products result in a portion of the Hg being converted to other forms, viz.,  $\text{Hg}^{2+}$  and  $\text{Hg}_p$ . The term *speciation* is used to denote the relative amounts of these three forms of Hg in the flue gas of the boiler. It is important to understand how Hg speciates in the boiler flue gas because, as discussed in Chapters 6 and 7, the overall effectiveness of different control strategies for capturing Hg often depends on the concentrations of the different forms of Hg species present in the boiler flue gas.

The speciation of Hg results from oxidation of  $\text{Hg}^0$  in the boiler flue gas, with the predominant oxidized Hg species believed to be  $\text{HgCl}_2$ . The mechanisms for this oxidation include gas-phase oxidation, fly-ash-mediated oxidation, and oxidation by post-combustion  $\text{NO}_x$  controls. Data reveal that gas-phase oxidation is kinetically limited and occurs due to reactions

of Hg with oxidizers such as Cl and Cl<sub>2</sub>. Research also suggests that gas-phase oxidation may be inhibited by the presence of NO, SO<sub>2</sub>, and water vapor.

Certain fly ashes have been shown to promote oxidation of Hg<sup>0</sup> more than others. The differences in oxidation appear to be attributable to the composition of the fly ash and the presence of certain flue gas constituents. The results of bench-scale research conducted at EPA reflect that the presence of HCl and NO<sub>x</sub> in flue gas and iron in fly ash assists in oxidation. Other research indicates that γ-Fe<sub>2</sub>O<sub>3</sub> may be causing Hg<sup>2+</sup> formation, and that surface area may be a dominant factor in this regard. Also, there are indications that HCl, NO<sub>2</sub>, and SO<sub>2</sub> in the flue gas may contribute to Hg<sup>0</sup> oxidation, while the presence of NO may suppress Hg<sup>0</sup> oxidation.

The understanding of Hg speciation in the flue gas of coal-fired electric utility boilers is far from being mature, and research and development efforts are currently underway to develop more information.

Mercury can be captured and removed from a flue gas stream by injection of a sorbent into the exhaust stream with subsequent collection in a PM control device such as an electrostatic precipitator or a fabric filter. However, adsorptive capture of Hg from flue gas is a complex process that involves many variables. These include the temperature and composition of the flue gas, the concentration of Hg in the exhaust stream, and the physical and chemical characteristics of the sorbent (and associated functional group). The implementation of an effective and efficient Hg control strategy using sorbent injection requires the development of low-cost and efficient Hg sorbents. Of the known Hg sorbents, activated carbon and calcium-based sorbents have been the most actively studied. However, improved versions of these sorbents and new classes of Hg sorbents can be expected, as this is still a very active field of study.

Adsorption of elemental Hg is enhanced by the presence of functional groups and/or catalytically active sites (that oxidize the Hg to Hg<sup>2+</sup>). Oxidation of elemental Hg to ionic species by the catalytic components that may be present in fly ash (especially iron compounds) is a critical step before adsorption of the species by the fly ash or some injected sorbents. Both the oxidant and binding sites for the adsorption of elemental Hg may also be provided by the injected sorbents. Also, alkaline components of the fly ash exhibit sorptive properties for oxidized Hg. Fly ashes, which contain higher unburned carbon contents, such as those produced from low-NO<sub>x</sub> burner systems, may have significant catalytic and sorptive properties. The unburned carbon appears to have some oxidant/adsorption sites similar to those that existed in the activated carbon sorbents.

Activated carbon binding sites may be enhanced by impregnation with an active additive (e.g., S, Cl, I) or pretreatment (e.g., with H<sub>2</sub>SO<sub>4</sub> or HCl). It appears that the presence of heteroatoms, such as sulfur and chlorine, on the activated carbon surfaces greatly enhance the adsorption of Hg. Other non-carbon-based sorbents may be enhanced by oxidant/catalyst additions. The enhancement is caused by the oxidation of the elemental Hg either by the added oxidant or by the added catalyst to the sorbents. A promising alternative appears to be the replacement of the coal-based activated carbons with a low cost, high-capacity, reactive sorbent. Such sorbents are currently under development.

Oxidized Hg is readily absorbed by alkaline solutes/slurries or adsorbed by alkaline PM (or by sorbents). Flue gas desulfurization systems, which use alkaline materials to neutralize the acidic SO<sub>2</sub> gas, remove oxidized Hg effectively in the flue gas. Current research is focusing on optimization of the existing desulfurization systems as a retrofit technology for controlling oxidized Hg emissions and on development of new multipollutant control technologies for simultaneously controlling both SO<sub>2</sub> and oxidized Hg emissions.

## 5.8 References

1. Senior, C.L., A.F. Sarofim, T. Zong, J.J. Helble, and R. Mamani-Paco. Gas phase transformation of mercury in coal-fired power plants. *Fuel Processing Technology*, 63, (2-3): 197-214 (2000).
2. Senior, C.L., L.E. Bool, J. Morency, F. Huggins, G.P. Huffman, N. Shah, J.O.L. Wendt, F. Shadman, T. Peterson, W. Seames, B. Wer, A.F. Sarofim, I. Olmeze, T. Zeng, S. Growley, A. Kolker, C.A. Palmer, R. Finkelman, J.J. Helble, and M.J. Wornat. *Toxic substances from coal combustion – a comprehensive assessment*. Physical Science, Inc., Final Report (Contract No. DE-AC-22-95, PC 951011, U.S. Department of Energy, Federal Energy Technology Center). September 1997.
3. Senior, C.L., J.J. Helble, and A.F. Sarofim. "Predicting the speciation of mercury emissions from coal-fired power plants." Paper presented at the *Conference on Air Quality II: Mercury, Trace Elements, and Particulate Matter*, McLean, VA. September 19-21, 2000.
4. Ghorishi, S.B., C.W. Lee, and J.D. Kilgroe. "Mercury speciation in combustion systems: studies with simulated flue gases and model fly ashes." Paper presented at the *92nd Annual Meeting of Air & Waste Management Association*, St. Louis, MO. June 20-24, 1999.
5. Edwards, J.R., R.K. Srivastava, and J.D. Kilgroe. A study of gas-phase mercury speciation using detailed chemical kinetics. Published in *Journal of Air & Waste Management Association*, 5: 869-877 (2001).
6. Niksa, S., J.J. Helble, and N. Fujiwara. "Interpreting laboratory test data on homogeneous mercury oxidation in coal-derived exhausts." Paper presented 94th Annual Meeting of the Air & Waste Management Association, Paper # 86, Orlando, FL. June 24 -28, 2001.
7. Lee, C. W., J.D. Kilgroe, and S.B. Ghorishi. "Speciation of mercury in the presence of coal and waste combustion fly ashes." Presented at the 93<sup>rd</sup> Annual Meeting of the Air & Waste Management Association, Salt Lake City, UT. June 18-22, 2000.
8. Lee, C.W., R.K. Srivastava, J.D. Kilgroe, and S.B. Ghorishi. "Effects of iron content in coal combustion fly ashes on speciation of mercury." Paper presented at the 94th Annual Meeting of the Air & Waste Management Association, Paper # 156, Orlando, FL. June 24 -28, 2001.

9. Galbreath, K.C., C.J. Zygarlicke, D.L. Toman, and R.C. Schulz. "Effects of NO<sub>x</sub> and α-Fe<sub>2</sub>O<sub>3</sub> on mercury transformations in a 7-kW coal combustion system." Paper presented at the 94th Annual Meeting of the Air & Waste Management Association, Paper # 767, Orlando, FL. June 24 -28, 2001.
10. Norton, G.A., H. Yang, R.C. Brown, D.L. Laudal, G.E. Dunham, J. Erjave, and J.M. Okoh. "Role of fly ash on mercury chemistry in simulated flue gas streams." Paper presented at the 94th Annual Meeting of the Air & Waste Management Association, Paper # 164, Orlando, FL. June 24 -28, 2001.
11. Haythornthwaite, S., S. Sjoström, T. Ebner, J. Ruhl, R. Slye, J. Smith, T. Hunt, R. Chang, and T.D. Brown. "Demonstration of dry carbon-based sorbent injection for mercury control in utility ESP's and baghouses." In Proceedings of the EPRI/DOE/EPA Combined Utility Air Pollutant Control Symposium, EPRI TR-108683-V3; Washington, DC. August 25-29, 1997.
12. Laudal, D.L., M.K. Heidt, T.D. Brown, and B.R. Nott. "Mercury speciation: a comparison between method 29 and other sampling methods." Presented at the 89<sup>th</sup> Annual Meeting of the Air & Waste Management Association, Nashville, TN, Paper 96-W64A.04. June 1996.
13. Brown, T. D., D.N. Smith, R.A. Hargis, Jr., and W.J. O'Dowd. "1999 Critical Review: Mercury Measurement and Its Control: What We Know, Have Learned, and Need to Further Investigate," *Journal of the Air & Waste Management Association*, June 1999. pp. 1-97. Available at: < <http://www.lanl.gov/projects/cctc/resources/pdfsmisc/haps/CRIT991.pdf> >.
14. Li, Z., and J.Y. Hwang. "Mercury distribution in fly ash compounds." Presented at the Air & Waste Management Association Annual Meeting, Toronto, Ontario, Canada. June 8-13, 1997.
15. Huggins, F.E., N. Yap, G.P. Huffman, and J.K. Neathery. "Investigation of mercury adsorption on Cherokee fly-ash using XAFS spectroscopy." Presented at the 93<sup>rd</sup> Annual Meeting of the Air & Waste Management Association, Salt Lake City, UT. June 18-22, 2000.
16. Carey, T.R., O.W. Hargrove, Jr., C.F. Richardson, R. Chang, F.B. Meserole. *Performance of Activated Carbon for Mercury Control in Utility Flue Gas Using Sorbent Injection*, In Proceedings of the EPRI/DOE/EPA Combined Utility Air Pollutant Control Symposium, Washington, DC; EPRI TR-108683-V3. August 25B29, 1997.
17. Galbreath, K.C., and C.J. Zygarlicke. Mercury transformation in coal combustion flue gas. *Fuel Processing Technology*, 65-66: 289-310 (2000).

18. Brunauer, S., P.H. Emmett, and E. Teller, *J. Am. Chem. Soc.*, 60, 309. 1938.
19. Hsi C., J. Rood, M. Rostam-Abadi, S. Chen, and R. Chang. "Effects of sulfur impregnation temperature on the properties and mercury adsorption capacities of activated carbon fibers (ACFs)." *Environmental Science and Technology*, 35, 2785-2791. 2001.
20. Bansal R.C., J.B. Donnet, and F. Stoecki. *Active Carbon*. New York, NY, and Basel, Switzerland: Marcel Dekker. 1988.
21. Ghorishi, S.B., and B.K. Gullett. Sorption of mercury species by activated carbons and calcium-based sorbents: effect of temperature, mercury concentration and acid gases. *Waste Management & Research*, 16: 6: 582-593. 1998.
22. Krishnan, S.V., B.K. Gullett, and W. Jozewicz. Sorption of Elemental Mercury by Activated Carbons. *Environmental Science and Technology*, 28(8): 1506-1512 (1994).
23. Serre, S.D., B.K. Gullett, and S.B. Ghorishi. Entrained-flow adsorption of mercury using activated carbon. *Journal of the Air & Waste Management Association*, 51: 733-741 (May 2001).
24. Helfritch, D.G., P.L. Feldman, and S.J. Pass. "A circulating fluid bed fine particulate and mercury control concept." Presented at the *EPRI/DOE/EPA Combined Utility Air Pollutant Control Symposium*, Washington DC. August 1997.
25. Hargis, R.A., W.J. O'Dowd, and H.W. Pennline. "Sorbent injection for mercury removal in a pilot-scale coal combustion unit." Presented at the 93<sup>rd</sup> Annual Meeting of the Air & Waste Management Association, Salt Lake City, UT. June 18-22, 2000.
26. Waugh, E.G., B.K. Jenson, L.N. Lapatrack, F.X. Gibbons, S. Sjostrom, J. Ruhl, R. Slye, and R.A. Chang. "Mercury control in utility ESP's and FFs through dry carbon based sorbent injection pilot-scale demonstration." In *Proceedings of the EPRI/DOE/EPA Combined Utility Air Pollutant Control Symposium*. Washington, DC, EPRI TR-108683-V3). August 23-29, 1997.
27. Carey, T.R., C. Richardson, R. Chang, and F.B. Meserole. "Assessing sorbent injection mercury control effectiveness." Paper presented at the 1999 Spring National Meeting of the American Institute of Chemical Engineers, Houston, TX. March 14-18, 1999.
28. Sjostrom, S., T. Ebner, T. Ley, R. Slye, C. Richardson, T. Machalek, M. Richardson, R. Chang, and F. Meserole. "Assessing the performance of mercury sorbents in coal combustion flue gas." Paper presented at the 94<sup>th</sup> Annual Meeting of the Air & Waste Management Association, Orlando, FL. June 24-28, 2001.

29. Rostam-Adadi, M., S.G. Chen, H-C. His, M. Rood, R. Chang, T. Carey, B. Hargrove, C. Richardson, W. Rosenhoover, and F. Meserole. "Novel vapor phase mercury sorbents." In *Proceedings of the First EPRI/DOE/EPA Combined Utility Air Pollution Control Symposium* (The Mega Symposium), Washington, DC, August 25-29, 1997.
30. White, D.M., W.E. Kelly, M.J. Stucky, J.L. Swift, and M.A. Palazzolo. *Emission test report: field test of carbon injection for mercury control, Camden County Municipal Waste Combustor*, EPA/600/R-93/181 (NTIS PB94-101540), U.S. EPA, Air and Energy Engineering Research Laboratory, Research Triangle Park, NC. September 1993.
31. Serre, S.D., B.K. Gullett, and S.B. Ghorishi. "Elemental mercury capture by activated carbon in a flow reactor." Paper presented at 93<sup>rd</sup> Annual Meeting of the Air & Waste Management Association, Salt Lake City, UT. June 18-22, 2000.
32. Serre, S.D., B.K. Gullett, and Y. H. Li. "The effect of water (vapor-phase and carbon) on elemental mercury removal in a flow reactor." Paper presented at 94th Annual Meeting of the Air & Waste Management Association, Paper # 164, Orlando, FL. June 24 -28, 2001.
33. Ghorishi, S.B., R. Keeney, W. Jozewicz, S. Serre, and B. Gullett. "In-flight capture of elemental mercury by a chlorine-impregnated activated carbon." Paper # 731 presented at the 94th Annual Meeting of Air & Waste Management Association, Orlando, FL. June 24-28, 2001.
34. Brown, T. D., D.N. Smith, R.A. Hargis, Jr., and W.J. O'Dowd. "1999 Critical Review: Mercury Measurement and Its Control: What We Know, Have Learned, and Need to Further Investigate," *Journal of the Air & Waste Management Association*, June 1999. pp. 1-97.
35. Ghorishi, S.B., R.M. Keeney, and B.K. Gullett. "Role of surface functional groups in the capture of elemental mercury and mercuric chloride by activated carbons." In *Proceedings of the Air Quality II Conference*, McLean, VA. September 19-21, 2000.
36. Gullett, B.K., S.B. Ghorishi, K. Raghunathan, and K. Ho. *Removal of Coal-Based Volatile Trace Elements: Mercury and Selenium*, Final Technical Report. September 1, 1995, through August 31, 1996.
37. Ghorishi, S.B., and C.B. Sedman. "Combined Mercury and Sulfur Oxides Control Using Calcium-Based Sorbents." Paper presented at the EPRI/DOE/EPA Combined Utility Air Pollutant Control Symposium, Washington, DC. August 25-29, 1997.
38. Ghorishi, S.B., and C.B. Sedman. Low concentration mercury sorption mechanisms and control by calcium-based sorbents: application in coal-fired processes, *Journal of the Air & Waste Management Association*, 48: 1191-1198, 1998.

39. Ghorishi, S.B., C. Singer, W. Jozewicz, C. Sedman, and R. Srivastava. "Simultaneous control of Hg<sup>0</sup>, SO<sub>2</sub>, and NO<sub>x</sub> by novel oxidized calcium-based sorbents." Paper # 243, Presented at the 94th Annual meeting of the Air & Waste Management Association. June 24-28, Orlando, FL, 2001.
40. EPRI Report 1000454. Development and evaluation of low cost mercury sorbents. November 2000.
41. EPRI Report TE-114043. Development and evaluation of mercury sorbents. November 1999.
42. EPRI Report TR-110532. Development and evaluation of low-cost sorbents for removal of mercury emissions from coal combustion flue gas. September 1998.
43. Rostam-Abadi, M., S. Chen, A.A. Lizzio, H-C. His, C.M.B. Lehmann, M. Rood, R. Chang, C. Richardson, T. Machalek, and M. Richardson. "Development of low-cost sorbents for mercury removal from utility flue gas." Paper presented at U.S. EPA/DOE/EPRI Combined Power Plant Air Pollutant Control Symposium, and the Air & Waste Management Association Specialty Conference on Mercury Emissions: Fate, Effects, and Control, Chicago, IL. August 20-23, 2001.
44. Korpiel, J.A., and R.D. Vidic. Effect of sulfur impregnation method on activated carbon uptake of gas-phase mercury. *Environmental Science and Technology*, 31: 2319-2326 (1997).
45. Vidlic, R. D. and D.P. Siler. Vapor-phase elemental mercury adsorption by activated carbon impregnated with chloride and chelating agents. *Carbon*. 3-14 (2001).
46. Li, Y. H., S.D. Serre, C.W Lee, and B.K. Gullett. "Elemental mercury adsorption by activated carbon treated with sulfuric acid." Presented at the U.S. EPA/DOE/EPRI Combined Power Plant Air Pollutant Control Symposium, and the Air & Waste Management Association Specialty Conference on Mercury Emissions: Fate, Effects, and Control, Chicago, IL. August 20 -23, 2001.
47. Li, Y. H., C.W. Lee, and B.K. Gullett. "Characterization of activated carbons' physical and chemical properties in relation to their mercury adsorption." Presented at the American Carbon Society CARBON '01, An International Conference on Carbon, University of Kentucky Center for Applied Energy Research, Lexington, KY. July 14 - 19, 2001.
48. Meserole, F., C. F. Richardson, T. Machalek, M. Richardson, and R. Chang. "Predicted Costs of Mercury Control at Electric Utilities Using Sorbent Injection." Presented at U. S. EPA/DOE/EPRI Combined Power Plant Air Pollutant Control Symposium, and the Air & Waste Management Association Specialty Conference on Mercury Emissions: Fate, Effects, and Control, Chicago, IL, August 20-23, 2001.

49. DeVito, M.S., and W.A. Rosenhoover. "Hg flue gas measurements from coal-fired utilities equipped with wet scrubbers." Presented at 92<sup>nd</sup> Annual Meeting of the Air & Waste Management Association, St. Louis, MO. June 20-24, 1999.
50. Redinger, K.E., A. Evans, R. Bailey, and P. Nolan. "Mercury emissions control in FGD systems." Presented at the EPRI/DOE/EPA Combined Air Pollutant Control System, Washington, DC. August 25-29, 1997.
51. McDermott Phase III Study Section, McDermott Technologies, Inc. *Advanced Emissions Control Development Program Phase III - Approved Final Report*, prepared for the U.S. Department of Energy (US DOE-FETC contract DE-FC22-94PC94251-22) and Ohio Coal Development Office (grant agreement CDO/D-922-13). July 1999. Available at: < <http://www.osti.gov/dublincore/servlets/purl/756595-LACvcL/webviewable/756595.pdf> >.
52. Hargrove, O.W., Jr., T.R. Carey, C.F. Richardson, R.C. Sherupa, F.B. Meserole, R.G. Rhudy, and T.D. Brown. "Factors affecting control of mercury by wet FGD." Paper presented at the EPRI/DOE/EPA Combined Utility Air Pollutant Control Symposium. Washington DC. August 25-29, 1997.
53. Livengood, C.D., and M.H. Mendelsohn. "Process for combined control of mercury and nitric oxide." Presented at the EPRI/DOE/EPA Combined Utility Air Pollutant Control Symposium, Atlanta, GA. August 16-20, 1999.

## Investigation of Mercury Transformation by HBr Addition in a Slipstream Facility with Real Flue Gas Atmospheres of Bituminous Coal and Powder River Basin Coal

Yan Cao,\*† Quanghai Wang,† Chien-wei Chen,† Bobby Chen,† Martin Cohron,†  
Yi-chuan Tseng,†‡ Cheng-chung Chiu,†‡ Paul Chu,§ and Wei-Ping Pan†

*Institute for Combustion Science and Environmental Technology, Western Kentucky University,  
Bowling Green, Kentucky 42101, Mingchi University of Technology, Taipei, Taiwan, and Electric Power  
Research Institute, Palo Alto, California 94304*

Received November 2, 2006. Revised Manuscript Received July 3, 2007

An investigation of speciated mercury transformation with the addition of hydrogen bromide (HBr) at elevated temperatures was conducted in a slipstream reactor with real flue gas atmospheres. A real flue gas atmosphere is composed of bituminous coal (with high sulfur and high chlorine contents) and Powder River Basin (PRB) coal (with lower sulfur and chlorine contents). The average sulfur, chlorine, and mercury contents in the tested bituminous coal were 1.31% and 1328 and 0.11 ppm and 0.61% and 170 and 0.08 ppm, respectively, for tested PRB coal. The average CaO, Fe<sub>2</sub>O<sub>3</sub>, and loss on ignition in collected fly ash contents of tested bituminous coal were 1.71, 17.51, and 7.13% and 22.95, 4.91, and 0.64%, respectively, for tested PRB coal. The different contents of coal chlorine, CaO, and Fe<sub>2</sub>O<sub>3</sub> in fly ash can be attributed to the different mercury speciations at baseline tests for these two coals in this study. The addition of HBr concentrations into the flue gas was controlled in the 3–15 ppm range. Semi-continuous mercury emission monitors were used to check the variation of mercury speciation at sampling locations. The Ontario Hydro Method (ASTM D6784-02) was used for data validation or comparison. For both methods, a high temperature inertial sampling probe was used to minimize the interference between vapor phase mercury and fly ash. Its temperatures were controlled consistently with flue gas temperatures at their installation locations in the slipstream reactor. Test results indicated that adding HBr into the flue gas at several parts per million strongly impacted the mercury oxidation and adsorption, which were dependent upon temperature ranges. Higher temperatures (in the range of 300–350 °C) promoted mercury oxidation by HBr addition but did not promote mercury adsorption. Lower temperatures (in a range of 150–200 °C) enhanced mercury adsorption on the fly ash by adding HBr. Test results also verified effects of flue gas atmospheres on the mercury oxidation by the addition of HBr, which included concentrations of chlorine and sulfur in the flue gas. Chlorine species seemed to be involved in the competition with bromine species in the mercury oxidation process. With the addition of HBr at 3 ppm at a temperature of about 330 °C, the additional mercury oxidation could be reached by about 55% in a flue gas atmosphere by burning PRB coal in the flue gas and by about 20% in a flue gas by burning bituminous coal. These are both greater than the maximum gaseous HgBr<sub>2</sub> percentage in the flue gas (35% for PRB coal and 5% for bituminous coal) by thermodynamic equilibrium analysis predictions under the same conditions. This disagreement may indicate a greater complexity of mercury oxidation mechanisms by the addition of HBr. It is possible that bromine species promote activated chlorine species generation in the flue gas, where the kinetics of elemental mercury oxidation were enhanced. However, SO<sub>2</sub> in the flue gas may involve the consumption of the available activated chlorine species. Thus, the higher mercury oxidation rate by adding bromine under the flue gas by burning PRB coal may be associated with its lower SO<sub>2</sub> concentration in the flue gas.

### 1. Introduction

Mercury emissions are regarded as one of the world's most problematic environmental issues because of their propensity to bioaccumulate by up to a factor of 10 000 within an aquatic food chain. Mercury, after bioaccumulation, will result in neuron damage in human beings.<sup>1</sup> A report for Congress from the U.S. Environmental Protection Agency (U.S. EPA) estimated that 80% of total anthropogenic mercury emissions from 1994 to

1995 were from combustion, of which 33% was associated with coal-fired utility boilers.<sup>2</sup> The EPA announced its final regulation on mercury emissions from coal-fired utility boilers in March 2005. This regulation stated that yearly mercury emissions will be reduced by 20.8% by 2010 and 68.8% by 2018 from levels in 1999 when this regulation was fully implemented.<sup>3</sup>

Mercury occurs in the flue gas of coal-fired utility boilers in three valence states: elemental mercury Hg(0), oxidized mercury

\* Corresponding author. E-mail: yan.cao@wku.edu.

† Western Kentucky University.

‡ Mingchi University of Technology.

§ Electric Power Research Institute.

(1) Westoo, G. Methylmercury as a Percentage of Total Mercury in Flesh and Viscera of Salmon and Sea Trout of Various Ages. *Science* 1973, 181, 567–568.

(2) Keating, M. H.; Mahaffey, K. R.; Schoeny, R.; Rice, G. E.; Bullock, O. R.; Ambrose, R. B., Jr.; Swartout, J.; Nichols, J. W. *Mercury Study Report to Congress*; EPA-452/R-97-003; 010' U.S. Environmental Protection Agency, Office of Air Quality Planning and Standard and Office of Research Development: Research Triangle Park, NC, 1997; Vols. I–VIII.

(3) U.S. Environmental Protection Agency. *Clean Air Mercury Rules*, March 2005; <http://www.epa.gov/mercuryrule/index.htm>.

Hg(2+), and particle-bound mercury Hg(P). Elemental mercury constitutes a global environmental issue because of its relative stability, its relative water insolubility, and its long-range transport in the atmosphere. Oxidized and particle-bound mercury produces risks to humans and the immediate environment because of its local deposition and water solubility. Studies on speciated mercury transformation in flue gas are critical to their environmental impacts and technical availabilities for effective control by Air Pollution Control Devices (APCDs) in utility boilers, such as a cold-side electric precipitator (ESP), a fabric filter (FF), and wet flue gas desulfurization (W-FGD). It was reported that cold-ESP and FF can capture Hg(P), W-FGD can capture Hg(2+) efficiently, and SCR can help to enhance Hg(0) oxidation.<sup>4-8</sup> Thus, the combination of SCR, W-FGD, and ESP or FF in coal-fired power utilities may be the economic means for mercury emission control with simultaneous abatement of SO<sub>x</sub> and NO<sub>x</sub>.

However, the U.S. EPA ICR Hg emission database and other field tests regarding the potential effects of combining SCR and W-FGD on mercury capture indicated an increased mercury capture when bituminous coals were burned but not when PRB coal or lignite was burned.<sup>4</sup> PRB coal or lignite is plentiful in the south central (Texas) and north central (Wyoming, Montana, and South Dakota) areas of the U.S. where lower sulfur and chlorine are present. A lower chlorine content in PRB and Texas lignite may be associated with their failure to enhance Hg(0) oxidation by SCR. On the other hand, mercury emission control using SCR to enhance the Hg(0) oxidation was dependent upon using a W-FGD to subsequently capture the Hg(2+). It was reported that only about 25% of utility boilers had a W-FGD installed for SO<sub>x</sub> control.<sup>4</sup> In comparison, 80% of utility boilers is equipped with a cold-ESP to control particle emission. Thus, methods to effectively convert Hg(0) to Hg(2+) or Hg(0) to Hg(P) are welcomed by a majority of utility owners who rely on these APCDs for simultaneous mercury emission control (especially those that use low sulfur PRB coal and lignite). Activated carbon injection (ACI) has been a prevailing technology for mercury control with a cold-ESP or other particle control devices available in coal-fired power plants.<sup>9-13</sup> However,

adding carbon to fly ash complicates the subsequent use of fly ash as an additive for cement production. Therefore, non-carbon based mercury adsorbents are being developed.<sup>14-16</sup> Whatever adsorbents are developed and utilized in coal-fired power plants, an additional expense will be added to the cost of electricity generation due to the higher cost of adsorbents and the unexpected control efficiency.

A new concept has been put forward that adds chemicals, such as bromine compounds, to flue gas to significantly enhance the mercury oxidation (from Hg(0) to Hg(2+)) or enhance its bonding to fly ash (Hg(P)).<sup>17,18</sup> However, the mercury transformation mechanism by adding bromine in the coal-fired flue gas atmosphere is not entirely understood. It is reported that the possible reaction routines of mercury and halogen species in atmospheric conditions are a photochemistry reaction mechanism,<sup>19-23</sup> which cannot be directly extended to that under the high temperature environment of coal-fired utility boilers. Mercury chemistry is highly dependent upon its interaction with fly ash and some unknown species in the flue gas, indicating that there are significant benefits to conducting tests using real flue gas. The greatest benefit of smaller pilot-scale slipstream tests is the ability to control variables and isolate specific factors. This paper attempts to answer several questions concerning mercury speciation chemistry under bromine addition using a pilot-scale slipstream facility with real flue gases. Two test sites that burn bituminous and sub-bituminous coal were selected. Because of the complexity of speciation prediction during coal combustion within such a multicomponent and multiphase system, thermodynamic equilibrium calculations<sup>24-26</sup> were also

(4) Kilgroe, J. D.; Sedman, C. B.; Srivastava, R. K.; Ryan, J. V.; Lee, C. W.; Thorneloe, S. A. *Control of Mercury Emission from Coal-Fired Electric Utility Boilers*; Interim Report EPA-600/R-01-109; U.S. Environmental Protection Agency: Washington, DC, 2001.

(5) Chu, P.; Laudal, D.; Brickett, L.; Lee, C. W. *Power Plant Evaluation of the Effect of SCR Technology on Mercury*, Presented at the Department of Energy-Electric Power Research Institute U.S. Environmental Protection Agency Air and Waste Management Association Combined Power Plant Air Pollutant Control Symposium, The Mega Symposium, Washington, D.C., May 19-22, 2003; paper 106.

(6) Richard, C.; Machalek, T.; Miller, S.; Dene, C.; Chang, R. *Effect of NO<sub>x</sub> Control Processes on Mercury Speciation in Flue Gas*, Presented at the Air Quality III Meeting, Washington, DC, September 10-13, 2002.

(7) Laudal, D. L.; Thompson, J. S.; Pavlish, J. H.; Brickett, L.; Chu, P.; Srivastava, R. K.; Lee, C. W.; Kilgore, J. Mercury Speciation at Power Plants Using SCR and SNCR Control Technologies. *EM* 2003.

(8) Hocquel, M. *The Behavior and Fate of Mercury in Coal-Fired Power Plants with Downstream Air Pollution Control Devices*; Forsch.-Ber. VDI Verlag: Dusseldorf, Germany, 2004.

(9) Holmers, M. J.; Pavlish, J. H.; Zhang, Ye.; Benson, S. A.; Frize, M. J. Pilot-Scale Evaluation of Activated Carbon-Based Mercury Control Options for Utilization Burning Lignite Coal. *Prepr. Pap.-Am. Chem. Soc., Div. Fuel Chem.* 2004, 49, 281.

(10) Measerole, F. B.; Chang, R.; Carey, T. R.; Machac, J.; Richardson, C. F. Modeling Mercury Removal by Sorbent Injection. *J. Air Waste Manage. Assoc.* 1999, 49, 694-704.

(11) Serre, S. D.; Gullett, B. K.; Ghorishi, S. B. Entrained-Flow Adsorption of Mercury Using Activated Carbon. *J. Air Waste Manage. Assoc.* 2001, 51, 733-741.

(12) Olson, E. S.; Crocker, C. R.; Benson, S. A.; Pavlish, J. H.; Holmers, M. J. Surface Compositions of Carbon Sorbents Exposed to Simulated Low-Rank Coal Flue Gases. *J. Air Waste Manage. Assoc.* 2005, 55, 747-754.

(13) Ghorishi, B. K.; Keeney, R. M.; Serre, S. D.; Gullett, B. K.; Jozewick, W. S. Development of Cl-Impregnated Activated Carbon for Entrained-Flow Capture of Elemental Mercury. *Environ. Sci. Technol.* 2002, 35, 4454-4459.

(14) Galbreath, K. C.; Zygarić, C. J. Mercury Transformation in Coal Combustion Flue Gas. *Fuel Process. Technol.* 2000, 65-66, 289-310.

(15) Biermann, J.; Voogt, N.; Sorochian, A.; Wendt, J. O. L.; Meritt, R.; Gale, T. K. *In-Flight Elemental and Oxidized Mercury in Coal Combustion Flue Gases by a Novel Mineral Sorbent between 320 and 1540 °C*, DOE-EPRI-EPA-A&WMA Power Plant Air Pollutant Control Mega Symposium, Washington, DC, May 19-22, 2003.

(16) Wu, J.; Cao, Y.; Li, S. G.; Cui, H.; Lu, P.; Pan, W. P. Evaluation of Mercury Sorbents on a Lab-Scale Multi-Phase Flow Reactor and on a Pilot-Scale Slipstream Reactor. *Prepr. Pap.-Am. Chem. Soc. Fuel Chem.* 2005, 51 (1).

(17) Vosteen, B. W. et al. U.S. Patent 6,878,358, April 12, 2005.

(18) Vosteen, B. W.; Kanefke, R.; Koser, H. Bromine-Enhanced Mercury Abatement from Combustion Flue Gases—Recent Industrial Applications and Laboratory Research. *VGB Power Tech—Int. J. Electricity Heat Generation* 2006, 86, 70-75.

(19) Raofie, F.; Ariya, P. A. Product Study of the Gas-Phase BrO-Initiated Oxidation of Hg<sup>0</sup>: Evidence for Stable Hg<sup>+</sup> Compounds. *Environ. Sci. Technol.* 2004, 38, 4319-4326.

(20) Goodsite, M. E.; Plane, J. M. C.; Skov, H. A Theoretical Study of the Oxidation of Hg<sup>0</sup> to HgBr<sub>2</sub> in the Atmosphere. *Environ. Sci. Technol.* 2004, 38, 1772-1776.

(21) Balabanov, N. B.; Peterson, K. A. Mercury and Reactive Alojen: Thermochemistry of Hg+ (Cl<sub>2</sub>, Br<sub>2</sub>, BrCl, ClO, and BrO). *J. Phys. Chem. A* 2003, 107, 7465-7470.

(22) Shepler, B. C.; Balabanov, N. B.; Peterson, K. A. Ab Initio Thermochemistry Involving Heavy Atoms: An Investigation of the Reactions Hg + IX (X = I, Br, Cl, O). *J. Phys. Chem. A*, accepted.

(23) Tossell, J. A. Calculation of Energetics for Oxidation of Gas-Phase Elemental Hg by Br and BrO. *J. Phys. Chem. A* 2003, 107, 7804-7808.

(24) Malykh, N. V.; Pertsikov, I. Z. A Thermodynamic Study of the Behavior of Selenium and Arsenic during Oxidative and Reductive Thermal Destruction of Coal. *Khim. Tverdogo Tela* 1990, 24, 50-54.

(25) Frandsen, F. J.; Erickson, T. A.; Kuhnelt, V.; Helble, J. J.; Linak, W. P. *Equilibrium Speciation of As, Cd, Cr, Hg, Ni, Pb, and Se in Oxidative Thermal Conversion of Coal—Comparison of Thermodynamic Packages*, Proceedings of the 3rd International Gas Cleaning Symposium, University of Karlsruhe, Karlsruhe, Germany, 1996; pp 18-20.

(26) Cenni, R.; Frandsen, F.; Gerhardt, T.; Splietho, H.; Hein, K. R. G.; Study on Trace Metal Partitioning in Pulverized Combustion of Bituminous Coal and Dry Sewage Sludge. *Waste Manage.* 1998, 18, 433-444.

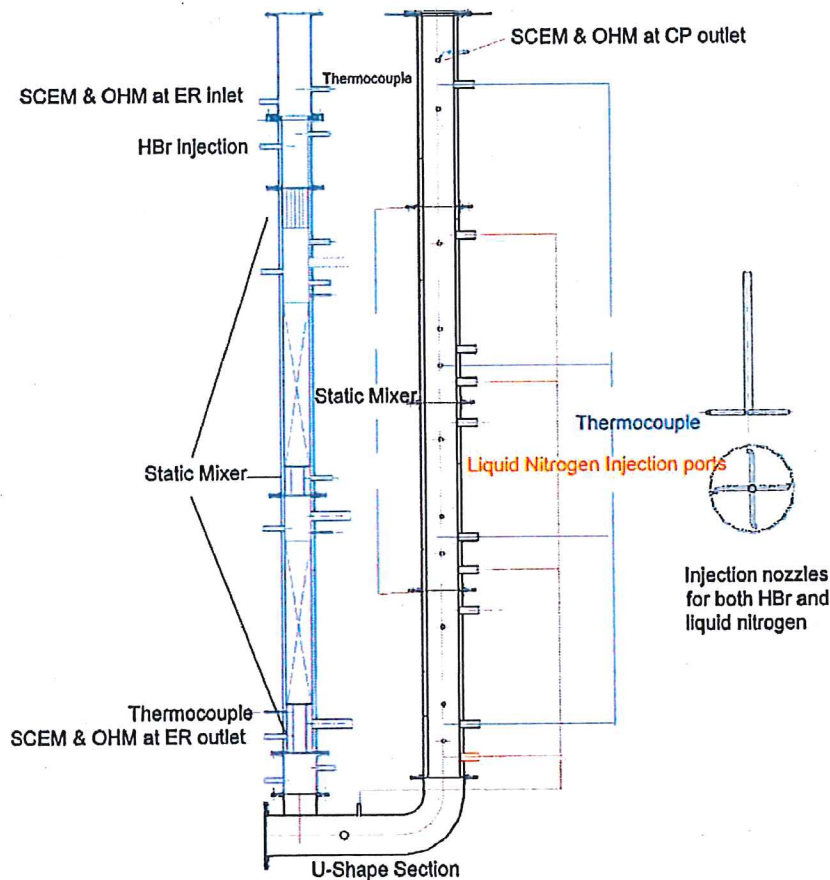


Figure 1. Schematic diagram of the slipstream reactor in a coal-fired power plant.

used to investigate the possible mercury species in the coal-fired flue gas bromine addition, which were within wide temperature windows.

## 2. Experimental Procedures and Thermodynamics Calculations

**2.1. Description of Testing Sites.** During testing, boiler loads of both units were kept stable. The oxygen concentration and temperature at the economizer outlet of the boiler were frequently checked to ensure the stability of the boiler performance during each day's test.

unit 1	unit 2
coal: sub-bituminous (PRB coal)	coal: bituminous (Kentucky medium-sulfur coal)
boiler: wall-fired	boiler: wall-fired
NO <sub>x</sub> control: low NO <sub>x</sub> burner	NO <sub>x</sub> control: low NO <sub>x</sub> burner
SO <sub>x</sub> control: none	SO <sub>x</sub> control: none
particulate control: cold-side ESP	particulate control: cold-side ESP

**2.2. Slipstream Facility and HBr Addition System.** A pilot-scale slipstream facility was designed and manufactured to simulate the full-scale applications of an SCR system and air-preheater (APH) in utility boilers. Its two components, the SCR reactor and the cooling pass (CP), are connected by a U-shaped section on the bottom. An ID Fan, at the outlet of the CP, generates negative pressure to pull the real flue gas from the economizer outlet of the boiler. Then, it passes through the SCR to the CP and finally delivers the flue gas downstream of the economizer outlet location. The schematic diagram of the experimental setup is shown in Figure 1.

The slipstream reactor was manufactured in a concentric configuration to provide good insulation to minimize the temperature drop inside the SCR reactor. The temperature drop was less than 20 °C during tests in this study.<sup>27</sup> The flue gas was split into two streams whose ratio was controlled by manual flashboard valves that adjust the section of the outside pass of the flue gas. The bypassed flue gas functions as a strengthened heat insulator, due to its higher temperature, which minimizes the heat transfer rate by decreasing the temperature difference between the introduced main stream of the flue gas and the bypassed flue gas stream. The average temperature inside the SCR reactor was about 330 °C. It may be varied with the operational load. The detailed description of a slipstream SCR reactor can be found in ref 27. In this study, the SCR reactor was left as an empty reactor without SCR catalyst loading. Thus, we renamed the SCR reactor the empty reactor (ER). There are two sampling ports at the inlet and outlet of the ER. The residence time of flue gas inside ER reactor was controlled to be about 1 s.

To control the temperature drop (from 330 to 170 °C) and quenching rate in the CP system, liquid nitrogen was used by injecting it into the CP in four stages through four injection ports by solenoid valves. Specially designed nozzles, as shown in Figure 1, distributed liquid nitrogen uniformly in the cross-section at the injection point with the assistance of two static mixers downstream of the injection nozzles. Liquid nitrogen vaporizes, cooling the hot flue gas to the desired temperature of 170 °C at the CP outlet by certain cooling rates. The thermocouple monitored the temperature and provided a feedback signal to the flow controller of liquid

(27) Cao, Y.; Chen, B.; Wu, J.; Cui, H.; Li, S. G.; Herren, S. M.; Smith, J.; Chu, P.; Pan, W. P. Study of Mercury Oxidation by Selective Catalytic Reduction Catalyst in a Pilot-Scale Slipstream Reactor at a Utility Boiler Burning Bituminous Coal. *Energy Fuels* 2007, 21, 145–156.

Table 1. Analysis of Coal and Ash Samples during Tests

Coal Analysis													
sample name	as determined			dry basis									
	ADL <sup>a</sup> (%)	moisture (%)	ash (%)	vol material (%)	sulfur (%)	Btu BT (U/lb)	carbon (%)	hydrogen (%)	nitrogen (%)	oxygen (%)	chloride (ppm)	fluoride (ppm)	mercury (ppm)
bituminous coal	3.04	5.41	10.30	37.13	1.31	13423	75.85	4.85	1.79	5.92	1328	ND	0.11
PRB <sup>b</sup> coal trial 1	20.75	11.37	6.20	47.07	0.42	12022	70.75	5.00	2.21	15.43	177	42	0.07
PRB <sup>b</sup> coal trial 2	18.52	12.15	7.59	45.45	0.81	12173	71.15	4.99	2.32	13.15	164	40	0.09
Av	19.63	11.76	6.89	46.26	0.61	12097	70.95	4.99	2.26	14.29	170	41	0.08
Ash Analysis													
sample name	Na <sub>2</sub> O (%)	MgO (%)	Al <sub>2</sub> O <sub>3</sub> (%)	SiO <sub>2</sub> (%)	P <sub>2</sub> O <sub>5</sub> (%)	SO <sub>3</sub> (%)	K <sub>2</sub> O (%)	CaO (%)	TiO <sub>2</sub> (%)	MnO (%)	Fe <sub>2</sub> O <sub>3</sub> (%)	BaO (%)	SrO (%)
bituminous coal	0.01	0.90	18.14	38.27	0.58	1.94	2.35	1.71	1.14	0.02	17.51	0.15	0.13
PRB <sup>b</sup> coal	1.02	4.70	14.89	28.63	0.69	11.93	0.39	22.95	1.17	0.02	4.91	0.49	0.30
Ash Analysis													
sample name	sulfur (%)	mercury (ppm)	chloride (ppm)	bromide (ppm)	fluoride (ppm)	LOI (%)							
bituminous coal	0.15	0.35	250	ND	ND	7.13							
PRB <sup>b</sup> coal trial 1	0.67	0.15	123	ND	95	0.59							
PRB <sup>b</sup> coal trial 2	0.89	0.18	177	ND	98	0.69							
Av	0.78	0.17	150	ND	97	0.64							

<sup>a</sup> ADL<sup>1</sup>: air-dry loss. <sup>b</sup> PRB<sup>2</sup>: Powder River Basin coal.

nitrogen. If the thermocouple returned a temperature signal higher than what was desired, the controller allowed more liquid nitrogen to be injected into the duct by enlarging the opening of the solenoid valve. Two pretests were conducted. One was performed by measuring oxygen concentrations at the inlet and outlet of the CP and indicated that less liquid nitrogen was needed to achieve the cooling rates of the flue gas, which simulated the APH in the utility boilers. The other was performed by investigating the temperature change during liquid nitrogen injection. It indicated that injecting the liquid nitrogen caused less of a temperature change. Therefore, the effect of the liquid nitrogen droplet formation could be ignored. Only one sampling location was used, which was at the outlet of the CP.

The mercury continuous emission monitor (CEM) was used for observing mercury variations during testing. The Ontario Hydro (OH) Method was also used for Hg-CEM data validation. For both methods, an inertial sampling probe was used to sample flue gas. The sampling probe temperatures were controlled like the temperatures of flue gases in the reactor at locations of the sampling probe installation. A detailed description of quality assurance and quality control (QA/QC) for both methods is shown in refs 27 and 28.

HBr gas from a pressurized cylinder, at a predetermined concentration using nitrogen as the carrier gas, was injected into the system. The desired spiking concentration of HBr inside the slipstream reactor could be adjusted by the mass flow controller (MFC). To ensure controlled and even distribution of HBr, three static mixers were installed at different locations on the SCR reactor. The HBr injection port was located below the sampling port at the ER inlet, which left this sampling port unaffected. The additional concentration of the HBr gas spike in the flue gas was controlled at about 3, 6, and 15 ppm to minimize potential hazards.

**2.3. Coal and Ash Analysis.** Bituminous coal, with medium sulfur and chlorine contents, and PRB coal, with low sulfur and chlorine contents, were burned during tests with the HBr addition. Coal and ash samples were collected once a day during testing. The proximate analysis, elemental analysis, and mineral metal analysis data of the coal samples are shown in Table 1. Analysis of fly ash samples from the ESP hopper, which was the front row, is also shown in Table 1. All data were presented on a dry basis, and the testing methods for all these samples can be found in ref 28. The average sulfur, chlorine, and mercury contents in the tested bituminous coal were about 1.31% and 1328 and 0.11 ppm, respectively. In comparison, the average sulfur, chlorine, and mercury contents in the tested PRB coal were about 0.61% and

170 and 0.08 ppm during tests, respectively. On the basis of approximate mass balance, 90% of the sulfur and chlorine content in coal existed in the flue gas during its combustion. CaO, Fe<sub>2</sub>O<sub>3</sub>, and loss on ignition (LOI) were about 1.71, 17.51, and 7.13% for collected fly ash of tested bituminous coal and 22.95, 4.91, and 0.64% for collected fly ash of tested PRB. The bromine contents in tested coals were under the detection limit.

**2.4. Thermodynamics Equilibrium Calculation.** The F\*A\*CT software package was used to implement the calculations of the equilibrium compositions for flue gas under different temperatures. The thermodynamic database attached to the F\*A\*CT software package is mostly based on the JANAF Thermochemical Tables.<sup>29</sup> It covers about 5000 species and compounds with thermodynamics data, in which data on mercury and bromine were among those when thermodynamic equilibrium calculations were used on coal combustion systems. Some general assumptions are as follows: (1) the stable species, which is predicted by thermodynamics calculations, can be obtained only when the chemical processes occurring in the system have reached equilibrium; (2) physical processes, such as particle nucleation, agglomeration, and adsorption in the flue gas, are not considered in thermodynamic equilibrium calculations. Then, the possible interaction of some gaseous species with the fly ash particles, which would affect the partitioning of the studied elements, is neglected; and (3) equilibrium analysis does not account for mixing due to content and/or temperature gradients. However, in real combustion, this may occur in localized areas.

In this study, the computational systems contain eight elements, all of which can be found in associated species of JANAF. In the calculations, we specifically included the interactions between mercury and halogen elements (mainly chlorine and bromine). Although the influence of other coexisting elements in coal may affect mercury's behavior, through sharing or depleting the total active dominant atoms in the combustion system, they still were negligible according to our previous studies. Mercury species considered in our equilibrium analysis are listed in Table 3.

### 3. Results

**3.1. Thermodynamics Equilibrium Analysis of Adding HBr to the Typical Coal-Fired Flue Gas.** Thermodynamic calculations can provide information on possible products and their equilibrium concentrations after the addition of HBr to the coal-fired flue gas. Three calculation conditions were used for thermodynamics equilibrium analysis, which are shown in

(28) Cao, Y.; Duan, Y. F.; Kellie, K.; Li, L. C.; Xu, W. B.; Riley, J. T.; Pan, W. P. Impact of Coal Chlorine on Mercury Speciation and Emission from a 100 MW Utility Boiler with Cold-Side Electrostatic Precipitators and Low-NO<sub>x</sub> Burners. *Energy Fuels* 2005, 19, 842–854.

(29) Chase, M. W.; Davies, C. A.; Downey, J. R. JANAF (Joint Army and Navy Air Force), JANAF Thermochemical Tables. *J. Phys. Chem. Ref. Data* 1985, 14, 1.

Table 2. Mercury Species Taken into Account in the Equilibrium Analysis<sup>a</sup>

compositions
Hg <sub>2</sub> (N <sub>2</sub> ) <sub>2</sub> (s), HgO(s, g), Hg <sub>2</sub> CO <sub>3</sub> (s), Hg <sub>2</sub> C <sub>2</sub> O <sub>4</sub> (s)
Hg <sub>2</sub> (C <sub>2</sub> H <sub>3</sub> O <sub>2</sub> ) <sub>2</sub> (s), HgS(s, g), Hg(l, g), HgSO <sub>4</sub> (s)
HgNOCl <sub>3</sub> (s), Hg <sub>2</sub> (CNS) <sub>2</sub> (s), HgCl <sub>2</sub> CH <sub>3</sub> OH(s), Hg <sub>2</sub> SO <sub>4</sub> (s)
HgCl(g), Hg <sub>2</sub> Cl <sub>2</sub> (s, g), HgCl <sub>2</sub> (l, s, g), Hg <sup>+</sup> (g)
Hg(CH <sub>3</sub> ) <sub>2</sub> (l, g), Hg <sub>2</sub> (g), HgH(g), HgBr(g), HgBr <sub>2</sub> (l, s, g), Hg <sub>2</sub> Br <sub>2</sub> (s)

<sup>a</sup> s: solid; l: liquid; and g: gas.

Table 3. Conditions of Typical Coal-Fired Flue Gas Compositions Set for Thermodynamic Calculations

species	N <sub>2</sub> , dry (%)	H <sub>2</sub> O, dry (%)	O <sub>2</sub> , dry (%)	CO <sub>2</sub> , dry (%)	NO, dry (ppm)	SO <sub>2</sub> , dry (ppm)	HCl, dry (ppm)	HBr, dry (ppm)	Hg, dry (ppb)
case I	80	7	6	13	300	1000	150	0 3 30	10
case II	80	7	6	13	300	1000	80	0 3 0	10
case III	80	12	6	13	300	300	10	3 30	10

Table 2. Calculation condition 1 refers to typical bituminous coal with medium sulfur and high chlorine contents (about 1000 ppm SO<sub>2</sub>, 300 ppm NO, and 150 ppm HCl at a 6% local O<sub>2</sub> concentration in the flue gas). Condition 2 refers to bituminous coal with high sulfur and medium chlorine contents (about 1000 ppm SO<sub>2</sub>, 300 ppm NO, and 80 ppm HCl in the flue gas at a 6% local O<sub>2</sub> concentration in the flue gas). Condition 3 refers to PRB coal with low sulfur and chlorine contents (about 300 ppm SO<sub>2</sub>, 300 ppm NO, and 10 ppm HCl in the flue gas at a 6% local O<sub>2</sub> concentration in the flue gas). The possible products found after HBr addition into these three kinds of flue gas compositions are shown in Figures 2–4, which correspond to the three calculation conditions. Hg(0) and HgCl<sub>2</sub> are the main products found in the flue gas for all three calculation cases at thermodynamic equilibrium conditions. Please note that all mercury species are in the gas phase and that HgBr<sub>2</sub> is a possible product after adding HBr to the coal-fired flue gas. However,

its concentration varied greatly with the ratio of HBr/HCl and the temperature range.

For a typical bituminous coal-fired flue gas with medium sulfur and high chlorine contents, as indicated in Figure 2, more than 90% of the mercury occurred as HgCl<sub>2</sub> when the temperature is below about 500 °C at the equilibrium status. Elemental mercury, Hg(0), is the major mercury species when the temperature is above about 700 °C at equilibrium status. Between 500 and 700 °C, HgCl<sub>2</sub> and Hg(0) have an inverse relationship. When the addition of HBr begins, HgBr<sub>2</sub> comes out at a temperature range between 300 and 700 °C, which partially overlaps the temperature range of the transition between HgCl<sub>2</sub> and Hg(0). HgCl<sub>2</sub> and Hg(0) equilibrium curves will shift a little due to HgBr<sub>2</sub> formation. With the minimum addition of HBr at 3 ppm, the maximum percentage of the HgBr<sub>2</sub> concentration relative to the total mercury in the flue gas is only 5% at about 550 °C. HgCl<sub>2</sub> and Hg(0) are still the major mercury species in the flue gas. Increasing the HBr concentration to 30 ppm can increase the maximum equilibrium concentration of HgBr<sub>2</sub> to 60% at about 550 °C, and simultaneously, the temperature range of the equilibrium curve of HgBr<sub>2</sub> is expanded. Corresponding to the actual test conditions in this study, in which the temperature is around 330 °C, the maximum HgBr<sub>2</sub> occurrence in the flue gas at equilibrium status is less than 5% with the addition of HBr below 30 ppm. Decreasing HCl concentrations in the flue gas by half can increase the equilibrium concentrations of HgBr<sub>2</sub>. However, the maximum HgBr<sub>2</sub> occurrence at the equilibrium status is still below 15% with the minimum addition of HBr, which is 3 ppm in the whole occurrence temperature of HgBr<sub>2</sub> (indicated in Figure 3).

For the typical coal-fired flue gas of PRB with low sulfur and chlorine contents, it was indicated in Figure 4 that more than 90% of the mercury occurred as HgCl<sub>2</sub> when the temperature was below 400 °C at the equilibrium state. Hg(0) is the major mercury species when the temperature is above 600 °C at equilibrium status. It seems that the temperature range for the simultaneous occurrence of Hg(0) and HgCl<sub>2</sub> shifts to a lower temperature, in comparison with the case of a higher

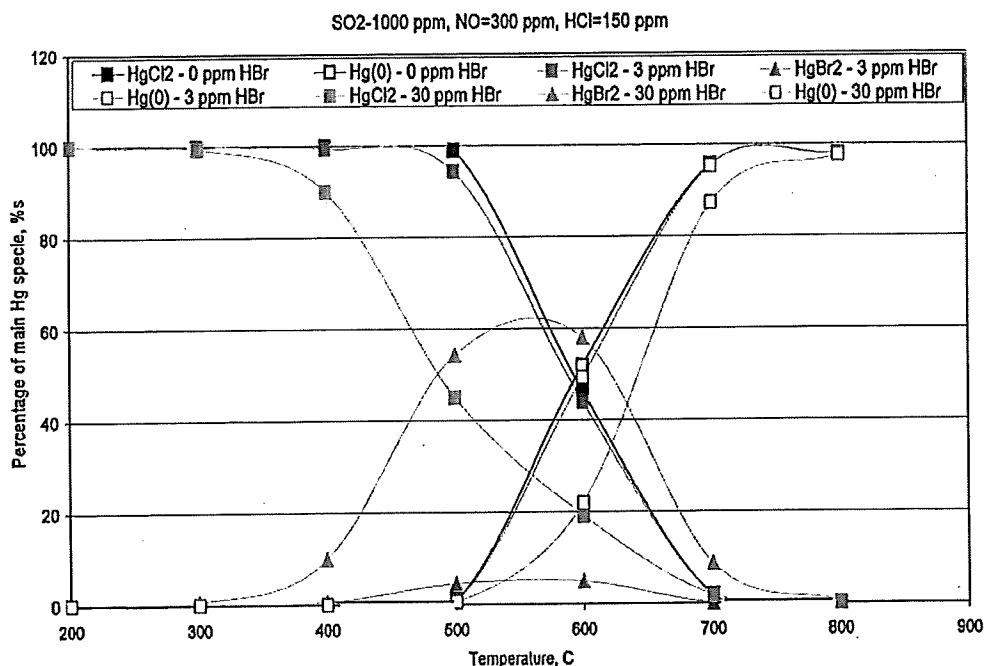


Figure 2. Equilibrium mercury species under typical flue gas conditions of bituminous coal with high sulfur and chlorine contents.

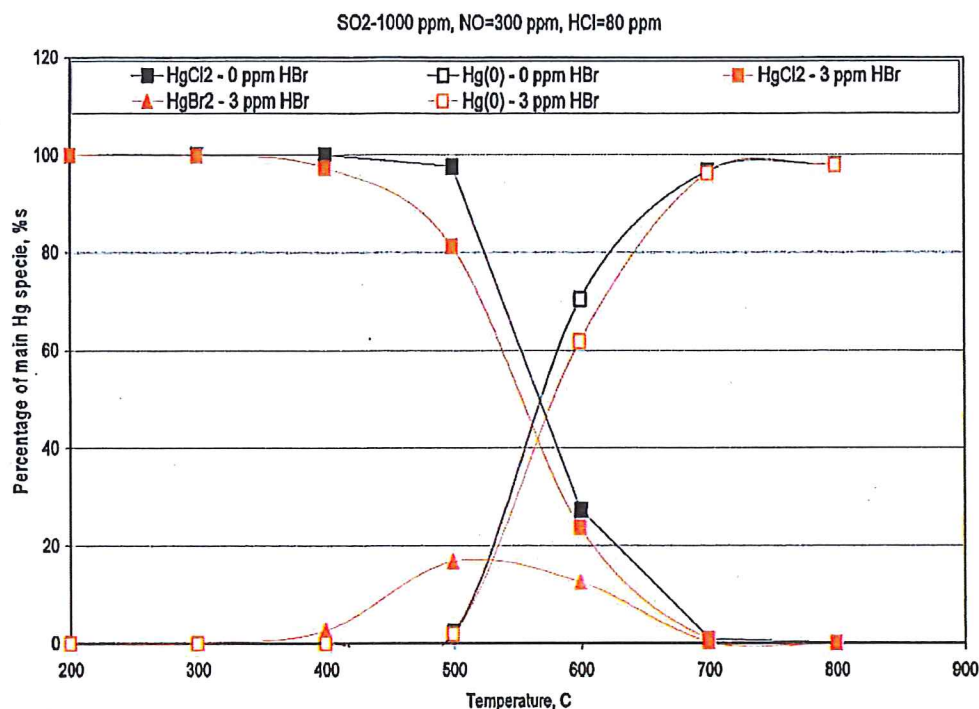


Figure 3. Equilibrium mercury species under typical flue gas conditions of bituminous coal with high sulfur and medium chlorine contents.

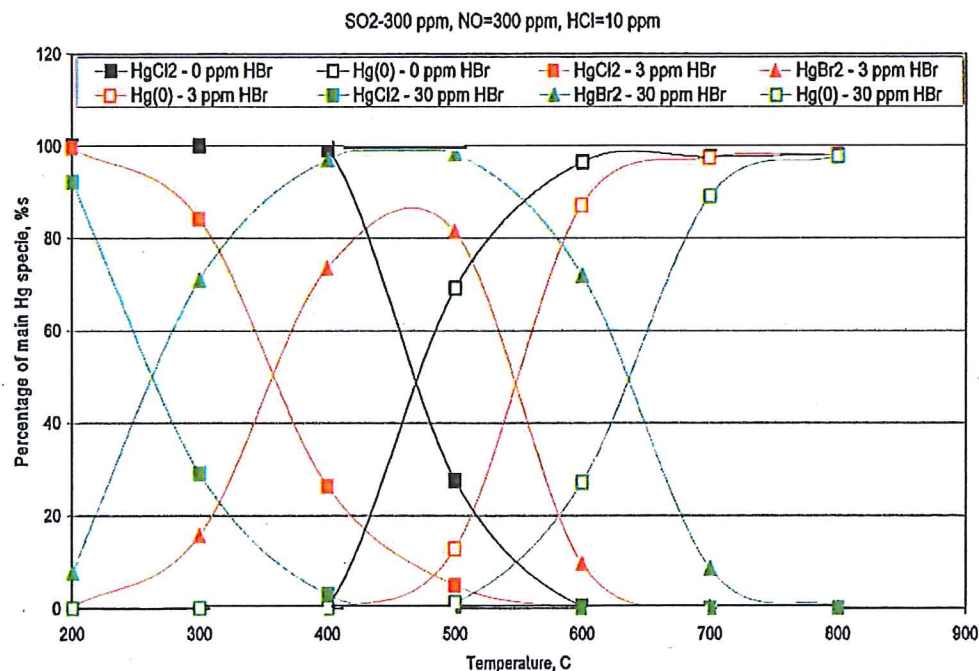


Figure 4. Equilibrium mercury species under typical flue gas conditions of PRB coal with low sulfur and chlorine contents.

chlorine concentration in the flue gas. After HBr addition begins at 3 ppm, HgCl<sub>2</sub> and Hg(0) equilibrium curves shift largely to low temperature and high temperature, respectively. The temperature range for the HgBr<sub>2</sub> occurrence is also widening within range of 200–800 °C. These shifts are dependent on HBr addition concentrations. With the minimum HBr<sub>2</sub> addition concentration at 3 ppm, the maximum percentage of HgBr<sub>2</sub> relative to the total mercury in the flue gas can be reached at about 80% at a temperature of 500 °C. Increasing the HBr addition concentration to 30 ppm will continue to enlarge the

temperature range of HgBr<sub>2</sub> occurrence and increase the maximum equilibrium concentration to 100% occurrence of HgBr<sub>2</sub> in the flue gas. However at temperatures below 330 °C, which is of interest in this study, the maximum occurrence of HgBr<sub>2</sub> in the flue gas is only about 35% for the addition of HBr at 3 ppm.

**3.2. Effects of HBr Addition on Mercury Transformation under a Bituminous Coal Atmosphere.** The variation of speciated mercury, monitored by the Hg-CEM system, in two tests of HBr addition at 3 ppm under a bituminous coal

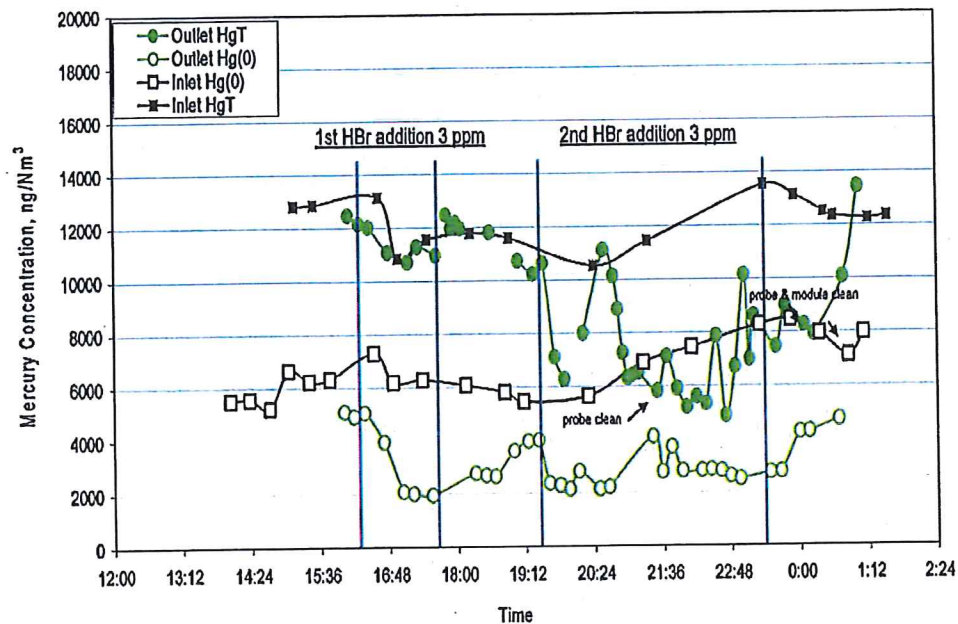


Figure 5. Effect of HBr addition on mercury speciation in a slipstream facility under a typical bituminous coal atmosphere (HBr addition trial 1 at 3 ppm and trial 2 at 3 ppm).

Table 4. Summary of Test Results

test condition						SCEM data (at 3% O <sub>2</sub> ) dry basis									OHMethod data (at 3% O <sub>2</sub> ) dry basis														
T (°C)						ER inlet Hg measurements (ng/N m <sup>3</sup> )			ER outlet Hg measurements (ng/N m <sup>3</sup> )			CP outlet Hg measurements (ng/N m <sup>3</sup> )			ER inlet Hg measurements (μg/N m <sup>3</sup> )				ER outlet Hg measurements (μg/N m <sup>3</sup> )				CP outlet Hg measurements (μg/N m <sup>3</sup> )						
ER in	ER out	APH out	cooling rate (F/s)	HBr (ppm)		Hg (0)	Hg (T)	% Hg(0)	Hg (0)	Hg (T)	% Hg(0)	Hg (0)	Hg (T)	% Hg(0)	Hg (0)	Hg (2+)	Hg (T)	% Hg(0)	Hg (0)	Hg (2+)	Hg (T)	% Hg(0)	Hg (0)	Hg (2+)	Hg (T)	% Hg(0)			
Bituminous Coal test																													
322	293			0		6612	12950	51.1	5016	12215	41.1				6.72	4.65	11.37	59.1	4.55	7.31	11.86	38.4							
322	293			3		6581	11849	55.5	2015	11006	18.3				7.9	3.96	11.86	66.6	1.47	10.21	11.68	12.6							
322	293			0		5770	11674	49.4	3980	11857	33.6																		
322	293			3		7068	11839	59.7	2340	6971	33.6																		
PRB Coal Test																													
341	330			0		8937	11635	76.8	8149	11534	70.7																		
341	330			0		9342	11721	79.7	9216	11483	80.3																		
341	330			0		7241	10135	71.4	7031	10369	67.8				7.4	1.2	8.6	86	4.95	2.31	7.26	68.2							
341	330	282		15		8332	10998	75.8	919	10765	8.5				6.37	2.33	8.7	73	1.25	5.96	7.21	17.3							
344	329	165	400	0		7793	10337	75.4	7811	9688	80.6	5863	7451	78.7															
344	328	163	400	6		6621	9787	67.7	934	7163	13.0	654	2123	30.8	7.91	0.92	8.83	90	2.52	6.08	8.6	29.3	0	3.45	3.45	0			
340	321	230	400	0		5124	8691	59.0	5107	9372	54.5	3980	5576	71.4															
344	321	227	400	3		5249	8141	64.5	892	9175	9.7	308	3398	9.1									0	3.68	3.68	0			

atmosphere is presented in Figure 5. Before HBr addition started, a baseline test was conducted until the speciated mercury concentration stabilized with a variation within 10%. The baseline tests indicated that Hg(0)/Hg(VT) (Hg(VT) is the total vapor phase mercury, which is the sum of Hg(0) and Hg(2+)) was about 55% at the ER inlet and 40% at the ER outlet, which is the typical mercury speciation at a higher temperature of about 330 °C by burning bituminous coal with a high chlorine content. In the first trial of HBr addition at 3 ppm, Hg(VT) at the ER outlet remained constant, which is the same as that at the ER inlet location. There was no evidence to show that HBr addition impacted the adsorption of the speciated mercury on fly ash in the flue gas at approximately 330 °C. However, Hg(0)/Hg(VT) decreased dramatically starting at its baseline concentration of about 40% to 18% during HBr addition at 3 ppm, above 20% of the additional Hg(0) oxidation rate. The elemental mercury concentration came back to its baseline level after the HBr addition stopped. However, this recovery process was slow and lasted for 2 h in the first trial. A memory effect of adding the HBr seemed to be left in the slipstream reactor after HBr

addition stopped. The OH Method data, for validation of the Hg-CEM data, are shown in Table 4. The ratio of Hg(0) and Hg(VT) at the ER outlet decreased from 35.7 to 12.6% with an additional drop of about 20% by the OH Method data, which supported the validation of Hg-CEM data observed at the first trial of the HBr addition at 3 ppm. However, test results from SCEM and OH Method disagreed with the maximum occurrence of 5% HgBr<sub>2</sub> from the thermodynamics predictions. It seems that additional mercury oxidation cannot be directly associated with the new Hg(2+) species, such as HgBr<sub>2</sub> with HBr addition in the flue gas.

For data validation, confirmation tests during HBr addition were conducted in the second trial with the same HBr addition concentration at 3 ppm. Differing from what we found in the first trial, Hg(VT) underwent a decrease of almost 50% and greatly fluctuated, except for the simultaneous decrease of Hg(0). It seems that adsorption of speciated mercury occurred somewhere in the sampling system. We purged and cleaned the sampling probe and the mercury speciation module during the HBr addition period. We could recover some of Hg(VT) but

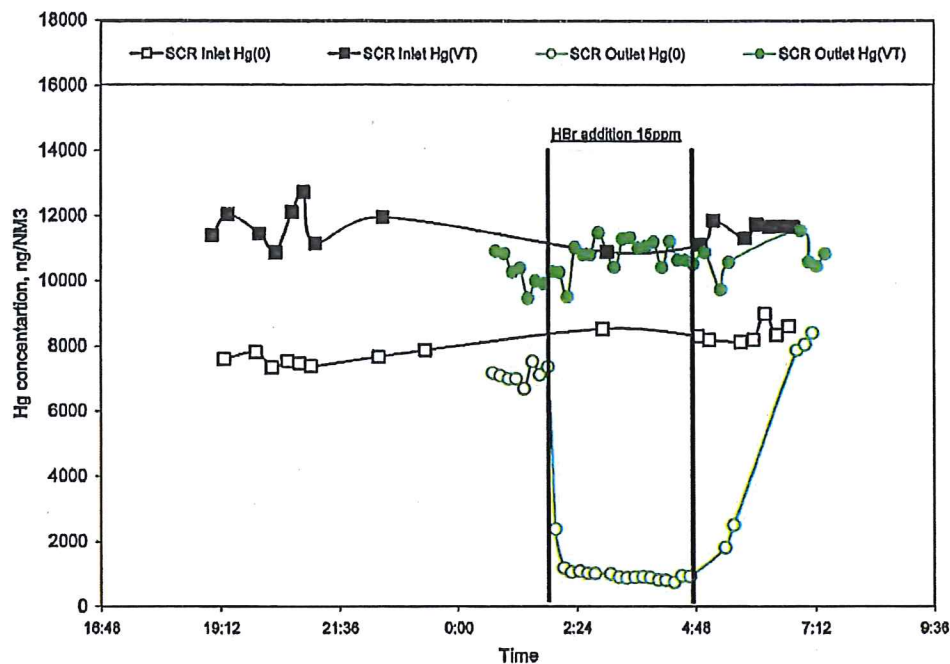


Figure 6. Effect of HBr addition on mercury speciation in slipstream facility under typical PRB coal atmosphere (HBr addition trial 1 at 15 ppm).

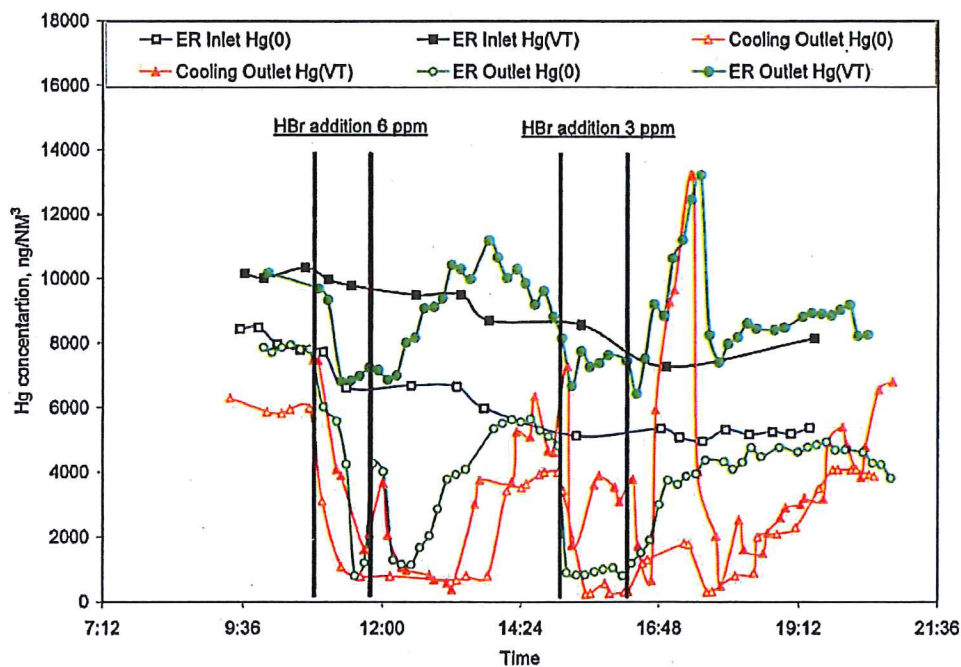


Figure 7. Effect of HBr addition on mercury speciation in slipstream facility under typical PRB coal atmosphere (HBr addition trial 2 for test 1 at 6 ppm and test 2 at 3 ppm).

not Hg(0). After the HBr addition stopped, the Hg(VT) varied and could not return to its baseline level automatically until the purging of the probe stopped. The memory effect of the HBr addition occurred after HBr addition was conducted. We noticed the probe heating system's failure, which resulted in a temperature drop in some parts of the inertial sampling probe during the second trial of the HBr addition. Fly ash deposition was found inside the inertial sampling probe. This was the result of moisture condensation and ash deposition after the temperature dropped. It seems that low temperatures could greatly impact mercury adsorption of the fly ash under the conditions

of HBr addition. This resulted in a measurement bias at the ER outlet location in the second trial.

**3.3. Effect of HBr Addition on Mercury Speciation under a PRB Coal Atmosphere.** The variation of speciated mercury at different HBr addition concentrations with PRB coal are presented in Figures 6 and 7, respectively. The baseline tests were conducted until the speciated mercury concentration stabilized within a 10% variation before HBr addition began. The baseline tests indicated that Hg(0)/Hg(VT) was varied between 70 and 80% in the flue gas, which is the typical mercury speciation at a higher temperature of about 330 °C by

burning PRB coal with a lower chlorine content. In the first trial of HBr addition at 15 ppm, Hg(VT) at the ER outlet followed the trend of Hg(VT) at the ER inlet and was kept almost constant (see Figure 6). There is no apparent evidence to show that HBr addition could impact mercury adsorption on the fly ash at a higher temperature of about 330 °C by burning PRB coal. However, the strong effect of HBr on mercury oxidation was found because Hg(0) underwent a dramatic decrease by about 70% as compared to its baseline concentration after HBr addition started. The recovery of Hg(0) to its baseline level was still slow and took about 2 h after HBr addition stopped in the first trial. The memory effect of HBr addition remained in the system after HBr addition stopped because probe purging and SCEM system cleanup did not help this recovery process. The test by the OH Method during the HBr addition at 15 ppm indicates that Hg(VT) was consistent with its baseline concentration of less than 10%. An apparent oxidation effect was confirmed by the OH Method that Hg(0)/Hg(VT) decreased dramatically from 68.2% at baseline conditions to 17.3% by about 50.9% during HBr addition at 15 ppm. Results from both Hg-CEM and OH Method confirmed the strong effect of the HBr addition on mercury oxidation in the flue gas atmosphere of PRB coal at higher temperatures of about 330 °C.

The second trial of HBr addition using the flue gas of PBR coal was conducted when the CP was combined with the ER slipstream reactor to study the temperature effect on mercury oxidation and adsorption. Results from Hg-CEM monitoring were at three test locations: the ER inlet, the ER outlet (also the CP inlet), and the CP outlet (shown in Figure 7). Hg(VT) at the ER outlet was consistent with that at the ER inlet. However, it was higher than that at the CP outlet due to mercury capture by fly ash at a lower temperature of the CP. The first addition of HBr during this term was about 6 ppm. After HBr addition, there was an apparent decrease of both Hg(0) and Hg(VT) at the ER outlet while Hg(0) and Hg(VT) at the ER inlet were relatively stable. However, the Hg(0) oxidation was found because the extent of the decrease of Hg(0) was much larger than that of Hg(VT) at the ER outlet during the HBr addition. At the same period, both Hg(0) and Hg(VT) decreased simultaneously by almost the same extent of about 70% at the CP outlet where the temperature was controlled at about 170 °C. An apparent oxidation effect was also confirmed by the OH Method because Hg(0)/Hg(VT) decreased dramatically by over 60% at the ER outlet location (from 90% at the ER inlet location to 29.3%) during HBr addition at 6 ppm. Hg(VT) dropped from about 9 to 3.5  $\mu\text{g}/\text{N m}^3$  at the CP outlet. This indicates a dramatic decrease of mercury with HBr addition as the temperature decreased. After HBr addition stopped, both Hg(0) and Hg(VT) at the ER and CP outlets could be recovered slowly to their baseline levels. Hg(VT) at the ER outlet was eventually greater than that at the ER inlet but not for that at the CP outlet. This indicates that mercury re-emission should be occurring within the sampling system at the ER's CP outlets. The second HBr addition was conducted at 3 ppm after both Hg(0) and Hg(VT) returned to their baseline. Similarly, Hg(0) underwent a dramatic decrease at both locations of the ER outlet and the CP outlet. Hg(VT) at the ER outlet just underwent a small decrease, as compared to a large decrease of Hg(VT) at the CP outlet. An apparent oxidation effect was confirmed at the ER outlet where Hg(0)/Hg(VT) decreased dramatically by about 55% at the ER outlet location (from 64.5% at the ER inlet location to 9.1%) during the HBr addition at 3 ppm. Hg(VT) dropped from about 9 to 3.7  $\mu\text{g}/\text{N m}^3$  at the CP outlet. We should point out that we focused on the expected variation

of mercury concentration at the outlet locations by HBr addition. Thus, rare data were obtained at the inlet location due to the availability of SCEM. Our previous experience on investigations on the stable concentrations of speciated mercury at the inlet location seemed valid if the boiler load was kept constant.

The mercury oxidation rates by experimental results from both Hg-CEM and OH Method disagreed with those predicted by thermodynamics analysis under the same conditions with PRB coal. With HBr addition at 3 ppm in the PRB flue gas, the maximum percentage of HgBr<sub>2</sub> was just 35%, as compared to an additional Hg(0)/Hg(VT) drop of over 50%. This may imply that the additional mercury oxidation cannot be solely associated with the formation of HgBr<sub>2</sub> by HBr addition. The possible clues to this disagreement may refer to the availability of other more active oxidation agents, which can greatly improve mercury oxidation kinetics without limiting the occurrence of HgCl<sub>2</sub> by the thermodynamic equilibrium at temperatures around 330 °C. The availability of this active chlorine species may come from the activation of the stable chlorine species being attacked by the bromine species. Some of inter-halogens, such as BrCl, can be formed under thermodynamically stable conditions. It may subsequently cause the improvement of Hg oxidation kinetics.<sup>30,31</sup>

**3.4. Characterization of Ash Samples from HBr Addition Tests.** Additional tests were conducted in a 1 in. lab-scale fixed bed reactor at approximately 300 °C, in which fly ash from bituminous coal was loaded. Fly ash was collected from the ESP hopper during HBr addition tests. The Hg(0) stream and HBr stream were delivered to the fixed bed subsequently or simultaneously to investigate the mechanisms of mercury adsorption by brominated fly ash and its temperature range. It was found that the mercury content of treated fly ash under higher temperatures (about 300 °C) did not change. However, the brominated fly ash, which was made by first delivering HBr to the fly ash sample in the fixed bed, did not capture any Hg(0) by subsequent addition in the Hg(0) stream, as shown in Figure 8 as Ash-B+SE(HBr+Hg(0)). Original mercury on the brominated fly ash (Hg(P)) was also almost entirely lost. Another test delivered HBr and Hg(0) simultaneously on the loaded fly ash in the fixed bed, as shown in Figure 8 as Ash-B+SI-(HBr+Hg(0)). This indicates the loss of Hg(P) in the fly ash, as compared to that of its original Hg(P) content in the fly ash. In both of these cases, the Br content in the fly ash was concentrated above 800 ppm, as compared to that in the original fly ash, which was under the detection limit. It seems that the bromine species on the fly ash caused the fly ash bound mercury to desorb under temperatures as high as 300 °C.

Fly ash, collected from both the slipstream facility and the ESP hopper of the boiler during HBr addition tests with PRB coal, were subjected to the determination of their mercury and bromine contents. Hg(P) in the ESP fly ash from the full-scale boiler was about 0.1 ppm. Hg(P) in the fly ash collected from the sampling location of the slipstream facility's CP outlet varied between 0.7 and 1.7 ppm. It was surprising to find that the bromine contents in all fly ash samples, during HBr addition from different sampling locations, were all under the detection limit. It seemed that Hg(P) in ash was independent of the bromine content on the fly ash, even at lower temperatures.

(30) Yeo, G. A.; Ford, T. A. Conformational Preferences of the Structures and Energetics of the Molecular Complexes of Trifluoride with Some Hydrogen Halides, Halogens, and Interhalogens. *J. Mol. Struct.* 2006, 1–8.

(31) Calvert, J. G.; Lindberg, S. E. A Modeling Study of the Mechanism of the Halogen–Ozone–Mercury Homogeneous Reactions in the Troposphere during the Polar Spring. *Atmos. Environ.* 2003, 37, 4467–4481.

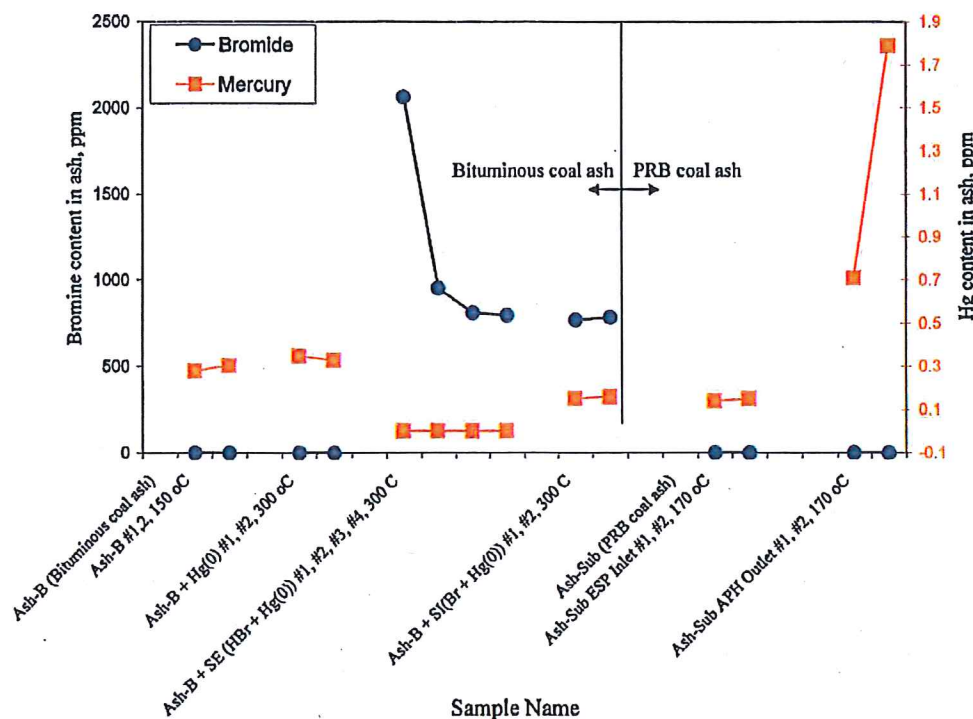


Figure 8. Variation of mercury content with the bromine content in the fly ash.

Results from the lab-scale fixed bed test provided evidence of the interaction of fly ash and bromine. First, under temperatures as high as 300 °C, mercury could not be captured on the fly ash, even when the fly ash was brominated. Second, there was a possibility that the original mercury reacted with bromine on the fly ash surface and was subsequently transferred to the gas phase. The bromine could extrude the originally captured mercury Hg(P) on the fly ash under high temperatures. Third, retaining HgBr<sub>2</sub> on the fly ash may occur as the temperature decreases, but it could be independent of the availability of the bromine species on the fly ash surface. Reaction between mercury and bromine species occurred in the gas phase.

#### 4. Discussion

The test results strongly suggest that bromine addition could result in enhanced mercury oxidation and adsorption on the fly ash in the two typical flue gas atmospheres by burning bituminous coal and sub-bituminous coal. The interaction between HBr and mercury was different under higher temperature range (300–350 °C) and lower temperature ranges (150–200 °C). Higher temperatures promote mercury oxidation but inhibit mercury adsorption on the fly ash. The enhanced mercury oxidation rate by HBr addition resulted from the improved kinetics of the elemental mercury oxidation. Lower temperatures strongly promote mercury adsorption on the fly ash in this study. A higher content of Fe<sub>2</sub>O<sub>3</sub> and LOI and a lower content of CaO were found in bituminous coal ash. However, test results did not provide any clear correlation between these fly ash constituents on the enhanced mercury oxidation, although previous studies suggested that Fe<sub>2</sub>O<sub>3</sub> and unburned carbon may be attributed to mercury transformation under a chlorine-dominant flue gas atmosphere.<sup>28,32–36</sup>

Under temperatures as high as 330 °C, thermodynamics studies indicated that there is a limited HgBr<sub>2</sub> occurrence in the coal-fired flue gas but not for HgCl<sub>2</sub>, which can proceed to 100% conversion in the temperature range of this study if the kinetics of mercury oxidation by chlorine is quick enough. The enhanced mercury oxidation rate by bromine addition in this test exceeded the limitation of the thermodynamics prediction. This may indicate that HgBr<sub>2</sub> formation was not the only new product by bromine addition. It is possible that simultaneous formation of HgBr<sub>2</sub> and HgCl<sub>2</sub> occurred. Bromine seems to have the capability of attacking a chlorine species in the flue gas to promote the generation of activated chlorine, which is involved in improving the kinetics of mercury oxidation. This may explain why the total mercury oxidation rate exceeded the thermodynamics limitation on the maximum occurrence of HgBr<sub>2</sub>. Under lower temperature ranges, test results in both present study and previous studies<sup>37,38</sup> supported the affinity of mercury on the surface of the fly ash or brominated adsorbents or fly ashes. For example, the brominated activated carbon could be used as

(33) Ghorishi, S. V.; Lee, C. W.; Kilgroe, J. D. *Mercury Speciation in Combustion Systems: Studies with Simulated Flue Gas and Model Fly Ash*, Presented at the 92nd Annual Meeting of the Air and Waste Management Association, St. Louis, MO, June 20–24, 1999; paper 199.

(34) Olson, E. S.; Mibeck, B. A.; Benson, S. A.; Laumb, J. D.; Crocker, C. R.; Dunham, G. E.; Sharma, R. K.; Miller, S. J.; Pavlish, J. H. The Mechanistic Model for Flue Gas Mercury Interaction on Activated Carbons: The Oxidation Site. *Prepr. Pap.-Am. Chem. Soc., Div. Fuel Chem.* 2004, 49, 279–280.

(35) Rodriguez, S.; Almquist, C.; Lee, T. G.; Furuuchi, M.; Hedrick, E.; Biswas, P. A Mechanistic Model for Mercury Capture with in Site-Generated Titania Particles: Role of Water Vapor. *J. Air Waste Manage. Assoc.* 2004, 54, 149–156.

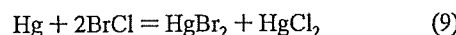
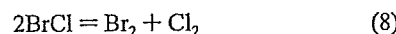
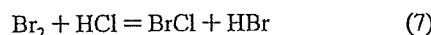
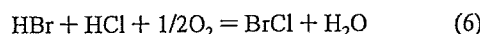
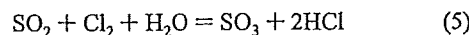
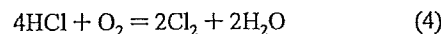
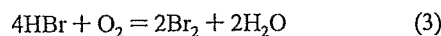
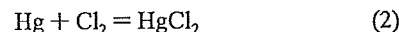
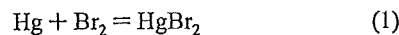
(36) Landreth, R.; Miller, J.; Rogers, W.; McCoy, M.; McMurry, R.; McGinnis, D. G.; Corey, Q.; Brickett, L. *Full-Scale B-PAC Mercury Control with Bituminous, Sub-bituminous, Lignite, and Blended Coals with Cold-Side ESPs, Fabric Filters, and a Hot-Side ESP*, 8th Annual Joint EPA, DOE, EEI, EPRI Conference on Air Quality, Global Climate Change, and Renewable Energy, Tucson, Arizona, January 24–26, 2005.

(37) Nelson, S., Jr.; Zhou, Q.; Miller, J. *Novel Duct-Injection Mercury Sorbents*, Presented at the Air Quality III Conference, Arlington, VA, Sept 9–12, 2002.

(32) Niksa, S.; Helble, J. J.; Fujiwara, N. *Interpreting Laboratory Test Data on Homogeneous Mercury Oxidation in Coal-Derived Exhausts*, Presented at the 94th Annual Meeting of the Air and Waste Management Association, Orlando, FL, June 24–28, 2001; paper 86.

an effective adsorbent to capture mercury in utility boilers by comparison to its parent activated carbon. The temperature ranges were an important factor for mercury capture by the brominated surface of solids. The brominated fly ash at the higher temperature of 330 °C did not show any mercury capture capability, which was indicated by the results from both the slipstream tests and the lab-scale fixed bed tests. Bromine species even caused the fly ash bound mercury to desorb under these higher temperatures.

Vosteen and et al. proposed possible mechanisms for enhanced mercury oxidation by the addition of the bromine species based on their extensive studies.<sup>18</sup> He pointed out that both the free bromine molecule (Br<sub>2</sub>) and the free chlorine molecule (Cl<sub>2</sub>) were more active for mercury oxidation than HBr and HCl; see eqs 1 and 2, respectively. However, the bromine Deacon reaction produced more free Br<sub>2</sub>, as shown in eq 3, than the chlorine Deacon reaction producing the chlorine molecule (Cl<sub>2</sub>), as shown in eq 4. The reason for enriched Br<sub>2</sub> in the flue gas by bromine species addition is because less Br<sub>2</sub> could be consumed by SO<sub>2</sub>, which is generally the main acid species in the coal-fired flue gas. The chlorine molecule, which was consumed by SO<sub>2</sub> as shown in eq 5, unfortunately could not largely exist in the coal-fired flue gas. However, it was noticed that bromine addition in the flue gas was conducted by co-combustion of the bromine species and coal in Vosteen's tests and that the oxidized mercury also included both HgBr<sub>2</sub> and HgCl<sub>2</sub> in their tests.<sup>18</sup> That means that the bromine species had enough residence time (several seconds) to produce Br<sub>2</sub>. Even in this longer residence time, Br<sub>2</sub> could not convert all mercury to HgBr<sub>2</sub> and left some Hg(0) to react with the Cl species to produce HgCl<sub>2</sub>. The chlorine species seemed to be involved in competition with the bromine species on the mercury oxidation process. This evidence could support our findings by thermodynamics predictions that there existed a limited mercury oxidation by the bromine species. Considering our study's test conditions where the residence time of the flue gas in the ER was about 1 s, which may be too short for total conversion of HBr to Br<sub>2</sub>, there must be other mechanisms regarding mercury oxidation with both bromine and chlorine species in the flue gas. Thermodynamics predictions provide the evidence of the maximum conversion rate of the reaction. The conversion rate of every reaction cannot exceed this line since the limitation of actual kinetics exists. To determine the conflict and thermodynamics prediction and test results, the occurrence of the intermediate species of BrCl<sup>20,31,39</sup> was proposed in this study, which brought in the competition of chlorine on mercury oxidation by bromine addition. Sulfur oxide in the flue gas, dependent on its concentration, will consume the available activated chlorine species based on Vosteen's theory.<sup>18</sup> The reduced oxidation rate by bromine addition under the flue gas atmosphere with a higher SO<sub>2</sub> concentration by burning bituminous coal seems to support this mechanism. BrCl could be generated or depleted as shown in eqs 6–8. Consequently, mercury is oxidized in the reaction shown in eq 9. All reactions listed in this study are presented as global reactions.



Mercury oxidation, associated with the Br species in the flue gas, actually occurs through two modes. The first was homogeneous in the gas phase, whose global reactions are shown in eqs 1, 2, and 9. The second was heterogeneous in nature, which occurred on the interface of the fly ash. Actual bonding between mercury and bromine on the fly ash surface was a definite initial step in the heterogeneous mode, which was further dependent on temperature. The weak bonding with fly ash resulted in the oxidation of mercury at higher temperature range. However, it may be developed into mercury adsorption on the surface of fly ash if this bonding is strong enough. Thus, fly ash can function as a mercury oxidation catalyst or a mercury adsorbent to retain the speciated mercury on its surface. Some fly ash-related mercury adsorption phenomena by the bromine addition supported the heterogeneous mechanism mentioned previously and also indicated the importance of the sampling method used in the study. We also noticed the complication of the complete explanation of the phenomena, which needs to be further studied.

Interaction of bromine and speciated mercury on the fly ash surface should be in the dynamics equilibrium status of adsorption and desorption, even at higher temperature ranges. This dynamics adsorption equilibrium can be changed in two directions by the variation of the flue gas conditions. Either the mercury was oxidized and subsequently kept out of the fly ash surface or it was retained on the fly ash surface. At higher temperatures, the dynamic adsorption and desorption equilibrium will shift to desorption of the oxidized mercury. Thus, there was a lesser possibility that speciated mercury could be retained on the surface of fly ash. At lower temperatures, there will be a reversion process that will be more favorable to retaining the captured mercury on the fly ash surface. In Figure 7, both Hg(VT) peaks at the ER outlet at approximately 330 °C and the outlet of the CP at approximately 170 °C appeared after stopping the HBr addition. The Hg(VT) peak at the CP outlet could be a possible consequence of the Hg(VT) peak at higher temperature areas in the ER because there was not enough time to capture mercury with concentrations suddenly increasing. In the ER, it seems that adsorbed bromine during bromine addition and adsorbed mercury on the fly ash continued to react and then abruptly left the fly ash surface in the gas phase when bromine addition stopped. The elemental mercury in the flue gas also continued to be reacted with the adsorbed bromine and thus made the Hg(0) recovery process slow down as indicated in the memory effect. Because of the fact that the bromine functioned differently at different temperature ranges, bias with a failure of the control temperature was attributed to some results in some cases in this study. For example, in Figure 5, Hg(VT)

(38) Zhou, Q.; Nelson, S., Jr.; Nelson, B. *Mercury Sorbent that Allows Fly Ash Use in Concrete*, Presented at the Air Quality IV Conference, Arlington, VA, Sept 22–24, 2003.

(39) Carpenter, L. J.; Hopkins, J. R.; Johns, C. E.; Lewis, A. C.; Parthipan, R.; Wevill, D. J.; Poissant, L.; Pilote, M.; Constant, P. Abiotic Source of Reactive Organic Halogens in the Sub-Arctic Atmosphere? *Environ. Sci. Technol.* 2005, 39, 8812–8816.

at the BR outlet occasionally decreased under HBr addition. Thus, frequent cleaning of the sampling probe and monitoring the status of the sampling probe was very important when the interaction of fly ash and mercury was prominent.

### 5. Conclusion

Mercury could be strongly oxidized or associated with fly ash with the addition of bromine in flue gas atmospheres by burning bituminous and PRB coal. Fly ash was an important factor in both mercury oxidation and adsorption with the bromine species available in the flue gas. However, it functioned differently under higher and lower temperature ranges. Higher temperatures (in a range of 300–350 °C) promoted mercury oxidation by bromine species but not mercury adsorption. Lower temperatures (in a range of 150–200 °C) enhanced mercury adsorption on the fly ash with the bromine species available in the flue gas. Flue gas atmospheres of different coals, such as bituminous and PRB, were shown to impact the mercury transformation by bromine addition, which was based on both test results and thermodynamics predictions. The chlorine species seemed to be involved in its competition with the bromine species on the mercury oxidation process. Thermodynamic equilibrium analyses indicated that gaseous  $\text{HgBr}_2$  was possibly formed at a maximum of 5% at equilibrium conditions under bituminous coal atmosphere and increased up to 35% under the PRB coal atmosphere at typical temperatures of the upstream APH in a utility boiler (approximately 350 °C). The disagreement in the thermodynamics predictions and test results

may indicate more complicated mercury oxidation mechanisms with HBr addition in the flue gas. One of these might be that bromine promoted the generation of the activated chlorine species, which may enhance the kinetics of  $\text{Hg}(0)$  oxidation with the chlorine species. However, depending on its concentration,  $\text{SO}_2$  in the flue gas will consume the available activated chlorine species. Thus, the higher mercury oxidation rate by bromine addition under flue gas by burning PRB coal may be associated with the lower  $\text{SO}_2$  concentration in such a flue gas.

**Acknowledgment.** This paper was prepared by the Western Kentucky University Research Group with support, in part, by grants made possible by the Electric Power Research Institute (EPRI Project EP-P13792/C6821) and the Kentucky Governor's Office of Energy Policy (Projects 05-GOEP-02 and 05-SEED-0001). Neither Western Kentucky University, nor the Electric Power Research Institute, nor the Kentucky Governor's Office of Energy Policy, nor any person acting on behalf of either (A) makes any warrant of representation, express or implied, with respect to the accuracy, completeness, or usefulness of the information contained in this paper or that the use of any information, apparatus, method, or process disclosed in this paper may not infringe privately owned rights or (B) assumes any liabilities with respect to the use of, or for damages resulting from the use of, any information apparatus, method, or process disclosed in this paper. Reference herein to any specific commercial product, process, or service by trade name, trademark, manufacturer, or otherwise does not necessarily state or reflect the endorsement of the Electric Power Research Institute and the Kentucky Governor's Office of Energy Policy.

EF060547K

# Impacts of Halogen Additions on Mercury Oxidation, in A Slipstream Selective Catalyst Reduction (SCR), Reactor When Burning Sub-Bituminous Coal

YAN CAO,<sup>\*,†</sup> ZHENGYANG GAO,<sup>†,‡</sup> JIASHUN ZHU,<sup>†</sup> QUANHAI WANG,<sup>†</sup> YAJI HUANG,<sup>†</sup> CHENGCHUNG CHIU,<sup>†,§</sup> BRUCE PARKER,<sup>||</sup> PAUL CHU,<sup>⊥</sup> AND WEI-PING PAN<sup>\*,†</sup>

*Institute for Combustion Science and Environmental Technology (ICSET), Western Kentucky University (WKU), Bowling Green, Kentucky 42101, North China Electric Power University, BaoDing 071003, HeBei, P.R. China, Mingchi University of Technology, Taipei, Taiwan, Electric Energy, Inc. (EED), Joppa, Illinois 62953, and Electric Power Research Institute (EPRI), Palo Alto, California 94304*

Received May 31, 2007. Revised manuscript received October 6, 2007. Accepted October 22, 2007.

This paper presents a comparison of impacts of halogen species on the elemental mercury (Hg(0)) oxidation in a real coal-derived flue gas atmosphere. It is reported there is a higher percentage of Hg(0) in the flue gas when burning sub-bituminous coal (herein Powder River Basin (PRB) coal) and lignite, even with the use of selective catalytic reduction (SCR). The higher Hg(0) concentration in the flue gas makes it difficult to use the wet-FGD process for the mercury emission control in coal-fired utility boilers. Investigation of enhanced Hg(0) oxidation by addition of hydrogen halogens (HF, HCl, HBr, and HI) was conducted in a slipstream reactor with and without SCR catalysts when burning PRB coal. Two commercial SCR catalysts were evaluated. SCR catalyst no. 1 showed higher efficiencies of both NO reduction and Hg(0) oxidation than those of SCR catalyst no. 2. NH<sub>3</sub> addition seemed to inhibit the Hg(0) oxidation, which indicated competitive processes between NH<sub>3</sub> reduction and Hg(0) oxidation on the surface of SCR catalysts. The hydrogen halogens, in the order of impact on Hg(0) oxidation, were HBr, HI, and HCl or HF. Addition of HBr at approximately 3 ppm could achieve 80% Hg(0) oxidation. Addition of HI at approximately 5 ppm could achieve 40% Hg(0) oxidation. In comparison to the empty reactor, 40% Hg(0) oxidation could be achieved when HCl addition was up to 300 ppm. The enhanced Hg(0) oxidation by addition of HBr and HI seemed not to be correlated to the catalytic effects by both evaluated SCR catalysts. The effectiveness of conversion of hydrogen halogens to halogen molecules or interhalogens seemed to be attributed to their impacts on Hg(0) oxidation.

\* Address correspondence to either author. E-mail: yan.cao@wku.edu (Y.C.), wei-ping.pan@wku.edu (W.P.).

† Western Kentucky University (WKU).

‡ North China Electric Power University.

§ Mingchi University of Technology.

|| Electric Energy, Inc. (EED).

⊥ Electric Power Research Institute (EPRI).

## 1. Introduction

Studies of the occurrence of speciated mercury (Hg) in flue gas are critical for reasons associated with both their environmental impacts and effective control by conventional air pollution control devices (APCDs) in coal-fired utility boilers (1–3). Mercury can be oxidized by the chlorine species in coal-fired flue gas. This oxidation process is likely to be enhanced by selective catalytic reduction (SCR) catalysts (4–9). The oxidized mercury could be easily captured by the wet flue gas desulfurization process (W-FGD) (10–14). Therefore, the combined utilization of SCR and W-FGD in coal-fired utilities has been regarded to be an economic means for multiple controls of SO<sub>x</sub>, NO<sub>x</sub>, and mercury (Hg). However, this works well for utilities when burning bituminous coals, but does not work well for utilities when burning Powder River Basin (PRB) coal. Thus, mercury control at utilities burning PRB coal has faced more challenges (1). PRB coal or lignite, with lower sulfur and chlorine content, is cheap and plentiful in the South Central (Texas) and North Central (Wyoming, Montana, and South Dakota) areas of the U.S. (15). They are widely used by American coal-fired utilities. However, lower chlorine content in PRB and lignite is reported to be associated with their lower Hg(0) oxidation even with the enhancement effect of SCR. Methods to effectively convert Hg(0) to Hg(2+) (the oxidized mercury) seem very critical for utility boilers where PRB coal or lignite is burned.

Generally, chlorine is the major halogen species in coals (16). According to the United States Geological Survey (USGS), there are some halogens other than chlorine, such as fluorine, bromine and iodine in coals (17–19). Chlorine and fluorine content in PRB coal is generally comparable, but always 100–1000 times higher than the bromine and iodine contents, which is too low to be detected by ASTM methods (20). This was why very few reports were made on halogens other than chlorine. Most previous studies indicated the correlation between chlorine and Hg(0) oxidation was largely scattered (1, 3), which inspired us to investigate the possible impact of halogens on Hg(0) oxidation and their mechanisms. This work attempts first to investigate performance of the SCR catalyst in PRB coal flue gas, including the impact of flue gas composition of PRB coal on NO<sub>x</sub> reduction and Hg(0) oxidation under SCR conditions. Second, to explore impacts of hydrogen halogens on Hg(0) oxidation and their mechanisms. Answering these questions could allow utilities to use some additives with or without SCRs as part of mercury compliance planning. This work was accomplished using a slipstream facility. The greatest benefits of slipstream tests can be flexible control and isolation of specific factors.

## 2. Experimental Section

**Test Utility, Slipstream Facility, and SCR Catalysts.** The detailed information on test utility, the schematic of the experimental setup and quality assurance and quality control (QA/QC) of mercury measurement can be found in previous studies (8, 21). The average temperature of the SCR facility in this study varied between 620 and 690 °F, which was dependent on boiler loads when tests were conducted. The residence time of flue gas inside the slipstream reactor was controlled to be about 1 s. When the SCR catalyst was loaded, the space velocity (the ratio of volumetric gas flow to catalyst volume) was set at 3600 h<sup>-1</sup>. Two tested honeycomb SCR catalysts were provided by two commercial vendors, CORMETECH, Inc. and BASF/CERAM, Inc. The pitch sizes and cell numbers are 8.4 mm and 18 × 18 for catalyst no. 1

(CORMETECH, Inc.), and 10 mm and 15 × 16 for catalyst no. 2 (BASF/CERAM, Inc.). The main components of both these two SCR catalysts are V<sub>2</sub>O<sub>5</sub>-WO<sub>3</sub>-TiO<sub>2</sub>.

**Characterizations of Coal, Ash, and Flue Gas of PRB Coal.** Coal was sampled as it was transferred into the coal bunkers. The sampled coal represents coal fueled to the test unit. Ash is a composite of all fly ash removed from the electrostatic precipitator (ESP) hoppers from the test unit. The coal and ash analysis results are shown in Table S1 in the Supporting Information (SI). Analysis methods and QA/QC procedures can be found in ref 21. There were three testing phases in this study. During phase 1, tests without SCR catalysts in the slipstream reactor were conducted. The average sulfur, chlorine, and mercury contents in the PRB coal burned were about 0.37%, 72 ppm, and 0.08 ppm. The bromine and iodine contents in tested coals were under the detection limit (less than 5 ppm). During phase 2 and phase 3, tests with SCR catalyst no. 1 and no. 2 in the SCR slipstream reactor were conducted, respectively. The average sulfur, chlorine, and mercury contents in the burned PRB coal were approximately 0.44%, 127 ppm, and 0.07 ppm in the second phase and 0.39%, 88 ppm, and 0.09 ppm in the third phase.

**Additive Injections.** NH<sub>3</sub>, HCl, and HBr gases were injected in the slipstream reactor by the control of a mass flow controller (MFC). HI and HF were injected using HI and HF solutions. Static mixers in the slipstream reactor ensured good mixing of additives and the flue gas. All additives were injected through several ports, which were located after the mercury sampling port at the SCR inlet, thus keeping the inlet sampling port unaffected by additives. In this study, the additional concentration of the individual additives or spike gases in the flue gas were controlled at ranges of 0–300 ppm for HCl, 0–9 ppm for HBr, 0–20 ppm for HF, and 0–15 ppm for HI.

**SCR Slipstream Facility and Mercury Measurement.** In this study, the SCR slipstream reactor was used as the testing facility. The detailed description of this facility, along with mercury measurement methods, are shown in ref 9.

### 3. Results and Discussion

**3.1. Performances of NO (Nitric Oxide) Reduction by SCR Catalysts.** The reduction performance of the two SCR catalysts were evaluated by monitoring the NO concentration at the inlet and outlet locations of the SCR slipstream reactor. IMR combustion-gas analyzer System 5000 with integrated gas-conditioning system, which is based on electro-chemical principle (from IMR Environmental Equipment, Inc.) was used as NO monitor (with detection limit of 1 ppm). Because of the low-NO burner installed in the test unit, NO concentration, which was introduced into the slipstream reactor, was found to be low: about 90 ppm (with 3% O<sub>2</sub> correction) at the SCR inlet location. Under NH<sub>3</sub> addition, both SCR catalysts worked properly in the SCR slipstream reactor. Lower NO at the slipstream outlet location could be achieved by SCR catalyst no. 1 than by SCR catalyst no. 2. A 92.5% NO reduction was observed by SCR catalyst no. 1 and 86.5% of NO reduction by SCR catalyst no. 2 when NH<sub>3</sub>:NO was close to 1, as indicated in SI Figure S1. The corresponding NO concentrations at the slipstream outlet were 6 and 12 ppm (3% O<sub>2</sub> correction), respectively.

**3.2. Effects of Halogen Additions on Mercury Oxidation.** Hg(0) oxidation in the SCR may occur through two processes (8, 22–24), (1) homogeneous oxidation, which occurs in the gas phase, and (2) heterogeneous oxidation, which occurs on the interface of solids (SCR catalyst or fly ash). To determine the contribution of SCR on Hg(0) oxidation, two kinds of tests were conducted. Tests with the empty bed of the slipstream reactor were conducted to investigate the possible Hg(0) oxidation mechanism including both Hg(0) homogeneous oxidation and Hg(0) heterogeneous oxidation

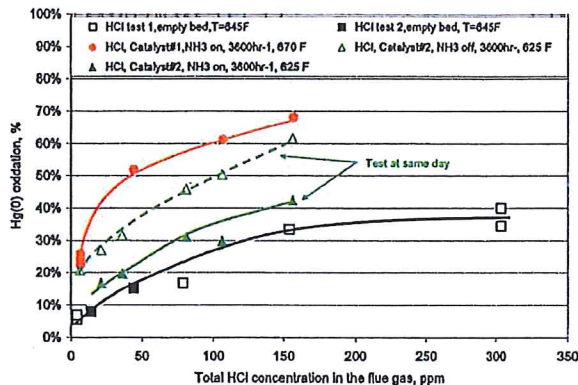


FIGURE 1. Effect of HCl addition on Hg(0) oxidation.

by interaction with “in-flight” fly ash. Tests with SCR catalyst in the SCR slipstream reactor were conducted to investigate the additional Hg(0) oxidation compared to the tests in the empty bed. The comparison of Hg(0) oxidation rates between two kinds of tests should be solely due to the catalytic effect of the SCR catalyst. Results were presented as the incremental percentage variation between the Hg(0) concentration at the SCR reactor inlet, (Hg(0)<sub>in</sub>), and the Hg(0) concentration at the SCR reactor outlet, (Hg(0)<sub>out</sub>), as indicated in eq (1).

$$\% \text{ Hg(0) oxidation} = 100 * \{ [\text{Hg(0)}]_{\text{in}} - \text{Hg(0)}_{\text{out}} \} / [\text{Hg(0)}]_{\text{in}} \quad (1)$$

**3.2.1. Addition of Hydrogen Chloride (HCl).** In the coal-derived flue gases, chlorine is believed to be mainly HCl. It is a most important species affecting mercury oxidation since the major oxidized mercury species in coal-fired flue gas is Hg(Cl)<sub>2</sub>. The effects of the spike gas HCl on the Hg(0) oxidation during tests in the empty slipstream reactor or those in the SCR slipstream reactor with two catalysts are shown in Figure 1. Whether the SCR catalysts were available or not, HCl showed a positive impact to increase Hg(2+) in the flue gas when burning PRB coal in this study. Tests in the empty slipstream reactor indicated that the percentage of Hg(0) oxidation increased to 7.9, 15.2, 16.7, 33.5, and 37.5% with incremented concentrations of HCl at 10, 40, 75, 150, and 300 ppm (total chlorine concentration in the flue gas at approximately 16.9, 44, 79, 154, and 304 ppm in the flue gas), respectively. When the HCl addition concentration was increased to above 150 ppm, the Hg(0) oxidation curve became flat.

During tests with SCR catalyst no. 1 in the SCR slipstream reactor at a NH<sub>3</sub> addition ratio at 1 (NH<sub>3</sub>/NO~1), the percentage of Hg(0) oxidation was largely increased by approximately 30% in comparison to those under tests in the empty slipstream reactor at similar HCl addition concentrations. With the HCl additions at 100 and 150 ppm, the Hg(0) oxidation increased to about 62 and 68%, respectively. During tests with SCR catalyst no. 2 at a similar NH<sub>3</sub> addition ratio (NH<sub>3</sub>/NO~1), the additional oxidations of Hg(0) were approximately 30 and 45%, respectively at HCl additions at 100 and 150 ppm. The additional Hg(0) oxidation with SCR catalyst no. 2 over those in the empty slipstream reactor was approximately only 10% at similar HCl addition concentrations. It was apparently lower than those tests with SCR catalyst no. 1. Thus, both SCR catalysts were shown to have catalytic effects, but to a different extent, on Hg(0) oxidation. For SCR catalyst no. 2, stopping injection of NH<sub>3</sub> apparently could improve Hg(0) oxidation by approximately 15%. That implies NH<sub>3</sub> had a negative impact on the Hg(0) oxidation process, at least for SCR catalyst no. 2. This study confirms that NO reduction by NH<sub>3</sub> and Hg(0) oxidation by chlorine

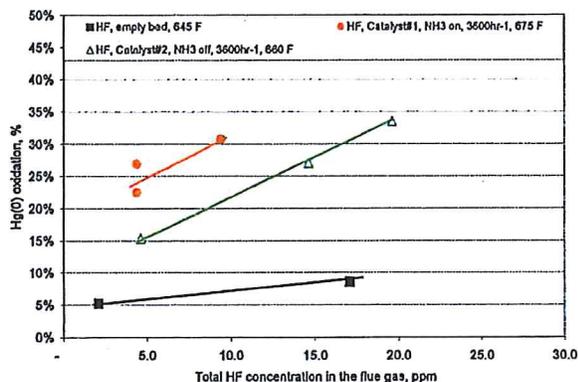


FIGURE 2. Effect of HF addition on Hg(0) oxidation.

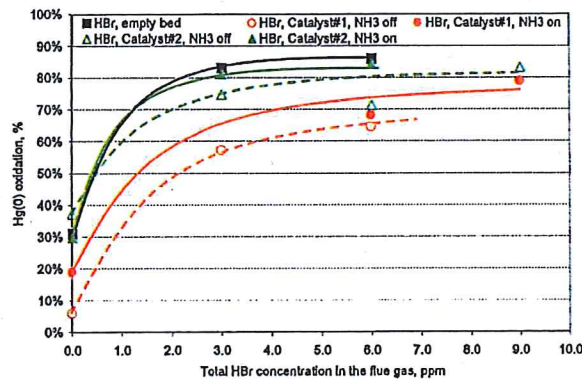


FIGURE 3. Effect of HBr addition on Hg(0) oxidation.

species simultaneously, but competitively occur on the surface of the SCR catalysts.

**3.2.2. Addition of Hydrogen Fluoride (HF).** Fluorine is another common halogen element in PRB coal, whose content varied between 20 and 50 ppm and was comparable to that of chlorine (100 ppm on average) in PRB coal, as indicated in SI Table S1. The effects of spike HF gases on Hg(0) oxidation during tests in the empty slipstream reactor and SCR slipstream reactor are shown in Figure 2. In both cases, HF additions showed a positive impact to increase the Hg(2+) in the flue gas of PRB coal. However, the capability of HF addition on the Hg(0) oxidation seemed limited as that of HCl. In the empty slipstream reactor, the percentage of Hg(0) oxidation was only 8.5% with HF addition, concentration up to 15 ppm (the total fluorine concentration in the flue gas was approximately 17.5 ppm). In the SCR slipstream reactor with catalyst no. 1 under the condition of NH<sub>3</sub> addition, the Hg(0) oxidations were about 25 and 30% with the addition of HF at about 3–8 ppm (the total fluorine concentrations in the flue gas at about 5 and 10 ppm). In the SCR slipstream reactor with catalyst no. 2, however without NH<sub>3</sub> addition, the Hg(0) oxidations were approximately 15, 26, and 34 with HF addition at 3, 13, and 18 ppm (the total fluorine concentrations in the flue gas at about 5, 15, and 20 ppm). Thus, both SCR catalysts in this study promoted Hg(0) oxidation in comparison to the case of the empty slipstream reactor. Considering the negative effect of NH<sub>3</sub> addition on the Hg(0) oxidation, SCR catalyst no. 1 should have higher oxidation activity than catalyst no. 2 during the addition of HF.

**3.2.3. Addition of Hydrogen Bromide (HBr).** The effects of HBr additions on Hg(0) oxidation in the empty slipstream reactor and in the SCR slipstream reactor are shown in Figure 3. Whether the SCR catalysts were available or not, HBr showed a very strong impact in increasing Hg(0) oxidation in the PRB coal-derived flue gas atmosphere. Tests in the

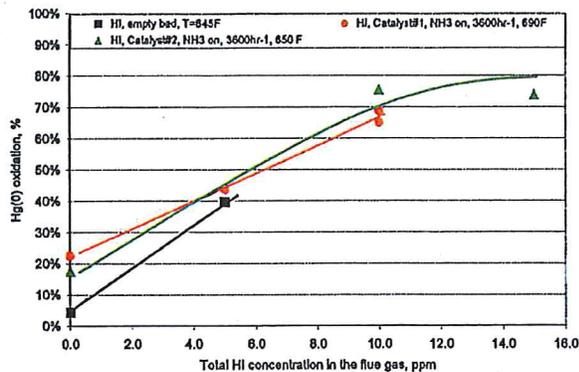


FIGURE 4. Effect of HI addition on Hg(0) oxidation.

empty slipstream reactor indicated the percentage of Hg(0) oxidation increased to 83 and 85.9% with additional concentrations of HBr at only 3 and 6 ppm, respectively. With the increase of HBr addition concentration from 3 to 6 ppm, the Hg(0) oxidation curve became flat. This may indicate that no apparent additional Hg(0) oxidation could be achieved by continuous addition of the HBr. During tests with SCR catalyst no. 1 at a preferred NH<sub>3</sub> addition ratio (NH<sub>3</sub>/NO~1), the percentages of Hg(0) oxidation were approximately 68.2 and 78.9% at HBr addition concentrations of 6 and 9 ppm, respectively. If addition of NH<sub>3</sub> was turned off, the percentages of Hg(0) oxidation were approximately 57.3 and 64.4% at HBr addition concentrations of 3 and 6 ppm, respectively. During tests with SCR catalyst no. 2, at a similar NH<sub>3</sub> addition ratio (NH<sub>3</sub>/NO~1), the percentages of Hg(0) oxidation were approximately 74.7 and 83.2% at HBr addition concentrations of 3 and 9 ppm, respectively. If addition of NH<sub>3</sub> was turned off, the percentages of Hg(0) oxidation were approximately 81 and 84.2% at HBr addition concentrations of 3 and 6 ppm, respectively.

There was good match between results from tests in the empty slipstream reactor and SCR slipstream reactor with both catalyst no. 1 and catalyst no. 2. This indicated the SCR catalyst did not have apparent promotion of Hg(0) oxidation and thus consequently was independent of impacts of NH<sub>3</sub> additions. This finding may indicate the promising function of HBr on Hg(0) oxidation and simultaneously Hg(0) oxidation was less dependent on the availability of SCR catalysts. This was different from those by additions of HCl or HF. In this study, The Hg(0) oxidation efficiencies were slightly lower at approximately 6.1 and 19% at baseline level (without addition of HBr) during tests with SCR catalyst no. 1 when NH<sub>3</sub> addition was on and off. During tests with SCR catalyst no. 2, its baseline values increased to 37.2 and 29.8% when NH<sub>3</sub> addition was on and off. During test with the empty slipstream reactor, this baseline value was also higher at approximately 29.5%. Thus, tests with SCR catalyst no. 1 showed a little lower Hg(0) oxidation efficiency by HBr addition, compared to cases in the empty slipstream reactor and SCR slipstream reactor with catalyst no. 2.

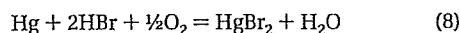
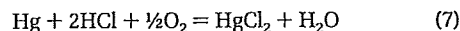
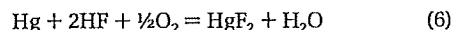
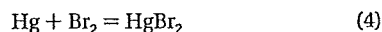
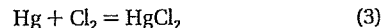
**3.2.4. Addition of Hydrogen Iodine (HI).** The effects of additions of HI on Hg(0) oxidation during tests in the empty slipstream reactor and SCR slipstream reactor are shown in Figure 4. In both cases, HI additions showed a stronger impact to increase the Hg(2+) in the flue gas of PRB coal. In the empty slipstream reactor, the addition of HI at 5 ppm could achieve approximately 40% of Hg(0) oxidation. With the same addition concentration of HI at 5 ppm in the SCR slipstream reactor with catalyst no. 1, similarly 40% Hg(0) oxidation efficiency could be achieved. When HI addition concentrations increased to 10 ppm, nearly the same Hg(0) oxidation efficiencies (approximately 70%) could be achieved for both SCR catalysts. These may indicate that Hg(0) oxidation by HI

addition was also independent of the availability of a SCR catalyst. A further increase of HI addition concentration to 15 ppm did not continuously increase Hg(0) oxidation efficiency for SCR catalyst no. 2, which is possibly limited by its reaction kinetics. Hg(0) oxidation was independent of the availability of SCR catalysts when HI was added in the flue gas. This was also observed when HBr was added, but was not observed when HCl and HF were added. It is believed that Hg(0) oxidation by HI and HBr may be through a similar mechanism.

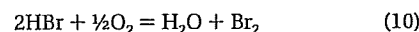
**3.3. Comparison of Impacts on Hg(0) Oxidation by Different Halogen Additives.** Figure S2 in the Supporting Information presents a comparison of impacts of different halogens (HCl, HF, HBr, and HI) on Hg(0) oxidation under a PRB coal-derived flue gas atmosphere, which was made using results from the empty slipstream reactor. The maximum Hg(0) oxidation efficiency at approximately 40% could be achieved by total HCl concentration at 300 ppm in the flue gas. The increase of Hg(0) oxidation efficiency by HF addition seemed to follow the same trend, and was also comparable to the HCl addition at the same addition concentration. As indicated in Figures 1 and 2, both SCR catalysts seemed to promote Hg(0) oxidation by HCl and HF at the same addition concentrations. The tests by additions of HCl and HF in this study were consistent with the lower Hg(0) oxidation efficiencies in the full scale utility boilers by burning PRB coal since its chlorine and fluorine contents are lower. As expected, addition of HCl could further increase Hg(0) oxidation, which can be catalyzed by both of the evaluated SCR catalysts. For comparison, by achieving the same Hg(0) oxidation efficiency at approximately 40% in the empty slipstream reactor (the baseline Hg(0) oxidation at about 5%), the addition of HI concentration in the flue gas only needed to be 5 ppm. Moreover, HBr addition concentration at only 3 ppm could achieve the Hg(0) oxidation efficiency as high as above 80% in the empty slipstream reactor (the baseline Hg(0) oxidation at about 30%). Both HBr and HI showed much stronger impacts on the Hg(0) oxidation than those by HCl and HF at the same addition concentrations. As indicated in Figures 3 and 4, the catalytic effects by SCR catalysts seemed not to be correlated with Hg(0) oxidation during additions of HBr and HI in the flue gas of PRB coal, at least for both evaluated SCR catalysts in this study.

The sequence, according to their impact strength on Hg(0) oxidation, were HBr, HI, and HCl or HF. It seemed to follow their inversed atom sequence in the Periodic Table of the Elements, except for the order between HBr and HI. The larger the halogen atom is, the greater its impact on Hg(0) oxidation. Two categories could be sorted by considering their interaction with the SCR catalyst and also interaction with NH<sub>3</sub> on the surface of SCR catalysts. SCR catalysts seemed to promote the Hg(0) oxidation through HCl and HF in Category 1, but not through HBr and HI in Category 2. NH<sub>3</sub> seemed to impact the Hg(0) oxidation only by HCl and HF through both SCR catalysts in Category 1.

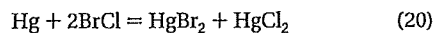
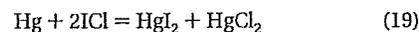
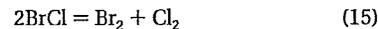
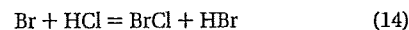
There were some clues to explicate the findings in this study. First, reaction paths for Hg(0) oxidation through halogen molecules (Br<sub>2</sub>, I<sub>2</sub>, Cl<sub>2</sub> and F<sub>2</sub>), as indicated in eqs 2–5 were generally favored in kinetics than those through hydrogen halogens, as indicated in eqs 6–9. This was at least clarified by previous investigation of Hg(0) oxidation mechanisms, which the chlorine or bromine species were involved in (25). That means kinetics of Hg(0) oxidation should be faster through halogen molecules than those through hydrogen halogens if previous studies on Hg(0) oxidation mechanisms by HCl and HBr could be further extended to those by HF and HI.



Second, additions of HBr and HI into the elevated temperature conditions would generate almost total conversion of HBr to Br<sub>2</sub>, and HI to I<sub>2</sub>. The generation of Br<sub>2</sub> could be through the Deacon reaction of bromine, as indicated in eq 10 (25). By a different reaction routine, I<sub>2</sub> could be generated through decomposition of HI (26, 27), as indicated in eq 11. However, this was not the case for HCl since the depletion of Cl<sub>2</sub> would occur by the enriched SO<sub>2</sub> in the coal-derived flue gases (8, 25), as indicated in eq 12.



Third, a more complicated mechanism was proposed to occur by additions of HBr and HI in the flue gas, in which interhalogen species (such as BrCl or ICl) were likely to be involved in the elemental mercury oxidation processes. The interhalogen of BrCl may be generated through reaction, as indicated in eqs 13 or 14, and depleted through reaction, as indicated in eq 15. And the interhalogen of ICl may be generated through reactions, as indicated in eqs 16 or 17, and depleted through reaction, as indicated in eq 18. Generally the interhalogens are unstable and extremely reactive chemically (28). The elemental mercury oxidation may occur through reactions by BrCl and ICl (29, 30), as indicated in eqs 19 and 20, respectively. Thus, outcomes of elemental oxidation may include mutual species of either HgCl<sub>2</sub> and HgBr<sub>2</sub>, or HgCl<sub>2</sub> and HgI<sub>2</sub>, respectively. Interhalogen species such as ClF also could be possibly generated, but did not seem important due to comparable impact of Cl and F on Hg(0) oxidation kinetics by tests in this study.



Under a temperature of around 300 °C, thermodynamics studies indicated there was a limitation on HgBr<sub>2</sub> or HgI<sub>2</sub> occurrence in the coal-fired flue gas, but not for HgCl<sub>2</sub> (9). HgCl<sub>2</sub> can proceed to the extent of approximately 100% conversion under the temperature range in this study if kinetics of mercury oxidation by chlorine is quick enough in the slipstream reactor. The enhanced Hg(0) oxidation rate by bromine additions in this study, and likely iodine additions, exceeded the limitation of thermodynamics prediction (9). It may indicate that the formation of HgBr<sub>2</sub> or likely HgI<sub>2</sub> were not the only new products by the addition of bromine or iodine. It was possible for the simultaneous formation of HgBr<sub>2</sub> and HgCl<sub>2</sub> by bromine addition, or HgI<sub>2</sub> and HgCl<sub>2</sub> by

iodine addition. Bromine or iodine seems to have the capability to attack chlorine species in the flue gas to promote the generation of activated chlorine, which was involved in improving the kinetics of mercury oxidation (28). This may explain why the total mercury oxidation rate exceeded the thermodynamics limitation on maximum occurrence of  $\text{HgBr}_2$  and  $\text{HgI}_2$ . Vosteen, et al. proposed the possible mechanisms on enhanced mercury oxidation by the addition of Bromine species based on their extensive studies (25). Larger generation of free bromine molecule ( $\text{Br}_2$ ), other than free chlorine molecule ( $\text{Cl}_2$ ) by HBr and HCl additions in the flue gas, was his point to distinguish the different impacts of bromine and chlorine on the elemental mercury oxidation kinetics. The bromine Deacon reaction will be favored to produce comparatively much more free  $\text{Br}_2$ , as shown in eq 10, whereas the reversed chlorine Deacon reaction will be favored by the depletion effect of  $\text{SO}_2$  in the flue gas. However, it was noticed that the bromine addition in the flue gas was conducted by cofiring of bromine species and coal in Vosteen's tests (higher temperature circumstance than in the current study) and the oxidized mercury included both  $\text{HgBr}_2$  and  $\text{HgCl}_2$  in their tests. This evidence may have revealed that, first bromine species had enough residence time (in several seconds) to produce  $\text{Br}_2$ ; and second,  $\text{Br}_2$  could not make a conversion of all mercury to  $\text{HgBr}_2$  and left some of the  $\text{Hg}(0)$  to be reacted with active Cl species to produce  $\text{HgCl}_2$ , even in this longer residence time than the current study. Chlorine species seemed to be involved in its competition to bromine species on the  $\text{Hg}(0)$  oxidation process. This evidence could support our findings by thermodynamics prediction that there exists a limitation of mercury oxidation by bromine species. Considering test conditions in this study that residence time of flue gas in an empty slipstream reactor was just one second, which may be too short for total conversion of HBr to  $\text{Br}_2$ , there must be other mechanisms regarding mercury oxidation with both bromine and chlorine species in the flue gas. To figure out the conflict and thermodynamics prediction and test results, the occurrence of the intermediate species of  $\text{BrCl}$  and  $\text{ICl}$ , was proposed in this study, which brought in the competition of chlorine on mercury oxidation under enhanced kinetics.

Thus, by a combination of findings in this study and previous studies, one may reasonably find that different impacts of halogens on  $\text{Hg}(0)$  oxidation should result from different kinetics between the  $\text{Hg}(0)$  and halogens in the kinetics-controlled  $\text{Hg}(0)$  oxidation process. Comparably, HCl was not effective to oxidize  $\text{Hg}(0)$  due to its ineffective conversion to their molecule ( $\text{Cl}_2$ ) under coal-fired flue gas atmospheres. Thus, eq 7 may be the main reaction routine for  $\text{Hg}(0)$  oxidation through HCl. HF addition most likely follows the same mechanisms, as indicated in eq 6, if the presumption of ineffective conversion of HF to  $\text{F}_2$  in the flue gas could be valid. With HBr or HI additions in the flue gas,  $\text{Hg}(0)$  oxidation will occur through two different routines, which are dependent on temperature ranges. Under higher temperature (generally higher than  $650^\circ\text{C}$  (27)), HBr and HI will be converted to  $\text{Br}_2$  and  $\text{I}_2$ .  $\text{Br}_2$  and  $\text{I}_2$  will make  $\text{Hg}(0)$  oxidation proceed very fast through reactions eqs 8 and 9), respectively. Thus,  $\text{HgBr}_2$  and  $\text{HgI}_2$  will be the main oxidized mercury in the flue gas, respectively. Under a lower temperature range (around  $300^\circ\text{C}$  such as in this study), HBr and HI will interact with HCl, which is available in the coal-fired flue gas, to generate interhalogens such as  $\text{BrCl}$  and  $\text{ICl}$  (30).  $\text{BrCl}$  and  $\text{ICl}$  also will make  $\text{Hg}(0)$  oxidation proceed fast through reactions eqs 19 and 20. Thus, both  $\text{HgBr}_2$  and  $\text{HgCl}_2$ , or  $\text{HgI}_2$  and  $\text{HgCl}_2$ , are occurrences of oxidized mercury in the flue gas. All reactions listed in this study were presented as global reactions. Detailed mechanism studies should be addressed in further studies.

## Acknowledgments

This paper was prepared by the Western Kentucky University Research Group with support, in part, by grants made possible by Electric Power Research Institute (EPRI project no. EP-P20247/C9896), Kentucky Office of Energy Policy Energy R&D Program (project no. PO2 855 0600002929 1), and the United States Department of Energy (DE-FC26-03NT41840). Neither Western Kentucky University nor the Electric Power Research Institute, Kentucky Office of Energy Policy and U.S. DOE, nor any person acting on behalf of either (A) makes any warrant of representation, express or implied, with respect to the accuracy, completeness, or usefulness of the information contained in this paper, or that the use of any information, apparatus, method, or process disclosed in this paper may not infringe privately owned rights; or (B) assumes any liabilities with respect to the use of, or for damages resulting from the use of, any information apparatus, method or process disclosed in this paper. Reference herein to any specific commercial product, process, or service by trade name, trademark, manufacturer, or otherwise, does not necessarily state or reflect the endorsement of the Electric Power Research Institute, Kentucky Office of Energy Policy and the United States Department of Energy.

## Supporting Information Available

Two figures and one table. This material is available free of charge via the Internet at <http://pubs.acs.org>.

## Literature Cited

- (1) Kilgroe, J. D.; Sedman, C. B.; Srivastava, R. K.; Ryan, J. V.; Lee, C. W.; Thorneloe, S. A. *Control of Mercury Emission from Coal-Fired Electric Utility Boilers: Interim Report, number EPA-600/R-01-109*; U.S. Environmental Protection Agency, Washington, DC, 2001.
- (2) Ravi, K.; Srivastava, N.; Hutson, B.; Martin, F.; Staudt, P. J. Control of mercury emissions from coal-fired electric utility boiler. *Environ. Sci. Technol.* 2006, 40, 1385-1393.
- (3) Pavlish, J. H.; Scordreal, E. A.; Mann, M. D.; Olson, E. S.; Galbreath, K. C.; Laudal, D. L.; Benson, S. A. Status review of mercury control options for coal-fired power plant. *Fuel Process. Technol.* 2003, 82, 89-165.
- (4) Lee, C. W.; Srivastava, R. K.; Ghorishi, S. B.; Hastings, T. W.; Stevens, F. M. Study of Speciation of Mercury under Simulated SCR NO<sub>x</sub> Emission Control Conditions. In *Air & Waste Management Association Combined Power Plant Air Pollution Control Symposium*; The Mega Symposium, Washington, DC, 2003.
- (5) Richard, C.; Machalek, T.; Miller, S.; Dene, C.; Chang, R. Effect of NO<sub>x</sub> Control Processes on Mercury Speciation in Flue Gas. In *Air Quality III Meeting*, Washington, DC, 2002.
- (6) Laudal, D. L.; Thompson, J. S.; Pavlish, J. H.; Brickett, L.; Chu, P.; Srivastava, R. K.; Lee, C. W.; Kilgroe, J. Mercury speciation at power plants using SCR and SNCR control technologies. *EM*, 2003, February 22.
- (7) Hocquel, M. *The Behavior and Fate of Mercury in Coal-Fired Power Plants with Downstream Air Pollution Control Devices*; Forsch.-Ber. VDI Verlag: Dusseldorf, Germany, 2004.
- (8) Cao, Y.; Chen, B.; Wu, J.; Cui, H.; Li, S. G.; Herren, S. M.; Smith, J.; Chu, P.; Pan, W. P. Study of mercury oxidation by selective catalytic reduction catalyst in a pilot-scale slipstream reactor at a utility boiler burning bituminous coal. *Energy Fuels* 2007, 21, 145-156.
- (9) Cao, Y.; Wang, Q. H.; Chen, W. C.; Chen, B.; Cohron, M.; Chiu, C. C.; Tseng, Y. C.; Chu, P.; Pan, W. P. Investigation of mercury transformation by HBr addition in a slipstream facility with real flue gas atmospheres of bituminous coal and Powder River Basin (PRB) Coal. *Energy Fuels* 2007, 21, 2719-2730.
- (10) Maxwell, W. H. Revised New Source Performance Standard (NSPS) Statistical Analytical for Mercury Emissions. 2006. <http://epa.gov/tm/atw/utility/NSPS-053106.pdf>.
- (11) Maxwell, B. Revised New Source Performance Standard (NSPS) Statistical Analytical for Mercury Emissions. 2005. <http://dnr.wi.gov/org/aw/air/reg/mercury/camr/Hgstatrevisiondoc.pdf>.
- (12) Shea, D. A.; Parker, L.; McCarthy, J. E.; Chapman, T. Mercury Emission from Electric Generating Units: A Review of EPA

- Analysis and MACT Determination: CRS Report for Congress. Order Code RL32744, 2005.
- (13) Niksa, S.; Fujiwara, N. Prediction the Impact of Wet FGD on Mercury Emissions. In *EUEC, 2005*, Tucson, AZ, 2005.
- (14) Mercedes, D. S.; Sven, U.; Klaus, R. G. Hein. Using wet-FGD systems for mercury removal. *J. Environ. Monit.* 2005, 7, 906-909.
- (15) U.S. Department of Energy, Energy Information Administration. *U.S. Coal Reserves: 1997 Update, DOE/EIA-0529(97)*; Office of Coal, Nuclear, Electric and Alternate Fuels, Office of Integrated Analysis and Forecasting: Washington, DC, 1999.
- (16) Davidson, R. Chlorine in coal combustion and co-firing. CCC/105, 2005, ISBN 92-9029-421-3.
- (17) Meij, R. Mass Balance Studies of Trace Elements in Coal-fired Power Plants Including Co-Combustion of Wastes and Biomass. In *Trace Elements Workshop Organized by IEA*; University of Warrick: Coventry, UK, 1999.
- (18) United States Department of the Interior Geological Survey. The U. S. Geological Survey Coal Quality Data Base (COALQUAL). <http://energy.er.usgs.gov>.
- (19) Bettinelli, M.; Spezia, S.; Minoia, C.; Ronchi, A. Determination of chlorine, fluorine, bromine, and iodine in coals with ICP-MS and IC. *At. Spectrosc.*, 2002, 23 (4).
- (20) Standard Test Method for Chlorine in Coal. ASTM: D236, 2001.
- (21) Cao, Y.; Duan, Y. F.; Kellie, K.; Li, L. C.; Xu, W. B.; Riley, J. T.; Pan, W. P. Impact of coal chlorine on mercury speciation and emission from a 100-MW utility boiler with cold-side electrostatic precipitators and low-NOx burners. *Energy Fuels* 2005, 19, 842-854.
- (22) Senior, C. L. Oxidation of mercury across selective catalyst reduction catalysts in coal-fired power plant. *J. Air & Waste Manage. Assoc.* 2005, 56, 23-31.
- (23) Niksa, S.; Fujiwara, N. A predictive mechanism for mercury oxidation on selective catalytic reduction catalysts under coal-derived flue gas. *J. Air & Waste Manage. Assoc.* 2005, 55, 1866-1875.
- (24) Edwards, J. R.; Srivastava, R. K.; Kilgroe, J. D. A study of gas-phase mercury speciation using detailed chemical kinetics. *J. Air Waste Manage.* 2001, 5, 869-877.
- (25) Vosteen, B. W.; Kanefke, R.; Koser, H. Bromine-enhanced mercury abatement from combustion flue gases - recent industrial applications and laboratory research. VGB Power Tech. *Int. J. Electr. Heat Generation* 2006, 86 (3), 70-75.
- (26) Sakuri, M.; Nakajima, H.; Onuki, K.; Ikenoya, K.; Shimizu, S. Preliminary process analysis for the closed cycle operation of the iodine-sulfur thermochemical hydrogen production process. *Int. J. Hydrogen Energy* 1999, 24, 603-612.
- (27) Giaconia, A.; Caputo, G.; Ceroli, A.; Diamanti, M.; Barbarossa, V.; Taruni, P.; Sau, S. Experimental study of two phase separation in the bunsen section of the sulfur-iodine thermochemical cycle. *Int. J. Hydrogen Energy* 2007, 32, 531-536.
- (28) Nebergell, W. H.; Schmidt F. C., Jr. Holtzclaw, H. F. In *College Chemistry with Qualitative Analysis* 5th ed; Heath and Company: Washington, DC, 1976.
- (29) Calvert, J. G.; Lindberg, S. E. The potential influence of iodine-containing compounds on the chemistry of the troposphere in the polar spring. II. mercury depletion. *Atmos. Environ.* 2004, 38, 5105-5116.
- (30) Geoffrey D. S. Senior, C. L.; O'Palko, A. Analysis of Bromine-Mercury Reactions in Flue Gas. In *University Coal Research/ Historically Black Colleges and Universities & Other Minority Institutions Contractors Review Meeting*; U. S. Department of Energy: Washington, DC, 2007.

ES071281E

# Field Testing of an FGD Additive for Enhanced Mercury Control

---



Gary Blythe  
URS Corporation



NETL Project DE-FC26-04NT42309  
COR: Charles Miller



EPRI Project Manager: Richard Rhudy

**EPRI**

**URS**

# Project Overview

- Field tests (pilot to full scale) of Degussa's TMT-15 additive for optimizing Hg capture by wet FGD
  - Prevent re-emissions
  - Minimize Hg in gypsum byproduct
- Co-funded by EPRI, TXU, Southern Company
- Test sites:
  - TXU Monticello (pilot wet FGD)
  - AEP Conesville (has dropped out due to recent OH results showing no re-emissions from Mg-lime FGD)
  - Southern Co. Plant Yates (pilot and full-scale JBR tests)

# Degussa TMT-15

---

- 15 wt% aqueous solution of trimercapto-s-triazine, tri-sodium salt ( $C_3N_3S_3Na_3$ )
- Primarily used to precipitate divalent heavy metals from wastewaters



- Currently used in 100's of incineration plants worldwide to precipitate Hg before re-emissions reactions can occur in wet scrubbers

# Hg-TMT Precipitates

- Divalent cation to trivalent anion precipitation leads to “cross linking”, produces precipitates large enough to filter, but much smaller than the bulk of the FGD solids
- Digestion of the Hg-TMT precipitate requires aqua regia under heat and pressure (i.e., more stable at low pH than other sulfides)
- Hg-TMT precipitates are thermally stable to 250°C (480°F)
  - Gypsum is calcined at 300°F to make wallboard

# TMT Properties

---

- Low toxicity to fish, water fleas, algae, etc.
- Mild irritant to skin, irritant to eyes
- No special PPE other than gloves, glasses or goggles with close-fitting side shields
- Not considered hazardous for transportation purposes

# Potential Economics for Enhanced Hg Co-removal Using TMT-15

- TMT-15 costs about \$4/kg as solution
- To prevent re-emissions:
  - Assume 20  $\mu\text{g}/\text{Nm}^3$  Hg in flue gas, 50% oxidized
  - Assume re-emissions at 2  $\mu\text{g}/\text{Nm}^3$  Hg
  - If TMT-15 is effective at 10x stoichiometric amount, cost is <\$500/lb additional Hg removed
- To lower Hg content of gypsum (same assumptions as above):
  - Annual value of gypsum for 500-MW plant is \$1.25 million (\$5/ton)
  - Annual TMT-15 cost ~\$30,000 or less

# Testing Completed to Date

---

- First week of 2-week effort on Monticello pilot wet FGD conducted in April
  - Did not see any Hg re-emissions with Hg SCEM under baseline (no catalyst upstream, no TMT) conditions
  - Decided to instead focus on ability to produce low Hg content gypsum

# Testing Completed to Date

- Delayed 2<sup>nd</sup> week of testing (week-long steady state test at optimum TMT dosage)
  - Since no re-emissions were seen (immediate SCEM feedback) needed to turn around analytical data on parametric test samples
  - Pilot wet FGD does not have primary dewatering
    - Need to add field separate gypsum from high Hg-content fines
    - New EPRI project is adding pump, hydrocyclones and tank to pilot wet FGD system for primary dewatering

# Interim Results of Parametric Tests at Monticello

---

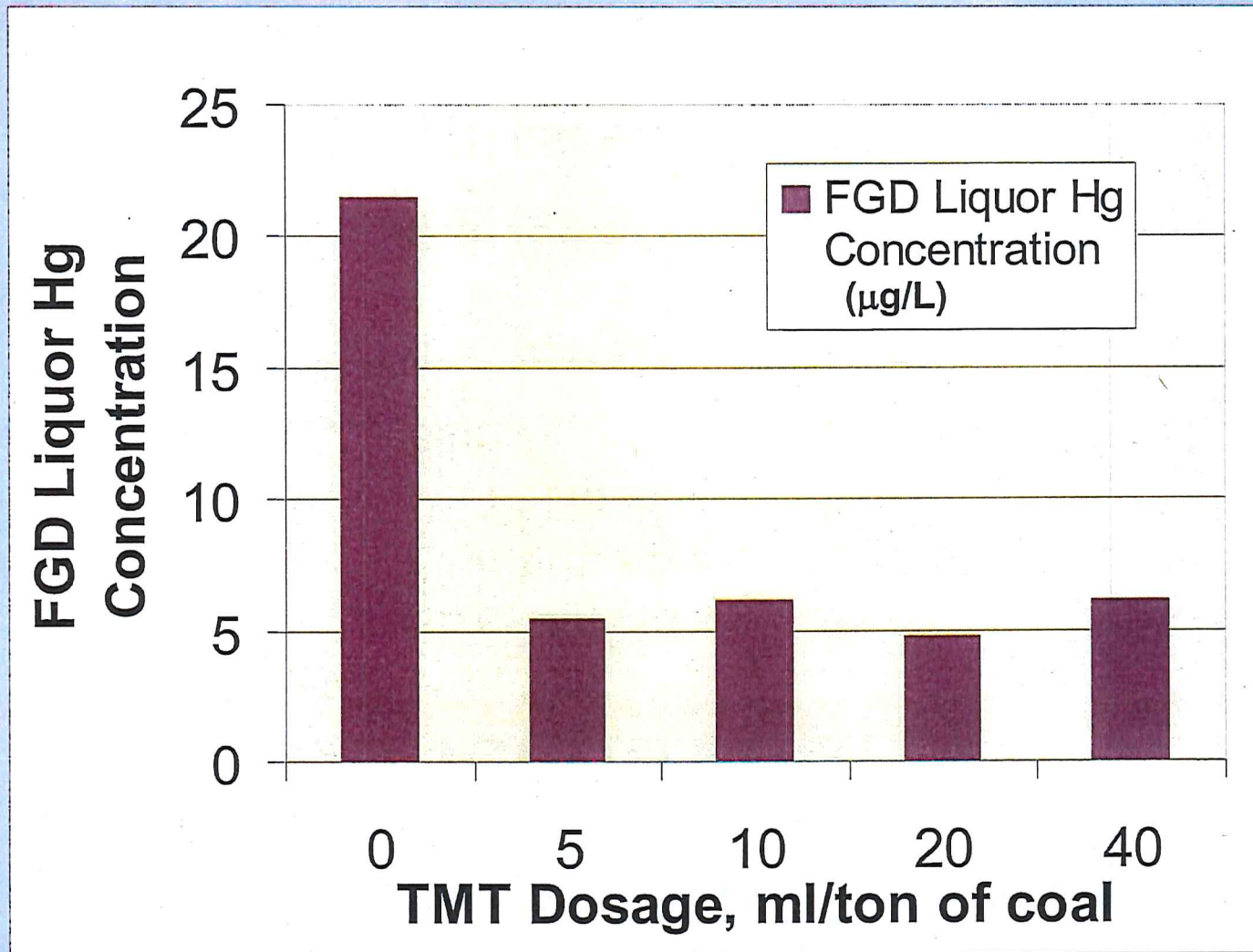
- No apparent affect of additive on Hg removal across FGD
- Saw decrease in FGD liquor Hg conc. with TMT
  - No apparent TMT dosage effect
- Separated gypsum from fines in the laboratory by settling
  - Modest decrease in gypsum Hg conc. with TMT
  - No apparent TMT dosage effect
  - Effectiveness of TMT may be masked by contamination of gypsum with fines in settled samples
  - Need field dewatering to determine true ability to separate high-Hg salts from gypsum

# FGD Pilot Unit at Monticello Station



TMT  
Injection

# FGD Liquor Hg Concentrations

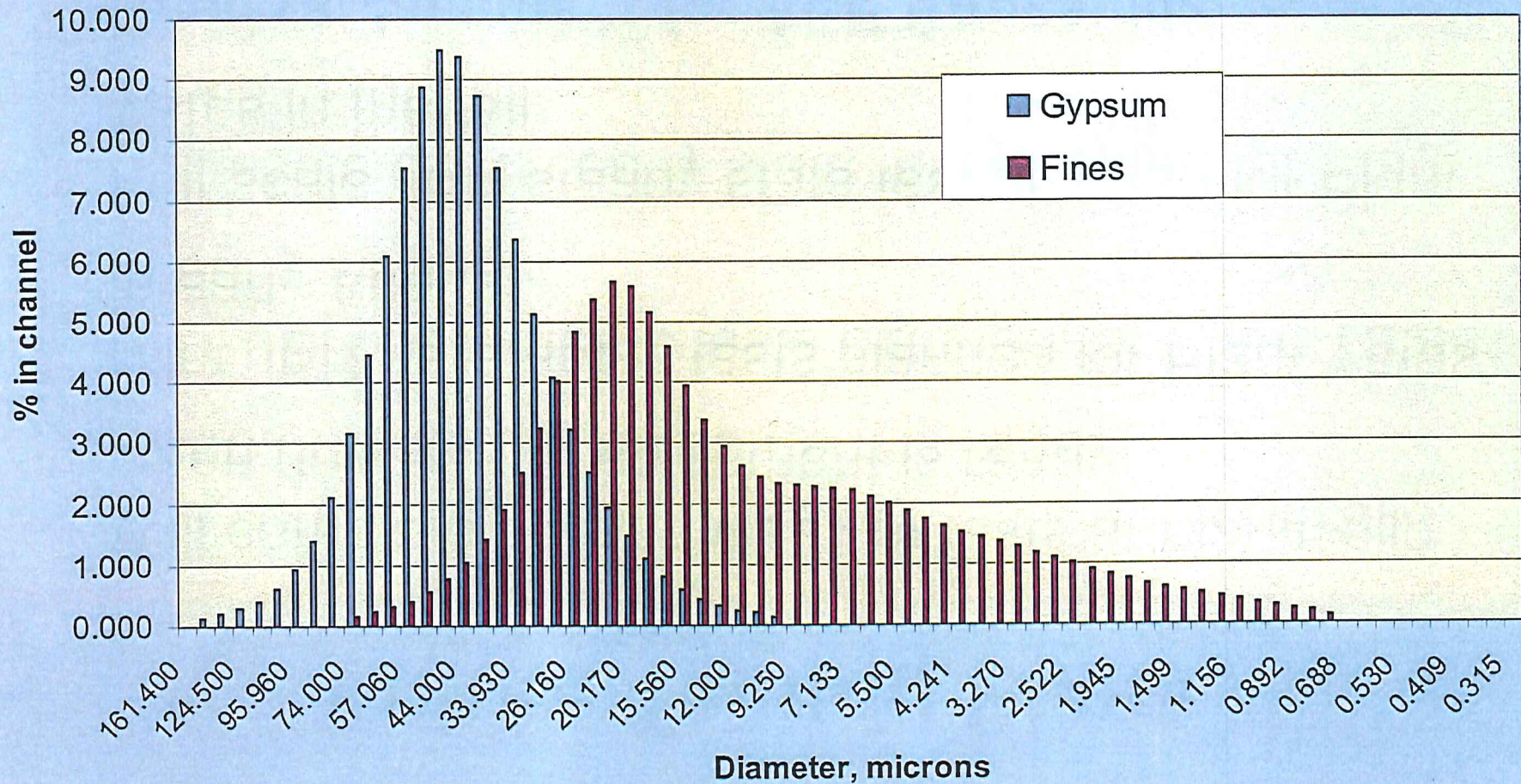


# Settled FGD Solids Sample Hg Concentrations

TMT Dosage (ml/ton of coal)	Wt% gypsum phase in slurry	Gypsum Hg Content, $\mu\text{g/g}$ (% of Hg in slurry)	Wt% fines in slurry	Fines Hg Content, $\mu\text{g/g}$ (% of Hg in slurry)
0	11.6	1.7 (53%)	0.3	55 (44%)
5	9.2	1.2 (33%)	0.5	39 (65%)
10	10.7	1.2 (36%)	0.3	75 (62%)
20	10.0	1.0 (33%)	0.4	52 (63%)
40	9.3	1.2 (36%)	0.3	57 (61%)

# Example PSD for Gypsum and Fines Phases (5 ml/ton TMT-15 dosage)

TMT Test 1 PSD Data



# Future Testing Plans

---

- Will complete second week of tests at Monticello when dewatering equipment is ready
- Pilot JBR parametric tests planned for Plant Yates in early August
- Full-scale JBR steady state test planned for Plant Yates in the fall
- **Need replacement for AEP Conesville**
  - Desire a site with known, significant re-emissions levels
  - Mg-lime FGD with natural oxidation, no SCR in service?

# Bench-scale Kinetics Study of Mercury Reactions in FGD Liquors



David W. DeBerry, Ph.D.

Gary Blythe

URS Corporation

NETL Project DE-FC26-04NT42314

COR: Sara Pletcher

EPRI Project Manager: Richard Rhudy

**EPRI**

**URS**

# Introduction

- **Project Goal** – develop a fundamental understanding of Hg “re-emissions” from wet FGD systems
  - Seen as FGD outlet  $\text{Hg}^0$  concentration  $>$  inlet  $\text{Hg}^0$
  - Apparent reduction of  $\text{Hg}^{+2}$  removed in FGD absorber
  - Limits overall Hg removal by FGD system
- **Technical Approach** – conduct kinetics experiments, kinetics modeling, and bench-scale wet FGD model validation tests
- **Expected Benefits** – the ability to predict FGD re-emissions, and optimize FGD conditions to minimize or eliminate

# Main Project Elements

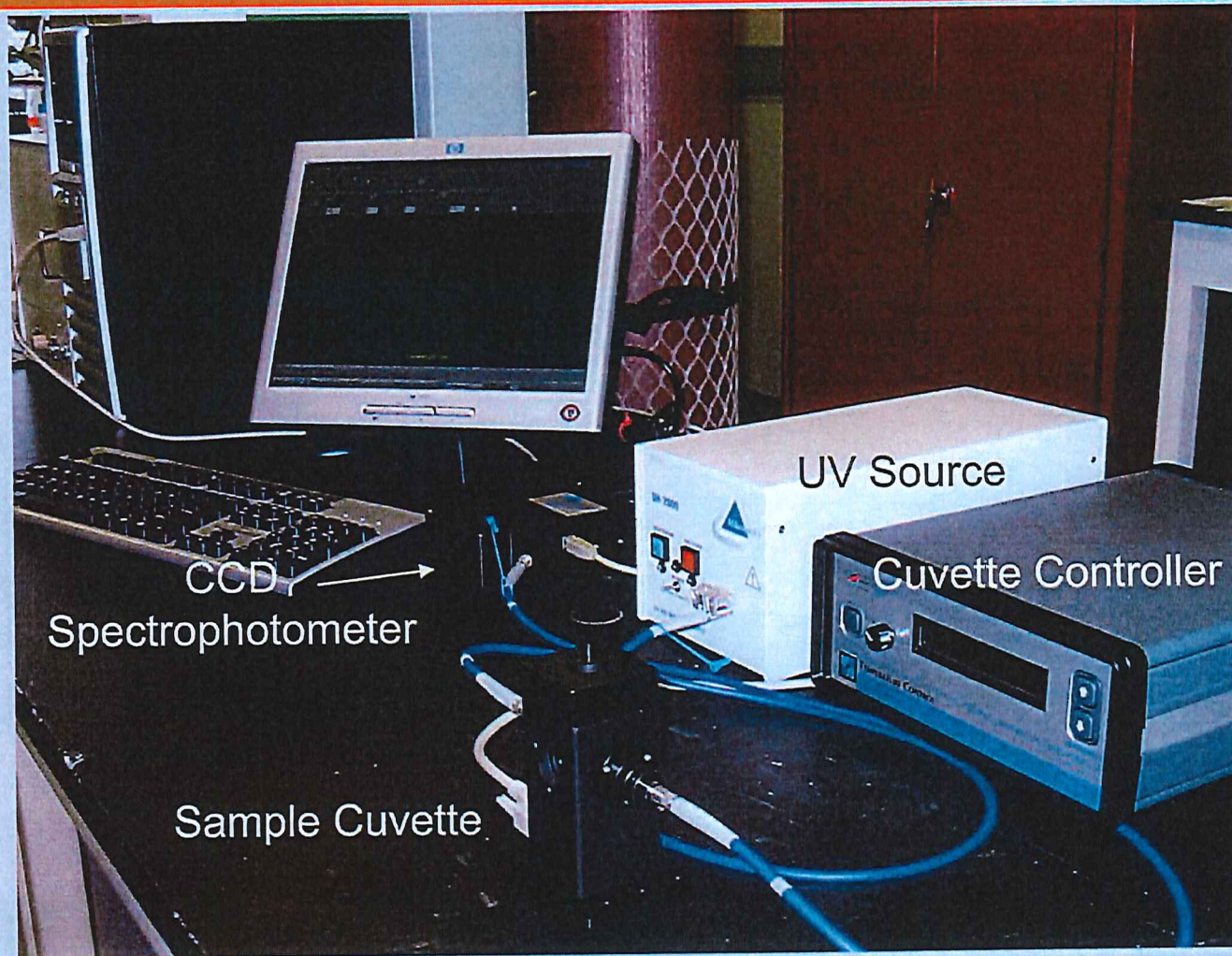
---

- Measure kinetics using both spectroscopy of the  $\text{Hg}^{2+}$ -Sulfite complex reactants, and production / stripping of  $\text{Hg}^0$
- Extend reaction conditions to include presence of chloride, thiosulfate and additives, and into the FGD pH region
- Construct a kinetics model which describes the results
- Test the model using the URS bench scale FGD

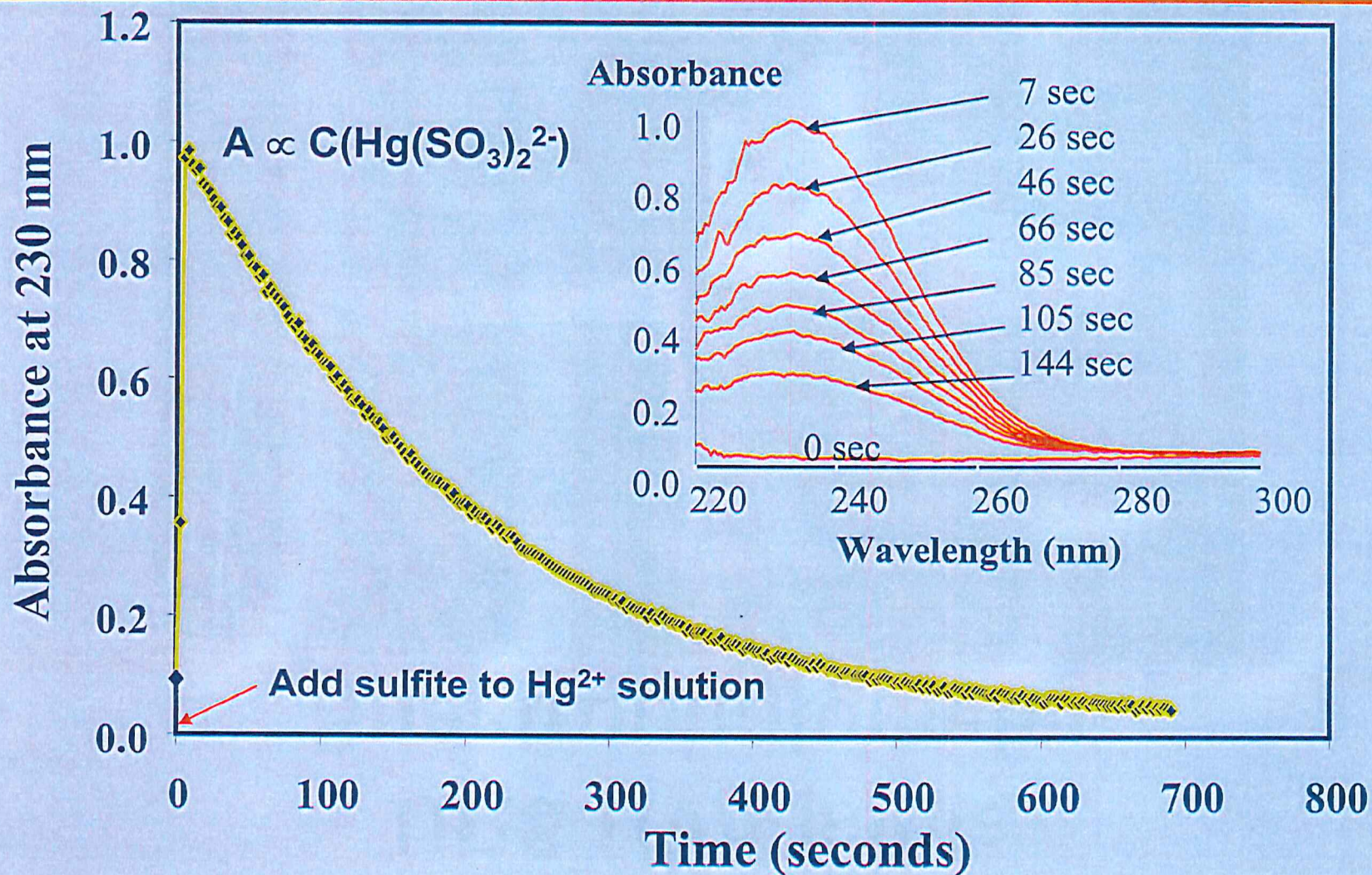
# Main Chemical Reactions for Hg Emission without Chloride

- Overall reaction:
  - $\text{Hg}^{2+} + \text{HSO}_3^- + \text{H}_2\text{O} \rightarrow \text{Hg}^0\uparrow + \text{SO}_4^{2-} + 3 \text{H}^+$
- Main pathway is through mercuric-sulfite complexes:
  - $\text{Hg}^{2+} + \text{SO}_3^{2-} \leftrightarrow \text{HgSO}_3$
  - $\text{HgSO}_3 + \text{SO}_3^{2-} \leftrightarrow \text{Hg}(\text{SO}_3)_2^{2-}$
- Equilibrium favors  $\text{Hg}(\text{SO}_3)_2^{2-}$  in presence of excess sulfite
- But only  $\text{HgSO}_3$  decomposes to give reduction of  $\text{Hg}^{2+}$ :
  - $\text{HgSO}_3 + \text{H}_2\text{O} \rightarrow \text{Hg}^0\uparrow + \text{SO}_4^{2-} + 2 \text{H}^+$

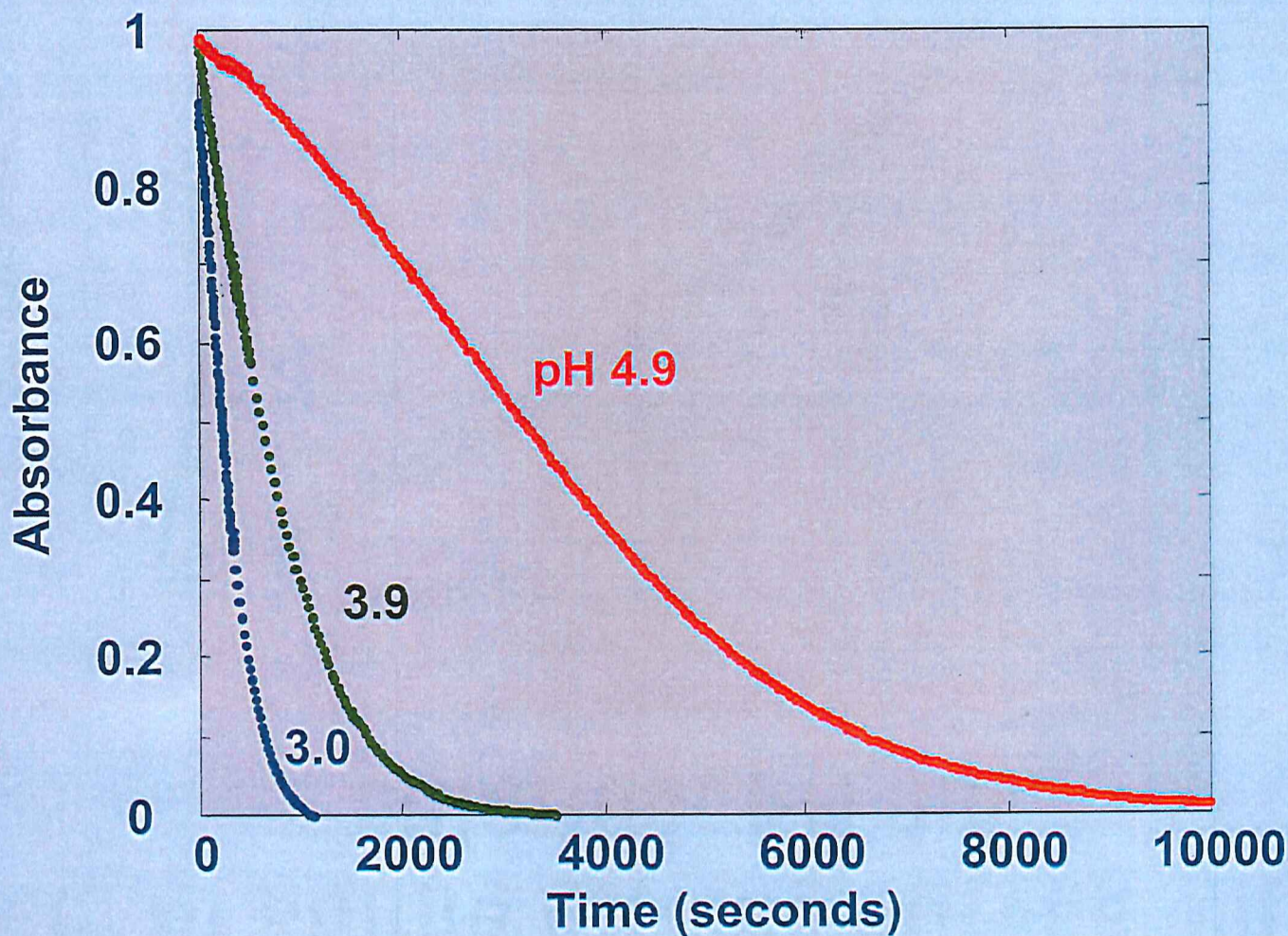
# URS UV/Visible Spectrophotometer



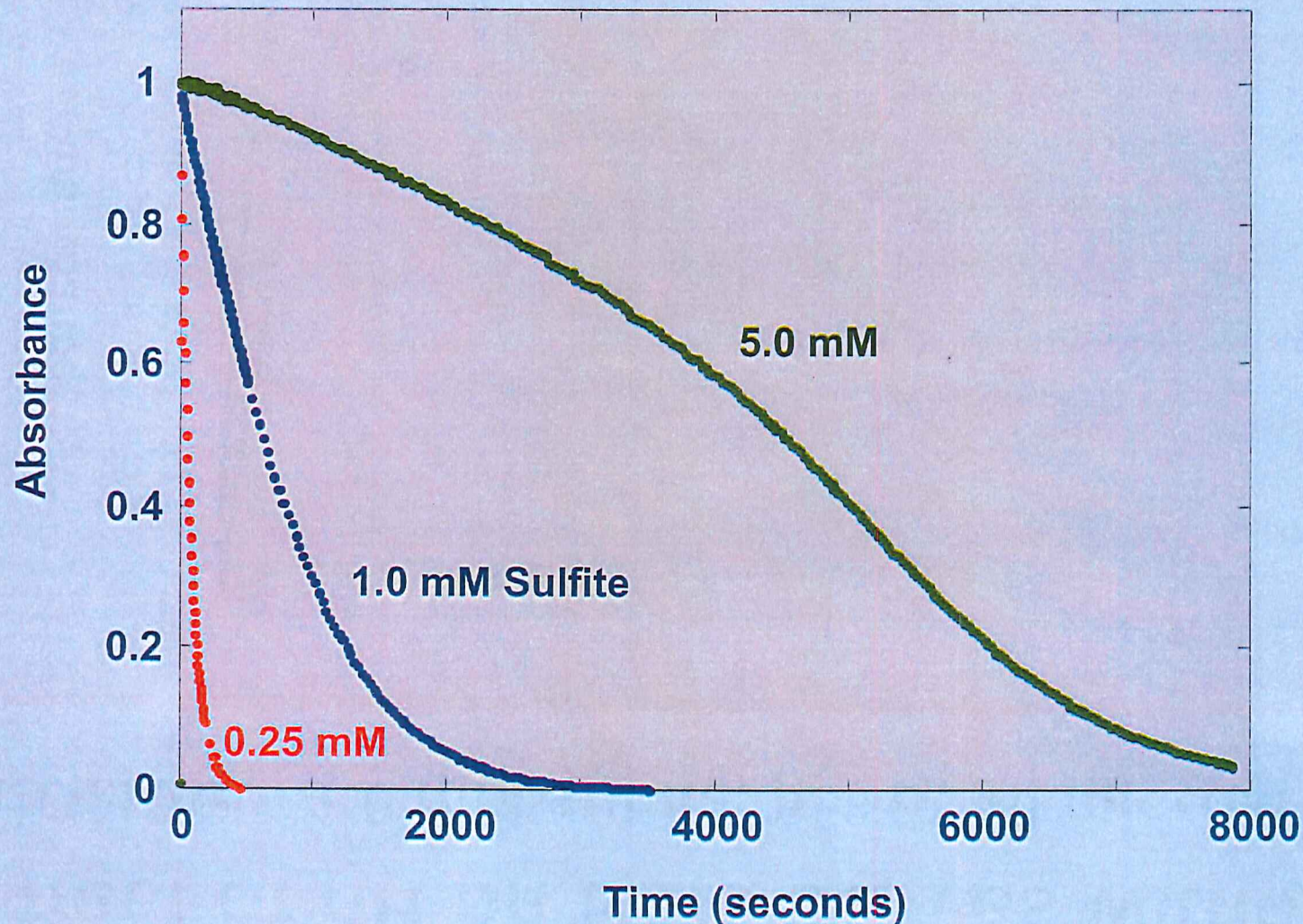
# Example Spectra and Rate Curve



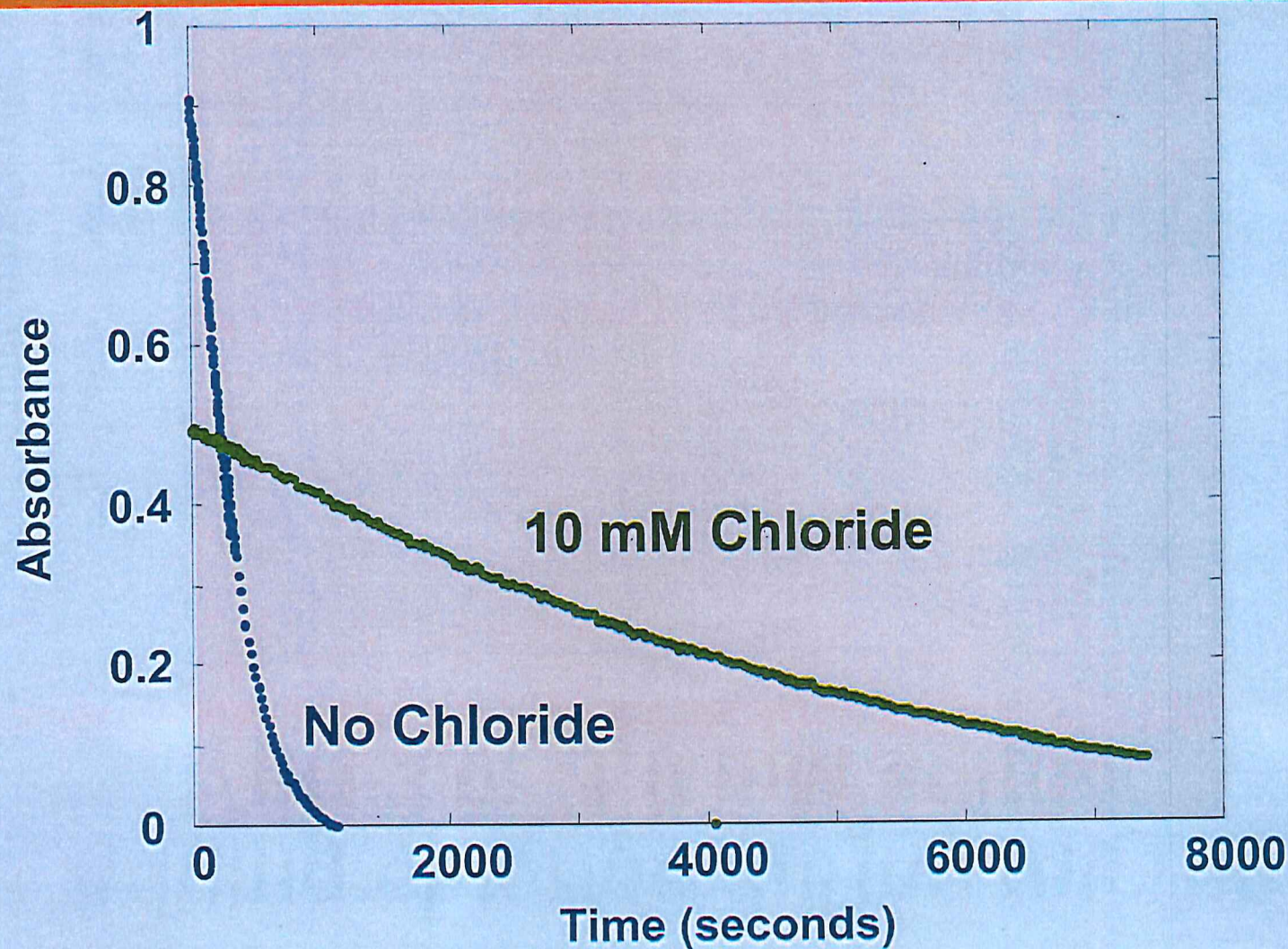
# Effect of pH on Rate Curves without Chloride. 1.0 mM sulfite, 55° C, 40 microM Hg<sup>2+</sup>



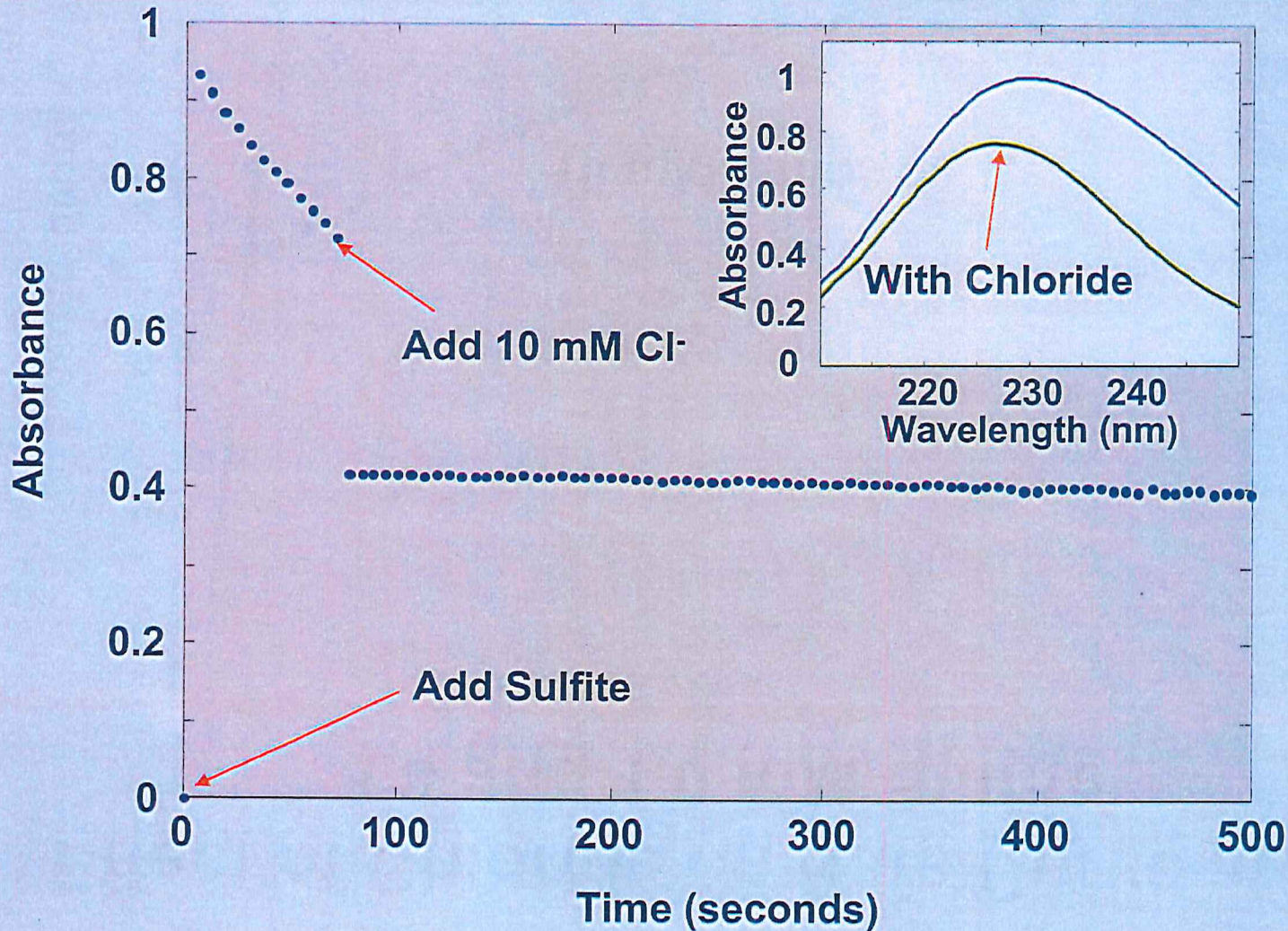
# Effect of sulfite on rate curves without chloride; pH 3.9



# Effect of Chloride on Rate Curve at pH 3.0 and 1.0 mM Sulfite



# Adding chloride during the run; pH 3.0; 1.0 mM sulfite

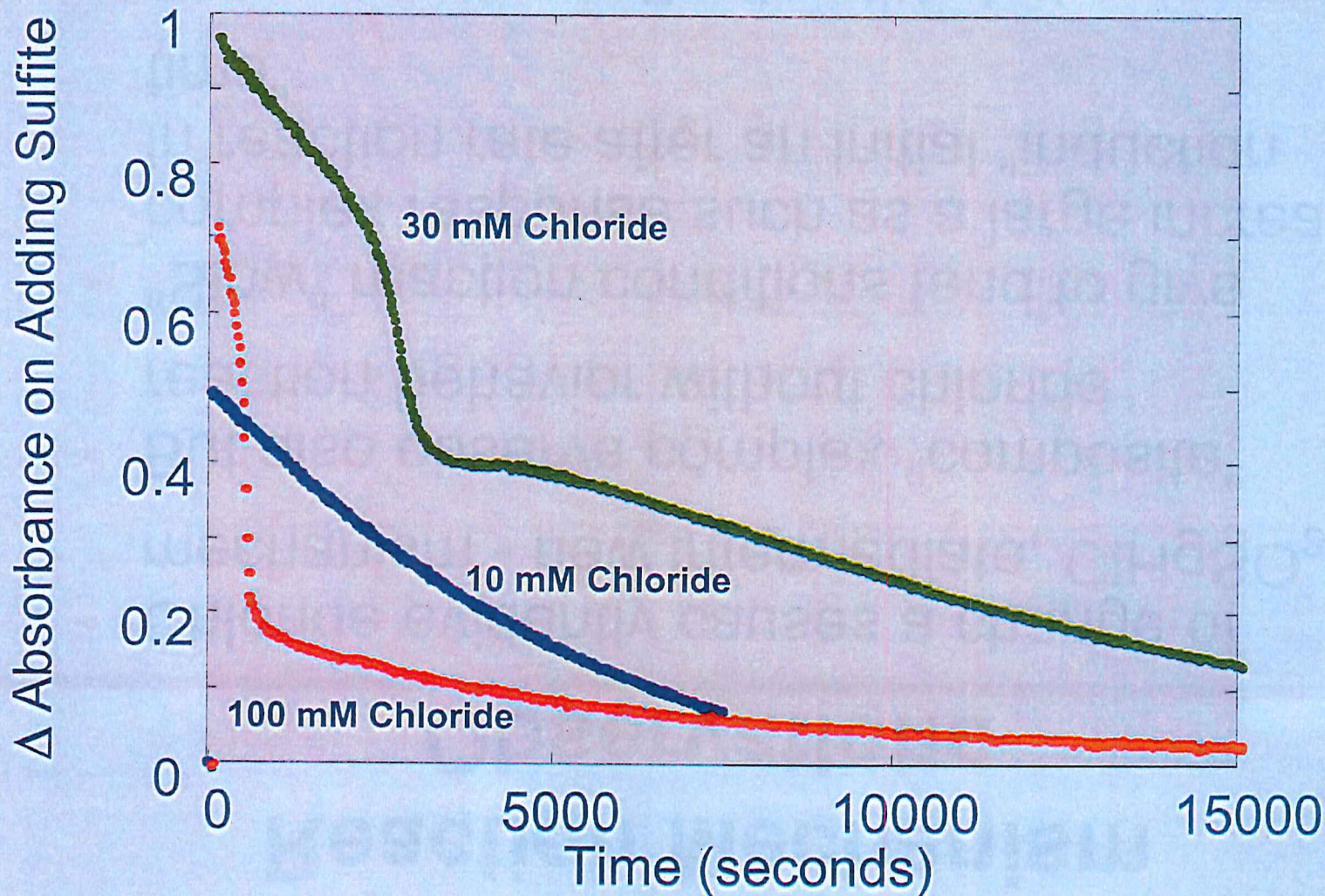


# Reaction Mechanism Observations

---

- Chloride evidently causes a change of mechanism - new intermediate,  $\text{ClHgSO}_3^-$
- But also observe complex “composite” reaction behavior without chloride
- “Slow” reaction conditions tend to give complex response such as a large increase in reaction rate after an initial “induction time”
- Several factors affecting this behavior are under investigation

# Induction Time Behavior in Chloride Solutions

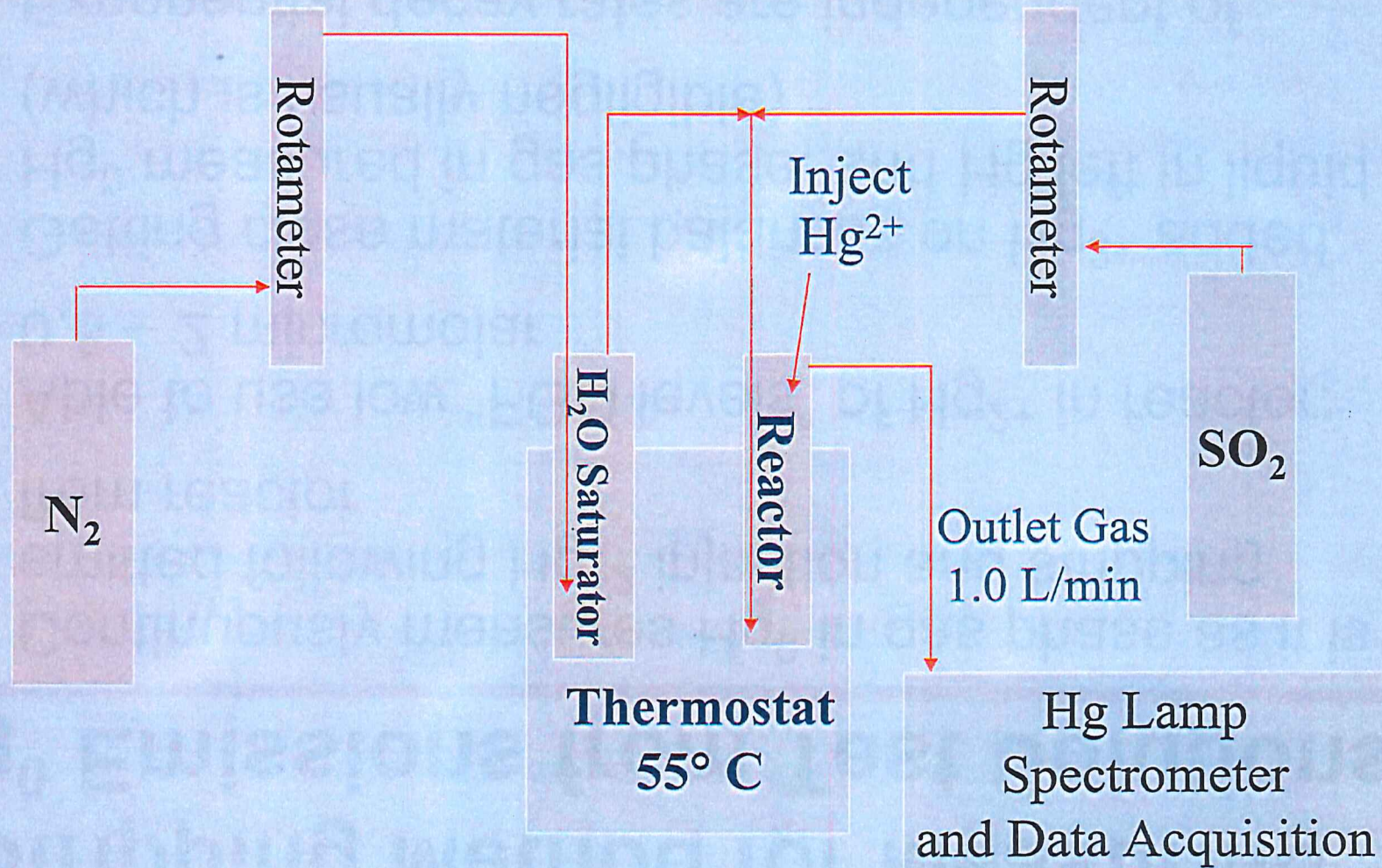


# Stripping Method for Measuring $\text{Hg}^0$ Emissions from Test Solutions

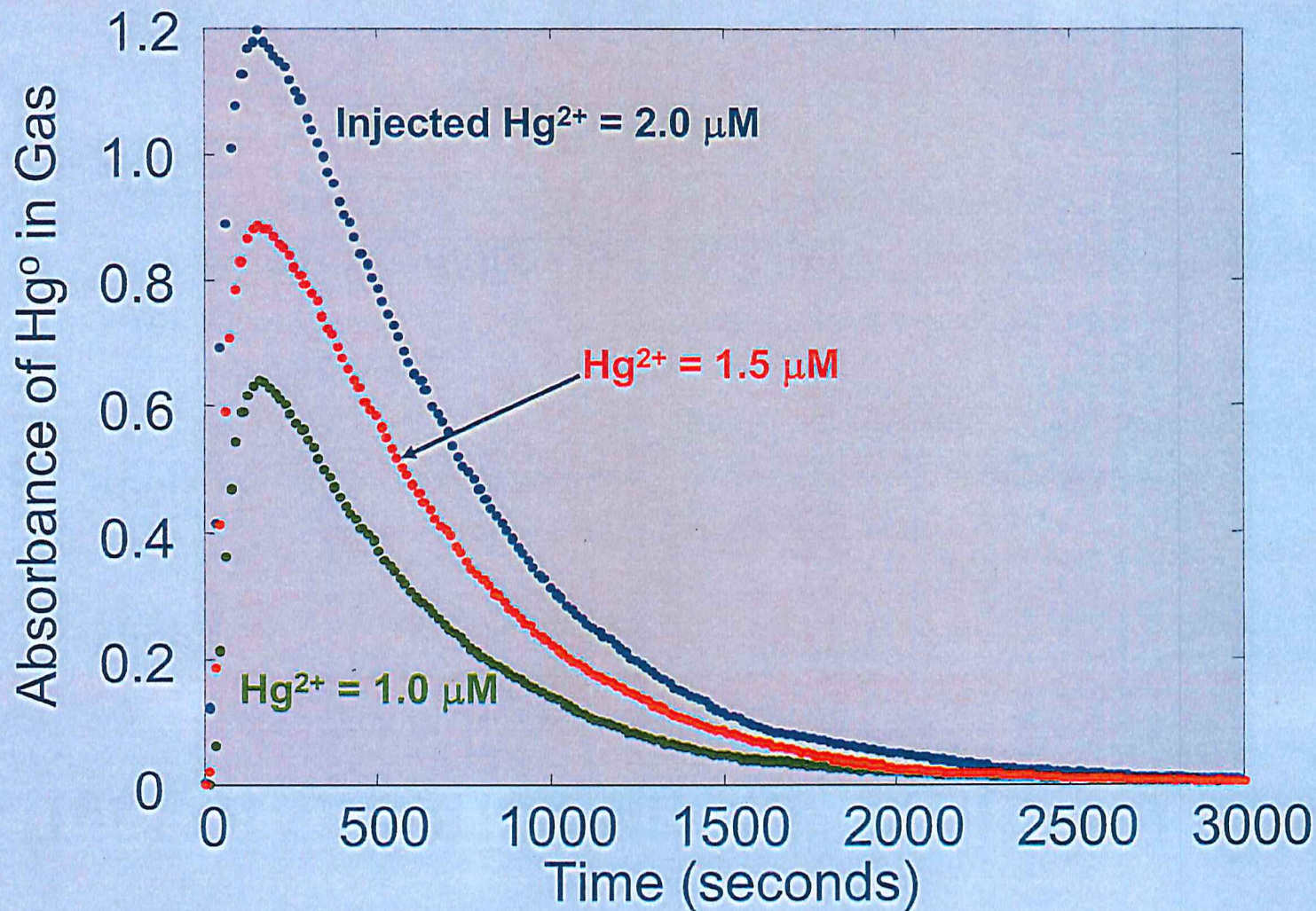
---

- Continuously measures  $\text{Hg}^0$  in gas phase as it is emitted following  $\text{Hg}^{2+}$  injection and stripping from reactor
- Able to use low “FGD levels” of  $\text{Hg}^{2+}$  in reactor: 0.5 – 2 micromolar
- Getting close material balances on  $\text{Hg}^{2+}$  added,  $\text{Hg}^0$  measured in gas phase, and  $\text{Hg}$  left in liquid (which is usually negligible)
- Exponential decay rates are independent of initial  $\text{Hg}^{2+}$  concentration, matching spectroscopic results

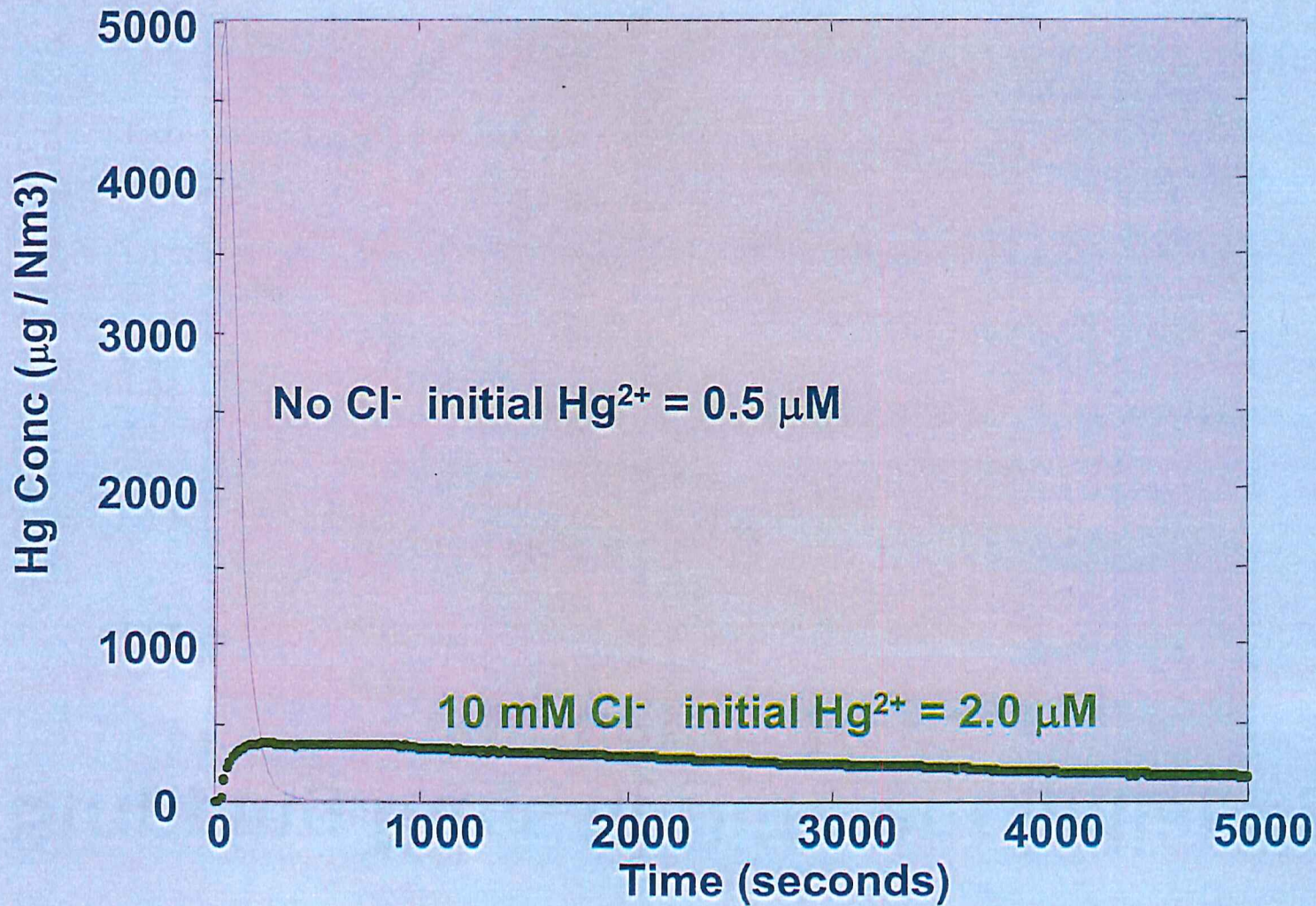
# Hg<sup>0</sup> Stripping Kinetics Apparatus



# Stripping Runs at Different Initial $\text{Hg}^{2+}$ Concentrations



# Effect of Chloride on $\text{Hg}^0$ Stripping Kinetics

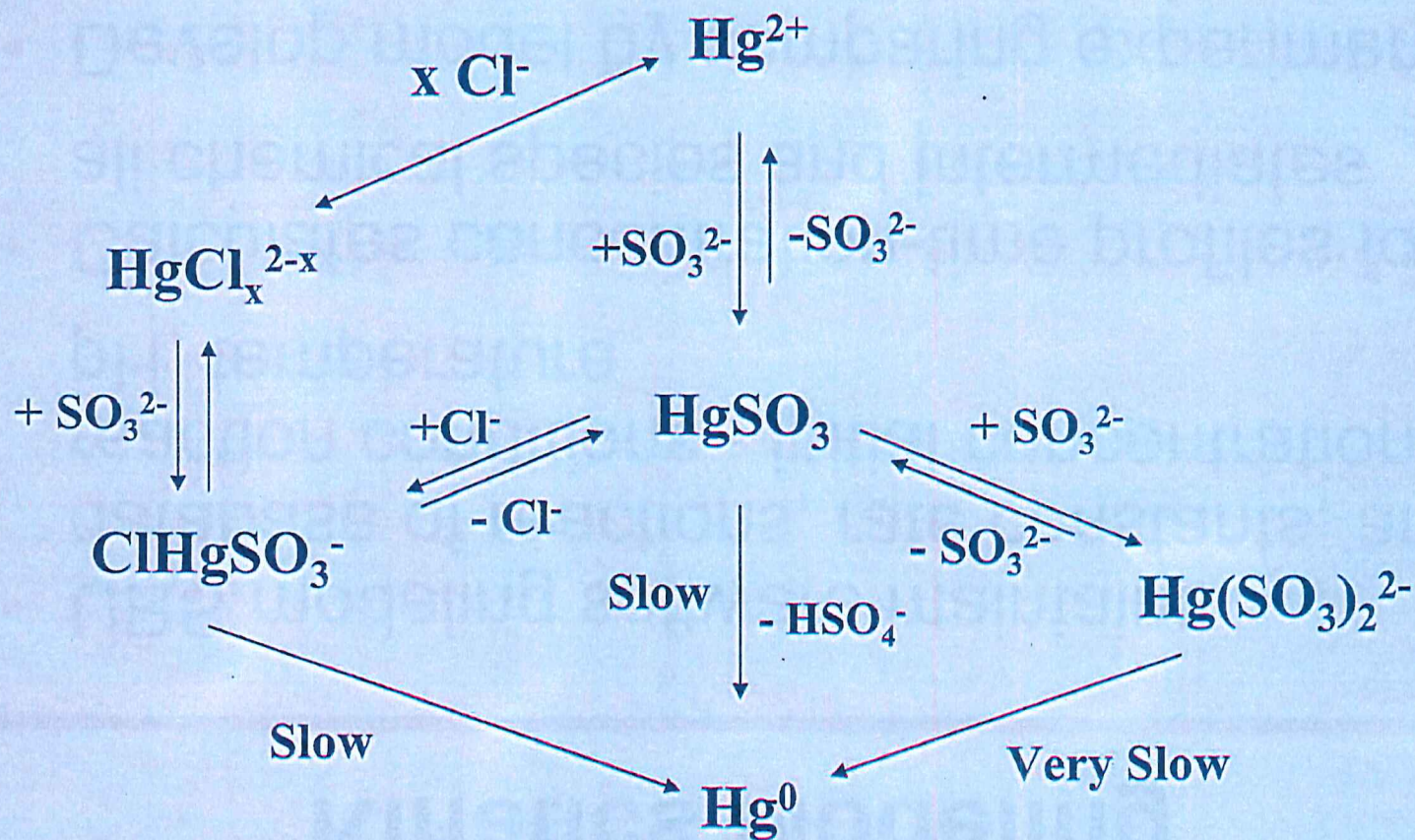


# Kinetics Modeling

---

- URS modeling software maintains database of reactions, rate constants, and reaction conditions - initial concentrations, pH, temperature
- Calculates concentration-time profiles for all chemical species and intermediates
- Develop model by comparing experimental and calculated results while varying rate parameters until results match experiment over a wide range of conditions

# Major Reaction Pathways



# Project Status and Conclusions

---

- Developed experimental methods for following reactants and products independently
  - Determining effects of pH, sulfite, temperature, ionic strength, and other "FGD" components on reaction rates
  - Chloride has major effects on reaction rates and mechanism
  - New reaction intermediates proposed; in process of constructing model using these mechanisms
-

# Pilot-Scale Study of a Wet Scrubber System for Control of SO<sub>2</sub>, NO<sub>x</sub>, and Hg in Coal Combustion Flue Gas

Paper # 47

Nick D. Hutson and John C.S. Chang

U. S. Environmental Protection Agency, Office of Research and Development, 109 T. W. Alexander Drive, Research Triangle Park, NC 27711

Yongxin Zhao

ARCADIS U.S., Inc., 4915 Prospectus Dr., Suite F, Durham, NC 27713

Renata Krzyzyska

Faculty of Environmental Engineering, Wroclaw University of Technology, Wybrzeze Wyspianskiego 27, 50-379 Wroclaw, Poland

## ABSTRACT

A pilot-scale study was performed in a wet flue gas desulfurization (WFGD) scrubber system aimed at enhancing mercury capture. The wet scrubber system was operated in forced oxidation mode to treat a simulated flue gas doped with Hg<sup>0</sup> vapor, variable amounts of SO<sub>2</sub>, and nitric oxide (NO). Results showed that the addition of a NaClO<sub>2</sub> solution is effective in increasing the amount of Hg captured in the scrubber. The additive is also effective in promoting the removal of NO<sub>x</sub>, but to a lesser extent. It was of interest to notice that the presence of SO<sub>2</sub> is critical in promoting Hg<sup>0</sup> oxidation and, in turn, enhanced Hg capture. At a scrubber inlet SO<sub>2</sub> concentration of 1100 ppm, the results showed that even if the injection point for the NaClO<sub>2</sub> solution was moved closer to the flue gas inlet, a significant amount of Hg capture was still achieved. However, when the SO<sub>2</sub> was increased to 2000 ppm, Hg capture was significantly lower. Experiments with different wet scrubber configurations revealed that the Hg-NaClO<sub>2</sub> reaction was less significant with respect to gaseous SO<sub>2</sub> concentrations than the concentration of aqueous sulfite ions.

## INTRODUCTION

In 2005, it was estimated that approximately one-third of U.S. coal-fired utility capacity was utilizing some type of flue gas desulfurization (FGD) technology. Nearly 90 percent of the installed systems are wet FGD scrubbers, with nearly 70 percent of those being limestone-based systems.<sup>1</sup> Overall, wet FGD technologies have been shown to routinely provide greater than 95 percent SO<sub>2</sub> removal, with good reliability.<sup>2</sup>

The U.S. Environmental Protection Agency (EPA) has recently proposed the Clean Air Transport Rule (CATR) which replaces EPA's 2005 Clean Air Interstate Rule. By 2014, the rule

and other state and EPA actions will reduce sulfur dioxide (SO<sub>2</sub>) emissions by 71 percent from 2005 levels. Because of these deep emission reduction requirements, a significant increase in the use of wet-FGD technology is expected in the next decade.

The CATR will also require reduction of NO<sub>x</sub> emissions – a reduction of 52% from 2005 levels by 2014. In the U.S., a majority of coal-fired utility boilers use combustion controls (e.g., low-NO<sub>x</sub> burners, staged combustion) to limit the formation of NO<sub>x</sub> in the flue gas. Some plants – especially those in ozone non-attainment areas – also employ selective catalytic reduction (SCR) or selective non-catalytic reduction (SNCR) technologies to further reduce NO<sub>x</sub> emissions.

EPA has also indicated an intention to regulate emissions of mercury and other hazardous air pollutants (HAPs) from coal-fired electric utility boilers. While wet-FGD scrubbers are installed specifically for SO<sub>2</sub> control, they may also effectively remove oxidized forms of mercury from flue gas<sup>3</sup> due to the good gas-liquid contact and the high solubility of most oxidized mercury compounds. This co-benefit control is only effective, however, for flue gas streams containing oxidized forms of mercury, as the elemental form is not soluble and tends to pass directly through the wet scrubber. For facilities utilizing low chlorine coals (e.g., western sub-bituminous coals), the majority of mercury is released in its elemental form. The presence of an SCR unit (used for NO<sub>x</sub> control) and adequate amount of chlorine can increase the conversion of Hg<sup>0</sup> to Hg<sup>2+</sup>. However, the use of SCR for mercury oxidation can be challenging when burning coals with low chlorine content. In addition, the catalyst can deactivate under high dust conditions.<sup>4</sup> Furthermore, not every plant has this SCR-FGD combination and, in some areas of the U.S., the SCRs are only used during the summer ozone season.

Researchers have explored the concept of multipollutant control in a wet scrubber system.<sup>5,6,7,8,9,10,11</sup> Theoretically, wet scrubbers can also be used for the removal of NO<sub>x</sub>. As NO has a very low solubility, effective removal of NO<sub>x</sub> by wet-scrubbing typically demanded oxidation of NO to NO<sub>2</sub>. One of the options is to add soluble oxidant to the scrubber liquor. Hutson et al.<sup>12</sup> recently reported on bench-scale results for the use of NaClO<sub>2</sub>/CaCO<sub>3</sub> for simultaneous control of SO<sub>2</sub>, NO<sub>x</sub> and Hg. This paper validates previous bench-scale results and focuses on explaining the impact of SO<sub>2</sub> on mercury capture.

## EXPERIMENTAL

The pilot-scale scrubber system used in this study (see Figure 1) has been described previously.<sup>13</sup> The system includes a spray tower and a forced oxidization tower. The spray tower consists of three absorber sections (marked 1, 2, and 3 in Figure 1). Each absorber section is 10 cm in diameter, 92 cm in length, and contains a 20 cm deep bed of plastic hollow balls (2 cm in diameter). The hollow balls are supported by a grid at the bottom of each absorber and are fluidized by the upward flow of the flue gas. Under forced oxidation operation, slurry is not discharged to the slurry hold tank at the bottom (marked 7 in Table 1), but to a separate 150-L oxidation tower (marked 6 in Figure 1). The hold tank contains ~10 L of 5 wt% CaSO<sub>4</sub> for pH adjustment. As shown in Figure 1, a stream of slurry in the hold tank is also drawn to the forced oxidation tower to allow the circulation pump to run smoothly. The two streams add up to ~30 L/min, resulting in a 4.9-min residence time for the slurry in the oxidation tower. Slurry

gravimetrically overflows to the slurry hold tank where pH is adjusted with  $\text{CaCO}_3$  before it is sent back to the spray tower.

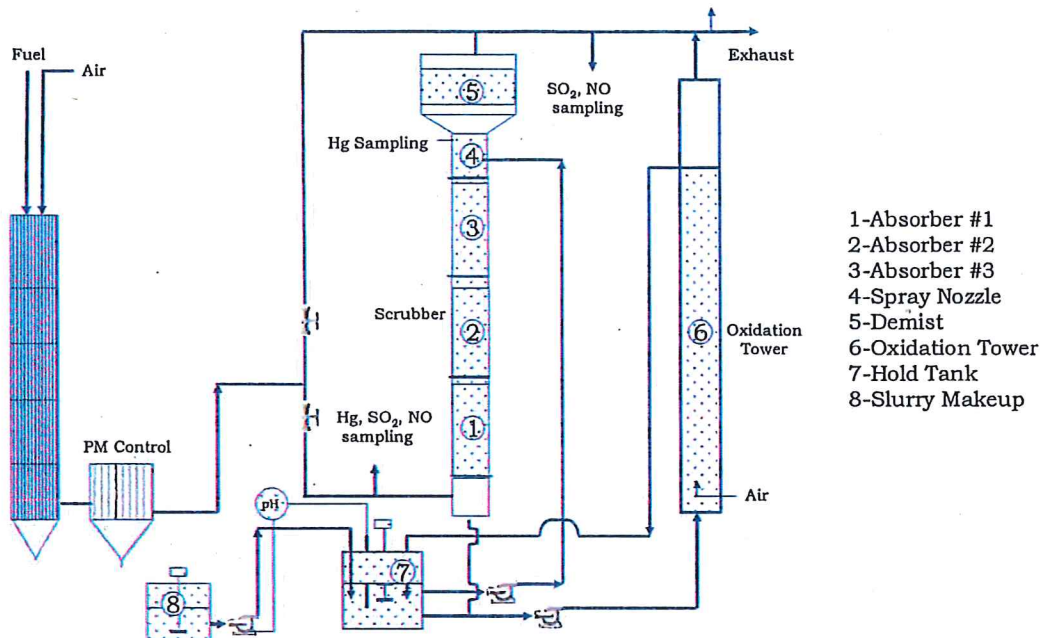


Figure 1: Schematic of the Pilot-scale Wet Scrubber System

The oxidation tower is sparged with air at a constant rate of  $\sim 45$  L/min to promote the conversion of  $\text{SO}_3^{2-}$  to  $\text{SO}_4^{2-}$ . Considering the potential consumption of  $\text{NaClO}_2$  by  $\text{SO}_3^{2-}$  ions,  $\text{NaClO}_2$  solution is added in the slurry recirculation line, approximately 0.3 m before the spray nozzle (marked 4 in Figure 1), unless otherwise indicated. The pH of the slurry is adjusted by adding reagent-grade calcium carbonate ( $\text{CaCO}_3$ ) into the hold tank. The addition is metered through a feedback control loop from the hold tank. The reagent-grade  $\text{CaCO}_3$  is added as a surrogate for natural limestone to ensure the results are not affected by impurities normally found in mined limestone. To simulate the real life wet scrubber operation conditions, pH of the slurry in the hold tank is 6.0 to 6.4. The circulating slurry is maintained at a liquid-to-gas ratio (L/G) of  $\sim 70$  gpm/1000 scfm. Slurry temperature is maintained at  $47 \pm 2$  °C.

Simulated flue gas is generated from a down-fired cylindrical furnace, known as the innovative furnace reactor (IFR). Though the furnace is capable of burning coal, it is typically fired with natural gas at a heating rate of 158,000 kJ/h. The fuel is introduced at the top of the furnace and combusted with air from axial and tangential directions. Since the natural-gas-derived flue gas contains no  $\text{SO}_2$  and only small amounts of NO, these components are added from gas cylinders. Gaseous  $\text{Hg}^0$  is produced in a permeation oven (VICI Metronics Dynacalibrator) and is carried by air into the duct before the scrubber. Unless otherwise indicated, the simulated flue gas contains approximately 7 percent  $\text{O}_2$ , 7 percent  $\text{CO}_2$ , 550 to 2000 ppm  $\text{SO}_2$ , 220 ppm NO; and  $17 \mu\text{g}/\text{m}^3$  Hg. The total flow of flue gas is controlled at  $800 \pm 50$  L/min.

The concentrations of Hg, SO<sub>2</sub>, and NO<sub>x</sub> are continuously monitored at both the scrubber inlet and outlet using continuous emission monitoring systems (CEMS). Measurements of Hg<sup>0</sup> are performed using ultraviolet (UV) spectrometers (Seefeldler-Hg 3000). Hg in the scrubber liquor is measured, when required, by cold vapor atomic absorption (CVAA) analyzer following EPA method 7040A. The NO<sub>x</sub> species are monitored by an NO<sub>x</sub> analyzer (API model 200AH) while SO<sub>2</sub> is measured by a fluorescence analyzer (API model 100AH).

## RESULTS AND DISCUSSION

### Hg Capture under a Typical Condition

A typical Hg capture result under forced oxidation operation is shown in Figure 2. In this case, a solution containing 1.62 M NaClO<sub>2</sub> was continuously added to the slurry circulation line at 5 mL/min. The specific location was 0.3 m from the spray nozzle so as to minimize potential NaClO<sub>2</sub> consumption by the sulfite ions. The slurry flowed through the absorbers at 8.3 L/min, and the pH in the hold tank was maintained at 6.4. Simulated flue gas generated by the furnace was 850 L/min. An SO<sub>2</sub> concentration of 1100 ppm was selected in order to understand how NaClO<sub>2</sub> influences the capture of Hg under a medium concentration level of SO<sub>2</sub>. As shown in Figure 2, 70 % Hg capture was observed immediately after NaClO<sub>2</sub> was sprayed into the system and this level lasted for 180 min. Significant removal of NO (~30%) and NO<sub>x</sub> (~15%) was also achieved, though the NO<sub>x</sub> (NO + NO<sub>2</sub>) scrubbing was less effective than the oxidation of the NO.

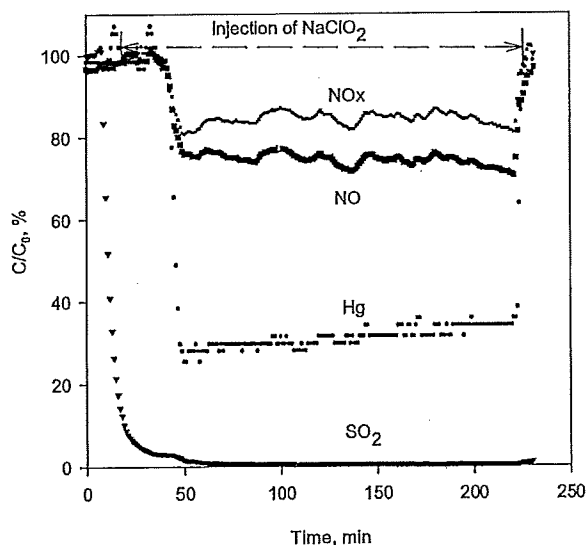


Figure 2: Hg Capture, SO<sub>2</sub>, and NO<sub>x</sub> Changes with Time across the Wet Scrubber System

With the same wet scrubber system, Chang and Zhao<sup>13</sup> have identified a significant amount of Hg reemission and determined that accumulated  $\text{Hg}^{2+}$  in the scrubber system is the dominant precursor of  $\text{Hg}^0$  reemissions. In their tests, Hg was added in the ionic form, and no oxidants were added to inhibit Hg emissions. Since Hg reemissions originated from accumulated ionic Hg in the slurry,  $\text{HgCl}_2$  was also added into the spray tower at a constant rate of  $15 \mu\text{g}/\text{min}$ . The  $\text{HgCl}_2$  was added to expedite  $\text{Hg}^{2+}$  accumulation in order to simulate Chang and Zhao's previous testing conditions. As shown in Figure 2, Hg reemissions across the spray tower were almost zero over the 180-min operation period. When measured from the top of oxidation tower, the Hg concentration reached  $\sim 4 \mu\text{g}/\text{m}^3$  at steady state. As the air flow through the forced oxidation tower was  $45 \text{ L}/\text{min}$ , the estimated Hg reemissions accounted for only 0.7 percent of total added Hg.

Scrubbing liquor was also sampled before being discharged into the forced oxidation tower. Solids were separated with a  $45 \mu\text{m}$  Teflon (PTFE) filter and all samples were quenched by immediately storing them in ice. Hg content in the samples was analyzed by CVAA using EPA Method 7470A. Anions, including  $\text{Cl}^-$  and  $\text{ClO}_3^-$ , were also analyzed as soon as practical by ion chromatography (IC) using EPA Method 300.0. Figure 3 plots the measured and estimated Hg and Cl species in the filtrate versus time. The results given in Figure 3 demonstrate that a good mass balance was achieved for both Hg and Cl species. The achievement of Hg mass balance further confirmed Chang and Zhao's<sup>13</sup> finding that the majority of captured Hg was in the liquid phase. This is also consistent with the nature of such reagents as  $\text{CaCO}_3$ ,  $\text{CaSO}_3$ , and  $\text{CaSO}_4$  whose crystal structure is not conducive to absorbing Hg.

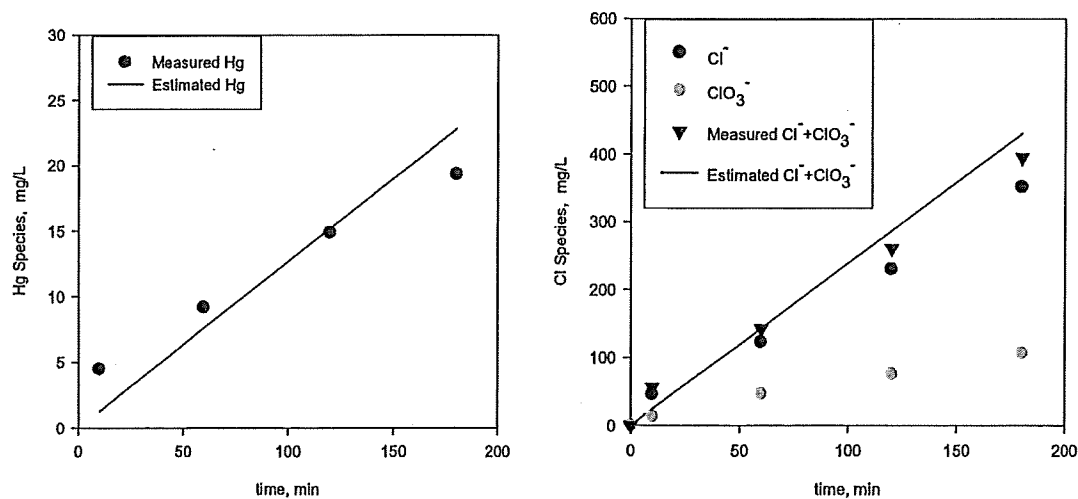


Figure 3: Aqueous Mercury and Chlorine Species in Slurry vs Time

When  $\text{NaClO}_2$  was added into the scrubber, the following reaction was suggested:<sup>7</sup>



However, the mass balance closure in Figure 3 implies that there was no gaseous  $\text{ClO}_2$  involved in reaction (1). Of interest was that a significant amount of  $\text{ClO}_3^-$  was detected in the scrubbing liquor, and it accumulated linearly against time. At the 180<sup>th</sup> minute, there was ~106 mg/L  $\text{ClO}_3^-$  found in the filtrated liquor. This finding was fully supported by our previous bench-scale tests that  $\text{ClO}_3^-$  is much less effective than  $\text{ClO}_2^-$  in oxidizing Hg and NO: when 50 mM  $\text{NaClO}_3$  was present in the liquid, Hg oxidation was nearly zero and only 3 percent NO was removed. By contrast, a much lower amount of  $\text{NaClO}_2$  (2.5 mM) in the liquid had led to 95 percent Hg being oxidized and to the corresponding NO removal of 36 percent.<sup>12</sup>

Reactions with  $\text{ClO}_2^-$  proceeding under an acidic environment are strongly supported by the results in Figure 4. In this case,  $\text{NaClO}_2$  (0.81 M at 5 mL/min) was first fed to the scrubber system for 90 min. During this operation period, the injection of  $\text{SO}_2$  was turned off. In the absence of  $\text{SO}_2$ , the slurry pH was 7.4. As shown in Figure 4, less than 20 percent of the Hg was removed by the scrubber system during the 90<sup>th</sup> minute time frame. Chlorine species (chloride and chlorite) in the liquid phase were also analyzed during this period of time. Of the two chlorine species, chlorite ions dominated, and the measured total chlorine species nearly equaled the estimates. At the 90<sup>th</sup> minute, when  $\text{SO}_2$  injection was turned on, a sharp drop of Hg was observed, accompanied by a quick drop in pH. The pH of the slurry was then maintained at 6.4. Due to the accumulation of chlorite in the slurry, Hg removal experienced a decrease at the 120<sup>th</sup> minute, followed by an increase back to ~55 percent at the 180<sup>th</sup> minute. Further analysis of liquid chlorine species highlighted that the originally existing chlorite was quickly consumed, and that the level of chloride ion increased at a fast rate.

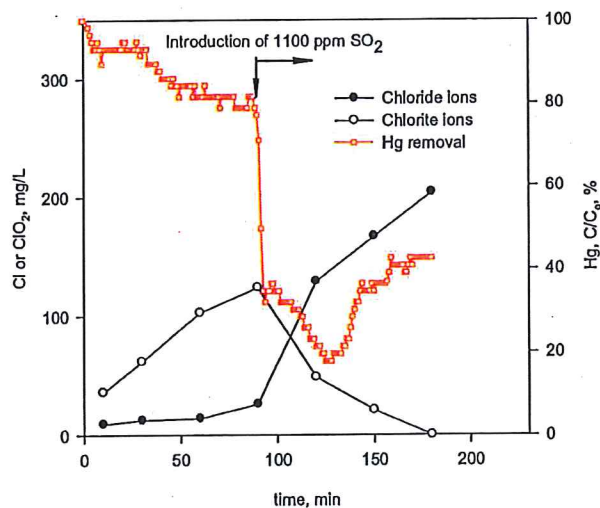


**Figure 4: Effect of  $\text{SO}_2$  Injection to Hg Oxidation and Chlorine Species Distribution in Liquid Phase**

NO removal followed the same pattern as Hg. Prior to the addition of  $\text{SO}_2$  to the flue gas, a small amount of NO was oxidized. An 80-percent drop in NO was immediately observed when  $\text{SO}_2$  was released to the scrubber system. As time proceeded, less and less NO was oxidized, until the

final NO oxidation ratio was stabilized at ~20 percent. It is thus clear that the occurrence of NO oxidation and Hg capture in this system demands a low level of pH as demonstrated in the bench-scale tests.<sup>12</sup>

### Hg Capture under Various Sulfur Dioxide Concentrations

Whereas the presence of SO<sub>2</sub> is critical for Hg capture in the wet scrubber systems, SO<sub>2</sub> nevertheless depletes NaClO<sub>2</sub>, thus deactivating the Hg-NaClO<sub>2</sub> reaction. Subsequent tests focused on the impact of varying SO<sub>2</sub> concentration in the flue gas. The test conditions were as previously described except that the SO<sub>2</sub> concentration was varied from 500 to 2000 ppm. Two levels of NaClO<sub>2</sub> concentration (0.81 M and 1.62 M) were employed for comparison. Figure 5 plots the impact that varying levels of SO<sub>2</sub> had on Hg capture across the wet scrubber system. For the cases where concentration of NaClO<sub>2</sub> solution was 1.62 M, the impact of SO<sub>2</sub> was not apparent until a decline to ~50 percent at 2000 ppm. However, a linear relation can be established for the cases where NaClO<sub>2</sub> solution was 0.81 M – Hg capture decreased with the increasing SO<sub>2</sub> concentration.

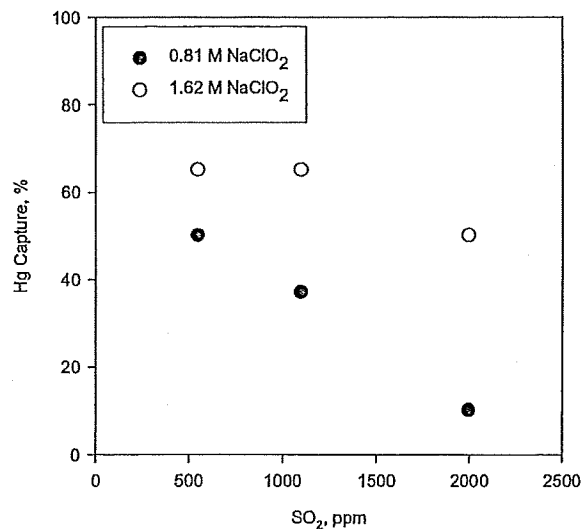


Figure 5: Impact of Varying Sulfur Dioxide (SO<sub>2</sub>) Concentration in the Flue Gas on Hg Capture

### Hg Capture with Different Injection Rates and Injection Locations

Since SO<sub>2</sub> is a dominant pollutant in the wet scrubber system, and its negative impact on Hg removal increases at high levels. The subsequent experiment was designed to include the effect of slurry residence on Hg capture. While maintaining SO<sub>2</sub> concentration at 1100 ppm NaClO<sub>2</sub> in the spray tower experiences a long residence time, a low level of SO<sub>2</sub> and a low level SO<sub>3</sub><sup>2-</sup> when sprayed from the top of absorber #3, On the other side of spectrum, injection of NaClO<sub>2</sub> to the top of absorber #1 leads to a short residence time, a high level of SO<sub>2</sub>, a high level of SO<sub>3</sub><sup>2-</sup>

immediately. For the latter, a low level of Hg/NO<sub>x</sub> capture has been expected. However, as seen in Figure 6 where Hg /NO<sub>x</sub> capture against NaClO<sub>2</sub> solution concentration is plotted, the extent of Hg/NO<sub>x</sub> capture weakly correlates to NaClO<sub>2</sub> injection location. Surprisingly, Hg capture was even reversely higher when 0.81 M or less NaClO<sub>2</sub> was injected from the top of absorber #1. Analysis of data presented in Figure 6 lend us to the conclusion that majority of NaClO<sub>2</sub> in the spray tower was consumed up within one or two absorbers. In addition, we have noticed that the pH at the exit of the wet scrubber is around 4.6 to 5.0. With the temperature of incoming flue gas being 95 to 100 °C, the reaction temperature in absorber #1 was 4 to 5 °C higher than that in absorber #3.

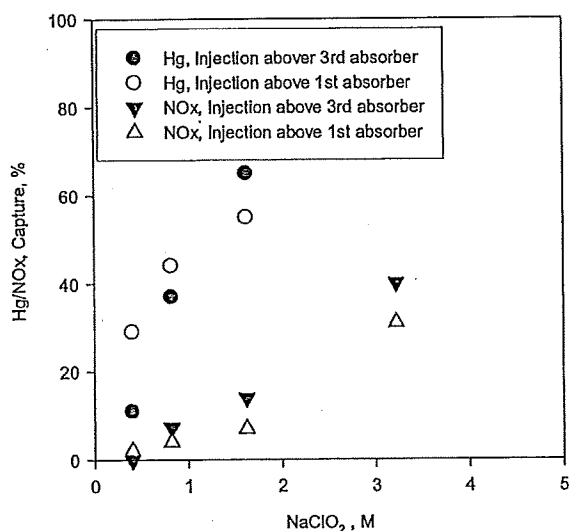


Figure 6: Hg, NO<sub>x</sub>, NO Captures with Different Injection Concentrations and Injection Locations

### Hg Capture with Various Numbers of Absorbers

As previously shown in Figure 6, we have determined that to reach ~70 percent Hg capture, the concentration of NaClO<sub>2</sub> solution should be 1.62 M. At this concentration, the effect of injection point location was insignificant, and the injected NaClO<sub>2</sub> was rapidly depleted within in one or two absorbers. One remaining question was to what extent gaseous SO<sub>2</sub> contributed to NaClO<sub>2</sub> consumption. It was not clear whether the consumption was rendered primarily by gaseous SO<sub>2</sub> or aqueous SO<sub>3</sub><sup>2-</sup>, or potentially both pathways, as shown below:<sup>12</sup>



Gaseous SO<sub>2</sub> participates in the depleting reaction at the gas-liquid interface where NaClO<sub>2</sub>-Hg reaction also exists. Aqueous SO<sub>3</sub><sup>2-</sup> was generated due to the capture of SO<sub>2</sub> by limestone. When

flowing down along the column of the spray tower, aqueous  $\text{SO}_3^{2-}$  depletes  $\text{NaClO}_2$  by reducing  $\text{NaClO}_2$  to ionic  $\text{Cl}^-$ . In most tests, more than 80 percent  $\text{SO}_2$  was captured by slurry. Although the aqueous  $\text{SO}_3^{2-}$  and  $\text{NaClO}_2$  reaction was deemed to dominate the depletion process, there was no direct evidence reported. In an attempt to understand the underlying  $\text{NaClO}_2$ - $\text{SO}_2$ - $\text{SO}_3^{2-}$  reactions in the wet scrubber system, slurry and  $\text{NaClO}_2$  were also alternatively sprayed from the top of absorber #2, or absorber #1. Consequently, the reaction space above the spray nozzle would be void, and no  $\text{Hg}$ - $\text{NaClO}_2$  reaction would be expected in these spaces. For this array of tests, the pH of the slurry in the hold tank was maintained at 6.4, and the solution of  $\text{NaClO}_2$  was 1.62 M.

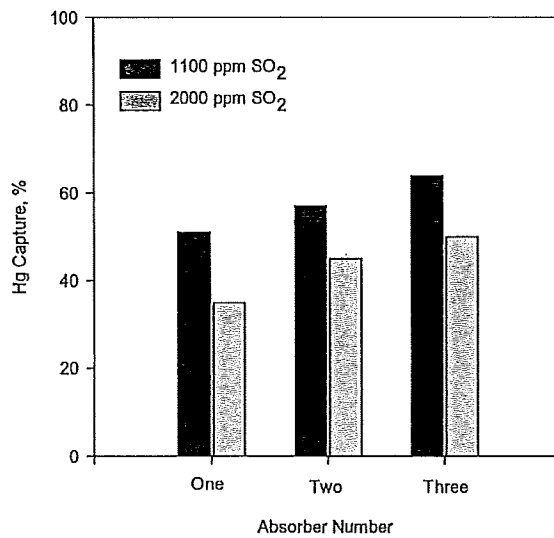


**Figure 7: Hg Capture with Different Number of Absorbers**

Figure 7 displays Hg capture as a function of the number of contact absorbers. When Slurry and  $\text{NaClO}_2$  were sprayed from the top of 1<sup>st</sup> absorber, the resulting mercury capture was 51 percent with 1100 ppm of  $\text{SO}_2$  and 35 percent with 2000 ppm. Increasing the number of absorbers did not dramatically enhance Hg capture, which is consistent with the analysis in Figure 6.

Table 1 gives the concentration changes of  $\text{SO}_2$  before and after  $\text{NaClO}_2$  injection. Assuming that the change was the result of gaseous  $\text{SO}_2$ - $\text{NaClO}_2$  reaction, one can see that the  $\text{SO}_2$  changes ranged from 25 to 77 ppm in the presence of 1100 ppm  $\text{SO}_2$  and from 47 to 86 ppm in the presence of 2000 ppm of  $\text{SO}_2$ . By comparison, the incremental  $\text{SO}_2$  removals were similar in each case. The calculation based on equation (2) shows that  $\sim 0.0015$  mol/min  $\text{NaClO}_2$  was being consumed by 80 ppm gaseous  $\text{SO}_2$ , accounting for 20 percent added  $\text{NaClO}_2$ . With only absorber #1, 625 ppm  $\text{SO}_2$  was turned into  $\text{HSO}_3^-/\text{SO}_3^{2-}$  for the case of 1100 ppm of  $\text{SO}_2$ . This amount increased to 975 ppm with 2000 ppm of  $\text{SO}_2$ . The corresponding Hg removal was 51 and 35 percent, respectively. Consequently, high levels of  $\text{SO}_2$  capture and, in turn, high levels of  $\text{HSO}_3^-/\text{SO}_3^{2-}$  concentration dominated the  $\text{NaClO}_2$  consumption in the wet scrubber system.

**Table 1. Hg removal and associated SO<sub>2</sub> concentrations with varying number of absorbers.**

Absorber #	SO <sub>2</sub> at Outlet before NaClO <sub>2</sub> Addition (1), ppm	SO <sub>2</sub> at Outlet after NaClO <sub>2</sub> Addition (2), ppm	(1)-(2)	Hg Capture
1 <sup>a</sup>	475	398	77	51%
2 <sup>a</sup>	147	80	67	57%
3 <sup>a</sup>	60	35	25	63%
1 <sup>b</sup>	1035	949	86	35%
2 <sup>b</sup>	457	410	47	45%
3 <sup>b</sup>	169	113	56	50%

a. 1100 ppm SO<sub>2</sub> in flue gas.

b. 2000 ppm SO<sub>2</sub> in flue gas.

When 3 absorbers were used for the case of 2000 ppm SO<sub>2</sub>, the resulting Hg capture was ~50 percent. This value was very close to Hg capture of ~57 percent in the case of passing 1100 ppm SO<sub>2</sub> through 2 absorbers. Together with the exiting SO<sub>2</sub> concentration in both cases, it again implied that nearly all NaClO<sub>2</sub> was consumed within one or two absorbers. Despite the potential massive consumption of NaClO<sub>2</sub>, a large amount of Hg was still oxidized through absorber #1, implying that Hg-NaClO<sub>2</sub> reaction proceeds at a very rapid rate.

### Hg Capture with Reconfigured Wet Scrubber

Now that the majority of NaClO<sub>2</sub> was consumed by HSO<sub>3</sub><sup>-</sup>/SO<sub>3</sub><sup>2-</sup> ions, not gaseous SO<sub>2</sub>, injecting NaClO<sub>2</sub> from the top of the scrubber is first proposed. To validate the above proposition, the wet scrubber was reconfigured – a portion of slurry was sprayed from the top of absorber #2, while a portion of slurry and NaClO<sub>2</sub> was injected from the top of absorber #3. The intention was to minimize consumption of NaClO<sub>2</sub> while improving Hg capture. Of the total flow of 8.3 L/min delivered by the recirculation pump, 1.7 L/min of slurry were sprayed with NaClO<sub>2</sub> from the top of absorber #3.

Figure 8 shows the status of Hg capture. In group 1 of the tests, a low concentration of SO<sub>2</sub> (~550 ppm) was used to simulate the case where there would be little SO<sub>2</sub> in absorber #3. All slurry was first sprayed at the top of absorber #2 to identify the SO<sub>2</sub> level in the absorber #3. With ~550 ppm SO<sub>2</sub>, the concentration of SO<sub>2</sub> out of absorber #2 was ~100 ppm. Then, a portion of slurry (1.7 L/min) was diverted to the top of absorber #3. The SO<sub>2</sub> concentration out of absorber #3 was slightly lower at ~85 ppm. When 1.62 M NaClO<sub>2</sub> was initiated at 5 mL/min, the SO<sub>2</sub> concentration from the wet scrubber quickly dropped to ~40 ppm. If the decrease of SO<sub>2</sub> was caused by a gaseous SO<sub>2</sub>-NaClO<sub>2</sub> reaction, then of the injected NaClO<sub>2</sub> (0.0081 mol/min), an estimate of ~0.000854 mol/min (or ~10%) NaClO<sub>2</sub> was depleted by gaseous SO<sub>2</sub>. As for the

oxidation of NO, which was ~225 ppm in the flue gas, its oxidation by NaClO<sub>2</sub> averaged 26.5 percent. However, the measured value for NO<sub>x</sub> capture was at a lower rate of 12.3 percent. Despite expecting a higher Hg capture, the resulting Hg capture was still ~70%. It held same for lowering the concentration of injected NaClO<sub>2</sub> to 0.81 M.

In group 2 of the tests, ~1100 ppm SO<sub>2</sub> was used. Slurry was circulated to both spray nozzles before the injection of NaClO<sub>2</sub> was initiated. At steady state, the SO<sub>2</sub> concentration out of the wet scrubber system was ~221 ppm. A higher concentration of SO<sub>2</sub>, in comparison to that in Table 1, was probably due to a lower slurry pH. During testing, a pH of 6.0 was selected. When the injection of NaClO<sub>2</sub> (solution concentration was 1.62 M) was turned on at a constant rate of 5 ml/min, the SO<sub>2</sub> concentration quickly dropped to ~170 ppm. Although a higher SO<sub>2</sub> concentration was used, the Hg removal across the wet scrubber system was not significantly lowered. At steady state, the corresponding Hg capture, NO oxidation, and NO<sub>x</sub> removal across the wet scrubber were ~65, ~25, and ~14 percent, respectively. Further calculations indicated that 12 percent (0.000987 mol/min) NaClO<sub>2</sub> was depleted by gaseous SO<sub>2</sub>. Total consumption of NaClO<sub>2</sub> by gaseous SO<sub>2</sub> and NO was 0.00203 mol/min or 25 percent. It should be noted that when the injection concentration of NaClO<sub>2</sub> was lowered to 0.81 M, Hg oxidation was improved by ~10 percent.

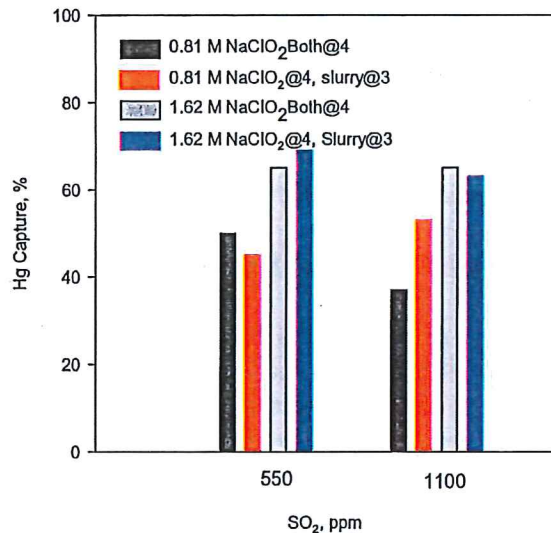


Figure 8. Hg Capture with Different Scrubber Configuration

## CONCLUSIONS

The pilot-scale tests confirmed our previously reported bench-scale results that NaClO<sub>2</sub> was effective in promoting Hg capture, but to a lesser extent NO/NO<sub>x</sub> capture in a wet scrubber system. Hg capture was as high as ~65 percent, while NO<sub>x</sub> capture was, in general, less than 20 percent. The results revealed that SO<sub>2</sub> was critical for the occurrence of Hg-NaClO<sub>2</sub> reaction, but it was also a limiting factor in minimizing NaClO<sub>2</sub> consumption. As an effort to understand the

consumption mechanism of  $\text{NaClO}_2$  in the wet scrubber system, analysis of data indicated that the consumption of  $\text{NaClO}_2$  was strongly related to aqueous sulfite ions, but to a lesser extent to gaseous  $\text{SO}_2$ . With 1100 to 2000 ppm  $\text{SO}_2$  to the wet scrubber system, an estimation of  $\text{NaClO}_2$  consumption by gaseous  $\text{SO}_2$  ranged from 10 to 20 percent.

**KEYWORDS:** Mercury, Sodium Chlorite, Wet Scrubber, Multi-pollutant Control

## REFERENCES

1. Srivastava, S. K.; Hutson, N. D.; Martin, G. B.; Princiotta, F.; Staudt, J. Control of Mercury Emissions from Coal-Fired Electric Utility Boilers. *Env. Sci. & Tech.* **2006**, *41*, 1385.
2. Srivastava, R. K.; Jozewicz, W. S.; Flue Gas Desulfurization: The State of the Art. *J. Air & Waste Management Assoc.* **2001**, *51*, 1676.
3. Srivastava, S. K.; Hutson, N. D.; Martin, G. B.; Princiotta, F.; Staudt, J.; Control of Mercury Emissions from Coal-Fired Electric Utility Boilers. *Env. Sci. & Tech.* **2006**, *41*, 1385.
4. Lee, C. W.; Serre, S. D.; Zhao, Y.; Lee, S. J.; Hastings, T. W.; Mercury Oxidation Promoted by a Selective Catalytic Reduction Catalyst under Simulated Powder River Basin Coal Combustion Conditions, *J. of the Air & Waste Management Association*, **2008**, *58*, 484.
5. Zhao, L. L.; Rochelle, G. T.; Mercury Absorption in Aqueous Oxidants Catalyzed by Mercury(II), *Ind. Eng. Chem. Res.*, **1998**, *37*, 380.
6. Zhao, L. L.; Rochelle, G. T.; Mercury Absorption in Aqueous Hypochlorite, *Chem. Eng. Sci.*, **1999**, *54*, 655.
7. Brogren, C.; Karlsson, H. T.; Bjerle, I.; Absorption of NO in an Aqueous Solution of  $\text{NaClO}_2$ , *Chem. Eng. Technol.*, **1998**, *21*, 61.
8. Sada, E.; Kumazawa, H.; Kudo, I.; Kondo, T.; Absorption of NO in Aqueous Mixed Solutions of  $\text{NaClO}_2$  and NaOH, *Chem. Eng. Sci.*, **1978**, *33*, 315.
9. Yang, C. L.; Shaw, H.; Aqueous Absorption of Nitric Oxide Induced by Sodium Chlorite Oxidation in the Presence of Sulfur Dioxide, *Env. Progress*, **1998**, *17*(2), 80.
10. Adewuyi, Y. G.; He, X.; Shaw, H.; Lolertpihop, W.; Simultaneous Absorption and Oxidation of NO and  $\text{SO}_2$  by Aqueous Solutions of Sodium Chlorite. *Chem. Eng. Sci.*, **1999**, *174*, 21.
11. Jozewicz, W.; Srivastava, R.K.; Ellison, W.; Ferrell, R.J. *Investigation of Multipollutant Scrubbing by Wet Flue Gas Desulfurization Systems*; joint presentation at 29th International Technical Conference on Coal Utilization & Fuel Systems: Clearwater, Florida, April 18-22, **2004**.
12. Hutson, N.D.; Krzyzyska, R.; Srivastava, S.K.; Simultaneous Removal of  $\text{SO}_2$ ,  $\text{NO}_x$ , and Hg from a Simulated Coal Flue Gas using a  $\text{NaClO}_2$ -enhanced Wet Scrubber, *Ind. Eng. Chem. Res.*, **2008**, *47* (16), 5825.

13. Chang, J. C.S.; Zhao, Y. Pilot Plant Testing of Elemental Mercury Reemission from a Wet Scrubber. *Energy & Fuels*, **2008**, *22*, 338–342

## Production of Activated Char from Illinois Coal for Flue Gas Cleanup<sup>†</sup>

Anthony A. Lizzio,\* Joseph A. DeBarr, and Carl W. Kruse

Illinois State Geological Survey, 615 East Peabody Drive, Champaign, Illinois 61820

Received November 8, 1996. Revised Manuscript Received January 6, 1997<sup>®</sup>

Activated chars were produced from Illinois coal and tested in several flue gas cleanup applications. High-activity chars that showed excellent potential for both SO<sub>2</sub> and NO<sub>x</sub> removal were prepared from an Illinois No. 2 bituminous coal. The SO<sub>2</sub> (120 °C) and NO<sub>x</sub> (25 °C) removal performance of one char compared favorably with that of a commercial activated carbon (Calgon Centaur). The NO<sub>x</sub> removal performance of the same char at 120 °C exceeded that of the Centaur carbon by more than 1 order of magnitude. Novel char preparation methods were developed including oxidation/thermal desorption and hydrogen treatments, which increased and preserved, respectively, the active sites for SO<sub>2</sub> and NO<sub>x</sub> adsorption. The results of combined SO<sub>2</sub>/NO<sub>x</sub> removal tests, however, suggest that SO<sub>2</sub> and NO<sub>x</sub> compete for similar adsorption sites and SO<sub>2</sub> seems to be more strongly adsorbed than NO. A low-activity, low-cost char was also developed for cleanup of incinerator flue gas. A three-step method involving coal preoxidation, pyrolysis, and CO<sub>2</sub> activation was used to produce the char from Illinois coal. Five hundred pounds of the char was tested on a slipstream of flue gas from a commercial incinerator in Germany. The char was effective in removing >97% of the dioxins and furans present in the flue gas; mercury levels were below detectable limits.

### Introduction

Concerns about air quality and our environment have led to increasing regulation of exhaust emissions from stationary combustion sources. More stringent regulations will likely be introduced in the future. Sulfur and nitrogen oxides are important air pollutants that cause photochemical smog formation and acid rain. One of the unique properties of activated carbon is that it can remove nearly every impurity found in flue gas including SO<sub>2</sub>, NO<sub>x</sub>, particulates, mercury, dioxins, furans, heavy metals, volatile organic compounds, and other trace elements.<sup>1-6</sup> No other existing sorbent has that capability. An activated-carbon-based process, typically placed after the precipitator and just before the stack, can be used alone or in conjunction with other control methods to remove sulfur and nitrogen oxides from flue gas.<sup>7-9</sup> This technology has been used in Europe and Japan for cleanup of flue gas from both coal combustion and waste incineration. Currently, no U.S. utility employs a carbon-based process to clean flue gas.

Worldwide interest in carbon-based processes for low-temperature (80–150 °C) removal of SO<sub>x</sub>, NO<sub>x</sub>, mercury, and other air toxics from coal combustion and waste incineration flue gas is growing. Several air pollution control systems now in commercial use and several more on the verge of commercialization could benefit from improvements in the adsorptive/catalytic properties of carbon used to remove these contaminants from flue gas. An ongoing research program<sup>10-20</sup> at the Illinois State Geological Survey (ISGS) is seeking to develop activated chars of various activities using Illinois bituminous coal as the feedstock. This paper discusses our recent efforts to produce activated char tailored for specific commercial or near-commercial flue gas cleanup applications.

<sup>†</sup> Paper presented at the National Meeting of the American Chemical Society, New Orleans.

<sup>®</sup> Abstract published in *Advance ACS Abstracts*, February 15, 1997.

(1) Brueggendick, H.; Pohl, F. G. In *Proceedings of 10th Annual International Pittsburgh Coal Conference*, Pittsburgh, PA, 1993; p 787.

(2) Brueggendick, H.; Gilgen, R. *Prepr. Pap.-Am. Chem. Soc., Div. Fuel Chem.* 1996, 41 (1), 899.

(3) Tsuji, K.; Shiraiishi, I. In *Proceedings of Electric Power Research Institute SO<sub>2</sub> Control Symposium*, Washington, DC, 1991; p 307.

(4) Tsuji, K.; Shiraiishi, I. *Prepr. Pap.-Am. Chem. Soc., Div. Fuel Chem.* 1996, 41 (1), 404.

(5) Hartenstein, H.-U. In *Proceedings of 85th Annual Air and Waste Management Association Meeting*, Kansas City, MO, 1992.

(6) Hartenstein, H.-U. *Prepr. Pap.-Am. Chem. Soc., Div. Fuel Chem.* 1996, 41 (1), 409.

(7) Richter, E.; Knoblauch, K.; Jungten, H. In *Proceedings of 1st International Conference on Processing and Utilization of High Sulfur Coals*, 1985; p 563.

(8) Richter, E.; Knoblauch, K.; Jungten, H. *Gas Sep. Purif.* 1987, 1, 35.

(9) Jungten, H.; Kuhl, H. *Chem. Phys. Carbon* 1989, 22, 145.

(10) Lizzio, A. A.; DeBarr, J. A.; Kruse, C. W.; Donnals, G. L.; Rood, M. J. *Production and Use of Activated Char for Combined SO<sub>2</sub>/NO<sub>x</sub> Removal*. Final Technical Reports to Illinois Clean Coal Institute, 1994, 1995.

(11) DeBarr, J. A.; Lizzio, A. A. In *Proceedings of International Conference on Carbon*, Granada, Spain, 1994; p 268.

(12) Lizzio, A. A.; DeBarr, J. A. *Fuel* 1996, in press.

(13) DeBarr, J. A. The Role of Free Sites in the Removal of SO<sub>2</sub> from Simulated Flue Gases by Activated Char. M.S. Thesis, University of Illinois, Urbana, IL, 1995.

(14) DeBarr, J. A.; Lizzio, A. A.; Rood, M. J. In *Proceedings of 88th Annual Air and Waste Management Association Meeting*, San Antonio, TX, 1995.

(15) DeBarr, J. A.; Lizzio, A. A. In *Proceedings of 22nd Biennial Conference on Carbon*, San Diego, CA, 1995; p 562.

(16) Lizzio, A. A.; DeBarr, J. A.; Kruse, C. W. In *Proceedings of 22nd Biennial Conference on Carbon*, San Diego, CA, 1995; p 744.

(17) Kruse, C. W.; Lizzio, A. A.; DeBarr, J. A.; Bhagwat, S. B. *Prepr. Pap.-Am. Chem. Soc., Div. Fuel Chem.* 1995, 40 (4), 838.

(18) Kruse, C. W.; Lizzio, A. A.; DeBarr, J. A.; Bhagwat, S. B.; Lytle, J. M. *Producing Activated Carbon for Cleaning Flue Gas from Incinerators*. Final Technical Report to Illinois Clean Coal Institute, 1996.

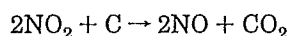
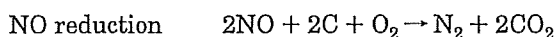
(19) Lizzio, A. A.; DeBarr, J. A. In *Proceedings of 12th International Annual Pittsburgh Coal Conference*, Pittsburgh, PA, 1995; p 652.

(20) Lizzio, A. A.; DeBarr, J. A. *Prepr. Pap.-Am. Chem. Soc., Div. Fuel Chem.* 1996, 41 (1), 201.

**SO<sub>2</sub> Removal.** Carbon adsorbents may be used to remove sulfur oxides from coal combustion flue gas at temperatures between 20 and 180 °C. The type of carbon used is probably the most important process consideration, with respect to both adsorption efficiency and maintenance of efficiency during extended operation. Numerous carbons have been tested for this application, ranging from highly activated carbon to untreated coal. The SO<sub>2</sub> adsorption capacity of an activated char prepared from the same coal can vary by 2 orders of magnitude depending on its preparation method.<sup>13</sup> Parameters that may affect SO<sub>2</sub> removal by carbon include flue gas temperature, pollutant concentration, particle size of sorbent, other components in the flue gas such as O<sub>2</sub> and H<sub>2</sub>O, and the physical/chemical properties of the carbon such as surface area and oxygen content. A high-quality carbon adsorbent for SO<sub>2</sub> removal should have the following properties: high adsorption capacity for SO<sub>2</sub>, rapid SO<sub>2</sub> adsorption kinetics, low reactivity with oxygen, minimal activation losses due to regeneration, high mechanical strength, and low cost. Removal of SO<sub>2</sub> from flue gas by activated carbon involves a series of reactions beginning with adsorption of SO<sub>2</sub> on free sites on the carbon surface. The resultant C-SO<sub>2</sub> complex reacts with gas phase O<sub>2</sub> to form C-SO<sub>3</sub>, which then reacts with adsorbed water to form sulfuric acid. A detailed mechanism and simplified rate expression for SO<sub>2</sub> removal by carbon was recently proposed.<sup>20</sup>

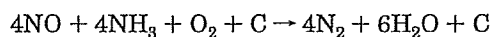
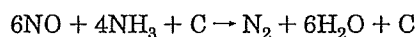
**NO<sub>x</sub> Removal.** Carbon can also be used to remove NO<sub>x</sub> from flue gas at temperatures between 20 and 150 °C. Carbon may act as both a sorbent<sup>21-23</sup> and a catalyst;<sup>24-26</sup> the extent of each depends on the physical/chemical properties of the carbon and flue gas conditions. The NO<sub>x</sub> adsorption capacity of an activated carbon can range from 0 to 15 wt % depending on sample preparation and flue gas conditions. Carbon, besides adsorbing NO<sub>x</sub>, can also catalyze NO<sub>x</sub> reduction, where N<sub>2</sub> and CO<sub>2</sub> are the principal products of the reaction. In either case, the carbon catalyst requires regeneration when a sufficient quantity of nitrogen oxide complexes accumulate on the carbon surface and block the sites responsible for the adsorption/reduction of NO<sub>x</sub>.

Nitrogen oxides are present in most flue gas mainly as NO and 5-10% NO<sub>2</sub>. Both can be reduced by reaction with carbon at temperatures between 20 and 200 °C.



Illan-Gomez et al.<sup>27</sup> found that the NO reduction activity of 10 carbons covering a wide range of surface area and pore size distributions correlated well with the N<sub>2</sub> BET surface area. It was concluded that at the temperatures studied (400-600 °C) all of the available surface area of the carbons was effective for the reaction and that accessibility problems due to diffusional limitations were not important. Yamashita et al.<sup>28</sup> studied the reaction of brown coal chars with NO and O<sub>2</sub> at 300 °C. A char loaded with 4% copper exhibited enhanced NO reduction activity in the presence of oxygen. The formation of reactive surface C(O) intermediates and stable C-O complexes during these reactions was investigated by a combination of transient kinetics and temperature-programmed desorption techniques. A mechanism for Cu-catalyzed NO reduction based on enhanced formation of reactive C(O) intermediates was proposed. There have been relatively few, if any, studies on NO<sub>x</sub> removal by carbon at temperatures <200 °C.

Another means to reduce NO<sub>x</sub> by carbon is by selective catalytic reduction (SCR) of NO with ammonia (NH<sub>3</sub>). Typically, the carbon catalysts used in commercial SCR processes are high surface area activated carbons (1000-1500 m<sup>2</sup>/g) made from bituminous coal. Carbo Tech (Essen, Germany) presently manufactures ton quantities of this material for carbon-based SCR processes operating throughout Europe. When NH<sub>3</sub> is added to the flue gas in the presence of carbon, the NO is reduced to nitrogen and steam. The stoichiometry of the overall reaction indicates that carbon is not consumed in the process.



The activity of carbon catalysts for SCR of NO<sub>x</sub> can be influenced by both the amount and types of functional groups present on the carbon surface. Singoredjo et al.<sup>29</sup> modified activated carbons with nitrogen and oxygen containing organic compounds, followed by pyrolysis and CO<sub>2</sub> activation, and studied low-temperature SCR of NO with NH<sub>3</sub> at temperatures between 110 and 280 °C. An increase in NO reduction activity was attributed to the creation of stable C-O complexes. These complexes could be removed only at high temperatures. The role of incorporated nitrogen was not clear. They concluded that overall NO reduction activity was the result of a combination of factors: number and type of C-O complexes on the char surface, nitrogen content of the char, and accessibility of the pores.

**Combined SO<sub>2</sub>/NO<sub>x</sub> Removal.** Retrofitting an existing utility boiler with an activated carbon FGD process should, in addition to improving SO<sub>2</sub>/NO<sub>x</sub> emissions, lower overall operating costs compared to competitive FGD processes. Richter et al.<sup>7</sup> described the flexibility of the Bergbau-Forschung (BF) carbon-based SO<sub>2</sub>/NO<sub>x</sub> removal process now in commercial use throughout Europe and its ease of incorporation into existing FGD processes. Four BF process configurations

(21) Rubel, A. M.; Stencil, J. M. *Prepr. Pap.-Am. Chem. Soc., Div. Fuel Chem.* 1996, 41 (1), 302.

(22) Groszek, A. J. *Prepr. Pap.-Am. Chem. Soc., Div. Fuel Chem.* 1996, 41 (1), 317.

(23) Nelson, S. G.; Bayak, R. A. *Prepr. Pap.-Am. Chem. Soc., Div. Fuel Chem.* 1996, 41 (1), 298.

(24) Jungten, H.; Richter, E.; Knoblauch, K.; Hoang-Phu, T. *Chem. Eng. Sci.* 1988, 43, 419.

(25) Ahmed, S. N.; Stencil, J. M.; Derbyshire, F. J.; Baldwin, R. M. *Fuel Process. Technol.* 1993, 34, 123.

(26) Spivey, J. J. *Catal. Today* 1994, 18, 155.

(27) Illan-Gomez, M. J.; Linares-Solano, A.; Salinas-Martinez de Lecea; Calo, J. M. *Energy Fuels* 1993, 7, 146.

(28) Yamashita, H.; Tomita, A.; Yamada, H.; Kyotani, T.; Radovic, L. R. *Energy Fuels* 1993, 7, 85.

(29) Singoredjo, L.; Kapteign, F.; Moulijn, J. A.; Martin-Martinez, J. M.; Boehm, H.-P. *Carbon* 1993, 31, 213.

were analyzed in detail. Perhaps the most interesting was a carbon-based process placed behind a conventional FGD unit (scrubber). With a flue gas of high SO<sub>2</sub> concentration, the scrubber was able to be operated at a relatively low SO<sub>2</sub> removal rate and was used only as a preliminary stage for the more efficient carbon-based process. Also, it was easier to integrate a carbon-based NO<sub>x</sub> reduction process into a power plant FGD scheme than to use a catalyst-based NO<sub>x</sub> reduction unit, which needed to be operated at relatively high temperatures (>250 °C). They also suggested that for smaller boilers, and those boilers burning high-sulfur coal, it would be more economical to operate conventional spray sorption methods at low efficiency and arrange behind them a suitable activated carbon FGD process to remove the bulk of SO<sub>2</sub>/NO<sub>x</sub>.

Mitsui Mining Co. Ltd. (Tokyo, Japan) modified the BF process to achieve both SO<sub>2</sub> and NO<sub>x</sub> removal in a single process.<sup>3,4</sup> The process consists of three sections: adsorption, regeneration, and byproduct recovery. Their process scheme achieves 100% removal of SO<sub>2</sub> and over 80% removal of NO<sub>x</sub> by contacting the flue gas with two consecutive moving beds of activated coke. Ammonia is injected into the second bed to reduce nitrogen oxides at a temperature of 200 °C. Halogen compounds, dioxins, and trace elements such as mercury vapor also contained in the flue gas are removed by chemical and/or physical adsorption onto the carbon. Particulates are also removed by the activated coke filter. Elemental sulfur, sulfuric acid, or liquid SO<sub>2</sub> is recovered in the regeneration section. Mitsui Mining also developed technology to produce the activated coke used in their process. The surface area and SO<sub>2</sub> adsorption capacity of their coke vary between 150 and 300 m<sup>2</sup>/g and between 60 and 110 mg/g, respectively. Mitsui Mining initially constructed and operated a pilot plant that produced 0.5 ton of activated coke per day. Bituminous coal was found to be the best feedstock, but lignite and petroleum coke were also used. An activated coke with high mechanical strength was achieved by controlled pyrolysis of bituminous coal, and a proper micropore structure was developed using a controlled chemical activation process. The ratio of activated coke to binder was critical to produce a final product with high mechanical strength. The surface of the activated coke was then chemically treated to increase its ability to remove SO<sub>2</sub> and NO<sub>x</sub>. Today, Mitsui Mining produces about 3000 tons of activated coke per year for their process that is installed on a 350 MW fluidized bed combustion power plant in Japan. The metallurgical coke is produced in coke ovens and then further activated to increase its surface area from 20 to 300 m<sup>2</sup>/g. The cost to produce the activated coke is \$800–1000/ton.

Gangwal et al.<sup>30,31</sup> developed the Research Triangle Institute (RTI)–Waterloo process, a novel low-temperature process employing carbon-based catalysts and operating downstream of the electrostatic precipitator. It is capable of removing more than 95% of the SO<sub>2</sub> and 75% of the NO<sub>x</sub> from coal combustion flue gas. Sulfur dioxide is catalytically oxidized to SO<sub>3</sub> at 100 °C and is removed as medium-strength sulfuric acid in a series

of periodically flushed trickle bed reactors containing an activated carbon catalyst. The SO<sub>2</sub> free gas is reheated to 150 °C and NH<sub>3</sub> is added. The gas is passed over a fixed bed of another carbon catalyst to reduce the NO<sub>x</sub> to N<sub>2</sub> and H<sub>2</sub>O. The technical feasibility of the process was demonstrated in laboratory scale experiments. A preliminary evaluation of the RTI–Waterloo process conducted for a 100 MW electric power plant burning a 2.8% sulfur coal showed that the RTI–Waterloo process was competitive with several combined SO<sub>2</sub>/NO<sub>x</sub> removal processes (conventional FGD/SCR, SNO<sub>x</sub>, E-beam). The carbon catalysts developed in the study, however, still need to be optimized with respect to cost and long-term durability.

**Incinerator Flue Gas.** Carbon-based systems for flue gas cleanup have been installed on commercial medical, hazardous, and municipal waste incinerators throughout Europe. The activated carbon technology is given preference over other alternatives because of its high removal efficiency for sulfur oxides, dioxins, furans, mercury, heavy metals, and other air toxics. Typically, flue gases pass through an activated carbon filter at temperatures between 100 and 150 °C. In the process developed by STEAG Aktiengesellschaft,<sup>1–2</sup> known as the *a/c/t* process, a three-layer moving bed of carbon separates and treats selectively pollutants in each layer. The spent carbon is returned to the incinerator where the adsorbed contaminants are either destroyed or released again for ultimate removal in a wet scrubber system situated upstream of the carbon filter. Operating results show that current European emission requirements are met with this type of system. Availability of this proven technology in the United States could prompt legislation to set incinerator emissions limits low enough to make incinerators acceptable to the American public. The potential market for activated char in the United States is estimated to be 80 000 tons/year, assuming 10% of U.S. incinerators adopt this technology to meet needs emanating from anticipated regulation of emissions from existing incinerators. The carbon used by STEAG is made from German brown coal and has a relatively low surface area (<270 m<sup>2</sup>/g) and price (<\$300/ton). A domestic source of this carbon is needed for *a/c/t* processes that will be installed on U.S. waste incinerators.

## Experimental Section

**Char Preparation.** Figure 1 presents a process flow sheet for production of high-activity (for coal combustion) and low-activity (for incinerator flue gas) char from Illinois coal. The four major processing steps are preoxidation, pyrolysis, activation, and surface modification by a novel oxygen deposition/thermal desorption treatment. The pyrolysis and activation steps were used in making both types of chars. The high- and low-activity chars were prepared from Colchester (Illinois No. 2) hvC bituminous coal obtained from two different mines in Illinois.

**High-Activity Char.** High-activity chars were produced from a Colchester (Illinois No. 2) coal (designated IBC-102 coal in the Illinois Basin Coal Sample Program<sup>32,33</sup>). A 48 × 100 mesh sample of this coal was used. Chars were prepared at 900 °C for 0.5 h in a 5 cm i.d. batch fluidized bed reactor (FBR). Typically, 200 g of IBC-102 coal was fluidized in flowing N<sub>2</sub> (6

(30) Gangwal, S. K.; Silveston, P. L.; Howe, G. B.; McMichael, W. J.; Spivey, J. J. Final Report to U.S. DOE, 1993.

(31) Gangwal, S. K.; Howe, G. B.; Spivey, J. J.; Silveston, P. L.; Hudgins, R. R.; Metzinger, J. G. *Environ. Prog.* 1993, 12, 128.

(32) Harvey, R. D.; Kruse, C. W. *J. Coal Qual.* 1988, 7, 109.

(33) Demir, I.; Lizzio, A. A.; Fuller, E. L.; Harvey, R. D. *J. Coal Qual.* 1994, 13, 93.

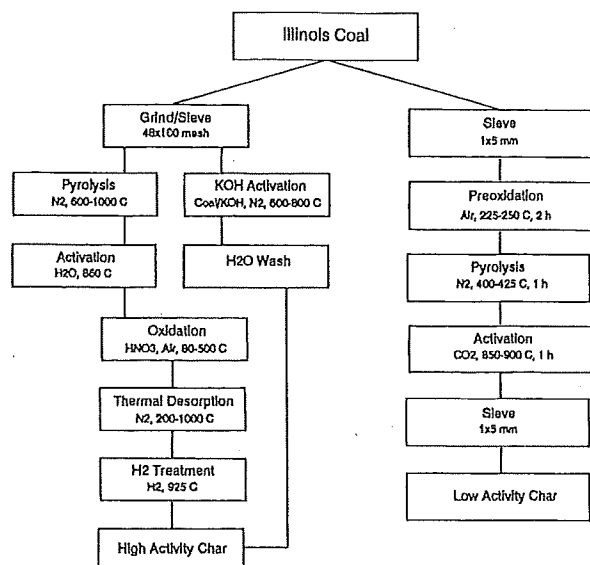


Figure 1. Production of high- and low-activity char from Illinois coal.

L/min) and heated to the desired pyrolysis temperature. A multistep heating procedure was used to minimize agglomeration of coal particles in the FBR.<sup>13</sup> Steam activation was performed to further develop microporosity and increase surface area. Typically, 50 g of char prepared at 900 °C was placed in the 5 cm i.d. FBR and heated to 860 °C in flowing N<sub>2</sub>. At 860 °C, the N<sub>2</sub> flow was replaced by 50% H<sub>2</sub>O/50% N<sub>2</sub> (6 L/min) for 0.75 h to achieve 30% char conversion.

The H<sub>2</sub>O-activated char was subjected to a nitric acid treatment. Typically, 10 g of the char was added to 0.2 L of 10 M HNO<sub>3</sub> solution and refluxed at 80 °C for 1 h. The HNO<sub>3</sub>-treated carbon was washed with distilled H<sub>2</sub>O to remove excess acid and vacuum-dried overnight at 25 °C. Using a 2.5 cm FBR, the HNO<sub>3</sub>-treated char was heated in 1 atm of N<sub>2</sub> (ultrahigh purity) to 525, 725, or 925 °C and held for 1 h to desorb C–O complexes formed by the HNO<sub>3</sub> treatment. To preserve active sites, the HNO<sub>3</sub>-treated char was exposed to 1 atm of H<sub>2</sub> (instead of N<sub>2</sub>) at 925 °C for 1 h.

A chemical activation method was also employed to enhance surface area development. Potassium hydroxide (KOH) was loaded onto the coal by impregnation to incipient wetness. Typically, 100 g of KOH was dissolved in 0.1 L distilled water and mixed thoroughly with 100 g of raw coal. The dried coal/KOH mixture was added to the 5 cm i.d. FBR and pyrolyzed in flowing N<sub>2</sub> at 600 and 800 °C for 0.5 h. The sample was cooled in N<sub>2</sub> and washed with distilled H<sub>2</sub>O to remove leftover potassium and air-dried overnight at 110 °C.

**Low-Activity Char.** The mine from which IBC-102 coal was obtained was closed at the time this study was performed (it reopened in 1996), so another Colchester (Illinois No. 2) coal, readily obtained from a nearby mine, was used instead to produce low-activity char. The conditions needed to produce low-activity char from this coal were identified using several types of reactors including a 4.5 cm i.d. horizontal tube furnace, 9 cm i.d., 1.2 m heated zone, continuous feed rotary tube kiln, and a continuous feed charring oven.<sup>10,17,18</sup> With the assistance of Allis Mineral Systems (Milwaukee, WI), the production steps were carried through two levels of scale up, culminating in the production of 277 kg of activated char in a 46 cm i.d., 3 m heated zone, externally fired rotary tube kiln. A 580 kg pound sample of size-graded bituminous coal having a free swelling index of 4.5 was used as feedstock for the production run. A three-step process, which included preoxidation, pyrolysis, and activation, was necessary to process the coal. The coal feed rate during preoxidation was 23 kg/h to maintain a 2 h residence time at 250 °C. Initial external temperatures in the

three heating zones of the kiln ranged from 420 °C for the first zone (entrance) to 250 °C for the final zone (exit). The pyrolysis step was carried out in flowing N<sub>2</sub> (227 L/min) in the temperature range 425–450 °C and a feed rate of 30 kg/h. The volatile matter was combusted in a gas-fired combustor. The activation step was conducted in flowing CO<sub>2</sub> (170 L/min) at 870–920 °C with a feed rate of 23 kg/h. The overall yield for the three steps was 48% (277 kg of char from 580 kg of coal) after screening to remove 11 kg of –16 mesh (–1 mm) material. Further details of the conditions used in the production runs have been described elsewhere.<sup>10,16–18</sup>

**Char Characterization.** The SO<sub>2</sub> adsorption capacities of prepared chars were determined by thermogravimetric analysis (Cahn TG-131). In a typical run, a 30–50 mg char sample was placed in a platinum pan and heated at 20 °C/min in flowing N<sub>2</sub> to 120 °C. Once the temperature stabilized, the flow of N<sub>2</sub> was switched to a mixture of gases containing 5% O<sub>2</sub>, 7% H<sub>2</sub>O, and the balance N<sub>2</sub>. Once there was no further weight gain due to adsorption of O<sub>2</sub> and H<sub>2</sub>O, SO<sub>2</sub> was added in concentrations representative of a typical flue gas for combustion of high-sulfur coal (2500 ppm of SO<sub>2</sub>).

A laboratory scale adsorption column/mass spectrometer (AC/MS) system was used to measure nitric oxide (NO) breakthrough curves. The AC consisted of a 1.25 cm i.d. × 30 cm stainless steel tube and was heated by a 2.5 cm i.d. split tube furnace. The temperature of the AC was monitored by a 0.6 cm type K thermocouple placed directly above the sample bed. Concentrations of 16 gas species were monitored continuously at 20 s intervals using a quadrupole mass spectrometer (Gastrace-A System, VG Quadrupoles, Fisons Instruments). In a typical run, 3–5 g of activated char was loaded into the AC (8 cm carbon bed) and placed between two layers of quartz wool packing. The AC was heated under 99.9999% He flowing at 0.2 L/min to the desired temperature. Once the temperature stabilized, the gas was switched to a mixture consisting of 500 ppm of NO, 5% O<sub>2</sub>, balance He. The concentration of NO in the effluent was monitored as a function of time. When the carbon bed became saturated, e.g., inlet and outlet concentrations of NO were identical, the gas was switched back to He and the AC cooled to room temperature. If the sorbent was regenerated, it was heated to 925 °C at 20 °C/min under flowing helium.

Temperature programmed desorption (TPD) experiments were carried out in a flow-through, 2.5 cm i.d. stainless steel fixed bed reactor system. In a typical run, 0.5 g of sample was heated in flowing nitrogen (0.5 L/min) at 5 °C/min to a final temperature of 1000 °C and held for 1 h to achieve nearly complete desorption of CO and CO<sub>2</sub> from the char surface. Rosemount Model 880 CO and CO<sub>2</sub> nondispersive infrared analyzers were used to continuously monitor the concentrations of CO and CO<sub>2</sub> in the effluent gas.

Surface areas were determined from the amount of N<sub>2</sub> and CO<sub>2</sub> adsorbed at 77 and 195 K, respectively, using a dynamic sorption method in conjunction with a single-point BET adsorption equation. Single-point N<sub>2</sub> BET surface areas were determined from N<sub>2</sub> (77 K) adsorption data obtained at a relative pressure (*P/P*<sub>0</sub>) of 0.30 with a Monosorb flow apparatus (Quantachrome Corp.). Single-point CO<sub>2</sub> BET surface areas were determined from CO<sub>2</sub> (195 K, dry ice–ethanol) adsorption data obtained in a custom-made U-tube apparatus at a *P/P*<sub>0</sub> of 0.15 (220 Torr of CO<sub>2</sub> in helium, *P*<sub>0</sub> = 1450 Torr).

## Results and Discussion

**SO<sub>2</sub> Removal.** The initial goal of this study was to identify process conditions for producing activated char with optimal SO<sub>2</sub> removal characteristics.<sup>10–15</sup> Chars with varying pore structure and surface chemistry were prepared from IBC-102 coal under a wide range of pyrolysis and activation conditions and tested for their ability to remove SO<sub>2</sub> from simulated flue gas. Table 1.

Table 1. Correlation of SO<sub>2</sub> Adsorption Capacity with Surface Area and Chemisorbed Oxygen

sample	SO <sub>2</sub> capacity <sup>a</sup> (mg of SO <sub>2</sub> / g of char)	N <sub>2</sub> BET (m <sup>2</sup> /g)	CO <sub>2</sub> BET (m <sup>2</sup> /g)	SO <sub>2</sub> /N <sub>2</sub> (mg/m <sup>2</sup> )	SO <sub>2</sub> /CO <sub>2</sub> (mg/m <sup>2</sup> )	O <sub>2</sub> (wt %)	SO <sub>2</sub> /O <sub>2</sub>
Calgon F400	206	1000	1000	0.21	0.21	0.5	41.2
Calgon Centaur	327	360	— <sup>b</sup>	0.91	—	—	—
IBC-102, N <sub>2</sub> , 500 °C, 0.5 h	19	1.2	270	15.8	0.07	8.8	0.22
IBC-102, N <sub>2</sub> , 700 °C, 0.5 h	33	10	315	3.3	0.10	1.5	2.20
IBC-102, N <sub>2</sub> , 900 °C, 0.5 h	7	1.2	98	5.8	0.07	0.5	1.40
IBC-102 + KOH, N <sub>2</sub> , 600 °C, 0.5 h	157	500	725	0.31	0.22	7.4	2.12
IBC-102 + KOH, N <sub>2</sub> , 800 °C, 0.5 h	176	800	1155	0.22	0.15	5.6	3.14
IBC-102, 500 °C; 10% O <sub>2</sub> , 390 °C	13	220	422	0.06	0.03	8.6	0.15
IBC-102, 700 °C; 10% O <sub>2</sub> , 440 °C	37	320	490	0.11	0.08	8.9	0.42
IBC-102, 900 °C; 10% O <sub>2</sub> , 500 °C	42	230	395	0.18	0.11	5.2	0.81
IBC-102, 900 °C; H <sub>2</sub> O, 860 °C	176	220	613	0.80	0.29	1.1	16.0
IBC-102, 900 °C; H <sub>2</sub> O, 860 °C; 45% HNO <sub>3</sub> , 2.5 h, 25 °C	—	400	585	0.06	0.04	16.4	—
IBC-102, 900 °C; H <sub>2</sub> O, 860 °C; 45% HNO <sub>3</sub> , desorbed at 525 °C	91	460	693	0.20	0.13	5.9	1.54
IBC-102, 900 °C; H <sub>2</sub> O, 860 °C; 45% HNO <sub>3</sub> , desorbed at 725 °C	241	500	727	0.48	0.33	1.6	15.0
IBC-102, 900 °C; H <sub>2</sub> O, 860 °C; 45% HNO <sub>3</sub> , desorbed at 925 °C	237	550	726	0.05	0.39	0.5	57.4

<sup>a</sup> SO<sub>2</sub> capacity determined after 6 h. <sup>b</sup>Not determined.

Table 2. SO<sub>2</sub> Removal Tests Performed by RTI

cycle	low emission (ppm of SO <sub>2</sub> )	20% breakthrough time (min)
HNO <sub>3</sub> -925 °C Char		
1	80	3
2	100	80
3	80	60
4	150	25
5	160	35
6	240	30
7	300	20
8	350	15
9	400	10
KOH-Activated Char		
1	25	45
2	1800	

summarizes the results. A novel char preparation method, involving nitric acid treatment followed by thermal desorption of carbon-oxygen (C-O) complexes, was developed to produce activated chars with SO<sub>2</sub> adsorption capacities comparable to those of commercial activated carbons (Calgon F400 and Centaur). An attempt was made to relate the observed SO<sub>2</sub> adsorption behavior to the physical and chemical properties of the char. There was no correlation between SO<sub>2</sub> capacity and N<sub>2</sub> BET surface area. A TPD method was used to determine the nature and extent of C-O complexes formed on the char surface. TPD data revealed that SO<sub>2</sub> adsorption was inversely proportional to the amount of stable C-O complex. The formation of stable C-O complex may have served only to occupy carbon sites that were otherwise reactive to SO<sub>2</sub> adsorption. TPD data have also revealed that SO<sub>2</sub> adsorption was directly proportional to the number of free adsorption sites on the carbon surface.<sup>12-15</sup>

The Research Triangle Institute performed SO<sub>2</sub> removal tests on five of the chars listed in Table 1 under conditions simulating those used in the RTI-Waterloo process: 100 °C, 2500 ppm of SO<sub>2</sub>, 5% O<sub>2</sub>, 10% H<sub>2</sub>O, balance helium, space velocity of 1400 h<sup>-1</sup>. Each adsorption cycle was followed by a 0.2 L wash with 4.32 N H<sub>2</sub>SO<sub>4</sub>. The results of nine adsorption/desorption cycles performed with the HNO<sub>3</sub>-925 °C char are summarized in Table 2. After the first cycle, the 20% breakthrough time (BT), i.e., when 20% of inlet concentration of SO<sub>2</sub> is measured in the effluent, was extended from 3 to 80 min; however, BT decreased steadily thereafter. Also, the lowest emission (LE), i.e., the

Table 3. Comparison of SO<sub>2</sub> Breakthrough Times

cycle	low emission (ppm of SO <sub>2</sub> )	5% breakthrough time (min)
HNO <sub>3</sub> -725 °C Char		
1	10	60
2	1200	
Centaur Carbon		
1	0	725
2	10	40

minimum SO<sub>2</sub> concentration detected in the effluent, increased with each subsequent cycle. It should be mentioned that the NO<sub>x</sub> removal tests for the HNO<sub>3</sub>-925 °C char were performed prior to these SO<sub>2</sub> removal tests. The rather poor performance of this char can be attributed to adsorbed NO, NH<sub>3</sub>, and O<sub>2</sub> poisoning of the SO<sub>2</sub> adsorption sites. Commercial processes typically remove SO<sub>2</sub> before NO<sub>x</sub> to avoid production of ammonium sulfate, which can also reduce catalytic activity.<sup>3-8</sup> All subsequent SO<sub>2</sub> removal tests were performed on carbons that were not previously exposed to NO or NH<sub>3</sub>. The KOH-activated char was also tested. Table 2 shows that a relatively low SO<sub>2</sub> emission in the effluent was achieved and the 20% BT was 45 min, but after the first cycle, performance decreased dramatically.

The SO<sub>2</sub> removal performance of the Centaur carbon was superior to that of all other carbons tested. Table 3, however, shows that its 5% BT also decreased after the first cycle. The IBC-102, HNO<sub>3</sub>-725 °C char performed best among the ISGS chars tested. Its initial LE was 10 ppm of SO<sub>2</sub> (equivalent to 99% removal efficiency), but this increased to 1200 ppm of SO<sub>2</sub> after just the first acid wash. An RTI carbon (not listed in Table 2 or 3) showed similar deactivation after the first cycle. The integral feature of the RTI-Waterloo process is its regeneration step involving a water wash with dilute H<sub>2</sub>SO<sub>4</sub>. One important advantage of doing this instead of thermal regeneration is that it does not consume carbon. Thus, a carbon catalyst in this process could last for many years without having to be replaced. The SO<sub>2</sub> removal performance of all the carbons tested by RTI in this study decreased markedly after the first cycle. Whether a low-cost carbon having a high concentration of free sites resistant to poisoning by the dilute acid wash can be developed for this process remains to be determined.

NO<sub>x</sub> Removal. Although SCR of NO<sub>x</sub> with ammonia

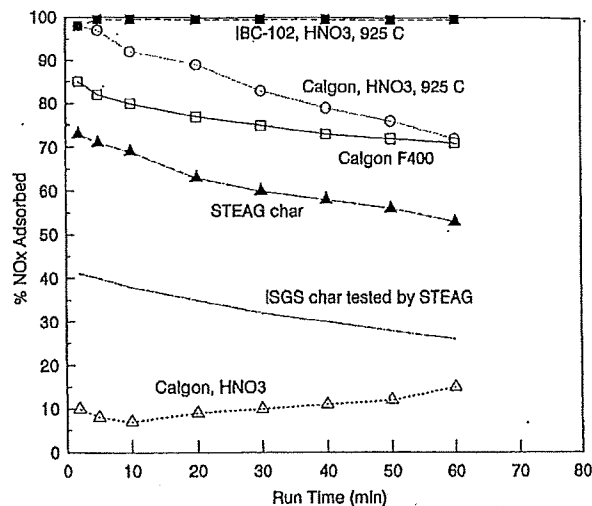


Figure 2.  $\text{NO}_x$  removal with various carbons at 25 °C.

is an available technology to remove  $\text{NO}_x$  from flue gas, this process has several drawbacks, e.g., ammonia slip (another air pollutant), equipment corrosion, higher operating temperature, which requires reheating of the flue gas, large reactor volumes, and high equipment costs. Consequently, SCR is not practical in many applications and may be problematical with coal-fired power plants. Coal-based carbons are an attractive alternative to traditional SCR catalysts (vanadium, titanium) for reducing  $\text{NO}_x$  emissions. Sorbent Technologies Corp. (STC) and the U.S. Air Force are presently developing a carbon-based process for low-temperature (20–100 °C) removal of  $\text{NO}_x$  from exhaust streams from jet engine test cells and other combustion sources such as diesel engines that would not require the use of ammonia.<sup>23</sup> The carbon filter being developed is a relatively simple  $\text{NO}_x$  control device that is placed directly into the exhaust duct path. There it substantially removes the  $\text{NO}_x$  as well as other contaminants such as  $\text{SO}_2$ , HCl, and organics. The ISGS and STC are working together to develop a carbon for low-temperature  $\text{NO}_x$  removal.

Several carbons prepared at the ISGS were tested by STC. The experimental conditions used were as follows: 10 g of carbon, 2.5 cm i.d. fixed bed reactor, 500 ppm of NO in air, and a flow rate of 4 L/min. Figure 2 shows that the IBC-102,  $\text{HNO}_3$ -925 °C char removed 100% of the  $\text{NO}_x$  during a 1 h test. Recall that this char also adsorbed the greatest amount of  $\text{SO}_2$  (Table 1). The  $\text{NO}_x$  removal efficiency of a similarly treated Calgon F400 carbon (Calgon,  $\text{HNO}_3$ , 925 °C) decreased from 100% to 70% after 1 h. The  $\text{HNO}_3$ -treated Calgon carbon that was not heat treated at 925 °C (Calgon,  $\text{HNO}_3$ ) removed only 10% of the  $\text{NO}_x$  after 60 min, illustrating the importance of the thermal desorption step in our char preparation method. Thermal desorption of C–O complexes opens closed porosity and widens pores but, more importantly, creates nascent sites on the carbon surface that react with  $\text{NO}_x$ .

Figure 3 presents NO and  $\text{NO}_2$  breakthrough curves obtained at 25 °C for the IBC-102,  $\text{HNO}_3$ -925 °C char and the Centaur carbon. The  $\text{HNO}_3$ -925 °C char achieves nearly 100%  $\text{NO}_x$  removal for the first 8 h compared to only 4 h for the Centaur carbon. For the  $\text{HNO}_3$ -925 °C char, the concentration of NO in the

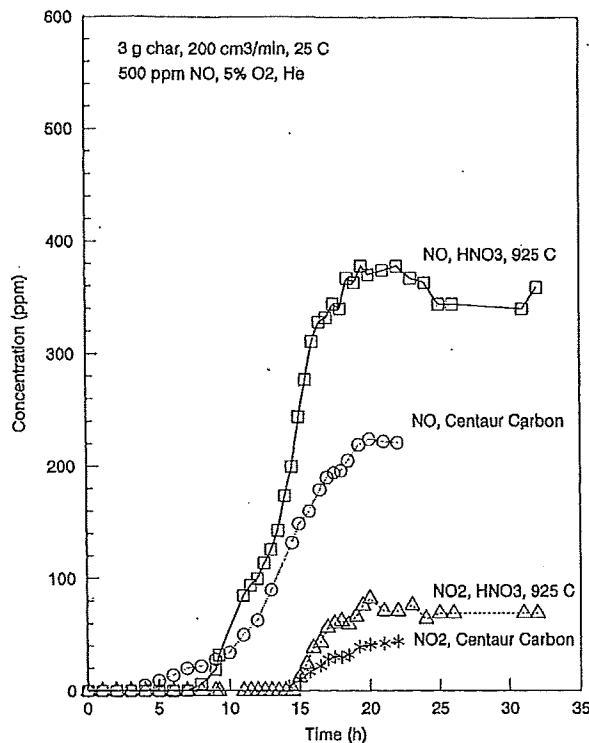


Figure 3. Comparison of high-activity char and Centaur carbon.

effluent increases from about 3% to 80% between 8 and 15 h, while the Centaur carbon continues to remove 50% of the NO after 20 h. It is interesting to note that  $\text{NO}_2$  is generated by both carbons and that its onset occurs at 15 h (50% of maximum breakthrough). The formation of  $\text{NO}_2$  during the low-temperature reaction of activated carbon fibers with NO was recently observed.<sup>34,35</sup> It seems that once the carbon surface becomes saturated with C–O, C–N, and C–NO functional groups,  $\text{NO}_2$  formation is initiated. Eventually, a char would require regeneration as these functional groups accumulate on the carbon surface and block the sites responsible for NO adsorption/reduction. Further work is needed to determine the mechanism by which this high-activity carbon removes  $\text{NO}_x$  from flue gas.

Selected IBC-102 chars were also tested in 500 ppm of NO, 5%  $\text{O}_2$ , balance He using the AC/MS system described under Experimental Section. Figure 4 shows the effect of flue gas temperature on the  $\text{NO}_x$  removal capacity of the nitric acid/thermally desorbed char (4 g of char, space velocity of 2000  $\text{h}^{-1}$ ). The  $\text{NO}_x$  removal capacity increases monotonically with decreasing temperature. At 150 °C, the char removes 19.2 mg of NO/g of char and at 60 °C the char removes 25.8 mg of NO/g of char. It is interesting to note that complete breakthrough was never achieved in these four runs. It appears that two  $\text{NO}_x$  removal mechanisms were in effect: the adsorption mechanism, where NO is simply adsorbed on the char surface; and the catalytic mechanism, where the char converts NO to  $\text{N}_2$ . The char adsorbs/reduces  $\text{NO}_x$  until its adsorption/catalytic sites

(34) Mochida, I.; Kismori, S.; Hironaka, M.; Kawano, S.; Matsumura, Y.; Yoshikawa, M. *Energy Fuels* 1994, 8, 1341.

(35) Jang, B. W.-L.; Spivey, J. J.; Kung, M. C.; Kung, H. H. *Prepr. Pap.-Am. Chem. Soc., Div. Fuel Chem.* 1996, 41 (1), 308.

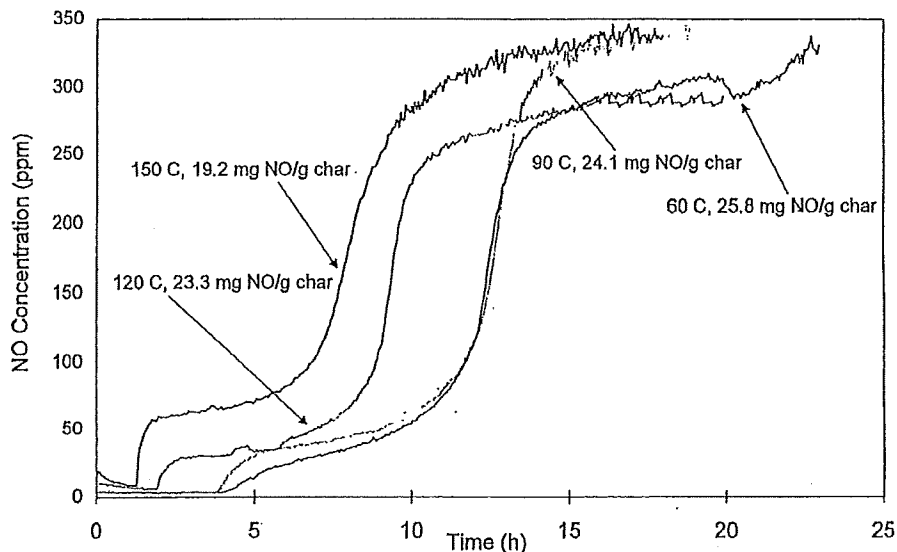


Figure 4. Effect of temperature on  $\text{NO}_x$  removal by IBC-102,  $\text{HNO}_3$ -925 °C char.

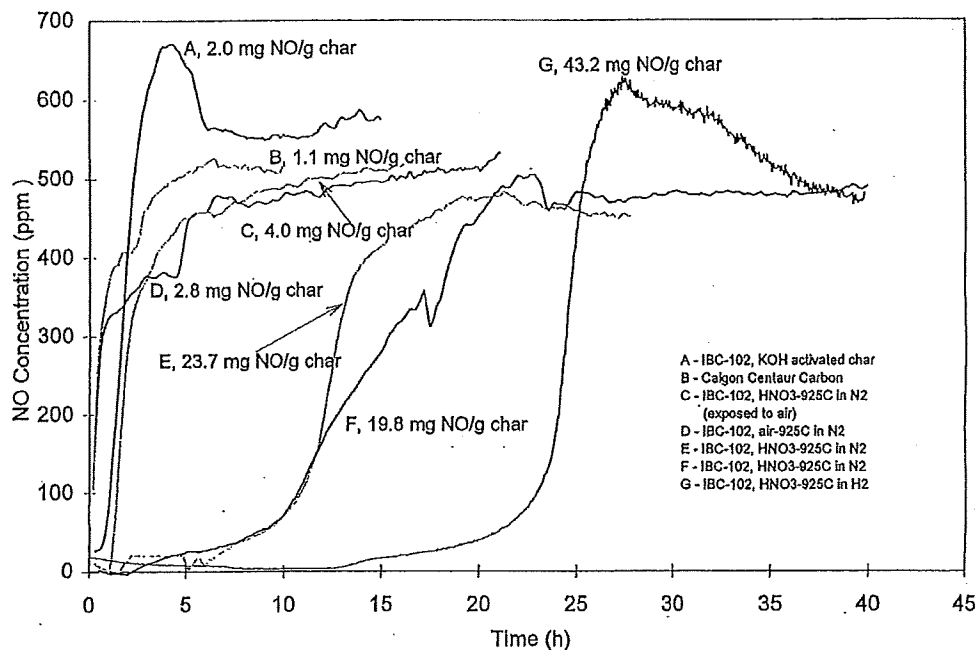


Figure 5.  $\text{NO}$  breakthrough curves for selected IBC-102 chars and a commercial activated carbon.

are saturated with C–O and C–N complexes. The catalytic component of the mechanism may be why complete breakthrough (500 ppm of  $\text{NO}$  in the exit gas) was not easily achieved in these experiments.

Figure 5 shows that Centaur carbon (B) had rather poor  $\text{NO}_x$  removal capacity at 120 °C, whereas the nitric acid treated, thermally desorbed chars (C–G) performed significantly better. It is interesting to note that the  $\text{NO}$  concentration in the effluent gas exceeds the  $\text{NO}$  input concentration in some cases (e.g., samples A and G). An air-oxidized/thermally desorbed char (D) was slightly better than the KOH-activated char (A), although potassium is known to be a good catalyst for  $\text{NO}_x$  reduction at higher temperatures (300–600 °C).<sup>36–38</sup> Exposure of the char sample to ambient air prior to a  $\text{NO}_x$  removal run had a detrimental effect on perfor-

mance (compare breakthrough curves of samples C and E). Sample C was exposed to air for at least 48 h before the run. Chemisorbed oxygen may poison the active sites for  $\text{NO}$  adsorption/reduction, although it was necessary to have oxygen in the simulated flue gas to achieve some  $\text{NO}_x$  removal.

Table 1 showed that a lack of oxygen, rather than a char surface loaded with oxygen, enhances  $\text{SO}_2$  removal. It seems that carbon atoms that are not occupied by an adsorbed oxygen atom have valence electrons that are available and more reactive toward  $\text{SO}_2$  adsorption.

(36) Illan-Gomez, M. J.; Linares-Solano, A.; Radovic, L. R.; Salinas-Martinez de Lecea, C. *Energy Fuels* 1995, 9, 97.

(37) Illan-Gomez, M. J.; Linares-Solano, A.; Radovic, L. R.; Salinas-Martinez de Lecea, C. *Energy Fuels* 1995, 9, 104.

(38) Garcia-Garcia, A.; Linares-Solano, A.; Salinas-Martinez de Lecea, C. *Prepr. Pap.-Am. Chem. Soc., Div. Fuel Chem.* 1996, 41 (1), 293.

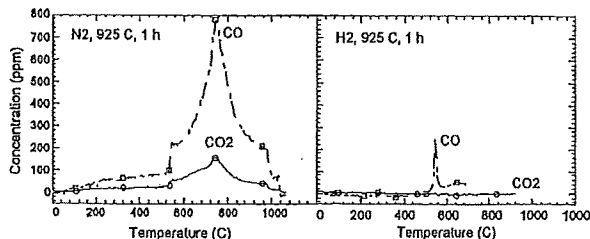


Figure 6. Effect of hydrogen treatment on TPD profiles of IBC-102,  $\text{HNO}_3$ -925 °C char exposed to air at 25 °C for 2 weeks.

Thus, the number of unoccupied or free sites should control the uptake of  $\text{SO}_2$ . This same concept of free sites may apply to  $\text{NO}_x$  removal by carbon. To regenerate the active sites (and also to preserve them), sample E was heated to 925 °C in flowing hydrogen (0.2 L/min) and held for 1 h at 925 °C. The reaction of hydrogen with carbon at this temperature serves to gasify the most reactive carbons, leaving behind a more stable surface but one that still contains an appreciable number of free sites. Some C-H complex may also form, and it remains to be determined what effect this would have on  $\text{NO}_x$  removal performance. The stable surface created by  $\text{H}_2$  treatment at 925 °C should adsorb less oxygen and water at room temperature, which should lead to more available sites to react with  $\text{NO}_x$  at higher temperatures. Figure 5 shows that the  $\text{NO}_x$  removal capacity of sample G increased by more than a factor of 2 with the hydrogen treatment as its breakthrough curve was shifted to the right by more than 10 h. Further work is needed to optimize the hydrogen treatment conditions used in this study, e.g., reduce the time and temperature of the treatment.

Figure 6 presents TPD profiles for the nitric acid treated IBC-102 chars thermally desorbed in nitrogen and hydrogen at 925 °C and then exposed to room temperature air for 2 weeks. There is a marked difference in the TPD profiles of these two chars. The char desorbed in nitrogen contains about 4.8 wt % oxygen, whereas the char desorbed in hydrogen contains only 0.2 wt % oxygen. Thus, a high-temperature  $\text{H}_2$  treatment appears to reduce significantly the amount of oxygen chemisorbed on the char surface, which in accordance with Figure 5, increases the  $\text{NO}_x$  removal capacity of the char by almost a factor of 2. Recently, Verma and Walker<sup>39</sup> treated a carbon molecular sieve with hydrogen at 150 °C to decrease its affinity for oxygen and water (aging), which in turn enhanced its air separation capabilities.

**Selective Catalytic Reduction.** The  $\text{NO}_x$  removal capabilities of selected IBC-102 chars in the presence of ammonia were also tested. The following reaction conditions were used by RTI: 40  $\text{cm}^3$  of carbon, 130–160 °C, 500 ppm of  $\text{NO}$ , 690 ppm of  $\text{NH}_3$ , 5%  $\text{O}_2$ , 10%  $\text{H}_2\text{O}$ , and 1400  $\text{h}^{-1}$  space velocity. Table 4 shows that the  $\text{NO}_x$  removal activity of the  $\text{HNO}_3$ -925 °C char, although highest among the ISGS chars tested, was still significantly lower than that of the carbon catalyst developed and tested by RTI (commercial activated carbon impregnated with a metal catalyst). The RTI carbon, although it achieving >99% conversion of  $\text{NO}$  to  $\text{N}_2$ , remains quite costly to produce. Table 4 also

Table 4.  $\text{NO}_x$  Reduction with Ammonia

sample	130 °C	140 °C	150 °C	160 °C
$\text{HNO}_3$ -925 °C	20	29	33	30
air-925 °C	14	8	3	0
$\text{H}_2\text{O}$ activated	16	14	14	14
$\text{HNO}_3$ -725 °C	3	6		22
KOH activated	22	8	7	
Centaur carbon	0			4
RTI carbon	99	99	99	99

Table 5. Comparison of Herdofenkoks and ISGS Char

property	Herdofenkoks	ISGS char
$\text{N}_2$ BET surface area ( $\text{m}^2/\text{g}$ )	275	110
iodine no.	349	137
$\text{SO}_2$ capacity (wt %, 120 °C, 4 h)	2.8	4.2
$\text{SO}_2$ capacity (wt %, 120 °C, 15 h)	7.6	5.8
bulk density ( $\text{lb}/\text{ft}^3$ )	29.8	23.8
carbon (wt %)	83.1	87.0
volatile matter (wt %)	7.7	4.7
ash (wt %)	8.7	8.3
mechanical strength	98.8	78.3
ignition point (°C)	405	395
$\text{CCl}_4$ activity (mg/100 mg of char)	17	51

shows that the five ISGS samples responded differently to variations in reaction temperature. The  $\text{NO}$  removal activity of the  $\text{HNO}_3$ -925 °C char went through a maximum at 150 °C.  $\text{NO}_x$  conversion with the air-925 °C char decreased with increasing temperature, while the steam-activated char maintained essentially the same level of activity between 130 and 160 °C. The  $\text{NO}_x$  reduction activity of the  $\text{HNO}_3$ -725 °C char increased from 3% to 22% between 130 and 160 °C, whereas that of the KOH-activated char decreased from 22% to 7%. The Centaur carbon performed rather poorly at the two temperatures studied. Note that the ISGS chars tested were not representative of chars optimized for this application. Activated carbons typically used in this application have relatively high surface areas (1000–1500  $\text{m}^2/\text{g}$ ). Singoredjo et al.<sup>29</sup> recently showed that  $\text{NO}_x$  removal with carbon in the presence of ammonia was influenced by a number of factors including the number and type of C-O complexes on the carbon surface, nitrogen content of the char, and accessibility of the pores. The oxygen contents of most of our chars were minimized due to the steam activation or thermal desorption treatments used in their preparation.

**Incinerator Flue Gas.** Incinerator flue gas typically contains much lower concentrations of  $\text{SO}_2$  and  $\text{NO}_x$  (20–100 ppm) compared to those found in coal combustion flue gas (500–3000 ppm) but also contains much higher levels of other pollutants such as mercury, dioxins, furans, heavy metals, and hydrochloric acid. Table 5 compares the properties of the ISGS low-activity char and the char presently used by STEAG (hereafter referred to as Herdofenkoks). It shows that ISGS char had a  $\text{N}_2$  BET surface area of only 110  $\text{m}^2/\text{g}$ , but an  $\text{SO}_2$  capacity after 4 h greater than that of the Herdofenkoks. The iodine number of the Herdofenkoks was about 3 times greater than that of ISGS char. (This number relates to the surface area contained in pores greater than 10 Å.) The mechanical strength of ISGS char, although not as good as Herdofenkoks, was still considered satisfactory for this application. Note that the carbon tetrachloride activity of ISGS char is 51 mg/100 g of char, about 3 times that of the Herdofenkoks (brown coal pyrolyzed at 950 °C for 0.75 h). The carbon tetrachloride activity is used as an indicator of carbon performance in vapor phase applications, e.g., VOC

Table 6. Pilot Plant Tests with ISGS Char

pollutant	inlet	outlet	efficiency (%)
dioxins, furans			
test 1 (ng/m <sup>3</sup> )	333.3	0.062	99.98
test 2 (ng/m <sup>3</sup> )	337.9	0.052	99.98
test 3 (ng/m <sup>3</sup> )	282.3	0.789	99.72
cadmium, titanium			
test 1 (mg/m <sup>3</sup> )	0.0140	0.0012	91
test 2 (mg/m <sup>3</sup> )	0.0062	0.0012	81
test 3 (mg/m <sup>3</sup> )	0.0052	0.0004	92
mercury			
test 1 (mg/m <sup>3</sup> )	0.0177	— <sup>a</sup>	—
test 2 (mg/m <sup>3</sup> )	0.0384	—	—
test 3 (mg/m <sup>3</sup> )	0.0223	—	—
Sb, As, Pb, Cr, Co, Cu, Mn, Ni, V, Sn			
test 1 (mg/m <sup>3</sup> )	0.2698	0.0744	72
test 2 (mg/m <sup>3</sup> )	0.0805	0.0347	57
test 3 (mg/m <sup>3</sup> )	0.0634	0.0185	71

<sup>a</sup> Below detection limits.

removal. Normally, one would not expect a carbon tetrachloride activity to be this high given the N<sub>2</sub> BET surface area of the char (110 m<sup>2</sup>/g). The observed value of 51 is more typical of carbons having surface areas of 800–1000 m<sup>2</sup>/g.

Commercial activated carbons available in the United States are believed to be too reactive for the STEAG /a/c/t process due to their relatively high surface area (>600 m<sup>2</sup>/g) and propensity to adsorb and react with NO<sub>x</sub>. The reaction of carbon with adsorbed NO<sub>x</sub> is exothermic and can ignite the carbon bed under certain conditions, e.g., in the absence of gas flow. The STEAG /a/c/t process requires the use of a low-activity char having a surface area <300 m<sup>2</sup>/g. A 550 pound sample of low surface area activated char produced in this study was shipped to Essen, Germany, where it was installed in a pilot plant unit and subjected to a NO<sub>x</sub> self-heating test. This involved adsorbing NO<sub>x</sub> on the carbon until saturated, shutting off the flow of gas to the adsorber, and measuring the temperature rise of the char bed. The ISGS char passed the test and is the only U.S. material known to have done so. (Figure 2 also shows that the NO<sub>x</sub> removal efficiency of this char was less than that of the Herdofenkoks.)

The test unit containing ISGS char was then installed on a slipstream of flue gas from a commercial waste incinerator in Germany. Flue gas velocity through the 800 mm char bed was 0.15 m/s. The ISGS activated char removed >99.7% of the dioxins and furans from the incinerator flue gas (Table 6). In addition, mercury, which was present in the inlet gas (average inlet concentration for the three tests was 0.0261 mg/m<sup>3</sup>), was not detected in the exit gas. [Although outlet Hg concentrations were not reported by STEAG, the Hg detection limits are presumed to be 0.0001 mg/m<sup>3</sup> (10 ppb) since inlet Hg concentrations were reported to that level of precision.] The removal efficiencies achieved by ISGS char were at least as good as, if not better than, those achieved with Herdofenkoks. The three 2-week tests, however, were not of ample duration to observe complete breakthrough of any of the pollutants listed in Table 6, so there was no information on total adsorption capacity. Typically other pollutants do not breakthrough the bed before SO<sub>2</sub>, so the SO<sub>2</sub> capacity is considered to be a good measure of the total adsorption capacity of the char. An economic analysis of our char production method was performed.<sup>17,18</sup> It indicated

that it would cost \$350 to produce one ton of ISGS char with a 80 000 tons/year plant, assuming a 20% rate of return on initial investment.

Serious consideration for producing this type of carbon in the United States by companies already in the activated carbon business awaits additional market studies. These studies will be influenced strongly by U.S. Environmental Protection Agency (U.S. EPA) regulations. Recent U.S. EPA regulations on municipal waste combustors require the installation of a carbon-based systems of some kind on both new and existing MWCs. The limits imposed in the United States on pollutants from MWCs are not as low as those in several European countries. The low limits there have forced the adoption of fixed bed technologies. U.S. EPA regulations for MWCs are currently based on carbon injection as the maximum achievable control technology. The mandating of lower pollution limits for hospital and hazardous waste incinerators is needed to provide granular carbon technology an opportunity to show its advantages.

**Additional Interest in ISGS Activated Char.** The successful pilot scale production of low-cost activated char by the ISGS has attracted the attention of several other organizations interested in utilizing inexpensive carbon to clean flue gas. One such company is NOXSO Corp., which has developed, under the Clean Coal Technology Program, a high-efficiency, dry, postcombustion flue gas treatment system that uses a regenerable sorbent to simultaneously remove SO<sub>2</sub> and NO<sub>x</sub> from coal combustion flue gas.<sup>40</sup> The process has no impact on boiler performance, is compact and easy to retrofit, generates a saleable byproduct (sulfuric acid, elemental sulfur, or liquid SO<sub>2</sub>), and creates no new waste streams, a distinct advantage over conventional FGD processes. The cost of the sorbent presently used in the NOXSO process, alumina substrate impregnated with 5% sodium, is \$2000/ton as compared to a projected \$350/ton for ISGS activated char. Thus, an opportunity exists to incorporate ISGS activated char into the NOXSO flue gas treatment process.

A joint effort between the ISGS and NOXSO is seeking to integrate additional SO<sub>2</sub>/NO<sub>x</sub> control into the NOXSO process via low-cost activated char, thereby creating a more cost effective and comprehensive pollution control system.<sup>41</sup> The technical and economic feasibility of integrating activated char into the NOXSO flue gas treatment system needs to be determined. The fluidized bed adsorber, a key attribute of the NOXSO process, is a novel and efficient reactor configuration for simultaneous removal of SO<sub>2</sub> and NO<sub>x</sub> as well as other air toxics from coal combustion flue gas. Through the installation of one additional fluidized bed of activated char within the main adsorber vessel, process improvement may be realized in terms of removal of vapor phase mercury and other air toxics as well. The commercial market potential for NOXSO technology is significant. Under Phase II of the Clean Air Act Amendments (CAAA), NOXSO expects U.S. and Cana-

(40) Bolli, R.; Haslbeck, J.; Zhou, Q. NOXSO: A No-Waste Emission Control Technology, Engineering Foundation. In *Proceedings of Economic and Environmental Aspects of Coal Utilization V*, Santa Barbara, CA, Feb 1993.

(41) Lizzio, A. A.; Cal, M. P.; DeBarr, J. A.; Donnals, G. L.; Lytle, J. M.; Haslbeck, J. L.; Chang, A. M.; Banerjee, D. D. Development of Activated Char for Combined SO<sub>2</sub>/NO<sub>x</sub> Removal. Final Technical Report to Illinois Clean Coal Institute, 1996.

Table 7. Comparison of Mitsui Coke and ISGS Char

property	Mitsui coke	ISGS char
N <sub>2</sub> BET surface area (m <sup>2</sup> /g)	200	105
CO <sub>2</sub> BET surface area (m <sup>2</sup> /g)		142
SO <sub>2</sub> capacity (mg of SO <sub>2</sub> /g)	100	27.1
DeNO <sub>x</sub> efficiency (%)	55	18.8
bulk density (g/mL)	0.60	0.39
micro strength (%)	70	48
ignition point (°C)	420	468

dian market requirements for SO<sub>2</sub>/NO<sub>x</sub> control systems to be as high as 10 000 MW annually in the years 1998–2005, roughly equivalent to 30 installations (300 MW average size) per year.

Our goal is to develop an activated char from Illinois coal that can be used in the NOXSO process, either alone or in conjunction with NOXSO sorbent, to more effectively remove SO<sub>2</sub> and NO<sub>x</sub> and other air toxics from coal combustion flue gas. Recent combined SO<sub>2</sub>/NO<sub>x</sub> removal tests performed in this study suggest that the high-activity HNO<sub>3</sub>–925 °C char can remove a significant amount of NO only when SO<sub>2</sub> is absent from the simulated flue gas. Four variables were examined in these tests: char particle size, gas/solid contact time, char regeneration, and water concentration in the flue gas stream. None of these variables affected this conclusion. The surface chemistry of the char, however, was not optimized for combined SO<sub>2</sub>/NO<sub>x</sub> removal. It seems that SO<sub>2</sub> and NO<sub>x</sub> compete for similar adsorption sites and that SO<sub>2</sub> is more strongly adsorbed. The nitric acid treated/thermally desorbed char was able to remove a significant amount of NO from the flue gas when SO<sub>2</sub> was not present. Whether this activated char can be modified in some way to adsorb significant amounts of both SO<sub>2</sub> and NO<sub>x</sub> remains to be determined.

Another company interested in using low-cost activated char for cleanup of coal combustion flue gas is Mitsui Mining. Mitsui Mining has licensed their technology to General Electric, and both are working together to develop new markets in the United States for their combined SO<sub>2</sub>/NO<sub>x</sub> removal process (the process can also be used to clean incinerator flue gas).<sup>4</sup> A carbon having a selling price of less than \$600/ton is needed. Our low-cost char was tested by Mitsui Mining under the following conditions: 140 °C, 1000 ppm of SO<sub>2</sub>, 200 ppm of NO<sub>x</sub>. Table 7 compares the properties of ISGS char and Mitsui Mining activated coke. The N<sub>2</sub> BET surface area and SO<sub>2</sub> adsorption capacity of ISGS char is less than that of Mitsui coke. Also, the NO<sub>x</sub> removal efficiency (selective catalytic reduction) of Mitsui coke is significantly greater than that of ISGS char. The surface of the Mitsui coke is said to contain functional groups (C–O, C–N, and C–OH) that react more effectively with SO<sub>2</sub> and NO<sub>x</sub>. Note that the ISGS char tested by Mitsui Mining was not made for this process. These tests were performed only to evaluate the potential of our low-cost char in other applications. A higher activity char would be needed to remove SO<sub>2</sub> and NO<sub>x</sub> from coal combustion flue gas.

### Conclusions

Chars with varying pore structure and surface chemistry were prepared from IBC-102 coal under a wide

range of pyrolysis and activation conditions and tested for their ability to remove SO<sub>2</sub> and NO<sub>x</sub> from simulated flue gas. A novel char preparation method, involving nitric acid treatment followed by thermal desorption of carbon–oxygen complexes, was developed to produce activated char with an SO<sub>2</sub> adsorption capacity approaching that of a commercial catalytic carbon (Calgon Centaur). An attempt was made to relate the observed SO<sub>2</sub> adsorption behavior to the physical and chemical properties of the char. There was no correlation between SO<sub>2</sub> capacity and N<sub>2</sub> BET surface area. TPD experiments revealed that SO<sub>2</sub> adsorption was inversely proportional to the amount of chemisorbed oxygen.

The NO<sub>x</sub> removal capabilities of selected IBC-102 chars were determined at temperatures between 25 and 120 °C and compared to those of the Centaur carbon. The NO<sub>x</sub> removal capability of the nitric acid treated/thermally desorbed IBC-102 char was about 20 times greater than that of the Centaur carbon. The NO<sub>x</sub> removal performance of this high-activity char, however, was sensitive to air exposure before a run. A method was developed to preserve the sites responsible for adsorption/reduction of NO<sub>x</sub>. By treating the char with hydrogen immediately following its preparation, the active sites were stabilized, making them less likely to react with O<sub>2</sub> or H<sub>2</sub>O during storage. The NO<sub>x</sub> removal performance of the hydrogen-treated char was significantly better than that of the untreated char. Additional work, however, is needed to optimize the hydrogen treatment conditions.

A low-activity, low-cost (\$350/ton) char was also developed for cleanup of incinerator flue gas. Five hundred pounds of the material was produced from Illinois coal using a three-step method, i.e., low-temperature preoxidation (at 250 °C), an intermediate pyrolysis step in nitrogen (at 425 °C), and activation in carbon dioxide (at 900 °C). The low surface area char (110 m<sup>2</sup>/g) was tested on a slipstream of flue gas from a commercial incinerator in Germany. The char removed >97% of the dioxins and furans from the incinerator flue gas. Mercury, also present in the flue gas, could not be detected in the exit gas. These tests showed the ISGS low-activity char to be quite effective for cleaning incinerator flue gas and qualified it for use in the STEAG /a/c/t process.

**Acknowledgment.** This work was supported by the Illinois Clean Coal Institute through the Illinois Coal Development Board and the U.S. Department of Energy. We appreciate the collaboration with Santosh Gangwal and Ben Jang of RTI, Sidney Nelson, Sr., and Sidney Nelson, Jr., of STC, Hermann Brueggendick, Herbert Schumann, and Volker Rummenhohl of STEAG, Ray Kucik of Allis Mineral Systems, Tak Inagaki, Tak Fujimoto, and Toshiyuki Nawa of Mitsui Mining, and John Haslbeck and Alex Chang of NOXSO Corp. We gratefully acknowledge the technical assistance of Gwen Donnals, Mark Cal, Sheila Desai, Athena Theodorakis, Gwen Murphy, and Manuel Canta of the ISGS.

EF960196H

# Control of heavy metals during incineration using activated carbon fibers

Zhen Shu Liu\*

*Department of Industrial Engineering and Management, Fortune Institute of Technology, Kaohsiung County, Taiwan, ROC*

Received 15 June 2006; received in revised form 22 August 2006; accepted 24 August 2006

Available online 30 August 2006

## Abstract

Activated carbon fibers (ACFs) were applied to control heavy metals in incineration flue gas. Three heavy metal species (Cr, Cd and Pb), three ACFs, various adsorption temperatures (150, 250 and 300 °C) and weights of ACFs were experimentally determined. The results indicated that the effects of the type of ACF and the weight of the ACFs on the solid-state Cr removal were insignificant. The extent of solid-state Cd and Pb removal was related to the knitting structure of ACFs and the physical characteristic of the metals. The removal efficiencies of the solid-state and gaseous metals at various reaction temperature followed the order 250 > 150 > 300 °C and 300 > 250 > 150 °C, respectively.

© 2006 Elsevier B.V. All rights reserved.

**Keywords:** Activated carbon fibers (ACFs); Adsorption; Condensation; Heavy metals; Incineration

## 1. Introduction

Incineration is one of the most effective techniques for disposing of municipal solid waste. However, poor design or operation can result in pollutants to be emitted. The pollutants contain heavy metals, organic compounds and acidic gases. When emitted to the atmosphere, they cause environmental hazards and diseases in humans [1].

During incineration, heavy metals cannot be destroyed but can be partially or completely vaporized at high temperature. Metal vapors nucleate to form new particles under supercritical conditions, or condense onto fly ash due to supersaturation as the temperature in the air pollution control devices (APCDs) decreases [2,3]. Earlier works examined the control of heavy metals from flue gas [4–8]. The conventional method of controlling heavy metals emitted from flue gas is to use powdered adsorbents to capture metals. Related results demonstrate that most silica aluminum species (such as kaolinite, bauxite, and aluminum oxide) can be used to adsorb heavy metals and each adsorbent has its own optimal operating conditions. However, fly ash that contains heavy metals cannot be removed using these powdered adsorbents.

In Taiwan, a spray dryer integrated with a fabric filter is conventional used as the air pollution control devices (APCDs) for

incinerators. Our previous study showed that the removal efficiency of fly ash by APCDs exceeded 95%. The results also indicated that APCDs effectively removed the heavy metals and acidic gases. However, the removal efficiency of polycyclic aromatic hydrocarbons (PAHs) using APCDs was only 40% [9]. Moreover, the conventional APCDs suffer from numbers shortcomings, including the need to add large amounts of alkaline chemicals to the spray dryer and the jamming of the spray nozzle by the alkaline chemicals during operation. Therefore, our recent study explores the removal of PAHs using an ACF adsorbent to reduce the disadvantages of conventional APCDs [10]. The results revealed that the removal efficiencies of PAHs exceeded 90%. Previous studies have also shown that ACFs effectively remove SO<sub>2</sub> [11,12]. This work is the first to investigate experimentally the removal of heavy metals by ACFs to evaluate the potential of an ACF adsorbent to replace conventional APCDs in incinerators and estimate the removal efficiencies of heavy metals, PAHs and SO<sub>2</sub> using ACFs as adsorbents during incineration.

Activated carbon fibers (ACFs) provide many advantages, including faster adsorption and desorption kinetics, much higher surface areas, a uniform micropore structure and a lower drop in pressure [13–18]. ACFs are widely utilized to remove low-concentration organic compounds from flue gas [13,17,18]. The use of ACFs to remove toxic heavy metals from wastewater has also been investigated [19,20]. However, the removal of heavy metals from flue gas by ACFs has rarely been studied.

\* Tel.: +886 7 7889888/8709; fax: +886 7 7889777.

E-mail address: zsliau@center.fotech.edu.tw.

Heavy metals produced by incineration can be condensed and adsorbed on fly ash or nucleate to form new particles. ACFs efficiently remove fly ash. Hence, heavy metals can be removed through adsorption and condensation by ACFs and by the interception of fly ash by ACFs. This work investigates the removal efficiencies of both gaseous metals and solid-state metals by ACFs. Gaseous metals and solid-state metals were defined according to the concentrations of the metals condensed or adsorbed on the ACFs and on the fly ash, intercepted by ACFs, respectively. Flue gases that contained organic compounds and heavy metals were generated using a fluidized bed incinerator to burn feedstocks. Three heavy metal species (Cr, Cd and Pb), three activated carbon fibers, three adsorption temperatures (150, 250 and 300 °C) and various weights of activated carbon fibers were used.

## 2. Experimental

### 2.1. Preparation of artificial feedstock

The artificial incinerator feedstock consisted of sawdust, polypropylene (PP) and a heavy metal solution to simulate real flue gas. These feed materials were enclosed in a polyethylene (PE) bag. Three metals (Cd, Cr and Pb) were dissolved in distilled water that contained 0.5 wt.% nitrate. Table 1 presents the feedstock compositions and operating parameters of the adsorption bed.

### 2.2. Adsorbents and apparatus

Three commercial ACFs obtained from Taiwan Carbon Technology Co. Ltd. in Taiwan were used in this experiment. All ACFs samples were used directly in this study with the original properties of the three commercial ACFs. The weight of the ACFs used for each test was 0.51–0.54 g (equal to 1–2 mm bed

Table 1  
Feedstock compositions and experimental operation parameters

Test	ACF type	Adsorption temperature (°C)	ACFs weight (g)	ACFs thickness (mm)
Run 1	ACF-A	150	0.53	1
Run 2	ACF-B	150	0.54	1
Run 3	ACF-C	150	0.54	2
Run 4	ACF-A	250	0.54	1
Run 5	ACF-A	300	0.51	1
Run 6	ACF-A	150	1.12	45
Run 7	ACF-A	150	1.64	45
Run 8	ACF-A	150	2.28	45

Composition of artificial feedstocks (g/bag): sawdust=0.7, polypropylene=0.33, PE bag=0.22, Cd=0.044, Cr=0.123, Pb=0.026.

height). Table 1 lists the operating parameters of the adsorption bed.

Fig. 1 displays the incineration system, which comprised a laboratory-scale fluidized-bed incinerator equipped with the ACFs adsorber. The height and inner diameter of the ACFs adsorber were 150 and 80 mm, respectively. The fluidized-bed material of 200 g silica sand was plunged into the combustion chamber. Three thermocouples were used to determine the temperature profile in the major incinerator, the inlet of the ACFs adsorber and the outlet of the ACFs adsorber. The combustion gases were treated in the ACFs adsorber, and then released into the atmosphere.

### 2.3. Experimental procedure

An excess air factor of 50% was applied to estimate the required amount of air and the 60 L/min of air was then introduced into the incinerator at room temperature (25 °C). The operating temperature of the combustion chamber was controlled at 800 °C. Initially, the combustion chamber was preheated to the desired temperature using electrical heaters. When the temper-

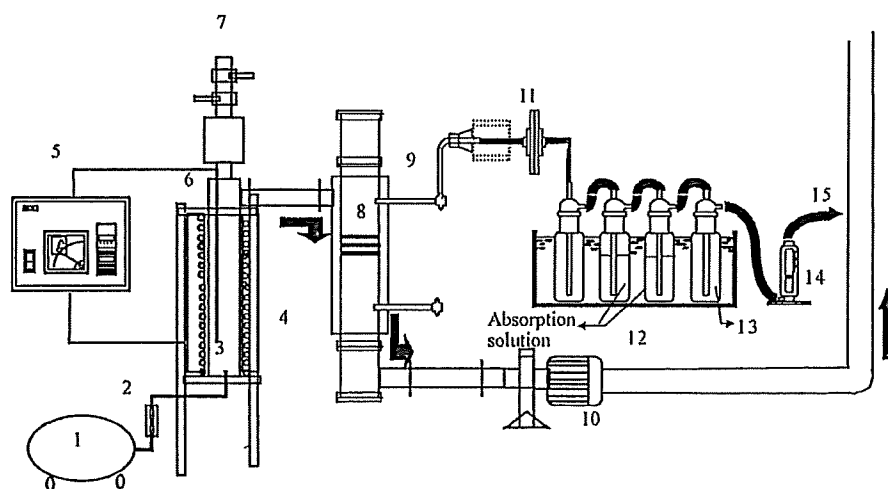


Fig. 1. Experimental system of fluidized-bed incinerator, ACFs adsorber and sampling train for heavy metal: (1) air compressor, (2) flowmeter, (3) combustion chamber, (4) electrical heater, (5) thermal feedback controller, (6) thermocouple, (7) feeder, (8) ACFs adsorber, (9) sampling probe, (10) induced fan, (11) filter holder, (12) impingers (50 mL HNO<sub>3</sub> + 50 mL H<sub>2</sub>O<sub>2</sub>), (13) silica gel, (14) flow meter, and (15) connect of vacuum pump.

Table 2  
Specific surface area and porosity of ACFs by N<sub>2</sub> isotherms

Sample	$S_{\text{BET}}^{\text{a}}$ (m <sup>2</sup> /g)	$V_{\text{T}}^{\text{b}}$ (cm <sup>3</sup> /g)	$V_{\text{micro}}$ (<2 nm) (nm, %)	$V_{\text{meso}}$ (2–50 nm) (nm, %)	Average pore diameter (by BET, nm)
ACF-A	1229	0.601	0.402 (67)	0.199 (33)	1.956
ACF-B	971	0.470	0.344 (73)	0.126 (27)	1.936
ACF-C	412	0.198	0.170 (86)	0.028 (14)	1.918
Run 1	3	0.004	0	0.004 (100)	4.849
Run 2	2	0.005	0	0.005 (100)	8.353

<sup>a</sup> BET surface area.

<sup>b</sup> Total pore volume at  $P/P_0=0.98$ .

ature reached a steady state, the artificial feedstock was fed into the incinerator at the rate of one bag per 15 s. The concentration and temperature of the flue gas were stable as the incinerator temperature reached a steady state. Then, the ACFs adsorber was actuated and the sampling was conducted. The sampling flow rate and time were 10 L/min and 4 min, respectively. The experiment was continuously conducted until the sampling was completed.

#### 2.4. Sampling and analytical methods

The flue gas was sampled prior to and after the ACFs adsorber to estimate the removal efficiency of the solid-state metals. The U.S. Environmental Protection Agency Method (M5) was used to sample the metals (Fig. 1). The flue gas, containing heavy metals and fly ash, was isokinetically sampled using a stainless probe and then passed through a filter holder that was packed with a glassy filter to collect particles. Finally, the flue gas was passed through impingers that contained a mixed solution of 200 mL 5% HNO<sub>3</sub> and 10% H<sub>2</sub>O<sub>2</sub> to absorb the remaining gaseous metals. The glassy filters were pretreated by microwave digestion (CEM MARS-5), and then the concentration of solid-state metals was analyzed by ICP-MS (Inductively Coupled Plasma Mass, PE-SCIEX ELAN 6100 DRC). The standard addition method was adopted, and a recovery efficiency of 100 ± 15% was obtained in each analysis. When the experiments were finished, the ACFs were also pretreated by microwave digestion and the digestion liquid was analyzed by ICP-MS to estimate the concentrations of gaseous metals.

#### 2.5. Characterization of ACFs

N<sub>2</sub> adsorption–desorption isotherms were obtained by using an ASAP 2010 vacuum volumetric sorption instrument at 77 K to determine the Brunauer–Emmett–Teller (BET) surface area and the Barrett–Joyner–Halenda (BJH) pore volume of various ACFs. Before N<sub>2</sub> sorption analysis, the samples were preheated at 493 K for degassing and cooled to room temperature in vacua. The photomicrographs of the ACFs were acquired from a Zeiss Axioplan 2 microscope equipped with an AxioCam HR color CCD (charge couple device) camera. An X-ray powder diffractometer (Siemens D5000) was used to identify the heavy metal species in the fly ash collected on the ACFs. The textural characteristics (pore volume, surface area and pore size) of the ACFs reported in this work were also discussed elsewhere [10].

### 3. Results and discussion

#### 3.1. Characterization of ACFs

Table 2 shows the specific surface area and porous structure of the ACFs. The results indicate that the specific surface areas of ACFs follow the order ACF-A > ACF-B > ACF-C. The order of the mesopore proportions in the ACFs is ACF-A > ACF-B > ACF-C. The micropore volumes of ACFs follow the order ACF-A > ACF-B > ACF-C. The BET surface areas are proportional to the total pore volumes [10].

#### 3.2. Effects of three ACFs on removal of mixed metals

Fig. 2 illustrates the effects of three ACFs on the removal efficiency of fly ash and solid-state metals (Cr, Cd and Pb). The results indicate that the removal efficiency of fly ash exceeded 90% and the best adsorbent of fly ash removal was ACF-C. Fig. 3 presents the knitted structure of the ACFs. The knitted structure of a piece of ACF-C was tighter than those of ACF-A and ACF-B. Moreover, the fly ash was removed immediately by the ACF-C at the beginning of the experiment. However, the fly ash wriggled through a gap in the ACF-A and ACF-B at the beginning of the experiment. Sampling was conducted immediately after the ACFs were placed in the fixed-bed reactor. Therefore, ACF-C removed more fly ash than did either ACF-A or ACF-B.

Fig. 2 also shows that ACF-C was the best adsorbent of solid-state Cd and Pb at 150 °C. Additionally, the removal of solid-state Cd by ACF-C exceeded that of Pb. The removal of solid-state metals was related to the physical properties of the

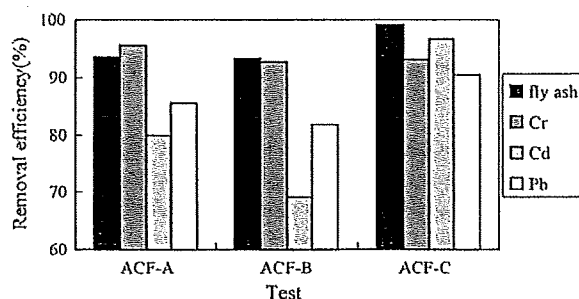


Fig. 2. The effects of three ACFs on the removal efficiency of fly ash and solid-state metals (Cr, Cd and Pb): Run 1 (ACF-A), Run 2 (ACF-B), and Run 3 (ACF-C).

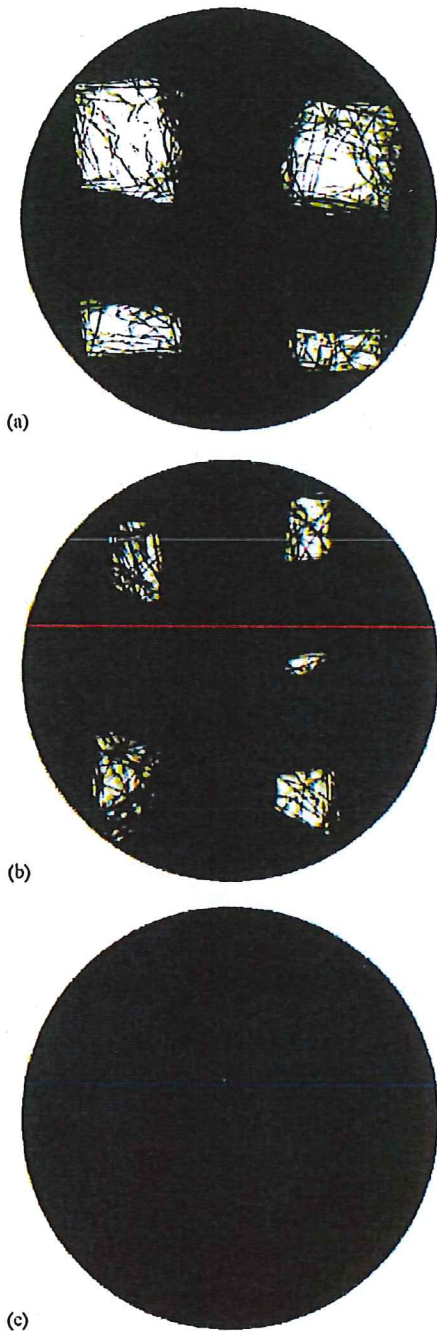


Fig. 3. The knitted structure of a piece of ACF: (a) ACF-A, (b) ACF-B, and (c) ACF-C (25 $\times$ ).

metals and the knitted structure of the ACFs. The high volatility of Cd and Pb resulted in the high concentrations of Cd and Pb distributed in the fly ash and gas phase. Our earlier study indicated that the proportions of metals in fly ash followed the order Cd > Zn > Pb > Cr > Cu [3]. Furthermore, the knitted structure of a piece of ACF-C is tighter than that of ACF-A or ACF-B (as shown in Fig. 3). The removal efficiency of fly ash by ACF-C exceeded that by the other two ACFs. Therefore, the removal efficiency of solid-state Cd and Pb by ACF-C

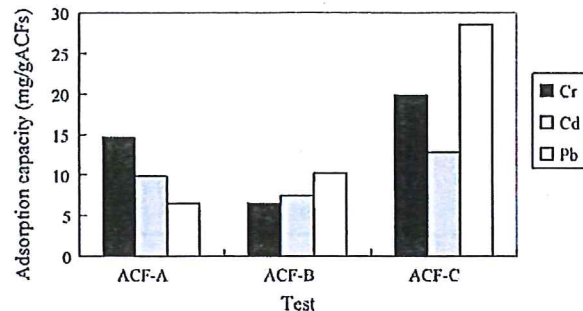


Fig. 4. The effects of three ACFs on the adsorption capacity of gaseous metals (Cr, Cd and Pb): Run 1 (ACF-A), Run 2 (ACF-B), and Run 3 (ACF-C).

exceeded by ACF-A or ACF-B and that of solid-state Cd by ACF-C exceeded that of Pb.

The effect of the type of ACF on the Cr removal was insignificant. Table 3 lists the boiling points and volatilities of various metals. The boiling points of various metal compounds of Cr (such as Cr and Cr<sub>2</sub>O<sub>3</sub>) may exceed the incineration temperature of 800 °C (Table 3) and the concentrations of Cr distributed in the fly ash and the gas phase may have been lower than that in the bottom ash. Therefore, the change in the surface structure of ACFs does not apparently affect the removal of Cr.

Fig. 4 plots the effects of three ACFs on the adsorption capacity of gaseous metals. The results reveal that the best adsorbent of the gaseous metals was ACF-C. The removal mechanisms of the gaseous metals by ACFs include condensation, physical adsorption and chemical adsorption. Since the ACFs controlled the metals at 150 °C by condensation, the metals condensed on the surfaces of the ACFs blocked the pores in the ACFs. Moreover, the removal efficiency of fly ash by ACF-C was the highest. The fly ash provided greater specific surface area and increased the opportunities for the condensation of metals onto the fly ash. Therefore, the removal efficiency of the mixed metals by ACF-C exceeded that by ACF-A or ACF-B.

Table 2 also shows the specific surface area and porous structure of various ACFs after the experiments. Since the BET surface areas and the pore volumes of micropores of ACFs decrease significantly during the experiments, the heavy metals in the flue gas not only adsorb or condense on the surface of ACFs but also enter the pores by diffusion to occupy the adsorption sites. Almost all of the surface areas of the ACFs are utilized.

### 3.3. Effects of adsorption temperature on removal of mixed metals

Fig. 5 shows the effect of adsorption temperature on fly ash and solid-state metals (Cr, Cd and Pb) removal. The effect of temperature on fly ash removal was insignificant, because ACFs removed the fly ash by the filtration mechanism. The removal efficiency of fly ash was related to the knitting structure of various ACFs.

Fig. 5 indicates that the removal efficiencies of solid-state metals at various adsorption temperatures follow the order 250 > 150 > 300 °C. The mixed metals that are adsorbed

Table 3  
Melting, boiling points and vapor pressures of various metal compounds [3,21–23]

	Cd	Pb	Cr
<b>Element</b>			
Melting point (°C)	320.9	327.5	1890
Boiling point (°C)	765	1744	2482
Vapor pressure (mmHg)	1 at 394 °C, 10 at 484 °C, 100 at 611 °C	1 at 973 °C, 10 at 1162 °C	1 at 1616 °C, 10 at 1845 °C
<b>Oxide</b>			
Melting point (°C)	900 (CdO)	888 (PbO)	2435 (Cr <sub>2</sub> O <sub>3</sub> )
Boiling point (°C)	1559	–	4000
Vapor pressure (mmHg)	1 at 1000 °C, 10 at 1149 °C	1 at 943 °C, 10 at 1085 °C	–

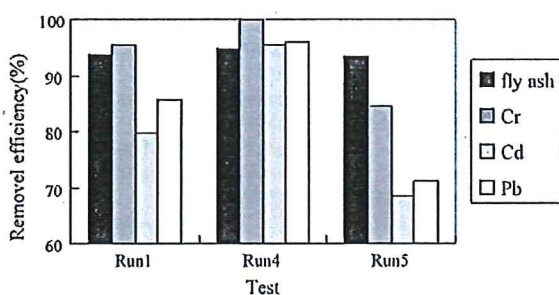


Fig. 5. The influences of adsorption temperature on fly ash and solid-state metals (Cr, Cd and Pb) removal: Run 1 (150 °C), Run 4 (250 °C), and Run 5 (300 °C).

physically or condensed on the fly ash may evaporate and desorb at 300 °C. Furthermore, the metals condensed on the ACFs surface at 150 °C blocked most of the pores on the surfaces of ACFs, reducing the opportunities for metals to enter the pores and reducing the concentration of metals physically adsorbed onto the ACFs. Consequently, the removal of mixed metals was highest at 250 °C.

Fig. 6 displays the effects of the adsorption temperature on the adsorption capacity of gaseous metals. The results indicate that the removal efficiency of the gaseous metals (Cr, Cd and Pb) increased with the adsorption temperature. Chemical adsorption may have occurred between the gaseous metals and the ACFs. The mixed metals adsorbed physically or condensed on the ACFs evaporated and desorbed at 300 °C, increasing the specific

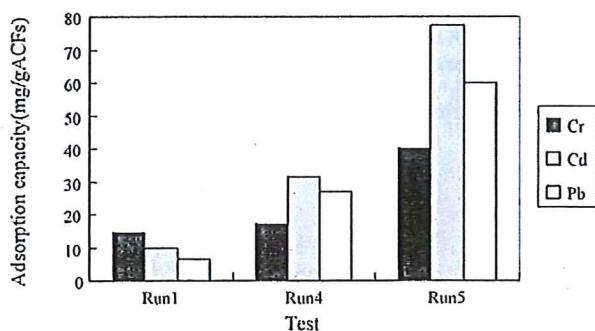


Fig. 6. The influences of adsorption temperature on the adsorption capacity of gaseous metals (Cr, Cd and Pb): Run 1 (150 °C), Run 4 (250 °C), and Run 5 (300 °C).

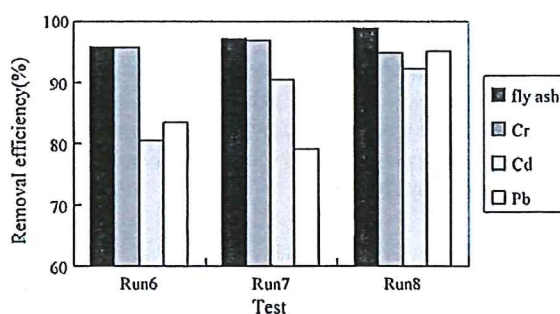


Fig. 7. The effects of the weight of ACFs on the removal efficiency of fly ash and solid-state metals (Cr, Cd and Pb): Run 6 (1.12 g), Run 7 (1.64 g), and Run 8 (2.28 g).

surface area for chemical adsorption. Therefore, the order of the removal efficiencies of gaseous metals at various adsorption temperature was 300 > 250 > 150 °C.

#### 3.4. Effects of the weight of ACFs on removal of mixed metals

Fig. 7 presents the effects of the weight of ACFs on the removal efficiency of fly ash and solid-state metals (Cr, Cd and Pb). The results indicate that the removal efficiency of Cd increased greatly with the weight of ACFs, whereas the removal of fly ash increased negligibly. However, the Pb removal increased greatly until the weight of ACFs was 2.28 g. The order of boiling points of the heavy metals is Cr > Pb > Cd (Table 3) and the proportion of Cd partitioned in fly ash greatly exceeded that of Pb [3]. Moreover, the increase in the weight of ACFs increases the filtration opportunity of the fly ash, especially for micro-particles. Therefore, a significant amount of Cd was removed by removing the fly ash and an increased adsorption capacity was required to control Pb in the flue gas.

The results revealed that the effects of the weight of ACFs on the Cr removal were insignificant. The boiling points of various metal compounds of Cr greatly exceeded 800 °C (the temperature of the incineration). Most metal compounds of Cr are distributed in the bottom ash and the concentration of the gaseous Cr is low [3]. Therefore, the adsorption capacity of a single ACF sufficed to adsorb Cr in flue gas.

Table 4  
Identification of heavy metal species distributed in fly ash collected on ACFs

Sample	Heavy metal species
Run 1	CrO, CdO, PbO, Cr <sub>2</sub> O <sub>3</sub>
Run 2	CrO, CdO, PbO, Cr <sub>2</sub> O <sub>3</sub>
Run 3	CrO, CdO, PbO, Cr <sub>2</sub> O <sub>3</sub>
Run 4	CdO, PbO, Cr <sub>2</sub> O <sub>3</sub>
Run 5	CdO, PbO, Cr <sub>2</sub> O <sub>3</sub>
Run 6	CdO, PbO, Cr <sub>2</sub> O <sub>3</sub>
Run 7	CdO, PbO, Cr <sub>2</sub> O <sub>3</sub>
Run 8	CdO, PbO, Cr <sub>2</sub> O <sub>3</sub>

### 3.5. Identification of heavy metal species in fly ash by X-ray diffraction (XRD)

Table 4 lists the heavy metal species in fly ash collected by the ACFs. It demonstrates that such oxide compounds as CrO, CdO, PbO and Cr<sub>2</sub>O<sub>3</sub> were present in fly ash, indicating that heavy metals really can condense and adsorb onto fly ash and then be removed by ACFs.

## 4. Conclusion

This study investigated the removal of three heavy metals from the incineration flue gas using the ACFs. The results demonstrated that the best adsorbent of gaseous metals at 150 °C was ACF-C. The effects of the type of ACF and the weight of ACFs on Cr removal were insignificant. The removal efficiency of Cd increased with the weight of ACFs and that of Pb increased to an ACF mass of 2.28 g. The results also indicated that the removal efficiencies of the solid-state metals and the gaseous metals at various reaction temperature follow the order 250 > 150 > 300 °C and 300 > 250 > 150 °C respectively. The results demonstrated the feasibility of using a ACFs adsorbent to remove the heavy metals from incineration flue gas.

## Acknowledgement

The author would like to thank associate Prof. J.C. Chen for allowing me to use their facilities to analyze the pollutants.

## References

- [1] M.Y. Wey, W.Y. Ou, Z.S. Liu, H.H. Tseng, W.Y. Yang, B.C. Chiang, Pollutants in incineration flue gas, *J. Hazard. Mater.* B82 (2001) 247–262.
- [2] W.P. Lin, P. Biswas, Metallic particle formation and growth dynamics during incineration, *Combust. Sci. Technol.* 101 (1994) 29–43.
- [3] Z.S. Liu, M.Y. Wey, C.L. Lin, The capture of heavy metals from incineration using a spray dryer integrated with a fabric filter using various additives, *J. Air Waste Manage. Assoc.* 51 (2001) 983–991.
- [4] J.C. Chen, M.Y. Wey, Y.C. Lin, The adsorption of heavy metals by different adsorbents under various incineration conditions, *Chemosphere* 37 (1998) 2617–2625.
- [5] J.C. Chen, M.Y. Wey, J.L. Su, S.M. Heish, Two stage simulation of the major heavy metal species under various incineration conditions, *Environ. Int.* 24 (1998) 451–466.
- [6] J.C. Chen, M.Y. Wey, Z.S. Liu, Adsorption mechanism of heavy metals on adsorbents during incineration, *J. Environ. Eng. ASCE* 127 (2001) 63–69.
- [7] T.C. Ho, T. Tan, J.M. Chen, S. Shukla, J.R. Hopper, Metal capture during fluidized bed incineration of solid wastes, *AIChE Symp. Ser.* 276 (1990) 51–60.
- [8] T.C. Ho, T. Tan, C. Chen, J.R. Hopper, Characteristics of metal capture during fluidized bed incineration, *AIChE Symp. Ser.* 281 (1991) 118–126.
- [9] Z.S. Liu, M.Y. Wey, C.L. Lin, Simultaneous control of acid gases and PAHs using a spray dryer combined with a fabric filter using different additives, *J. Hazard. Mater.* B91 (2002) 129–141.
- [10] Z.S. Liu, Control of PAHs from incineration by activated carbon fibers, *J. Environ. Eng. ASCE* 132 (2006) 463–469.
- [11] M.A. Daley, C.L. Mangun, J.A. Debar, S. Riha, A.A. Lizzio, G.L. Donnals, J. Economy, Adsorption of SO<sub>2</sub> onto oxidized and heat-treated activated carbon fibers (ACFs), *Carbon* 35 (1997) 411–417.
- [12] L. Ling, K. Li, L. Liu, S. Miyamoto, Y. Korai, S. Kawano, I. Mochida, Removal of SO<sub>2</sub> over ethylene tar pitch and cellulose based activated carbon fibers, *Carbon* 37 (1999) 499–504.
- [13] M.P. Cal, S.M. Larson, M.J. Rood, Experimental and modeled results describing adsorption of acetone and benzene onto activated carbon fibers, *Environ. Prog.* 13 (1994) 26–29.
- [14] J. Muñiz, G. Marbán, A.B. Fuertes, Low temperature selective catalytic reduction of NO over modified activated carbon fibers, *Appl. Catal. B: Environ.* 27 (2000) 27–36.
- [15] S.J. Park, K.D. Kim, Influence of activation temperature on adsorption characteristics of activated carbon fiber composites, *Carbon* 39 (2001) 1741–1746.
- [16] Z. Yue, C.L. Mangun, J. Economy, Preparation of fibrous porous materials by chemical activation. I. ZnCl<sub>2</sub> activation of polymer-coated fibers, *Carbon* 40 (2002) 1181–1191.
- [17] A.B. Fuertes, G. Marban, D.M. Nevskaja, Adsorption of volatile organic compounds by means of activated carbon fiber-based monoliths, *Carbon* 41 (2003) 87–96.
- [18] Z.H. Huang, F. Kang, K.M. Liang, J. Hao, Breakthrough of methylethylketone and benzene vapors in activated carbon fiber beds, *J. Hazard. Mater.* B98 (2003) 107–115.
- [19] C. Faur-Brasquet, K. Kadirvelu, P.L. Cloirec, Removal of metal ions from aqueous solution by adsorption onto activated carbon cloths: adsorption competition with organic matter, *Carbon* 40 (2002) 2387–2392.
- [20] J.P. Chen, L. Wang, Characterization of metal adsorption kinetic properties in batch and fixed-bed reactors, *Chemosphere* 54 (2004) 397–404.
- [21] R.C. Weast, S.M. Selby, *Handbook of Chemistry and Physics*, 48th ed., Chemical Rubber Pub, New York, 1968.
- [22] J.C. Bailar, H.J. Emeleus, S.R. Nyholm, A.F. Trotman-Dickenson, *Comprehensive Inorganic Chemistry*, Pergamon Press, New York, 1973.
- [23] R.H. Perry, C.H. Chilton, *Chemical Engineers' Handbook*, 5th ed., McGraw-Hill, New York, 1973.



For more information: Sweden +46 480 41 75 50, Finland +358 9 843 602,  
Germany +49 69 7191070, United Kingdom +44 151 6498344, United States +1 215 546-3900.  
[www.jacobi.net](http://www.jacobi.net)



**Jacobi**  
CARBONS

# Activated Carbon for Flue Gas Purification





Jacobi Carbons manufactures the DioxSorb® range of activated carbons from coal and coconut shell raw materials by steam activation, using the latest production techniques in modern purpose built facilities. DioxSorb® activated carbons are supplied as fine ground powders and impregnated cylindrical extruded pellets, which have been specifically designed to adsorb dioxins, mercury and heavy metals from flue gas. These materials are proven adsorbents which are used extensively in waste-to-energy, hazardous waste and clinical waste incineration plants.

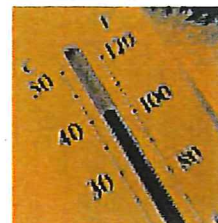
- Coal and coconut shell activated carbons designed to meet individual process requirements.
- Fine ground powders for optimum adsorption kinetics.
- Maximum pore volume and extensively developed transport pore system for rapid diffusion of contaminants into internal surface area.
- Highly developed internal surface area for maximum adsorption capacity.
- Maximum ignition temperature to ensure safe operation.
- Sulphur impregnated cylindrical extruded pellets for use in fixed bed adsorption systems.



**PROPERTIES OF DIOXSORB® ACTIVATED CARBON**

Grade	Type	Form	Surface Area m <sup>2</sup> g <sup>-1</sup>	Pore Volume cm <sup>3</sup> g <sup>-1</sup>	Density kg m <sup>-3</sup>	Mean Particle Diameter, µm	Application
BP5	Coal	Powder	600	1.05	600	21	Standard dioxin and mercury adsorbent
BP4	Coal	Powder	750	1.20	550	21	Standard dioxin and mercury adsorbent
BP2	Coal	Powder	1000	1.55	500	21	Optimum dioxin and mercury loading capacity
CP2	Coconut	Powder	950	0.55	550	21	Standard dioxin adsorbent
CP1	Coconut	Powder	1050	0.68	500	21	Excellent performance against dioxin
BPS	Coal	Powder	950	1.05	520	21	High mercury concentrations
VQ1	Coal	Extruded	1050	0.80	600	Extruded	Packed bed, maximum mercury loading capacity

Hazardous waste that can contain mercury is destroyed using high temperature incineration. The flue gas is treated using DioxSorb® activated carbon.



# Flue Gas from Hazardous Waste Incinerators

As the chemical manufacturing industry strives to meet the increasingly complex demands of the consumer market it is inevitable that hazardous waste materials will result as a by-product of certain process techniques.

High temperature incineration is widely recognised as the most environmentally acceptable method of destroying these materials. The resulting flue gas requires purification before being discharged to atmosphere. In the semi-dry process this involves dosing DioxSorb® activated carbon into the humidified flue gas. This material is subsequently deposited on the fabric filters where the removal of dioxins, mercury and heavy metals take place.

In order to optimise the destruction efficiency of the incinerator, the DioxSorb® may be returned to the start of the process together with incoming hazardous waste.

## STANDARD DESIGN CONDITIONS

PARAMETER	TYPICAL VALUE
Processing capacity	9000 kg h <sup>-1</sup> (total)
Injection method	Semi-dry
Particle collection	Fabric filters
Flue gas volume	65000 Nm <sup>3</sup> h <sup>-1</sup> (total)
Dioxin	
- inlet	2-4 ng TEQ Nm <sup>-3</sup>
- outlet	< 0.1 ng TEQ Nm <sup>-3</sup>
Mercury	
- inlet	50 mg Nm <sup>-3</sup>
- outlet	< 30 µg Nm <sup>-3</sup>
DioxSorb® injection	7 kg h <sup>-1</sup> (105 mg Nm <sup>-3</sup> )
Injection temperature	160°C
Relative humidity	20-25%
Outlet gas	
- rel. conditions	9-10% O <sub>2</sub> , v/v dry
Emission standard	EC 892:1997
Comment	Data based on average results obtained during three year period of operation using DioxSorb® BP2

For easy conversion to imperial units, please visit [www.jacobel.net](http://www.jacobel.net) and use FastConvert™.

Industrialised nations manufacture significant quantities of chemicals and consequently the waste by-products arising from these operations must be disposed of in a safe and environmentally acceptable manner. The licensing and regulation of hazardous waste incinerators is stringently controlled, resulting in a small number of large scale operations. Hazardous waste will often be difficult to burn, requiring a high flue gas volume relative to the quantity of waste being incinerated.

Dioxins in the flue gas are usually due to the presence of liquid halogens in the waste and mercury is common due to thermometers and electrodes, however, the concentrations will be variable. Due to the variability of the waste and the need for a high safety factor, the dosage of DioxSorb® may range from 100 to 200 mg Nm<sup>-3</sup>.

DioxSorb® may be used at temperatures up to 250°C, subject to the operation conditions and equipment design of the flue gas cleaning plant.

## STORAGE AND PACKING

DioxSorb® powdered activated carbon is supplied in 500-800 kg moisture proof, laminated, poly-propylene, liner-free, FIBCs (big bags). Dimensions are 95x95x125 cms (500 kg) and 93x93x180 cms (800 kg).

Section of a clinical waste  
incineration unit manufactured by Evans  
Tabo Universal Ltd. In Leeds (UK).



# Flue Gas from Clinical Waste Incinerators

The operation of a modern day hospital is a highly demanding responsibility, requiring skillful management of the available resources and a detailed understanding of the impact on the local environment. Due to the complexity of advanced medical techniques, the nature of the equipment which is used and the large number of surgical operations which are undertaken, hospitals generate a substantial quantity of chemical and bio-hazardous wastes. In order to safely dispose of these materials, maximise heat recovery and minimise environmental impact, many of the larger hospitals will operate on-site incineration plants. In common with industrial incineration units the flue gas will become contaminated with dioxins, mercury and heavy metals, requiring treatment before being discharged to atmosphere.

## STANDARD DESIGN CONDITIONS

PARAMETER	TYPICAL VALUE
Processing capacity	1000 kg h <sup>-1</sup> (total)
Injection method	Dry
Particle collection	Fabric filters
Flue gas volume	10000 Nm <sup>3</sup> h <sup>-1</sup> (total)
Dioxin	
- inlet	10-20 ng TEQ Nm <sup>-3</sup>
- outlet	< 0.1 ng TEQ Nm <sup>-3</sup>
Mercury	
- inlet	10-20 mg Nm <sup>-3</sup>
- outlet	< 50 µg Nm <sup>-3</sup>
DioxSorb <sup>®</sup> Injection	1.5 kg h <sup>-1</sup> (150 mg Nm <sup>-3</sup> )
Injection temperature	130°C
Relative humidity	8-10%
Outlet gas	
- ref. conditions	11% O <sub>2</sub> w/v dry
Emission standard	Directive 94/67/EC
Comment	Data based on average results obtained during three year period of operation using DioxSorb <sup>®</sup> BP2

For easy conversion to Imperial units, please visit [www.jacobinet.com](http://www.jacobinet.com) and use FastConvert<sup>™</sup>.

Clinical waste incineration units are generally designed for the treatment of waste generated on-site (or for the treatment of waste from the immediate vicinity) and consequently they tend to be relatively small plants. However, due to the nature of the waste they are processing they tend to have specialist characteristics.

Plastics from medical equipment will inevitably form a very high proportion of the waste leading to a relatively high concentration of dioxins, although this is usually of secondary importance.

The principal consideration is generally the incineration of electrical equipment, batteries and thermometers which give rise to extremely high concentrations of mercury in the flue gas. In order to ensure efficient removal of mercury to below consent level (European limit of 50 µg Nm<sup>-3</sup>) DioxSorb<sup>®</sup> activated carbon may be dosed into the flue gas at concentrations of 100-300 mg Nm<sup>-3</sup>. Lime is often used for acid gas removal at flue gas temperatures ranging from 130-180°C, above this temperature bicarbonate compounds may be used which provide increased reactivity.

## STORAGE AND PACKING

Robust multi-ply paper sacks of 20-25 kg net, shrink wrapped on 500 kg pallets, 100x120x110 cms.

In many major cities domestic waste is used as a fuel for the production of electricity and district heating.



# Flue Gas from Waste-to-Energy Plants

Disposal of domestic waste is undertaken using high temperature incineration and the recovered energy is used to preheat boiler feed water and to provide district heating for the local area. During the incineration process the flue gas becomes contaminated with particulate matter, acid gases, dioxins and gaseous heavy metals.

Purification of the flue gas involves cooling to the correct temperature followed by dry adsorption. Hydrated lime is injected for neutralisation of the acid gases and DioxSorb® activated carbon is injected for the adsorption of dioxins, mercury and heavy metals. The particulate matter, hydrated lime and DioxSorb® are removed from the flue gas using fabric filters.

The fabric filters are automatically cleaned and the resulting fly ash is disposed of as a non-hazardous material.

## STANDARD DESIGN CONDITIONS

PARAMETER	TYPICAL VALUE
Processing capacity	11000 kg h <sup>-1</sup> x 2
Injection method	Dry
Particle collection	Fabric filters
Flue gas volume	64800 Nm <sup>3</sup> h <sup>-1</sup> x 2
Dioxin	
- inlet	7 ng TEQ Nm <sup>-3</sup>
- outlet	0.07 ng TEQ Nm <sup>-3</sup>
Mercury	
- inlet	0.15 mg Nm <sup>-3</sup>
- outlet	< 2 µg Nm <sup>-3</sup>
DioxSorb® injection	4 kg h <sup>-1</sup> (30 mg Nm <sup>-3</sup> )
Injection temperature	130°C
Relative humidity	13–15%
Outlet gas - ref. conditions	11% O <sub>2</sub> w/v dry
Emission standard	EPA 1990 (IPR 5/3)
Comment	Data based on results obtained during three year period of operation using DioxSorb® BP2

For easy conversion to imperial units, please visit [www.jacobi.net](http://www.jacobi.net) and use FastConvert™.

Due to the need to dispose of the domestic waste from many major cities and the requirement for efficient energy production, waste-to-energy plants are often very large scale operations. Processing a substantial quantity of waste with a low calorific value, which is primarily organic in nature, results in huge flue gas volumes and relatively low levels of contaminants.

Dioxins are usually the principal contaminants due to the presence of plastics in the waste. Mercury may also be present as a secondary contaminant due to the presence of old batteries in the waste. Consequently the quantity of DioxSorb® activated carbon injected into the flue gas may be very low, values of 30–50 mg Nm<sup>-3</sup> are typical. The temperature at the point of injection has been reduced to 130°C to minimize the volatility of the contaminants, which consequently optimises the adsorption efficiency.

## STORAGE AND PACKING

DioxSorb® activated carbons can be supplied in pneumatic bulk trailers. This mode of delivery ensures dust free handling as the DioxSorb® activated carbon is discharged directly into a storage silo by a pressurised blower.



# Jacobi CARBONS

**Jacobi Carbons AB – Sweden**  
Varvsholmen, SE-392 30 Kalmar  
Tel: +46 480 41 75 50. Fax: +46 480 41 75 59.  
Email: [Info@jacobi.net](mailto:Info@jacobi.net). Web: [www.jacobi.net](http://www.jacobi.net)

**Jacobi Carbons GmbH – Germany**  
Feldbergstraße 21, D-60323 Frankfurt.  
Tel: +49 69 7191070. Fax: +49 69 71910720.  
E-mail: [Infode@jacobi.net](mailto:Infode@jacobi.net). Web: [www.jacobi.net](http://www.jacobi.net)

**Jacobi Carbons (Suomen Siv.) – Finland**  
Ratakatu 1BA3, SF-00120 Helsinki.  
Tel: +358 9 643 602. Fax: +358 9 642 900.  
Email: [Infofin@jacobi.net](mailto:Infofin@jacobi.net). Web: [www.jacobi.net](http://www.jacobi.net)

**Jacobi Carbons, Inc. – United States**  
1518 Walnut Street, Suite 1100, Philadelphia,  
PA 19102. Tel: +1 215 546-3900. Fax: +1 215 546-9921.  
E-mail: [Infous@jacobi.net](mailto:Infous@jacobi.net). Web: [www.jacobi.net](http://www.jacobi.net)

**Jacobi Carbons Ltd – United Kingdom**  
Nord House, Lord Street, Birkenhead,  
Merseyside CH41 1HT.  
Tel: +44 151 649 8344. Fax: +44 151 649 8345.  
E-mail: [Infouk@jacobi.net](mailto:Infouk@jacobi.net). Web: [www.jacobi.net](http://www.jacobi.net)

## Sales and Marketing



**Jacobi Carbons AB – Sweden**  
Headquarters of the Jacobi Carbons Group,  
coordinating worldwide sales and marketing



**Jacobi Carbons (Suomen Siv.) – Finland**  
Sales and marketing of activated carbon in  
Finland and the Baltic States.



**Jacobi Carbons GmbH – Germany**  
Sales and marketing of activated carbon in  
Germany and Continental Europe.



**Jacobi Carbons Ltd – United Kingdom**  
Sales and marketing of activated carbon in  
the United Kingdom and Republic of Ireland



**Jacobi Carbons, Inc. – United States**  
Sales and marketing of activated carbon in  
the United States and Canada.



**Jacobi Carbons Agents – Worldwide**  
A diverse network of agents and distributors  
strategically located around the world.

## Production and Engineering



**Jacobi Carbons Co. Ltd. – China**  
The manufacture of extruded and granular coal  
based activated carbons – ANS/NSF 61 facility



**Jacobi Carbons (Pvt.) Ltd. – India**  
The manufacture of granular coconut shell  
based activated carbon.



**Jacobi Carbons AB – Sweden**  
Powdered activated carbon manufactured from  
coal, coconut shell and wood.



**Jacobi Carbons Ltd – United Kingdom**  
Specialist impregnation facility, technical  
activated carbons, media handling and  
adsorption equipment.



Jacobi Carbons operate  
in full accordance with  
approved ISO-9000 quality  
control procedures

Chapter  
**4**

## Adsorption

### OBJECTIVES

#### Terminal Learning Objective

At the end of this chapter, the student will understand the basics of adsorption systems.

#### Enabling Learning Objectives

- 4.1 Distinguish among the various types of adsorption systems.
- 4.2 Identify the principles of operation that apply to adsorption systems.
- 4.3 Identify the factors that affect the performance of an adsorption system.
- 4.4 Determine the areas that need to be monitored in an adsorption system.

Adsorption processes have been used since the 1950s for the high-efficiency removal of a wide variety of organic vapors and several types of inorganic gases. The use of adsorption processes has been expanding recently due to innovations in the designs of the systems and to the development of new adsorbents.

Adsorption systems designed for odor control and other low contaminant concentration applications (<10 ppm) are relatively simple. In these cases, the adsorbent bed is discarded as it approaches saturation with the contaminant. These systems are termed *nonregenerative* because the adsorbent material is not reused.

Adsorption processes are also used extensively on large-scale applications having solvent vapor concentrations in the range of 10 to 10,000 ppm. Because of the large quantities of adsorbent needed, it is uneconomical to discard the adsorbent. Prior to becoming saturated with the solvents, the adsorbent is isolated from the gas stream and treated to drive the solvent compounds out of the solid adsorbent and into a small-volume, high-concentration gas stream. The desorbed gas stream is then treated to recover and reuse the solvents. The adsorbent is cooled (if necessary) and returned to adsorption service.

Adsorber systems that operate continuously must have (1) multiple fixed beds of adsorbent, (2) fluidized bed contactors with separate adsorption and desorption vessels, or (3) rotary bed adsorbents that cycle continuously between adsorption and desorption operations. Because the adsorbent is treated and placed back in service, these adsorption processes are termed *regenerative*.

Adsorption systems are being used as preconcentrators for thermal or catalytic oxidizer systems. The high-concentration, lower-volume organic vapor stream generated during adsorber bed desorption is well-suited for oxidation because fuel requirements in the oxidizer are minimized. This preconcentrator application has expanded the use of adsorption for low-concentration sources (10 to 1,000 ppm organic vapor) and for multi-component organic vapor streams.

Adsorption processes usually operate at efficiencies of 90% to 98% over long time periods. They can be vulnerable to a variety of operating problems, such as the gradual loss of adsorption capacity, plugging of the adsorbent beds, and

corrosion. The onset of these problems can usually be identified by shifts in the operating conditions and by increases in the stack contaminant concentrations.

## 4.1 Types and Components of Adsorption Systems

### Adsorbents

During adsorption, the gas stream passes through a bed or layer of highly porous material called the *adsorbent*. The compound or compounds to be removed, termed the *adsorbate(s)*, diffuse to the surface of the adsorbent and are retained because of weak attractive forces, while the carrier gas passes through the bed without being adsorbed. Adsorption occurs on the internal surfaces of the materials as shown in Figure 4-1.

The most common types of adsorbents for pollution control applications are activated carbons, zeolites (molecular sieves), and synthetic polymers. Other types of adsorbents, such as silica gel and activated alumina, are used primarily for dehydrating gas streams.

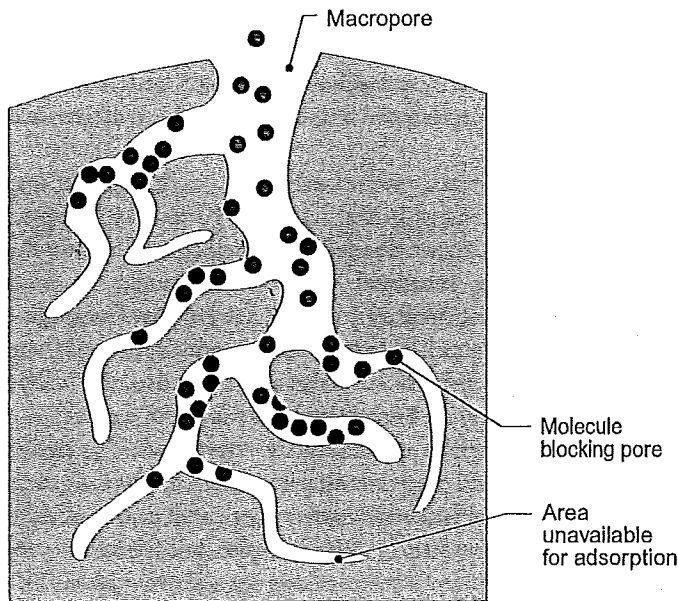


Figure 4-1. Vapor adsorbed into pores of adsorbent.

### Activated Carbon

Activated carbon can be produced from a variety of raw materials such as wood, coal, coconut, nutshells, and petroleum-based products.

The activation process takes place in two steps:

1. First, the feedstock is *pyrolyzed*. This involves heating the material in the absence of air to a temperature high enough (e.g., 1,100°F or 590°C) to drive off all volatile material. Carbon and small quantities of ash are left.
2. To increase the surface area, the carbon is then "activated" by using steam, air, or carbon dioxide at higher temperatures. These gases attack the carbon and increase the pore structure. The temperatures involved, the amount of oxygen present, and the type of feedstock all greatly affect the adsorption qualities of the carbon.

Manufacturers vary these parameters to produce activated carbons suitable for specific purposes. There are a large number of commercial brands available that have significantly different properties to serve various applications. Accordingly, the term *activated carbon* applies to an entire category of diverse materials, not to a specific material.

Because of its nonpolar surface, activated carbon is used to control emissions of a wide variety of organic solvents and toxic gases. Carbons used in gas phase adsorption systems are manufactured in a granular form or in a carbon fiber form. The granular carbon pellets are usually between 4 x 6 and 4 x 20 mesh. Bulk density of the granular-pellet-packed beds can range from 5 to 30 lb<sub>m</sub>/ft<sup>3</sup> (0.08 to 0.48 gm/cm<sup>3</sup>), depending on the internal porosity of the carbon. Total surface area of the macropores and micropores in activated carbon can range from 600 to 1,600 m<sup>2</sup>/gm.

#### *Zeolites (Molecular Sieves)*

Unlike activated carbon adsorbents that are amorphous in nature, molecular sieves have a crystalline structure. The pores are uniform in diameter.<sup>1, 2</sup> Molecular sieves can be used to capture or separate gases on the basis of molecular size and shape. Simplified sketches of several zeolites are shown in Figure 4-2.

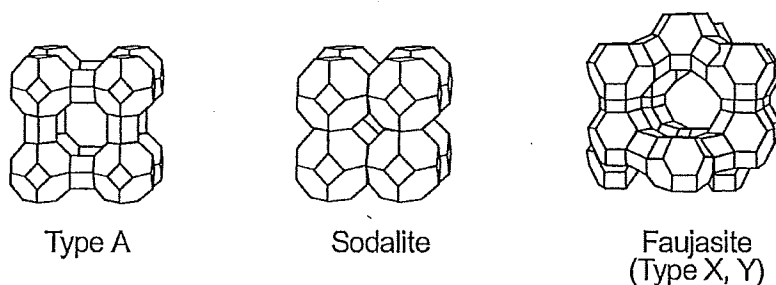


Figure 4-2. Sketches of zeolites.<sup>3</sup>  
(Reprinted by permission of Chemical Engineering Progress,  
American Institute of Chemical Engineers.)

The main uses of molecular sieves have been to remove moisture from exhaust streams, to separate hydrocarbons in refining processes, and to remove nitrogen oxide compounds from air pollution sources. Because of the development of new synthetic zeolites, their applications are expanding into the

volatile organic compound (VOC) control field. The surface areas of molecular sieves range from 590 to 700 m<sup>2</sup>/gm.

*Synthetic Polymers*

Polymeric adsorbents are formed by crosslinking long chain polymers that have a variety of functional groups. The polymeric materials have a rigid microporous structure with surface areas of more than 1,000 m<sup>2</sup>/gm.<sup>4</sup> The ash content is less than 0.01%.<sup>4,5</sup> The chemical structure of one commercial brand of synthetic polymer is shown in Figure 4-3.

These materials have very high adsorption capacities for selected organic compounds, and they can be regenerated more rapidly than activated carbon adsorbents. Regeneration can occur using hot air, hot nitrogen, steam, indirect contact heating, and microwaves. The main applications of this type of adsorbent are the control of organic compounds such as ketones, aldehydes, and reactive compounds that can undergo various chemical reactions on the surfaces of activated carbon.

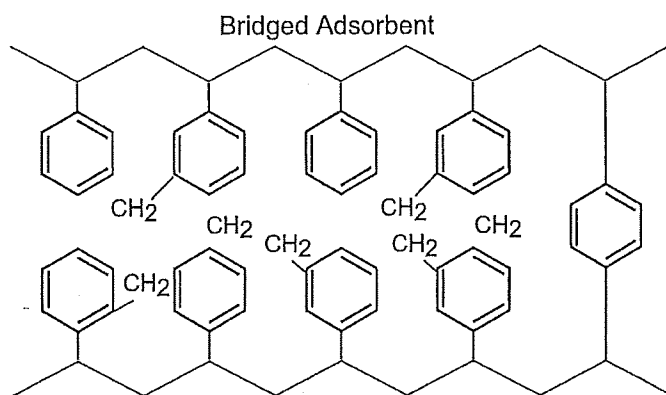


Figure 4-3. Example of a synthetic polymer.  
(Reprinted courtesy of Dow Chemical, Inc.; Midland, Michigan.)

Polymeric adsorbents are also used for gas streams containing high water vapor concentrations (>50% relative humidity) because they are less prone to adsorb water vapor than conventional activated carbon adsorbents. The main limitation to the use of polymeric adsorbents is cost. These materials are more expensive than activated carbon and zeolite adsorbents.<sup>4</sup>

*Silica Gel*

Silica gels are made from sodium silicate. Sodium silicate is mixed with sulfuric acid, resulting in a jelly-like precipitant from which the name "gel" comes. This precipitant is then dried and roasted. Different grades can be produced depending on the processes used in manufacturing the gel. Silica gels have surface areas of approximately 750 m<sup>2</sup>/gm. They are used primarily to remove moisture from exhaust streams. Silica gels are ineffective at temperatures above 500°F (260°C).

*Activated Alumina (Aluminum Oxides)*

Activated alumina is an amorphous form of aluminum oxide manufactured by heating aluminum trihydrate in an inert atmosphere to produce a porous, high-surface-area adsorbent. The primary use of activated alumina is for drying gases and they are not commonly used in air pollution applications. The surface areas of activated alumina adsorbents can range from 2 to 300 m<sup>2</sup>/gm.

**Characteristics of Adsorbents**

The physical properties of the adsorbent affect the adsorption capacity, adsorption rate, and pressure drop across the adsorbent bed. Table 4-1 summarizes these properties for the adsorbents discussed earlier.

Adsorbent <sup>2</sup>	Internal Porosity (%)	Surface Area (m <sup>2</sup> /gm)	Pore Volume (cm <sup>3</sup> /gm)	Bulk Dry Density (gm/cm <sup>3</sup> )	Mean Pore Diameter (Å)
Activated Carbon	55-75	600-1600	0.80-1.20	0.35-0.50	1500-2000
Activated Alumina	30-40	200-300	0.29-0.37	0.90-1.00	1800-2000
Zeolites (Molecular Sieves)	40-55	600-700	0.27-0.38	0.80	300-900
Synthetic Polymers <sup>1</sup>	-	1080-1100	0.94-1.16	0.34-0.40	-

1. Data provided applied to Dow XUS -43493.02 and XUS-43502.01 adsorbents.<sup>4</sup>

2. Data on silica gels not available.

Because adsorption occurs at the gas-solid interface, the surface area available to the vapor molecules determines the effectiveness of the adsorbent. Generally, the larger the surface area, the higher the adsorbent's capacity is. However, the surface area must be available in certain pore sizes if it is to be effective as a vapor adsorber.

Dubinin<sup>6</sup> classified the pores in activated carbon as *micropores*, *macropores*, or *transitional pores*. Micropores have diameters of 10-100 Angstroms (Å; Angstrom = 1.0 x 10<sup>-10</sup> meters) or less. Pores larger than 1,000 Å are considered macropores, and pores with diameters in the range of 100 to 1,000 Å are defined as transitional.

Many gaseous air pollutant molecules are in the 40 to 60 Angstrom size range. Thus, if a large portion of an adsorbent's surface area is associated with pores smaller than 60 Å, many contaminant molecules will be unable to reach these sites.

The large pores serve mainly as passageways to the smaller pores where the adsorption forces are stronger. These forces are strongest in pores that are smaller than approximately twice the size of the contaminant molecule where the molecules experience overlapping attraction of the closely-spaced walls.

*APTI 415: CONTROL OF GASEOUS EMISSIONS*

Capillary condensation occurs when multiple layers of adsorbed contaminant molecules build up from both sides of the pore wall, totally packing the pore and condensing in it. This activity usually occurs only in the micropores. The amounts of contaminant removed increase because additional molecules condense on the surface of the liquid that has formed.

## Adsorption Systems

### *Nonregenerative Adsorption Systems*

Nonregenerative adsorption systems are manufactured in a wide variety of physical configurations. They usually consist of thin adsorbent beds, ranging in thickness from 0.5 to 4 inches (1 to 10 cm). These thin beds have low-pressure drops, normally below 0.25 in W.C. (0.06 kPa) depending on the bed thickness, gas velocity, and particle size of the adsorbent. Bed areas are sized to control the gas velocity through them from 20 to 60 ft/min (6 to 18 m/min). Service time for these adsorption units can range from six months for "heavy" odor concentrations to two years for trace concentrations or intermittent operations.<sup>7</sup> Nonregenerative adsorption systems are used mainly as air purification devices for small air flow streams such as offices and laboratory exhausts.

These thin bed adsorbers are flat, cylindrical, or pleated. The granules of activated carbon are retained by porous support material, usually perforated sheet metal. An adsorber system usually consists of a number of retainers or panels placed in one frame. Figure 4-4 shows a nine-panel, thin-bed adsorber. The panels are similar to home air filters except that they contain activated carbon as the filter instead of fiberglass.

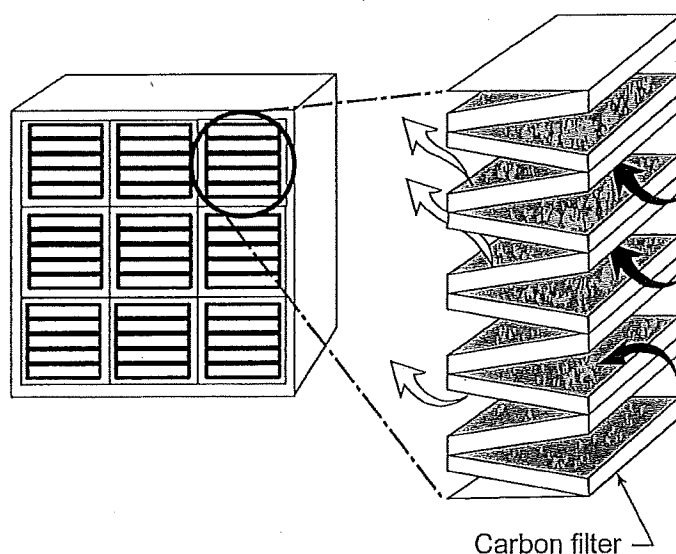


Figure 4-4. Thin-bed adsorber — nine-cell system.

The pleated cell adsorber (Figure 4-5) consists of one continuous retainer of activated carbon, rather than individual panels. Cylindrical canisters (Figure 4-5) are usually small units designed to handle low flow rates of approximately 25 ACFM (0.7 m<sup>3</sup>/min). Cylindrical canisters are made of the same materials as the panel and pleated adsorbers, but their shape is round rather than square. Panel and pleated beds are dimensionally about the same size, normally 2 ft by 2 ft (0.6

m by 0.6 m). Flat panel beds are sized to handle higher exhaust flow rates of approximately 2,000 ACFM ( $57 \text{ m}^3/\text{min}$ ), while pleated beds are limited to flow rates of 1,000 ACFM ( $28 \text{ m}^3/\text{min}$ ).

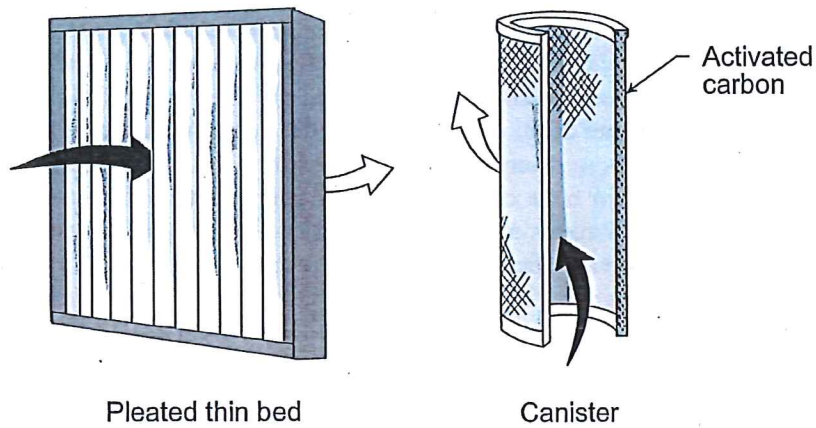


Figure 4-5. Nonregenerative adsorbers.

Thick-bed nonregenerative systems are also available. One system, shown in Figure 4-6, is essentially a 55-gallon drum. The bottom is filled with a material such as gravel to support a bed of activated carbon weighing approximately 150 lb<sub>m</sub> (70 kg). These units are used to treat small flow rates of 100 ACFM ( $2.8 \text{ m}^3/\text{min}$ ) from laboratory hoods, chemical storage tank vents, or chemical reactors.

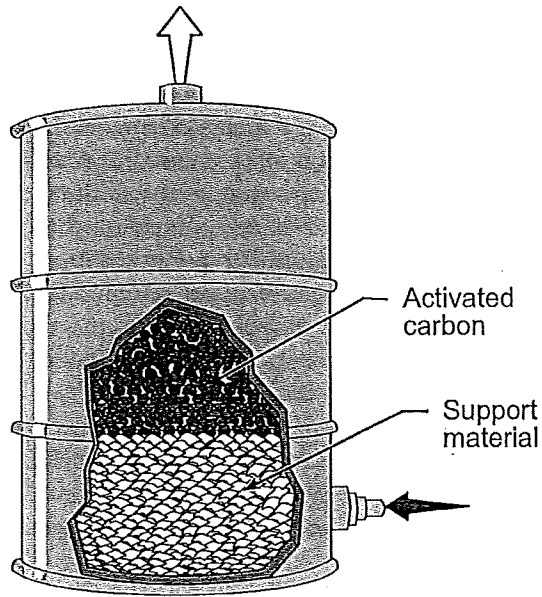


Figure 4-6. Thick bed nonregenerative adsorber.

A flowchart of a simple system containing a small-scale nonregenerative adsorber is shown in Figure 4-7. Solvent-laden air (SLA) is generated in a laboratory hood or small-scale industrial process that is almost entirely enclosed in a hood. A centrifugal fan discharges the SLA at positive pressure first to a particulate filter and then into the activated carbon panels or barrels. The cleaned gas stream is then exhausted directly to the atmosphere.

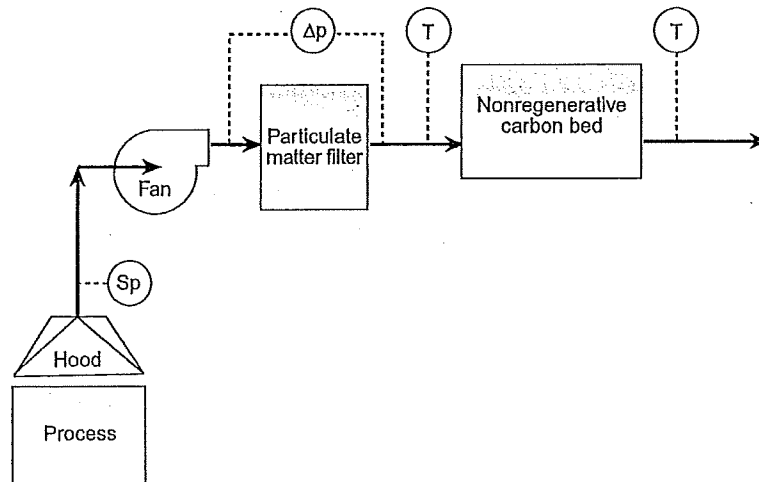


Figure 4-7. Flowchart of a simple nonregenerative adsorber.

The instrumentation on these systems is usually limited. In some cases, gas stream temperature monitors (usually dial-type thermometers) are mounted in the inlet and outlet ducts of the activated carbon panel units or barrels. An increase in the inlet temperature from the design or baseline levels indicates that the service life of the activated carbon may be reduced. An increase in the outlet temperature compared to the inlet temperature may indicate that liquid droplets of solvent are being captured in the bed and increasing the bed temperature. High outlet temperatures must be monitored to prevent fires.

Particulate filters may be used to prevent the accumulation of dusts, fibers, and other debris from plugging the passages through the activated carbon bed. The static pressure drop across these filters provides an indication of filter overloading, which reduces gas flow through the system.

Due to the physical scale of the nonregenerative systems, it is uneconomical to include outlet organic vapor concentration monitors since these instruments can cost several times the total cost of the control system. Accordingly, with these small systems, there is no direct indication that the unit is approaching saturation.

#### *Regenerative Adsorption Systems – Fixed-Bed Designs*

Large regenerative adsorption systems can be categorized as *fixed*, *moving*, or *fluidized* beds. The name refers to the manner in which the gas stream and adsorbent are brought into contact. The choice of a particular system depends on the pollutants to be controlled and the recovery requirements.

Fixed carbon adsorption beds are commonly used to control a variety of organic vapors and are often regenerated by low-pressure steam. They are best used when the liquid organic is immiscible with water when steam is used during the regeneration step. Relatively pure organic liquids may be recovered by condensing the regeneration exhaust and separating the water and the organic based on different densities.

Fixed-bed adsorption systems usually involve multiple beds. One or more beds treat the process exhaust, while the other beds are either being regenerated or cooled. A flowchart of a typical two-bed adsorption system is shown in Figure 4-8.

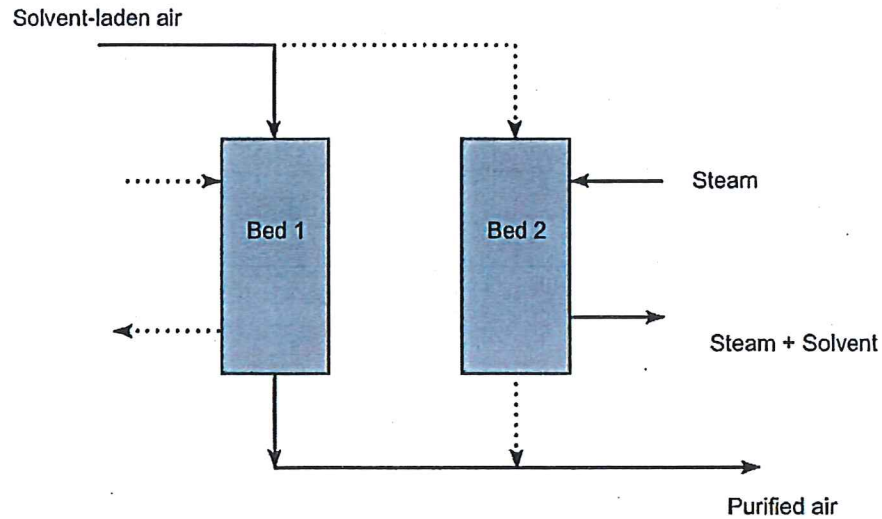


Figure 4-8. Two-bed adsorption system.

As shown, solvent-laden air enters Bed 1, which is in the adsorption mode. Gas flow is usually in the downward direction to avoid possible entrainment of carbon particles that might occur in the upflow mode. Solvent is adsorbed while purified air is discharged to the atmosphere. At the same time Bed 2 is in the regeneration mode. Steam is fed to Bed 2 and steam plus solvent exit the bed and are fed to the solvent recovery system. The functions of the two beds are switched periodically by opening and closing appropriate dampers. The switching may be based either upon a time cycle or when the adsorption bed approaches saturation and the solvent concentration in the purified air increases to some predetermined level. Three or more beds may be required if the duration of the adsorption and regeneration/cooling cycles cannot be matched.

A more complete three-bed system is shown in Figure 4-9. The SLA stream is first pretreated to remove any solid particles that could plug the carbon bed and prevent proper contact between the gas stream and the adsorbent bed. The solvent-laden air stream is often passed through an indirect heat exchanger (cold water tubes) to lower the gas temperature to the range of 60°F to 100°F (15°C to 40°C) where adsorption efficiency and adsorbent service life are both optimum. The pretreated gas stream then enters one of the parallel vessels that house the adsorbent beds. In Figure 4-9 we can imagine that the top bed is in the adsorption mode while the second bed is being regenerated and the third is cooling prior to its next adsorption phase. The steam plus regenerated solvent pass first to a condenser and, if the steam and solvent are immiscible, to a decanter where separation occurs due to density differences in the two phases. If the solvent and steam are miscible, distillation may be required for separation.

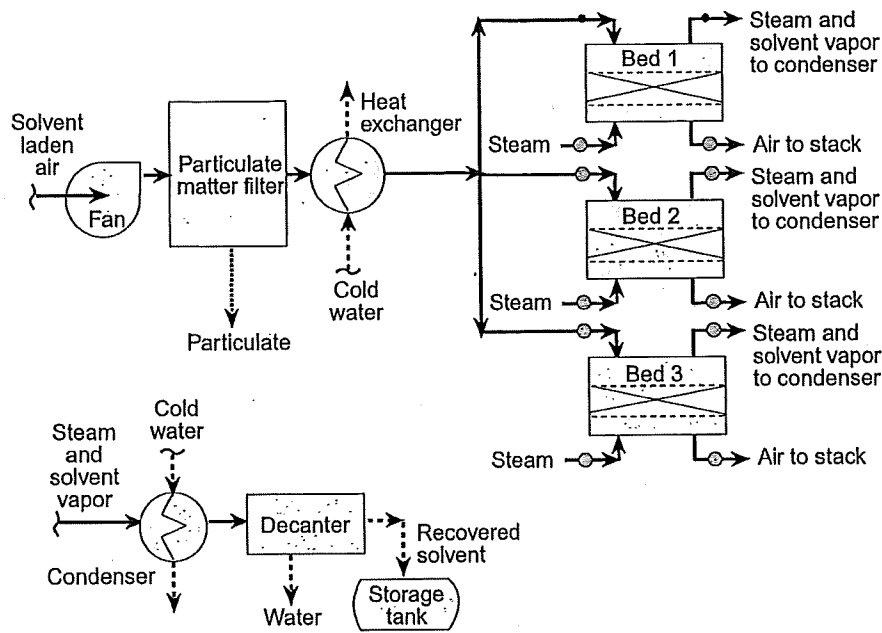


Figure 4-9. Multi-bed, fixed-bed-type adsorption system.

Regenerative fixed carbon beds are usually from 1 to 4 ft (0.3 to 1.2 m) thick. The maximum adsorbent depth of 4 ft (1.2 m) is based on pressure drop considerations.<sup>8</sup> Superficial gas velocities through the adsorber range from 20 to 100 ft/min (6 to 30 m/min). Pressure drops normally range from 3 to 15 in. W.C. (0.75 to 3.75 kPa), depending on the gas velocity, bed depth, and carbon pellet size.<sup>3</sup> A cutaway sketch of a fixed-bed adsorber vessel is shown in Figure 4-10.

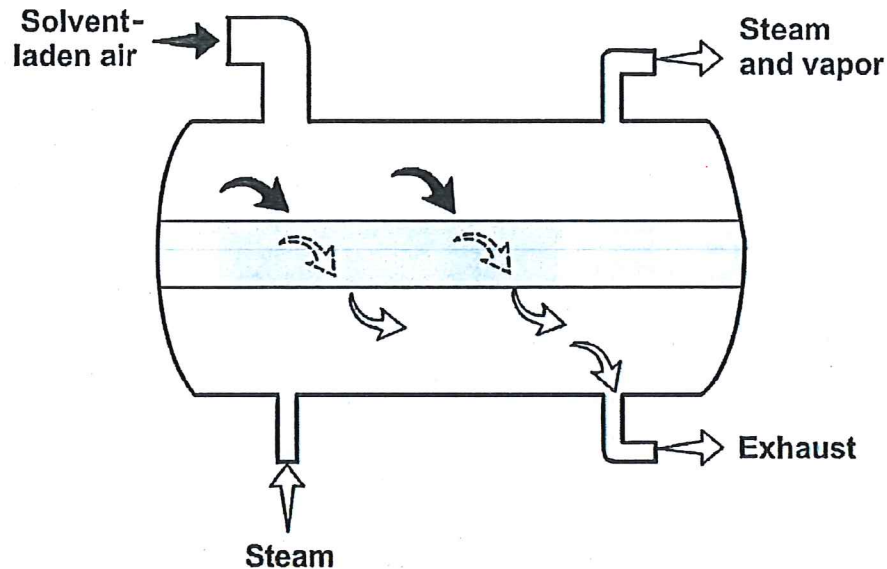


Figure 4-10. Cutaway sketch of horizontal adsorber vessel.

Adsorbers of this type are manufactured as a package system capable of handling flow rates up to 400,000 ACFM (11,500 m<sup>3</sup>/min). Larger units must be engineered and fabricated for the specific application.

Some fixed-bed adsorbers have been designed recently with "multi-pass" capability in order to increase the solvent vapor removal efficiency. The last adsorber vessel that has been regenerated is placed as a second stage<sup>9</sup> by using a series of dampers and connecting ductwork. The air stream passing out of the first adsorber is then directed through this second vessel in order to remove the solvent vapors that penetrated the first unit. This approach is also called *series/parallel*.

Two-chamber, fixed-bed adsorbers have also been developed using carbon fiber adsorbent elements. The activated carbon is prepared as fiber-coated surfaces, a number of which are mounted in a single chamber. The carbon fiber is a thin layer of material with micropores leading directly from the adsorbent surface.<sup>10</sup> With the two-chamber design, one of the chambers is in adsorption mode, while the other is desorbed using hot steam. Because of the thin depth of the material, desorption times are shorter than those for the conventional deep-bed, carbon pellet designs. A diagram of a two-bed, carbon fiber adsorber is shown in Figure 4-11.

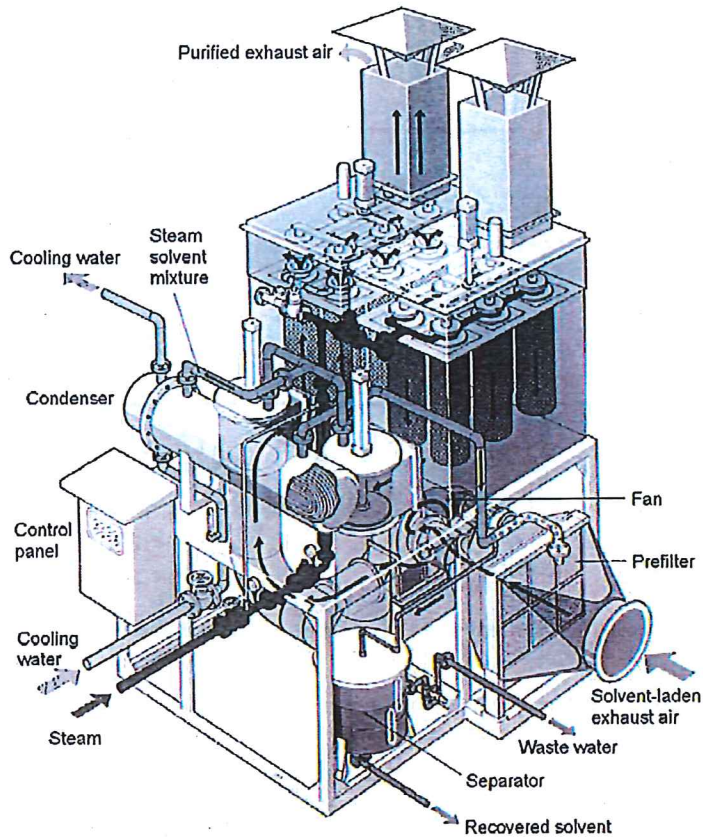


Figure 4-11. Carbon fiber system.  
(Reprinted courtesy of Durr Industries, Inc.; Plymouth, Michigan.)

*Regenerative Adsorption Systems – Moving-Bed Designs*

Moving-bed systems can use a carbon bed more effectively than a fixed-bed system because the solvent-laden air stream passes only through the unsaturated portion of the carbon bed, reducing the distance the air stream travels through the bed; therefore, the static pressure drop is low.

One type of moving-bed adsorber is the rotary wheel zeolite adsorber, such as shown in Figure 4-12. The zeolite adsorbent is mounted in a vertically oriented wheel that rotates at a rate of approximately five revolutions per hour. Three quarters of the wheel are in adsorption service while one quarter is being desorbed using hot air. The desorbed gas stream has a VOC content that is concentrated by approximately a factor of 10 to 15 over the inlet level and a flow rate that is less than 10% of the inlet gas stream. Overall VOC adsorption efficiencies are in the range of 90% to 98%.

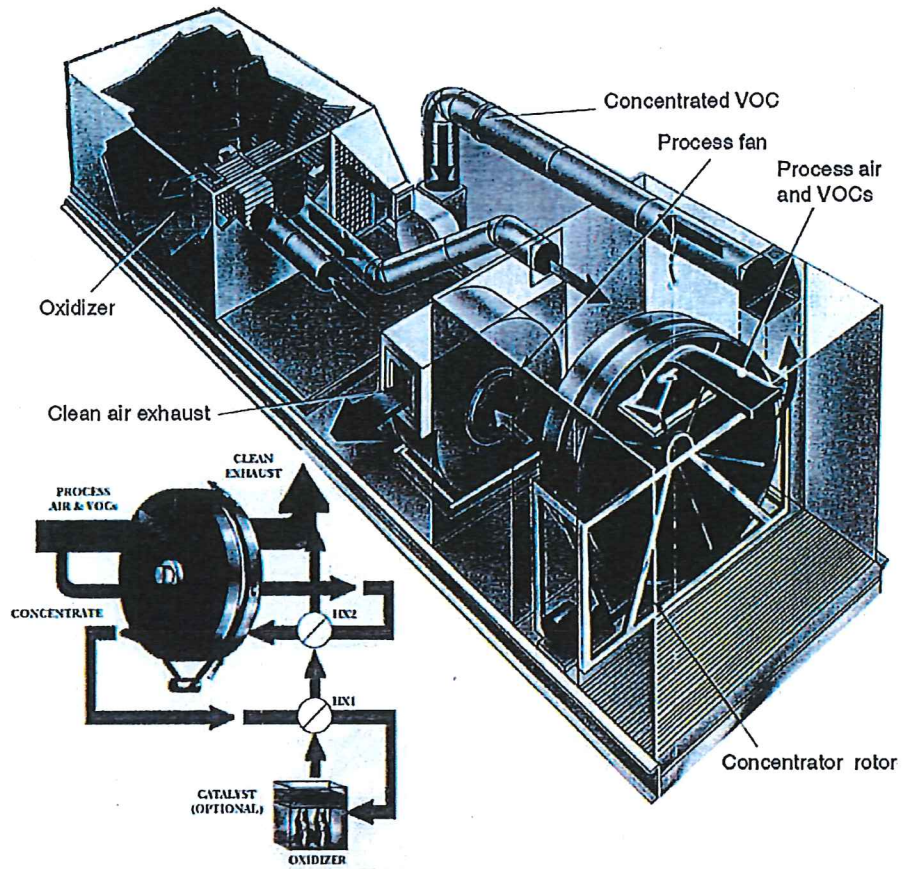


Figure 4-12. Rotary wheel zeolite adsorber.

Another type of moving-bed adsorber is the rotary carbon-fiber adsorber. This adsorber uses activated carbon-fiber paper prepared in a corrugated honeycomb arrangement (Figure 4-13a). The adsorbent is mounted in a rotor that turns continuously at a speed of 1 to 9 revolutions per hour.<sup>12</sup> Desorption is accomplished using hot air that passes through the honeycomb as it rotates into position.

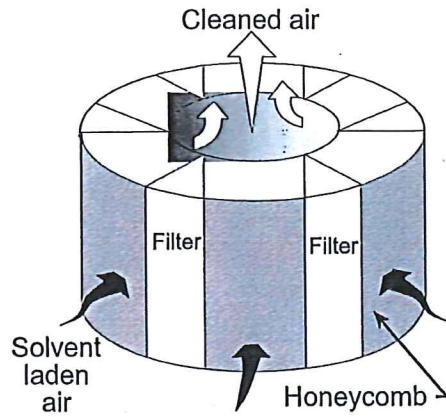


Figure 4-13a. Rotor for carbon-fiber system.

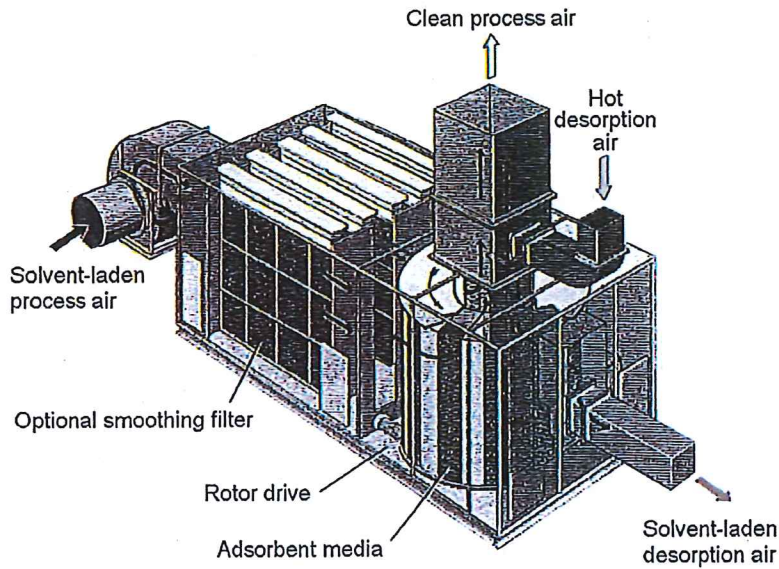


Figure 4-13b. Rotor system.

(Reprinted courtesy of Durr Industries, Inc.; Plymouth, Michigan.)

Adsorption and desorption are performed simultaneously on different sectors of the rotor. The desorbed solvent vapors are at concentrations of 5 to 15 times the inlet levels. Accordingly, the system is attractive for the pretreatment of dilute solvent-laden air streams prior to incineration. The carbon-fiber rotor system is shown in Figure 4-13b.

*Regenerative Adsorption Systems – Fluidized-Bed Adsorbers*

A fluidized bed system, shown in Figure 4-14, uses the motion of the solvent-laden gas stream to entrain adsorbent material and thereby facilitate good gas-solid contact. The VOC-laden gas stream is introduced at the bottom of the adsorber vessel and passes upward through the fluidized adsorbent with the purified gas exiting at the top. The adsorbent plus VOC is pneumatically conveyed to the desorption vessel for regeneration. Regeneration gas plus VOC exit from the top and are ready for further treatment. The regenerated adsorbent is then pneumatically conveyed back to the adsorption vessel. Because the adsorption and desorption processes are physically separate, organic contaminants can be concentrated by a factor of 10 to 50.

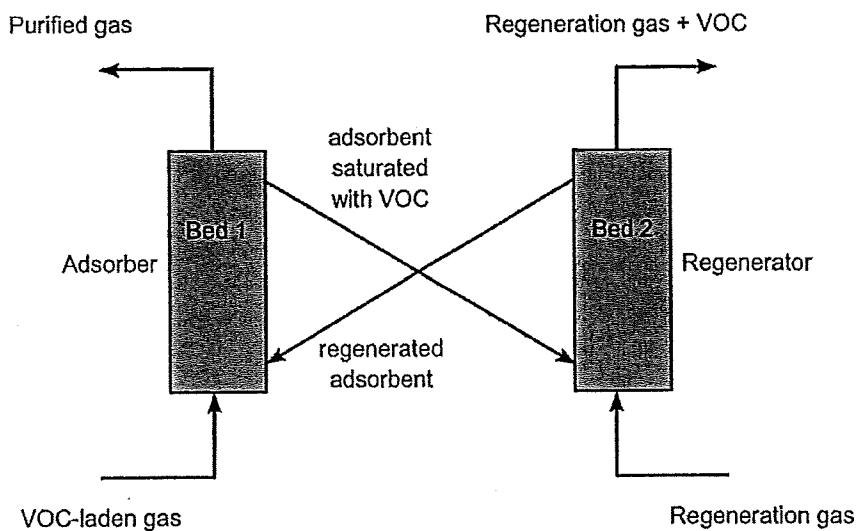


Figure 4-14. Fluidized bed adsorber/regenerator.

A system that consists of multiple fluidized beds is shown in Figure 4-15. VOC-laden gas enters at the bottom of the adsorber and passes upward through a series of beds. The adsorbent flows downward from bed to bed until it reaches the bottom. The saturated adsorbent is then transported pneumatically to the desorption vessel for regeneration. In this system regeneration is accomplished by indirect contact with hot gases from the oxidizer. The regenerated adsorbent is then transported back to the adsorption vessel while the desorbed VOC is destroyed in the oxidizer.

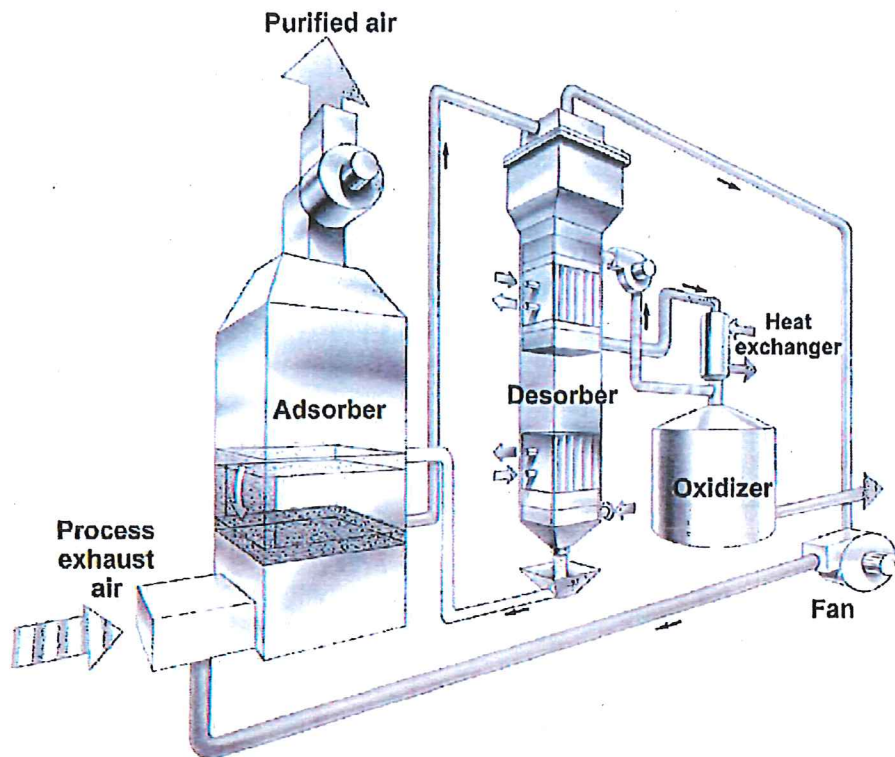


Figure 4-15. Fluidized-bed adsorber.  
(Reprinted courtesy of Weatherly, Inc.; Atlanta, Georgia.)

Both the moving bed and fluidized bed systems provide continuous operation and more efficient utilization of the adsorbent. These systems can be used with either polymeric adsorbents or activated carbon adsorbents. It is necessary to use an adsorbent that can withstand the physical attrition inherent in the system. A "beaded" activated carbon that minimizes attrition loss has been developed. The beaded shape is inherently stronger and has better fluidity properties than granular carbon. This type of carbon has been used in a few installations and is reported to reduce the attrition losses to 2% to 5% per year.

## 4.2 Operating Principles

### Adsorption Steps

Adsorption occurs in a series of three steps. In the first step, the contaminant is transferred from the bulk gas stream to the external surface of the adsorbent material. In the second step, the contaminant molecule diffuses from the relatively small area of the external surface (a few square meters per gram) into the macropores, transitional pores, and micropores within each adsorbent. Most adsorption occurs in the micropores because the majority of available surface area is there (hundreds of square meters per gram). In the third step, the

contaminant molecule adsorbs to the surface in the pore. Figure 4-16 illustrates this overall mass transfer, diffusion, and adsorption process.

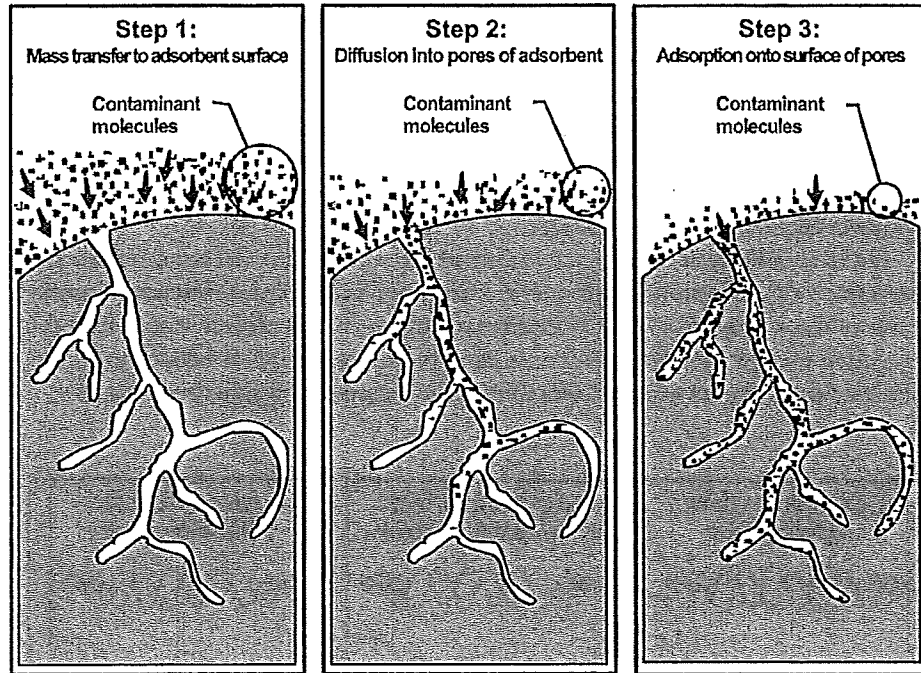


Figure 4-16. Adsorption steps.

Steps 1 and 2 occur because of the concentration difference between the bulk gas stream passing through the adsorbent and the gas near the surface of the adsorbent. Step 3 is the actual physical bonding between the molecule and the adsorbent surface. This step normally occurs more rapidly than steps 1 and 2.

### **Adsorption Forces**

The adsorption process is classified as either *physical* or *chemical*. The basic difference is the strength in which the gas molecule is bonded to the adsorbent. In physical adsorption, the gas molecule is held to the solid surface by weak forces of intermolecular cohesion. The chemical nature of the adsorbed gas remains unchanged; therefore, physical adsorption is a readily reversible process. In chemical adsorption a strong chemical bond is formed between the gas molecule and adsorbent. Chemical adsorption, or chemisorptions, is not easily reversed.

### *Physical Adsorption*

The forces active in physical adsorption are electrostatic in nature and occur under suitable conditions in most gas-solid systems. These forces are present in all states of matter: gas, liquid, and solid. They are the same forces of attraction that cause gases to condense and deviate from ideal behavior under extreme

conditions. Physical adsorption is also referred to as van der Waals' adsorption. Because of van der Waals' forces, physical adsorption can form multiple layers of adsorbate molecules, one on top of another.

The electrostatic effect that produces van der Waals' forces depends on the polarity of both the gas and solid molecules. Molecules in any state are either polar or nonpolar depending on their chemical structure. Polar substances exhibit a separation of positive and negative charges within the compound, which is referred to as a *permanent dipole*. Water is a prime example of a polar substance. Nonpolar substances have both their positive and negative charges in one center so they have no permanent dipole. Most organic compounds are nonpolar because of their symmetry.

Physical adsorption can result from three different effects: orientation, dispersion, or induction (Figure 4-17). For polar molecules, attraction occurs because of the *orientation effect*. The negative charge of one molecule is attracted to the positive charge of the other. An example of this type of adsorption is the removal of water vapor (polar) from an exhaust stream using silica gel (polar).

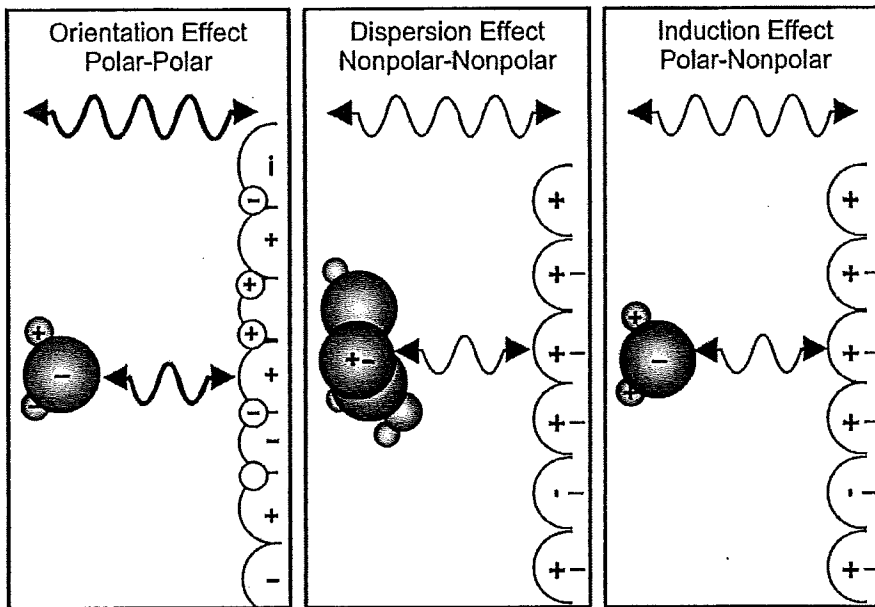


Figure 4-17. Physical forces causing adsorption.

The adsorption of a nonpolar gas molecule onto a nonpolar surface is accounted for by the *dispersion effect*. This effect is based on the fact that although nonpolar substances do not possess a permanent dipole, they do have a fluctuating or oscillating dipole. Fluctuating dipoles are a result of momentary changes in electron distribution around the atomic nuclei. In a nonpolar substance, when two fluctuating dipoles come close to one another, their total energy decreases, and they fluctuate in phase with each other. This is the origin

of the name *dispersion effect*. The adsorption of organic vapors onto activated carbon is an example of nonpolar molecular attraction.

The attraction between a molecule with a permanent dipole (polar molecule) and a nonpolar molecule is caused by the *induction effect*. A molecule with a permanent dipole can induce polarity into a nonpolar molecule when they come in close contact. The energy of this effect is determined by the polarizability of the nonpolar molecules. The induction effect is, however, small when compared to the orientation or dispersion effects. Therefore, adsorption systems use polar adsorbents to remove polar contaminants. This ensures that the inter-molecular forces of attraction between the gas and solid will be greater than those between similar molecules in the gas phase.

*Chemisorption*

Chemical adsorption (chemisorption) results from a chemical interaction between the gas and the solid. The gas is held to the surface of the adsorbate by the formation of a chemical bond. Adsorbents used in chemisorption can be either pure substances or chemicals deposited on an inert carrier material. One example of the former is the use of pure iron oxide chips to adsorb hydrogen sulfide gas. An example of the latter is the use of activated carbon that has been impregnated with potassium iodide to remove mercury vapors.

All adsorption processes are exothermic whether adsorption occurs from chemical or physical forces. The fast-moving gas molecules lose kinetic energy when adsorbed on the solid, which results in the liberation of heat.

In chemisorption, the heat of adsorption is comparable to the heat evolved from an exothermic chemical reaction, usually over 10 Kcal/gm moles. The heat given off by physical adsorption is much lower, approximately 0.1 Kcal/gm mole, which is comparable to the heat of condensation. Molecules that are chemisorbed are very difficult (and, in some cases, impossible) to remove from the adsorbent surface. Either increasing the operating temperature or reducing the pressure of the adsorbent bed can usually remove physically adsorbed molecules. Chemisorption stops when all the active sites on the surface of the adsorbent have reacted, forming only a monolayer of adsorbate molecules on the surface. Multilayers of adsorbed molecules can often be formed in physisorption. While the physical adsorption rate decreases with increasing temperature, the chemisorption rate increases with increasing temperature. Chemisorption is a highly selective process. A gas molecule must be capable of forming a chemical bond with the adsorbent surface for chemisorption to occur. Physisorption, in contrast, is a more general phenomenon. For these reasons physical adsorption is more desirable for air pollution control. A summary of the characteristics of physical versus chemical adsorption is presented in Table 4-2.

Table 4-2. Summary of the characteristics of chemisorption and physical adsorption.	
Chemisorption	Physical Adsorption
Releases high heat, 10 Kcal/gm mole	Releases low heat, 0.1 Kcal/gm mole
Forms a chemical compound	Gas retained by dipolar interaction
Desorption difficult	Desorption easy
Adsorbate recovery impossible	Adsorbate recovery easy

**Adsorption-Capacity Relationships**

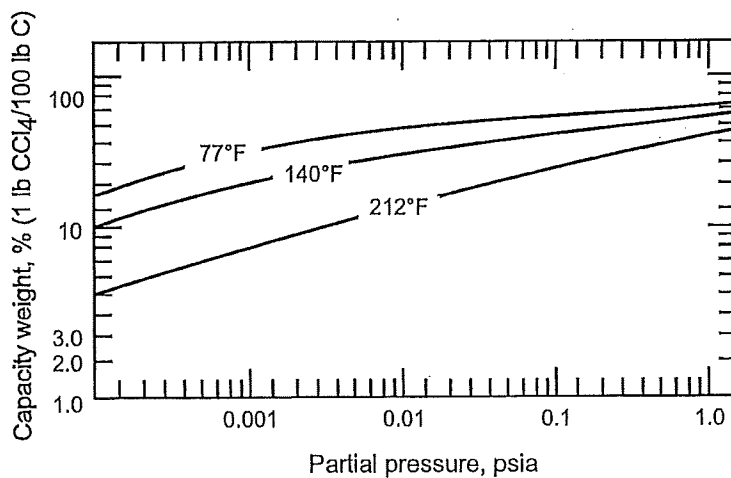
Most available data on adsorption systems are determined at equilibrium conditions. The equilibrium capacity is the maximum amount of vapor that can be adsorbed at a given set of operating conditions. Adsorption equilibrium is the set of conditions at which the number of molecules arriving on the surface of the adsorbent equals the number of molecules leaving. The adsorbent bed becomes “saturated with vapors” and cannot remove any more vapors from the exhaust stream. Although a number of variables affect adsorption capacity, gas temperature and pressure are the two most important.

Adsorption equilibrium data may be presented in three forms: isotherm at constant temperature, isobar at constant pressure, and isostere at constant amount of vapor adsorbed.

*Isotherm*

The most common and useful method of presenting adsorption equilibrium data is the adsorption isotherm, a plot of the adsorbent capacity versus the partial pressure of the adsorbate at a constant temperature. Figure 4-18 is an example of an adsorption isotherm for carbon tetrachloride on one specific activated carbon. Adsorption capacity may be presented in many different of units, with pounds of adsorbate per 100 pounds of adsorbent being typical. Data of this type are used to estimate the size of adsorption systems as demonstrated in Problem 4-1.

Attempts have been made to develop generalized equations to predict adsorption equilibrium from physical data. This is difficult because adsorption isotherms take many shapes depending on the forces involved. Isotherms can be concave upward, concave downward, or “S” shaped. To date, most of the theories agree with data only for specific adsorbate-adsorbent systems and are valid over limited concentration ranges.



Source: Adapted from Technical Bulletin, Calgon Corp.

Figure 4-18. Adsorption isotherm for carbon tetrachloride on one specific commercial activated carbon adsorbent product.

**Problem 4-1**

A dry cleaning process exhausts a 15,000 SCFM air stream containing 680-ppm carbon tetrachloride. Given Figure 4-18, and assuming that the exhaust stream is at approximately 140°F and 14.7 psia, determine the saturation capacity of the activated carbon.

**Solution:**

Step 1. In the gas phase, the mole fraction ( $y$ ) is equal to the ppm divided by  $10^6$ .

$$y = 680 \text{ ppm} = 0.00068$$

The partial pressure is the product of the total pressure and the mole fraction.

$$P^* = yP = (0.00068)(14.7 \text{ psia}) = 0.010 \text{ psia}$$

Step 2. From Figure 4-17, at a partial pressure of 0.01 psia and a temperature of 140°F, the carbon capacity is read as approximately 45 lb  $\text{CCl}_4$ / 100 lb C, or 45%. This is also equal to 45 gm  $\text{CCl}_4$ /100 gm C.

It must be noted that, in practical applications, adsorbents use more carbon than is required at saturation to ensure that uncaptured vapors are not exhausted to the atmosphere. Problem 4-2, presented later in this chapter, illustrates this point.

*Isostere*

The isostere is a plot of the natural log of the pressure versus the reciprocal of absolute temperature ( $\ln[p]$  vs.  $1/T$ ) at a constant amount of vapor adsorbed. Adsorption isostere lines are straight for most adsorbate-adsorbent systems. Figure 4-19 shows an isostere for the adsorption of  $\text{H}_2\text{S}$  gas onto molecular sieves. The isostere is important because the slope of the isostere corresponds to the differential heat of adsorption. The total or integral heat of adsorption is determined by integration over the total quantity of material adsorbed.

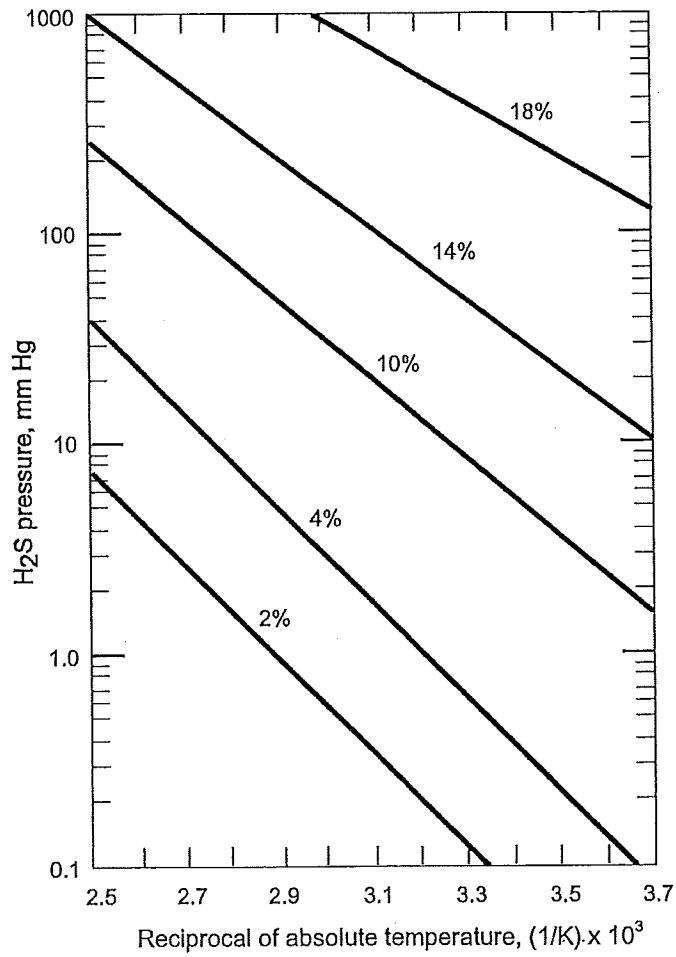


Figure 4-19. Adsorption isosteres of H<sub>2</sub>S on 13X molecular sieve (loading in % H<sub>2</sub>S by weight).

*Isobar*

The isobar is a plot of the amount of vapor adsorbed versus temperature at a constant partial pressure of the adsorbate. Figure 4-20 shows an isobar for the adsorption of benzene vapors on an activated carbon.

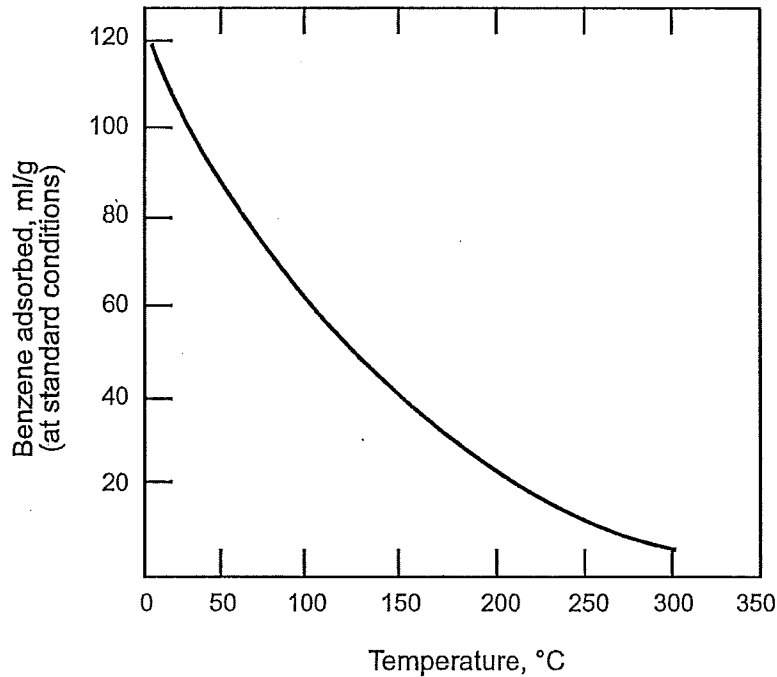


Figure 4-20. Adsorption isobar for benzene on an activated carbon ( $P_{\text{benzene}} = 10.0 \text{ mm Hg}$ ).

Note that the capacity units in this isobar are ml benzene/gm C. Also note that the amount adsorbed decreases with increasing temperature. This is always the case for physical adsorption.

Because the isotherm, isostere, and isobar for a given adsorbate-adsorbent system are developed at equilibrium conditions, they are mutually dependent. By determining one, such as the isotherm, the other two relationships can be determined. In the design of an air pollution control system, the adsorption isotherm is by far the most commonly used equilibrium relationship.

### 4.3 Adsorption System Performance

#### Applicability

##### Nonregenerative Systems

Nonregenerative systems are applicable to a wide variety of small, low-concentration organic vapor sources. As a very approximate guideline, organic compounds having molecular weights greater than 50 and/or boiling points greater than 68°F (20°C) can be adsorbed. Because these units are not regenerated, it is often possible to use them up to 50% of the saturation level

indicated by the applicable adsorption isotherm. This is generally a higher adsorbent utilization than is practical in regenerative systems. Accordingly, nonregenerative units can have a relatively long service life despite the limited quantity of adsorbent present.

*Regenerative Systems*

Conventional regenerative carbon bed adsorbers are used primarily for the removal and/or recovery of organic compounds having molecular weights between approximately 50 and 200.<sup>10</sup> These compounds usually have boiling points between 68°F and 350°F (20°C to approximately 175°C).<sup>10</sup> Very high molecular weight, high boiling point compounds have such a strong affinity for the adsorbent that it is impractical to desorb these materials.

Table 4-3 presents examples of organic compounds suitable for regenerative carbon adsorption. This is not a complete list because carbon adsorption is used for a wide variety of organic compounds. Other compounds, such as those listed in Table 4-4, are not suitable for regenerative adsorption because of their reactivity or high molecular weights and boiling temperatures.

Organic Compound	Boiling Point °F (°C)	Molecular Weight	Water Soluble	Flammable Liquid	Lower Explosive Limit, % Vol
<b>Aliphatic</b>					
Heptane	209 (98.4)	100.2	No	Yes	1.20
Hexane	156 (68.7)	86.2	No	Yes	1.20
Pentane	97 (36.1)	72.2	No	Yes	1.50
Naptha	288 (142)	-	No	Yes	0.92
Mineral Spirits	381 (194)	-	No	Yes	<1.00
Stoddard Solvent	379 (193)	-	No	Yes	1.10
<b>Aromatic</b>					
Benzene	176 (80.0)	78.1	No	Yes	1.40
Toluene	231 (110.6)	92.1	No	Yes	1.40
Xylene	292 (144.4)	106.2	No	Yes	1.00
<b>Ester</b>					
Butyl Acetate	259 (126.1)	116.2	No	Yes	7.60
Ethyl Acetate	171 (77.2)	88.1	Yes	Yes	2.50
<b>Halogenated</b>					
Carbon Tetrachloride	170 (76.7)	153.8	No	No	N.F.
Ethylene Dichloride	210 (98.9)	85.0	No	Yes	6.20
Methylene Chloride	104 (40.0)	84.9	Yes	No	N.F.
Perchloroethylene	250 (121.1)	165.8	No	No	N.F.
Trichloroethylene	189 (87.2)	131.4	No	No	N.F.
Trichloroethane	165 (73.9)	133.4	No	No	N.F.
<b>Ketones</b>					
Acetone	133 (56.1)	58.1	Yes	Yes	2.60
Diacetone Alcohol	293 (145.0)	116.2	Yes	Yes	-
Methyl Ethyl Ketone	174 (78.9)	72.1	Yes	Yes	1.80
Methyl Isobutyl Ketone	237 (113.9)	100.2	Yes	Yes	1.20
<b>Alcohols</b>					
Butyl Alcohol	241 (116.1)	74.1	Yes	Yes	1.40
Ethanol	165 (73.9)	46.1	Yes	Yes	4.30
Propyl Alcohol	205 (96.1)	60.1	Yes	Yes	2.10

Table 4-4. Organic compounds not usually suitable for carbon adsorption.	
Reactive Compounds	High Boilers
Organic acids	Plasticizers
Aldehydes	Resins
Monomers (some)	Long Chain HCs (+C <sub>14</sub> )
Ketones (some)	Glycols, Phenols, Amines

### Adsorption Capacity

Three important terms are used in actual systems to describe the capacity of the adsorbent bed, measured, for example, in pounds of vapor per pound of adsorbent.

- *Breakthrough capacity* is defined as the capacity of the bed at the time where unadsorbed vapor begins to be emitted.
- *Saturation capacity* (or equilibrium capacity) is the maximum amount of vapor that can be adsorbed per unit weight of carbon. This is the capacity read from the adsorption isotherms.
- *Working capacity* is a fraction of the saturation capacity, often in the range from 0.1 to 0.5 of the saturation capacity, that is used for design purposes. Smaller working capacities increase the amount of carbon required. The designer selects the appropriate fraction for individual systems by balancing the cost of carbon and adsorber operation versus preventing breakthrough.

It is generally uneconomical to desorb all vapor during the regeneration cycle. The small amount of residual vapor left in the bed is referred to as the *heel*, which accounts for a large portion of the difference between the saturation capacity and the working capacity. In some cases, the working capacity can be estimated by assuming that it is equal to the saturation capacity minus the heel.<sup>16</sup> Problem 4-2 illustrates one method of estimating the working capacity. In all of the examples in this course, a design factor of 0.25 of the saturation capacity is used. This is the same as assuming that the working amount of carbon is four times the amount required at saturation.

#### Problem 4-2

A dry cleaning process exhausts a 15,000 SCFM air stream containing 680 ppm carbon tetrachloride. Based on Figure 4-17 and gas stream conditions of 140°F and 14.7 psia, estimate the amount of carbon required if the adsorber operates on a four-hour cycle. Note that saturation capacity of the activated carbon is 45% by weight. The molecular weight of CCl<sub>4</sub> is 154. Use a working capacity of 25% of the saturation capacity.

Solution:

Step 1. Compute the flow rate of  $\text{CCl}_4$ .

$$Q_{\text{CCl}_4} = 15,000 \text{ SCFM} \times 0.00068 = 10.2 \text{ SCFM } \text{CCl}_4$$

Convert to pounds per hour:

$$\frac{10.2 \text{ ft}^3}{\text{min}} \times \frac{\text{lb mole}}{385.4 \text{ ft}^3} \times \frac{154 \text{ lb}_m}{\text{lb mole}} \times \frac{60 \text{ min}}{\text{hour}} = 245 \text{ lb}_m \text{ CCl}_4/\text{hour}$$

For a four-hour cycle:

$$4 \times 245 = 980 \text{ lb}_m \text{ CCl}_4$$

Step 2. The amount of activated carbon (at saturation) required is:

$$980 \text{ lb}_m \text{ CCl}_4 \times \frac{100 \text{ lb}_m \text{ carbon}}{30 \text{ lb}_m \text{ CCl}_4} = 3270 \text{ lb}_m \text{ activated carbon}$$

The actual amount of activated carbon required can be estimated by multiplying the amount needed at saturation by four (based on the working capacity of 25% of the saturation capacity).

$$4 \times 2178 = 8710 \text{ lb}_m \text{ carbon per four-hour cycle per adsorber}$$

Note: This gives only a rough estimate of the amount of carbon needed. Actual working capacity may be 25% to 75% of the saturation capacity.

### **Factors Affecting Adsorption System Performance**

A number of factors or system variables that influence the performance of a physical adsorption system are discussed in the following sections.

#### *Temperature*

The capacity of an adsorbent decreases as the temperature of the system increases, as illustrated in Figure 4-21. As the temperature increases, the vapor pressure of the adsorbate increases, raising the energy level of the adsorbed molecules. Adsorbed molecules now have sufficient energy to overcome the van der Waals' attraction and migrate back to the gas phase. Molecules already in the gas phase tend to stay there due to their high vapor pressure. As a general rule, adsorber temperatures are kept below 130°F (54°C) to ensure adequate bed capacities. Temperatures above this limit can be avoided by cooling the exhaust stream to be treated.

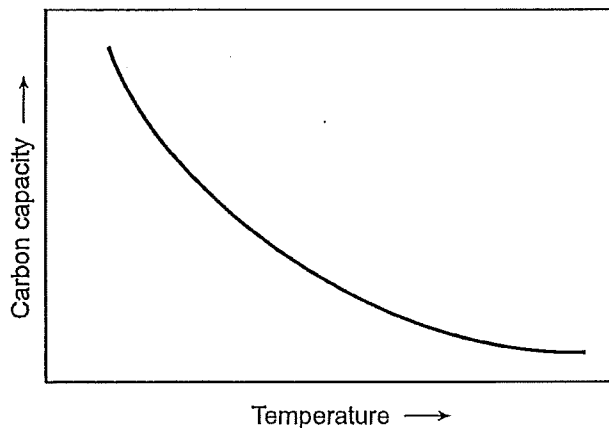


Figure 4-21. Carbon capacity versus gas stream temperature.

Adsorption is an exothermic process with the heat released for physical adsorption approximately equal to the heat of condensation. At low concentrations (below 1,000 ppm), the heat release is minimal and is quickly dissipated by the gas flowing through the bed. At higher concentrations (e.g., 5,000 ppm), the bed temperature can increase, thus causing the adsorption capacity to decrease. In addition, granular carbon is a good insulator that inhibits heat dissipation from the interior of the bed. In some cases, especially ketone recovery, the temperature rise can cause auto-ignition of the carbon bed.

*Pressure*

Adsorption capacity increases with an increase in the partial pressure of the vapor, which is proportional to the total pressure of the system. Any increase in pressure will increase the adsorption capacity. The increase in capacity occurs because of a decrease in the mean free path of vapor at higher pressures. Simply, the molecules are packed more tightly together. More molecules have a chance to "hit" the available adsorption sites, increasing the number of molecules adsorbed.

*Gas Velocity*

The gas velocity through the adsorber bed determines the contact or residence time between the gas stream and adsorbent. The residence time directly affects capture efficiency. The lower the gas velocity (the longer the contact time) through the adsorbent bed, the greater is the probability of a contaminant molecule reaching an available site. In order to achieve 90% or more capture efficiency, most carbon adsorption systems are designed for a maximum gas velocity of 100 ft/min (30 m/min) through the adsorber. A lower limit of at least 20 ft/min (6 m/min) is maintained to avoid flow problems such as channeling.

Gas velocity through the adsorber is determined by dividing the gas volumetric flow rate by the cross-sectional area of the adsorber. By specifying the gas velocity through the adsorber, the cross-sectional area is also specified.

**Problem 4-3**

A regenerative carbon bed system has three beds in parallel, each having a gas flow rate of 9,000 SCFM, a gas temperature of 100°F, and a gas pressure of +4 in. W.C. The barometric pressure is 30.3 in. Hg. What is the minimum cross-sectional area of each bed if the gas velocity must be maintained below 100 feet per minute?

**Solution:**

Step 1. Calculate the absolute static pressure.

$$SP_{\text{absolute}} = (4 \text{ in. W.C.}) + 30.3 \text{ in.Hg} \left( \frac{407 \text{ in. W.C.}}{29.92 \text{ in.Hg}} \right) = 416 \text{ in. W.C.}$$

Step 2. Calculate the gas flow rate in ACFM.

$$ACFM = 9,000 \text{ SCFM} \left( \frac{460^\circ\text{R} + 100^\circ\text{F}}{528^\circ\text{R}} \right) \left( \frac{407 \text{ in. W.C.}}{416 \text{ in. W.C.}} \right) = 9,340 \text{ ACFM}$$

Step 3. Calculate the minimum cross-sectional area of the bed to maintain a maximum of 100 ft/min.

$$\text{Velocity} = \left( \frac{\text{Gas flow rate in ACFM}}{\text{Area}} \right)$$

$$100 \text{ ft/min} = \left( \frac{9,340 \text{ ACFM}}{\text{Area}} \right)$$

$$\text{Area} = 93.4 \text{ ft}^2$$

Increasing the gas flow rate through the absorber increases the pressure drop. Within the above stated maximum and minimum flow rates, the allowable pressure drop usually dictates the required tower cross-sectional area and flow rate. The pressure drop across the bed also depends on the depth of adsorbent.

*Humidity*

As stated previously, activated carbon will preferentially adsorb nonpolar hydrocarbons over polar water vapor. The water vapor molecules in the exhaust stream exhibit stronger attractions for each other rather than the adsorbent. However, at high relative humidity the number of water molecules increases to the extent that they begin to compete with the hydrocarbon molecules for active adsorption sites, thus reducing the capacity and efficiency of the adsorption system.

Exhaust streams with humidities greater than 50% may require installation of additional equipment. Condensers to remove a portion of the water are one solution. Dilution air containing less moisture than the process stream has also been used. The contaminant stream may also be heated to reduce the humidity as long as the increase in temperature does not greatly affect adsorption efficiency. Additional adsorbent can be added to help offset the reduced efficiency.

*Bed Depth*

Providing a sufficient depth of adsorbent is very important in achieving efficient VOC removal due to the fact that adsorption rate is not infinitely fast. There are practical minimum and maximum limits to the bed depth.

The minimum depth is based primarily on the length of the mass transfer zone (MTZ) that, at fixed conditions such as temperature, partial pressure, and gas velocity, is related to the rate of adsorption. The MTZ is the volume of the bed where mass transfer occurs at any one time. The MTZ starts on the gas inlet side of the bed and moves through the bed as illustrated in Figure 4-22. The actual length of the MTZ remains fairly constant throughout the adsorption step. As long as the leading edge of the MTZ is above the bed outlet, the effluent concentration  $c_2$  remains very low, because that portion of the bed in front of the MTZ has not yet been exposed to VOC.

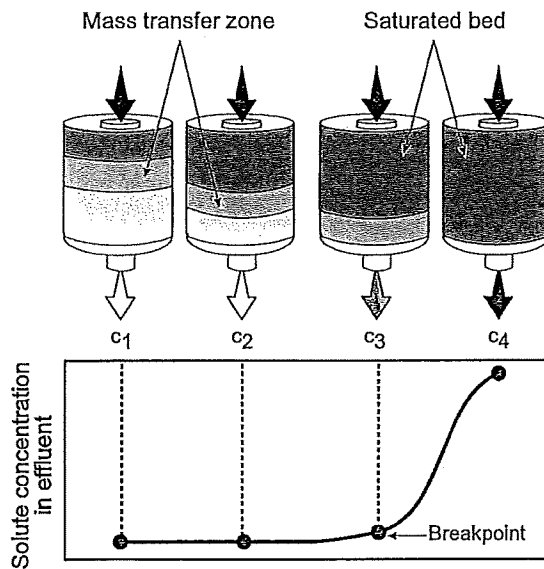


Figure 4-22. Mass transfer zone.

When the leading edge of the MTZ reaches the outlet of the bed, the concentration of contaminant in the effluent suddenly begins to rise. This is referred to as the breakthrough point. If the contaminated gas stream is not switched to a newly regenerated bed, the concentration of contaminant in the outlet will quickly rise until it equals the initial concentration,  $c_4$ .

If the adsorber bed depth is shorter than the required MTZ, breakthrough will occur almost immediately, rendering the system ineffective. Estimating the

MTZ is important in determining the minimum bed depth.

Estimating the length of the MTZ is difficult because it depends on six separate factors: (1) adsorbent particle size, (2) gas velocity, (3) adsorbate concentration, (4) fluid properties of the gas stream, (5) temperature of the system, and (6) pressure of the system. The MTZ can be estimated from experimental data using Equation 4-1.<sup>17</sup> To obtain the necessary data, vendors will usually test a small portion of the exhaust stream on a pilot adsorber column, operating at several different bed depths.

$$\text{(Eq. 4-1)} \quad \text{MTZ} = \frac{1}{1 - X_s} D \left( 1 - \frac{C_B}{C_s} \right)$$

Where: MTZ = length of MTZ (meters)  
 $X_s$  = degree of saturation in the MTZ (%), usually assumed to be 50%  
 D = bed depth (meters)  
 $C_B$  = breakthrough capacity (%)  
 $C_s$  = saturation capacity (%)

In the absence of experimental data, empirical factors are often used to estimate the MTZ.

Actual bed depths are usually several times longer than the length of the MTZ. The additional bed depth allows for adequate cycle times. Equation 4-1 can be rearranged to solve for breakthrough capacity for a fixed bed depth.

$$\text{(Eq. 4-2)} \quad C_B = \frac{(X_s)(C_s)(\text{MTZ}) + C_s(D - \text{MTZ})}{D}$$

Often the actual adsorbent depth is fixed by the maximum allowable static pressure drop across the bed. Pressure drop data for typical carbons are presented in Figure 4-23.<sup>16</sup> The pressure drop per meter of bed depth is plotted versus the gas velocity with the carbon mesh size as a parameter. From the figure, an adsorber with a flow rate of 80 ft/min (24 m/min) using 4x10 mesh carbon will have a pressure drop of approximately 6 in. W.C. per foot (1.5 kPa per meter) of bed depth. Therefore, if the total pressure drop across the bed is limited to 18 in. W.C. (4.5 kPa), the total bed depth should not exceed 3 ft (0.9 m).

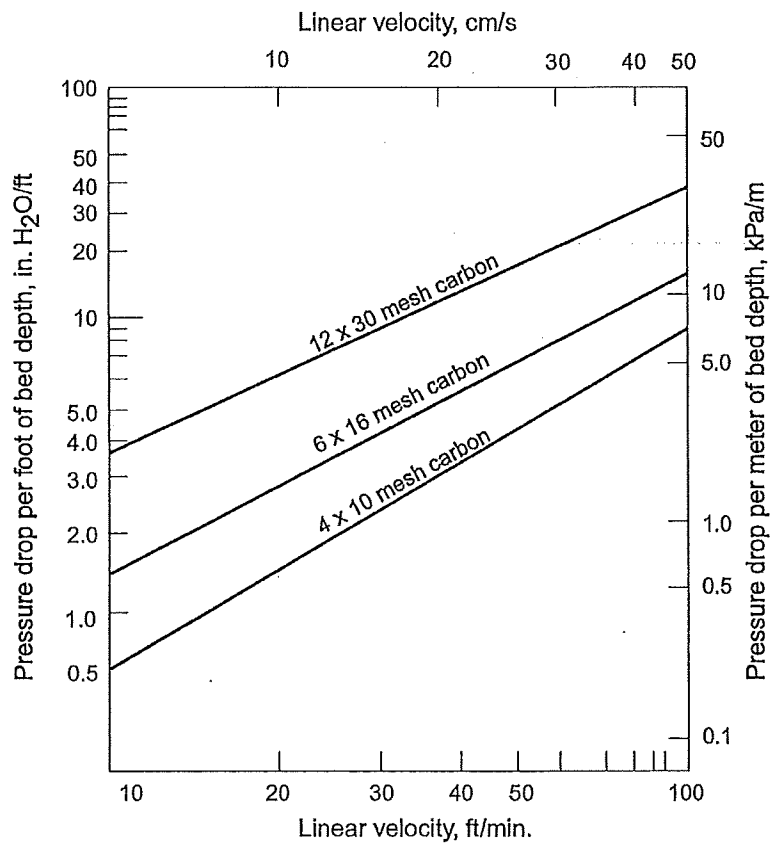


Figure 4-23. Pressure drop versus gas velocity through a deep bed granular carbon.

*Contaminants*

Particulate matter, organic compounds that have high boiling points, and entrained liquid droplets can also reduce adsorber efficiency if present in the gas stream.

Dust or lint greater than 3 micrometers in size can cover the surface of the adsorbent and reduce the surface area available to the gas molecule for adsorption. Covering active adsorption sites by an inert material is referred to as “blinding” or “deactivation.” To avoid this situation, almost all industrial adsorption systems are equipped with some type of upstream particulate matter removal device.

High boiling point and high molecular weight compounds have such an affinity for the carbon that it is extremely difficult to remove them by standard desorption practices. These compounds also tend to react chemically on the carbon surface, forming solids or polymerization products that are extremely difficult to desorb. Loss of carbon activity in this manner is termed *chemical deactivation*.

Entrained liquid droplets can also cause operational problems. Liquid

droplets that are non-adsorbing can act the same way as particulate matter by covering the surface and blinding the bed. Liquid adsorbate droplets result in high heats of adsorption, thereby increasing the temperature and decreasing the adsorption capacity. In the limit, the liquid organic droplets carried over from the process can cause bed fires from the released heat. An entrainment separator may be required when liquid droplets are present.

### ***Adsorbent Regeneration Methods***

Periodic replacement or regeneration of the adsorbent bed is mandatory in order to maintain continuous operation. When the adsorbate concentration is high, and/or the cycle time is short (less than 12 hours), replacement of the adsorbent is not feasible, and in situ regeneration is required. Regeneration is accomplished by reversing the adsorption process, usually increasing the temperature or decreasing the pressure. Four methods are used commercially for regeneration.

#### *Thermal Swing*

The bed is heated so that the adsorption capacity is reduced. The adsorbate leaves the surface of the carbon and is removed from the vessel by a stream of purge gas. Cooling must be provided before the subsequent adsorption cycle begins. Steam regeneration is a common example of thermal swing regeneration.

#### *Pressure Swing*

The pressure is lowered at a constant temperature to reduce the adsorbent capacity.

#### *Inert Purge Gas Stripping*

Purging with an inert gas reduces the partial pressure of the contaminant in the gas phase, reversing the concentration driving force. Molecules desorb from the surface into the gas stream.

#### *Displacement Cycle*

The adsorbates is displaced by a compound that is preferentially adsorbed. This method is usually a last resort for situations in which the adsorbate is both valuable and heat sensitive and in which pressure swing regeneration is ineffective.<sup>7</sup>

#### *Thermal Swing—Steam Stripping*

Steam stripping is the most common desorption technique because it is simple and relatively inexpensive. There are several additional advantages to using steam for desorption.

- A low steam temperature of 230°F (110°C) is sufficient to desorb most adsorbates of interest without damaging the carbon.
- Steam readily condenses in the adsorber bed, releasing its (the steam's) heat of condensation and aiding in desorption.
- Immiscible organic compounds can be easily separated by condensation

and decantation. Miscible compounds will require condensation followed by distillation.

- Residual moisture in the bed can be removed easily by a stream of cool, dry air (either pure or process-effluent).
- Steam is a more concentrated source of heat than hot air and is effective in raising the temperature of the adsorber bed quickly. Steam also avoids the potential fire hazard associated with air.

The amount of steam required for regeneration depends on the adsorbate and the adsorbate loading of the bed. The longer a carbon bed is steamed, the more adsorbate will be desorbed. It is usually not cost-effective to try to desorb all of the adsorbate. Acceptable working capacities can be achieved by using less steam and leaving a small portion of adsorbate in the bed (the heel). During the initial heating period, only a small amount of organic is desorbed because a fixed amount of steam is first required to raise the temperature of the bed to the desorption temperature. As the bed temperature increases, the rate of desorption increases until a plateau is reached. The plateau represents the optimum steam requirement, usually in the range of 0.25 to 0.35 pound of steam/pound of carbon.<sup>18</sup> The steam is usually supplied at pressures ranging from 3 to 15 psig, and steam usage can range anywhere from 0.3 to 10 pounds of steam per pound of solvent removed.

Some disadvantages are associated with steam regeneration:

- The aqueous effluent from the condenser can pose a water pollution problem unless the condensate is sent to a wastewater treatment facility.
- Some organic compounds may hydrolyze or form corrosive solutions in the presence of water. Corrosive substances can greatly reduce the life of the adsorption equipment unless expensive corrosive resistant materials are used.
- A hot, wet carbon bed will not effectively remove organic vapors. The bed will need to be cooled and dried to ensure adequate removal efficiencies at the beginning of a subsequent cycle.

#### *Pressure Swing - Vacuum Desorption*

Pressure swing or vacuum desorption has one primary advantage over thermal (steam) desorption. Desorption is accomplished by a change in pressure rather than temperature, so the time required to heat and cool the carbon bed is avoided. Thus pressure swing allows the bed to be in the adsorption mode for a greater fraction of the total cycle time. Smaller units may also be used because there is no increase in air volume due to heating of the bed. Both of these conditions allow for higher throughputs or smaller adsorber designs than can be accommodated by thermal swing desorption systems. Importantly, the desorbed vapors can be condensed directly, thus avoiding the need for additional downstream processing equipment, such as decanters or distillation columns.

The principle disadvantages of a pure pressure swing cycle are its high operating and construction costs. A vacuum system is required, unless the adsorber is initially operated at elevated pressures so that the pressure swing can

be accomplished by reducing the vessel to atmospheric pressures. In vacuum systems, the adsorber vessel and valving must be constructed of materials capable of withstanding vacuums of 28 in. Hg. Vacuum systems operating cyclically may require more operating attention than other regeneration systems. To be effective, pressure regeneration systems must operate so that a small decrease in pressure will result in a drastic shift in the direction of mass transfer.

**Problem 4-4**

A solvent degreaser is designed to recover toluene from an 8,000 ACFM air stream at 80°F (27°C) and atmospheric pressure. The company is planning to use a two-bed carbon adsorption system with a cycle time of 4 hours. The average concentration of toluene is 2,400 ppm. Given the adsorption isotherm for toluene (Figure 4-24), and the additional operational data given below, estimate the following:

- The amount of carbon required for a 4-hour operating cycle (operating time between desorption steps).
- The square feet of cross-sectional area required based on a 100 ft/min maximum velocity.
- The depth of the carbon bed.

Given: Molecular weight of toluene = 92.1  
 Activated carbon density = (30 lb<sub>m</sub>/ft<sup>3</sup>)

**Solution:**

Step 1. First calculate the toluene flow rate.

$$(8,000 \text{ ACFM}) \frac{528^\circ\text{R}}{540^\circ\text{R}} = 7,820 \text{ SCFM}$$

$$(7,820 \text{ SCFM}) \left( \frac{\text{lb moles total}}{385.4 \text{ scf}} \right) \left( \frac{0.0024 \text{ lb moles toluene}}{\text{lb moles total}} \right)$$

$$= 0.0487 \text{ lb moles toluene/min}$$

The mass flow rate of toluene is:

$$(0.0487 \text{ lb mole/min})(92.1 \text{ lb}_m/\text{lb mole}) = 4.49 \text{ lb}_m/\text{min}$$

Step 2. To determine the saturation capacity of the carbon, calculate the partial pressure of toluene at the adsorption conditions.

$$P^* = yP = \left( \frac{2400 \text{ ppm}}{1,000,000} \right) (14.7 \text{ psia}) = 0.0353 \text{ psia}$$

From Figure 4-24, the saturation capacity of the carbon is 45% or 45 pounds

toluene per 100 pounds of carbon at 0.0353 psia.

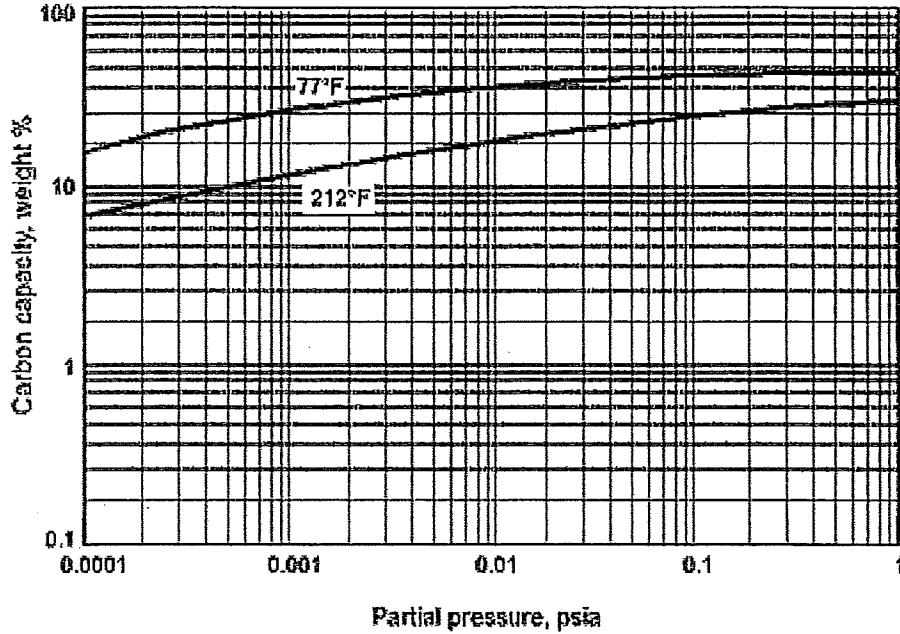


Figure 4-24. Toluene isotherm.

Step 3. The amount of carbon at saturation for a 4-hour cycle is:

$$\left(4.49 \frac{\text{lb}_m \text{ toluene}}{\text{min}}\right) \left(\frac{60 \text{ min}}{\text{hr}}\right) \left(\frac{100 \text{ lb}_m \text{ carbon}}{38 \text{ lb}_m \text{ toluene}}\right) \left(4 \frac{\text{hr}}{\text{cycle}}\right)$$

$$= 2,390 \text{ lb}_m \text{ of carbon (at saturation)}$$

The working charge of carbon can be estimated by multiplying the saturation capacity by four. Therefore, the working charge is:

$$(4)(2,390 \text{ lb}_m \text{ of carbon}) = 9,680 \text{ lb}_m \text{ of carbon for a 4-hour cycle}$$

The cross-sectional area of the bed is the volumetric flow rate divided by the allowable velocity of 100 ft/min through the adsorber.

The required cross-sectional area is:

$$A = \frac{Q}{\text{Maximum Velocity}} = \frac{8,000 \text{ ACF/min}}{100 \text{ ft/min}} = 80 \text{ ft}^2$$

Step 4. Estimate the bed depth.

Each bed of the proposed two-bed system would have to handle the 8,000 ACFM gas flow rate because one bed would be in desorption mode a portion of the operating time.

At a carbon density of 30 lb<sub>m</sub>/ft<sup>3</sup>, the bed depth would be:

$$\begin{aligned} \text{Vol. carbon} &= 9,680 \text{ lb}_m \text{ carbon} / (30 \text{ lb}_m / \text{ft}^3) = 320 \text{ ft}^3 \\ \text{Bed depth} &= 320 \text{ ft}^3 / 80 \text{ ft}^2 = 4 \text{ ft} \end{aligned}$$

This bed depth may result in excessively high pressure drop, so it may be preferable to use a larger vessel and a lower gas velocity. The required cross-sectional area is recalculated below using an average velocity of 60 ft/min rather than the 100 ft/min value used earlier in this problem.

$$A = \frac{Q}{\text{Maximum Velocity}} = \frac{8,000 \text{ acf/min}}{60 \text{ ft/min}} = 133 \text{ ft}^2$$

The bed depth for this modified approach would be:

$$320 \text{ ft}^3 / 133 \text{ ft}^2 = 2.4 \text{ ft}$$

## 4.4 Performance Monitoring

The factors that contribute to premature organic breakthrough in a large fixed-bed, regenerative system or a large nonregenerative system are relatively similar. The problems include but are not limited to the following:

- Corrosion and subsequent collapse of the pellet beds
- Infrequent desorption
- Loss of adsorptive capacity due to high boiling point compounds
- Plugging of activated carbon pellet beds due to particulate matter
- Physical deterioration of the activated carbon pellets or carbon fiber materials
- Increased operating temperature
- Increased organic vapor concentration

A conventional regenerative deep, fixed-bed system will be used to illustrate the techniques available to evaluate performance and to identify the problems listed above. Although the techniques are relatively similar for all types of fixed-bed systems, some small-scale fixed-bed units will not have all of the on-site instruments that are economically reasonable for the large installations.

The example fixed-bed system flowchart is shown in Figure 4-25. This shows three adsorber beds in parallel. The SLA stream from the process equipment is discharged by the centrifugal fan through a particulate matter filter and an indirect heat exchanger into the top of the on-line adsorber vessel. Low-pressure steam is used to desorb the organic vapors from the off-line adsorber vessel. The

typical types of instruments present on a large-scale system are shown in this flowchart.

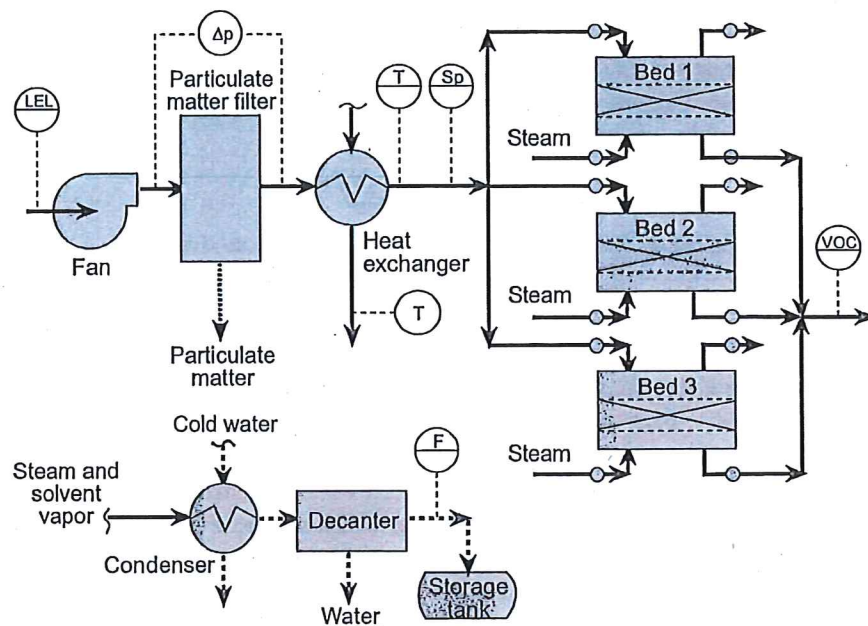


Figure 4-25. Flowchart of a three-bed (deep bed) adsorber.

A control room or control panel for the adsorber system is usually located in an area close to the adsorber vessels. One or more storage tanks are usually also close to the system.

### Outlet VOC Concentration Monitor

The most direct measure of the performance of the adsorber is provided by the outlet VOC concentration monitor. This instrument draws a sample gas stream from the outlet of each bed on a frequent basis. Common types of instruments include photoionization and flame ionization detectors (FID). The outlet concentrations are determined and recorded on a data acquisition system (DAS) or strip chart recorder at the control panel for the adsorber system. Premature breakthrough or other improper operation will be indicated by high outlet concentration.

It should be noted that these instruments provide an accurate indication of the outlet concentration only when they are calibrated for the specific organic compound, or compounds, present in the gas stream. The instruments are usually calibrated using a readily-available organic compound such as methane, propane, n-hexane, or 1,3 butadiene that can be prepared in a stable form at relatively high concentrations (100 to 10,000 ppm). Stable gas samples are much more difficult to prepare for compounds such as toluene, halogenated organics, and ketones. When calibration gases such as methane, propane, or 1,3 butadiene are used for calibration, the instrument reading is only a qualitative indicator of performance. However, instrument readings above baseline levels for the unit are

a clear indication of adsorber performance problems.

The accuracy of the VOC data should be checked regularly. The instruments should be calibrated on a daily basis using gas cylinders. Calibration gas is usually injected near the sample port on each adsorber bed (Figure 4-26) so that the integrity of the sample line to the instrument can be confirmed. A variety of problems in these sample lines can lead to lower-than-actual organic vapor concentration readings; these include:

- VOC outlet monitor sample line problems
- Air infiltration due to leaking connections or corroded tubing
- Adsorption and absorption along the tubing walls due to low surface temperatures and water condensation
- Reduced sample gas flow rates due to partial plugging of the tubing (primarily affects flame ionization detectors)
- Inoperative valves controlling sample gas flow from each adsorber vessel

The calibration frequencies and procedures for the instruments should be checked. A single point calibration and a zero check should be made on a daily basis. Outlet concentration data obtained since the last calibration period may be corrected for calibration drift and zero drift by computerized data acquisition systems.

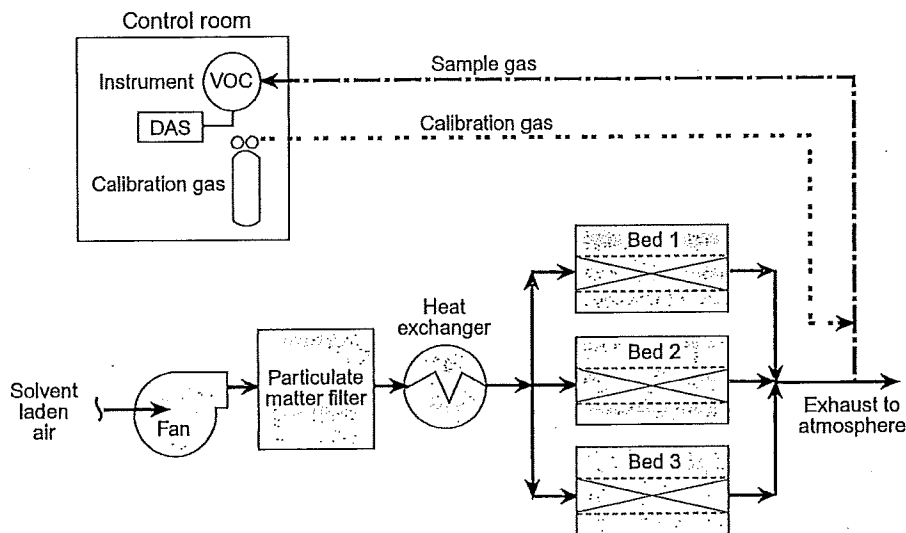


Figure 4-26. Calibration gas injection locations to check for sample line tubing problems.

### **Portable Organic Vapor Concentration Detectors**

There are a variety of portable detectors (often termed portable VOC analyzers) that can be used for small-scale fixed-bed adsorbers where it is uneconomical to have permanently mounted instruments. The most common types include (1) flame ionization detectors, (2) catalytic combustion analyzers, and (3)

photoionization detectors. All of these are battery-powered instruments that can be used to obtain a small gas sample and provide a qualitative indication of the total outlet VOC concentration. These instruments are subject to the same calibration gas limitations that affect the permanently mounted units on large-scale adsorber systems.

#### *Flame Ionization Detectors*

The flame ionization detector (FID) extracts 10 to 50 cc/min of the sample gas that is mixed with either pure hydrogen or a hydrogen/helium blend. The mixture is injected and combusted along with "clean" air in the FID. The organic compounds oxidized in the hydrogen flame form positive gas ions that are driven to a collector electrode in the burner chamber. The electrical current flowing through this electrode is amplified and provides an indication of the total mass of organic vapor in the sample gas stream. Any compounds that can be oxidized in the burner chamber can be detected, including essentially all organic compounds with the exception of low molecular weight, highly oxygenated or halogenated compounds, such as formaldehyde and carbon tetrachloride).

#### *Catalytic Combustion Analyzers*

The catalytic combustion analyzer is similar to the FID analyzer in that the organic compounds in the sample gas stream are entirely oxidized during the analysis. A small sample gas stream passes through a sintered metal detector that has a catalyst-coated wire. Oxidation of the organic compounds in this detector changes the electrical resistance of the coated wire. This change in resistance is converted to a current signal that is proportional to the total organic vapor concentration. This type of instrument responds to approximately the same types of compounds as the flame ionization detector; however, it is not quite as sensitive.

#### *Photoionization Detectors*

A photoionization detector (PID) pulls a sample gas stream through a small chamber where the organic compounds are irradiated with ultraviolet light. A small fraction of the organics is photoionized to form positive ions that are accumulated on an electrode creating a current proportional to the organic vapor concentration. The current is amplified to indicate the total organic vapor concentration. Unlike the flame ionization analyzer, the photoionization detector is essentially nondestructive. The sample gas stream passing through the instrument can be recovered in a sample gasbag and returned to a laboratory for more detailed analysis. Photoionization detectors can detect organic compounds with ionization potentials close to or below the ionization energy level of the lamp (e.g., 9.0, 10.0, 10.2, and 11.3 electron volts). Most organic compounds can be detected, including the highly oxygenated or halogenated compounds that cannot be measured by the flame ionization detector. Photoionization detectors are not useful for low molecular weight paraffinic compounds such as methane, propane, and butane, because these compounds have high ionization potentials. This is not a problem with respect to carbon adsorber evaluation, however, because these same compounds have very low affinity for activated carbon and

are not controlled by these systems.

All three types of instruments can be used to measure the outlet VOC concentration from an adsorber. Because of the limited pump capacity of all three instrument types, the sample should be obtained from a positive pressure portion of the outlet duct. A single point measurement can usually be made, and the monitoring times are relatively short.

Organic vapor concentration measurements using portable VOC analyzers should be made near the end of the adsorption cycle. At this time, the outlet VOC concentration is at a maximum. The measurements must not be conducted when the adsorber is in the cooldown-purge cycle just prior to returning to adsorption service. During this period, the gas stream humidity is high and water droplets may be present. Moisture can damage the sensors of all three types of instruments.

### ***Additional Monitoring Considerations***

#### *LEL Inlet Monitor*

Adsorbers designed to operate with feed gas containing more than 10% to 25% of the LEL usually have an LEL monitor in the inlet duct to the adsorber system. The primary purpose of this instrument is to shut down the fan and other system components in the event that the inlet concentration increases above the safety limit.

This instrument can be used to provide a qualitative indication of changes in the inlet VOC concentration. Increased inlet concentrations could lead to organic vapor breakthrough unless the adsorption cycle time is decreased.

#### *Gas Inlet Temperature*

The gas inlet temperature is one of the most important variables affecting performance. Due to the weak physical forces involved in adsorption, increased gas temperatures result in substantially reduced adsorption capacity which leads to increased prebreakthrough concentrations and premature breakthrough. The inlet gas temperatures should be compared during the last several months to identify significant increases above baseline values. Furthermore, gas inlet temperatures above 100°F may indicate inadequate performance.

#### *Adsorber Vessel Bed Static Pressure Drop*

The static pressure drop across a fixed-bed adsorber is usually between 0.5 and 3.0 in. W.C. (0.1 and 0.75 kPa) per foot of bed. The static pressure drop across moving-bed adsorbers is usually considerably lower than the levels for the fixed-bed designs.

Changes from baseline pressure drop levels are usually associated with conditions that adversely affect performance. An increase in the static pressure drop (no change in the gas flow rate) can be caused by the accumulation of dust and particulate matter on the inlet side of the bed. Gas flow maldistribution will lead to decreased adsorption efficiency. A decrease in the static pressure drop may indicate partial or complete collapse of the fixed bed due to corrosion of the support grid.

*Gas Flow Rate*

Gas flow rates above the design range of the absorber vessel create a longer-than-anticipated MTZ. Breakthrough will occur if the MTZ reaches the outlet of the carbon bed before the adsorber is brought off-line for desorption. Usually, the maximum gas velocities through the bed are limited to less than 100 feet per minute. Increased gas flow rates are indicated by increased centrifugal fan motor currents, increased adsorber vessel pressure drop, and/or increased hood static pressures.

Decreased gas flow rates may also indicate performance problems. Increased fugitive emissions from the process equipment served by the adsorber could be due to reduced gas flow rates. This problem may be indicated by reduced fan motor current, decreased hood static pressure, decreased static pressure drop across the adsorber vessels, and/or decreased static pressure drop across the particulate matter filter.

*Hood Static Pressure*

The hood static pressure provides a useful indicator of the gas flow conditions at the pick-up point on the process equipment where the organic vapors are being released. The typical values of the hood static pressure range from approximately -0.3 in. W.C. (-0.075 kPa) to more than -2.0 in. W.C. (-0.5 kPa). If the hood static pressure becomes less negative (moves toward 0.0 in. W.C.), the gas flow rate has probably decreased, and fugitive emissions have probably increased.

## **Review Exercises**

### Types and Components of Adsorption Systems

1. What types of adsorbents are often used in adsorption systems? Select all that apply.
  - a. Activated carbon
  - b. Carbon fiber
  - c. Zeolites
  - d. Polymeric materials
  
2. What is the primary purpose for using a preconcentrator adsorption system?
  - a. Achieve high VOC concentrations to facilitate higher saturation capacities
  - b. Improve collection efficiency in the adsorber vessel
  - c. Reduce the gas stream volume and increase the VOC concentration in an incinerator inlet gas stream
  - d. Increase the gas stream concentration prior to treatment in a condenser
  
3. What materials and/or techniques are used to desorb VOCs from regenerative type adsorption systems? Select all that apply.
  - a. Low pressure steam
  - b. Hot air
  - c. Vacuum
  - d. Hot water flush
  
4. What is the adsorber bed inlet concentration limit for VOC-containing gas streams?
  - a. 25% of the LEL
  - b. 75% of the LEL
  - c. 95% of the LEL
  - d. 99% of the LEL
  
5. What problems can potentially be created by the presence of particles larger than approximately 3 micrometers? Select all that apply.
  - a. Plugging of the inlet side of the bed
  - b. Increased channeling of the solvent-laden air through the bed
  - c. Increased static pressure drop

- d. Reduction in adsorbent saturation capacity
- 6. What is the normal maximum gas temperature used in VOC adsorption systems?
  - a. 75°F
  - b. 100°F
  - c. 130°F
  - d. 160°F
- 7. What type of solvent separator is needed for an activated carbon adsorber system that uses low-pressure steam for desorption and is collecting water-insoluble organic compounds?
  - a. Condenser and decanter
  - b. Distillation column
  - c. Stripping column
  - d. None of the above
- 8. What is the typical VOC removal efficiency of a properly designed and operated adsorption system?
  - a. 50% to 75%
  - b. 75% to 90%
  - c. 90% to 98%
  - d. 98% to 99.5%
- 9. Is an activated carbon adsorber system applicable to the removal of methane and ethane from a gas stream?
  - a. Yes
  - b. No
  - c. It depends on the solvent-laden gas temperature.
  - d. It depends on the solvent-laden gas pressure.

#### Operating Principles of Adsorption Systems

- 10. How does the saturation capacity of an activated carbon bed change when the VOC concentration increases?
  - a. It increases.
  - b. It decreases.
  - c. It remains unchanged.
  - d. It depends on the specific VOC.
- 11. How does the saturation capacity of an activated carbon bed change when the temperature of the solvent-laden air increases?

- a. It increases.
  - b. It decreases.
  - c. It remains unchanged.
  - d. It depends on the specific VOC.
12. How does the saturation capacity of an activated carbon bed change when the humidity of the solvent-laden air increases?
- a. It increases.
  - b. It decreases.
  - c. It remains unchanged.
  - d. It depends on the specific VOC.
13. Can the adsorption isotherm shown in Figure 4-20 be used for sizing an adsorber using a different commercial activated carbon product?
- a. Yes
  - b. No
  - c. It depends on the temperature of the solvent-laden air entering system and the sample gas used to develop the isotherm.
  - d. It depends on the temperature and relative humidity of the solvent-laden air entering the system and the sample gas used to develop the isotherm.
14. Why are high molecular weight compounds ( $>$  molecular weight of 200) difficult to handle in a regenerative adsorber system?
- a. They are not adsorbed efficiently.
  - b. They have too high an affinity and cannot be efficiently desorbed.
  - c. They cannot be separated in decanters, condensers, and distillation columns.
  - d. They are likely to decompose at the elevated adsorption temperature.

#### Adsorption System Performance

15. Using Figure 4-24, what is the saturation capacity of activated carbon for toluene at a temperature of 77°F and a toluene concentration of 600 ppm?
16. Based on the saturation capacity determined in Question 15, how much activated carbon would be needed in a three-bed regenerative system to treat a gas stream having a toluene concentration of 600 ppm and a gas flow rate of 30,000 SCFM? Assume that each bed is desorbed every third hour and that two beds are in service during all operating times. Assume that the working capacity is 25% of the saturation capacity.
17. Is the superficial velocity within the normal range for activated carbon fixed-bed systems if the three beds evaluated in Question 16 have cross-sectional areas of 180 ft<sup>2</sup> each? Use a gas temperature of 77°F, an inlet static pressure

of + 6 in. W.C., and a barometric pressure of 29.65 in. Hg, if necessary in solving the problem.

18. What is the approximate static pressure drop across the carbon bed described in Question 17? The bed contains 4 x 10 mesh carbon having a density of 30 lb<sub>m</sub>/ft<sup>3</sup>.
19. The static pressure drop of a fixed-bed carbon adsorber system has increased from 4 in. W.C. to 5.5 in. W.C. The static pressure drop across the particulate matter filter has decreased from 1.5 in. W.C. to 1.3 in. W.C. The fan motor current has also decreased. Have the fugitive emissions from the process equipment probably increased or decreased due to these changes?
  - a. Increased
  - b. Decreased
20. Which techniques are used to determine the adsorption isotherms that are used to size adsorbent beds?
  - a. Pilot plant tests
  - b. Laboratory tests with the specific type or brand of adsorbent
  - c. Theoretical adsorption models
  - d. Other

#### Performance Monitoring

21. What technique can be used to determine if breakthrough is occurring on a VOC adsorption system handling toluene?
  - a. Monitoring of the outlet VOC concentration
  - b. Measuring the bed static pressure drop
  - c. Measuring the bed inlet gas temperature
  - d. All of the above
22. What is the primary purpose of measuring the hood static pressure?
  - a. Evaluate changes in the gas flow rate that could adversely affect the adsorption bed
  - b. Determine if there is a need to adjust the desorption frequency
  - c. Identify possible increases in fugitive emissions from process equipment
  - d. Identify need to change the rate of water flow to an indirect heat exchanger upstream of the adsorber beds
23. What is the primary purpose of installing the adsorber bed inlet LEL gauge?
  - a. Detect potentially explosive conditions so that the system can be rapidly de-energized

**APTI 415: CONTROL OF GASEOUS EMISSIONS**

- b. Detect increased VOC concentrations that could require increased desorption frequency
  - c. Detect increased VOC concentrations that could confirm improved fugitive emission capture at the process source
  - d. Provide data for compiling a material balance of VOC materials around the adsorption system
24. What is the purpose of installing a solvent-laden air temperature gauge at the inlet of the adsorption beds?
- a. Detect potentially explosive conditions so that the system can be rapidly de-energized
  - b. Detect increased gas temperatures that could require increased desorption frequency
  - c. Detect decreased gas temperatures that could indicate impaired fugitive emission capture at the process source
  - d. Detect increased gas temperatures that could cause the VOCs to decompose.

## **Review Answers**

### Types and Components of Adsorption Systems

1. What types of adsorbents are often used in adsorption systems? Select all that apply.
  - a. Activated carbon
  - b. Carbon fiber
  - e. Polymeric materials
  
2. What is the primary purpose for using a preconcentrator adsorption system?
  - c. Reduce the gas stream volume and increase the VOC concentration in an incinerator inlet gas stream
  
3. What materials and/or techniques are used to desorb VOCs from regenerative type adsorption systems? Select all that apply.
  - a. Low pressure steam
  - b. Hot air
  - c. Vacuum
  
4. What is the adsorber bed inlet concentration limit for VOC-containing gas streams?
  - a. 25% of the LEL (Note – in some facilities, 10% of the LEL is the maximum allowed.)
  
5. What problems can potentially be created by the presence of particles larger than approximately 3 micrometers? Select all that apply.
  - a. Pluggage of the inlet side of the bed
  - b. Increased channeling of the solvent-laden air through the bed
  - c. Increased static pressure drop
  
6. What is the normal maximum gas temperature used in VOC adsorption systems?
  - c. 130°F
  
7. What type of solvent separator is needed for an activated carbon adsorber system that uses low-pressure steam for desorption and is collecting water-insoluble organic compounds?
  - a. Condenser and decanter

8. What is the typical VOC removal efficiency of a properly designed and operated adsorption system?
  - c. 90% to 98%
9. Is an activated carbon adsorber system applicable to the removal of methane and ethane from a gas stream?
  - b. No

Methane and ethane have molecular weights below 50.

### Operating Principles of Adsorption Systems

10. How does the saturation capacity of an activated carbon bed change when the VOC concentration increases?
  - a. It increases.
11. How does the saturation capacity of an activated carbon bed change when the temperature of the solvent-laden air increases?
  - b. It decreases.
12. How does the saturation capacity of an activated carbon bed change when the humidity of the solvent-laden air increases?
  - b. It decreases.
13. Can the adsorption isotherm shown in Figure 4-20 be used for sizing an absorber using a different commercial activated carbon product?
  - b. No
14. Why are high molecular weight compounds (> molecular weight of 200) difficult to handle in a regenerative adsorber system?
  - b. They have too high an affinity and cannot be efficiently desorbed.

### Adsorption System Performance

15. Using Figure 4-24, what is the saturation capacity of activated carbon for toluene at a temperature of 77°F and a toluene concentration of 600 ppm?

Step 1. In the gas phase, the mole fraction (y) is equal to the ppm divided by 10<sup>6</sup>.

$$y = 600 \text{ ppm} = 0.0006$$

Obtain the partial pressure:

$$P^* = yP = (0.0006)(14.7 \text{ psia}) = 0.0088 \text{ psia}$$

Step 2. From Figure 4-24, at a partial pressure of 0.0088 psia and a temperature of 77°F, the carbon saturation capacity is read as about 40%.

16. Based on the saturation capacity determined in Problem 15, how much activated carbon would be needed in a three-bed regenerative system to treat a gas stream having a toluene concentration of 600 ppm and a gas flow rate of 30,000 SCFM? Assume that each bed is desorbed every third hour, desorption requires exactly one hour, and that two beds are in service during all operating times. Assume that the working capacity is 25% of the saturation capacity.

Step 1. First calculate the toluene flow rate per bed.

$$(15,000 \text{ SCFM}) \left( \frac{\text{lb mole total}}{385.4 \text{ SCF}} \right) \left( \frac{0.0006 \text{ lb mole toluene}}{\text{lb mole total}} \right) \\ = 0.0234 \text{ lb mole toluene/min}$$

The mass flow rate of toluene is:

$$(0.0234 \text{ lb moles/min})(92.1 \text{ lb}_m/\text{lb mole}) = 2.16 \text{ lb}_m/\text{min}$$

From Question 15, the saturation capacity of the activated carbon is 40% or 40 pounds toluene per 100 pounds of carbon at 0.0088 psia.

Step 2. The amount of carbon at saturation for a 3-hour cycle is:

$$\left( \frac{2.16 \text{ lb}_m}{\text{min}} \right) \left( \frac{100 \text{ lb}_m \text{ carbon}}{40 \text{ lb}_m \text{ toluene}} \right) \left( \frac{60 \text{ min.}}{\text{hr}} \right) \left( \frac{3 \text{ hours}}{\text{cycle}} \right) = 970 \text{ lb}_m \text{ carbon per bed}$$

The working charge of carbon can be estimated by multiplying the saturation capacity by 4.

Therefore, the working charge is calculated as:

$$(4)(970 \text{ lb}_m \text{ of carbon}) = 3870 \text{ lb}_m \text{ of carbon for a 3-hour cycle}$$

17. Is the superficial velocity within the normal range for activated carbon fixed-bed systems if the three beds evaluated in Question 16 have cross-sectional areas of 180 ft<sup>2</sup> each? Use a gas temperature of 77°F, an inlet static pressure of + 6 in. W.C., and a barometric pressure of 29.65 in. Hg., if necessary in solving the problem.

Step 1. Calculate the absolute static pressure.

$$SP_{\text{absolute}} = (6 \text{ in. W.C.}) + 29.65 \text{ in. Hg} \left( \frac{407 \text{ in. W.C.}}{29.92 \text{ in. Hg.}} \right) = 409 \text{ in. W.C.}$$

Step 2. Calculate the gas flow rate in ACFM.

$$= \left( \frac{15,000 \text{ SCFM}}{\text{Bed}} \right) \left( \frac{460^\circ\text{R} + 77^\circ\text{F}}{528^\circ\text{R}} \right) \left( \frac{407 \text{ in.W.C.}}{409 \text{ in.W.C.}} \right) = 15,200 \text{ ACFM}$$

Step 3. Determine the superficial velocity through bed.

$$\text{Velocity} = \text{Flow Rate}/\text{Area} = (15,200 \text{ ft}^3/\text{min})/180 \text{ ft}^2 = 84.4 \text{ ft/min}$$

Yes, the velocity is in the normal range (< 100 ft/min).

18. What is the approximate static pressure drop across the carbon bed described in Question 17? The bed contains 4 x 10 mesh carbon having a density of 30 lb<sub>m</sub>/ft<sup>3</sup>.

Step 1. Calculate the depth of the activated carbon bed.

At a carbon density of 30 lb<sub>m</sub>/ft<sup>3</sup>, the bed depth would be:

$$\text{Vol. carbon} = 3,870 \text{ lb}_m \text{ carbon}/(30 \text{ lb}_m/\text{ft}^3) = 129 \text{ ft}^3$$

$$\text{Bed depth} = 129 \text{ ft}^3/180 \text{ ft}^2 = 0.72 \text{ ft}$$

Step 2. Calculate the static pressure drop.

From Question 18, linear velocity = 84 ft/min, therefore from Figure 4-23, the pressure drop per foot of bed depth is approximately 7 in. W.C./ft.

$$\text{Static pressure drop} = 0.72 \text{ ft} (7.0 \text{ in. W.C./foot of bed}) = 5.0 \text{ in. W.C.}$$

19. The static pressure drop of a fixed-bed carbon adsorber system has increased from 4 in. W.C. to 5.5 in. W.C. The static pressure drop across the particulate matter filter has decreased from 1.5 in. W.C. to 1.3 in. W.C. The fan motor current has also decreased. Have the fugitive emissions from the process equipment probably increased or decreased due to these changes?

a. Increased

20. Which techniques are used to determine the adsorption isotherms that are used to size adsorbent beds?

b. Laboratory tests with the specific type or brand of adsorbent

#### Performance Monitoring

21. What technique can be used to determine if breakthrough is occurring on a VOC adsorption system handling toluene?

a. Monitoring of the outlet VOC concentration

**APTI 415: CONTROL OF GASEOUS EMISSIONS**

22. What is the primary purpose of measuring the hood static pressure?
  - c. Identify possible increases in fugitive emissions from process equipment
  
23. What is the primary purpose of installing the adsorber bed inlet LEL gauge?
  - a. Detect potentially explosive conditions so that the system can be rapidly de-energized
  
24. What is the primary purpose of installing a solvent laden air temperature gauge at the inlet of the adsorption beds?
  - b. Detect increased gas temperatures that could require increased desorption frequency

## References

1. Ruthven, D.M. Zeolites as Selective Adsorbents. *Chemical Engineering Progress*, February 1988, 42-50.
2. Vaughan, D.E.W. The Synthesis and Manufacture of Zeolites. *Chemical Engineering Progress*, February 1988, 25-31.
3. Bethea, R.M. *Air Pollution Control Technology*. New York: Van Nostrand Reinhold, 1978.
4. Goltz, H.R.; Jones, K.C.; Tegen, M.H. *High Surface Area Polymeric Adsorbents for VOC Capture and On-Site Regeneration*. Paper presented at the Air & Waste Management Association, 87th Annual Meeting and Exhibition, Cincinnati, OH, June 1994.
5. Danielsson, M.A.; Hudon, V. VOC Emission Control Using a Fluidized-Bed Adsorption System. *Metal Finishing*, June 1994, 89-91.
6. Dubinin, M.M.; Saverina, E. *The Porosity and Sorptive Properties of Active Carbon*. USSR: Acta Physicochem, 1936.
7. Environmental Protection Agency. *Package Sorption Device System Study*. Research Triangle Park, NC: EPA-R2-73-202, 1973.
8. Vic Manufacturing. *Carbon Adsorption/Emission Control, Benefits and Considerations*. Minneapolis, MN: April 1979.
9. Lobmeyer, D.A. *VOC Abatement and Solvent Recovery Using Activated Carbon Adsorption Technology*. Presented at the 86th Annual Meeting & Exhibition of the Air & Waste Management Association, Denver, CO, June 13-18, 1993.
10. Durr Industries, Inc. *Environmental System Solutions, Ecopure Exhaust Air Purification Plants*. Plymouth, MI. Undated.
11. Kenson, R.E. *Preconcentration and Recovery of Solvent Using Activated Carbon Fiber Adsorption*. Presented at the 86th Annual Meeting & Exhibition of the Air & Waste Management Association, Denver, CO, June 13-18, 1993.
12. Union Carbide. *Purasiv HR for Hydrocarbon Recovery*. Technical Bulletin. New York. Undated.
13. Cannon, T.E. Carbon Adsorption Applications. In *Air Pollution Control and Design Handbook*; Cheremisinoff, P.N., Young, R.A., Eds.; New York: Marcel Dekker, Inc., 1977.
14. Cerny S.; Smesek, M. *Active Carbon*. New York: Elsevier Publishing Company, 1970.

**APTI 415: CONTROL OF GASEOUS EMISSIONS**

15. Turk, A. Adsorption. In *Engineering Control of Air Pollution: Air Pollution, Volume IV*; Stern, A.C., Ed.; New York: Academic Press, 1977.
16. Kovach, L.J. Gas-Phase Adsorption and Air Purification. In *Carbon Adsorption Handbook*; Cheremisinoff, P.N., Ellerbush, F., Eds.; Ann Arbor, MI: Ann Arbor Science Publishers, Inc., 1978.
17. Parmele, S.C.; O'Connell, W.L.; Basdekis, H.S. Vapor-Phase Adsorption Cuts Pollution, Recovers Solvent. *Chemical Engineering*, December 31, 1979, 58-70.
18. Parmele, S.C.; O'Connell, W.L.; Basdekis, H.S. Vapor-Phase Adsorption Cuts Pollution, Recovers Solvent. *Chemical Engineering*, December 31, 1979, 58-70.

## Impact of Sulfur Oxides on Mercury Capture by Activated Carbon

ALBERT A. PRESTO AND  
EVAN J. GRANITE\*

National Energy Technology Laboratory, United States  
Department of Energy, P.O. Box 10940, MS 58-103A,  
Pittsburgh, Pennsylvania 15236-0940

Recent field tests of mercury removal with activated carbon injection (ACI) have revealed that mercury capture is limited in flue gases containing high concentrations of sulfur oxides ( $\text{SO}_x$ ). In order to gain a more complete understanding of the impact of  $\text{SO}_x$  on ACI, mercury capture was tested under varying conditions of  $\text{SO}_2$  and  $\text{SO}_3$  concentrations using a packed bed reactor and simulated flue gas (SFG). The final mercury content of the activated carbons is independent of the  $\text{SO}_2$  concentration in the SFG, but the presence of  $\text{SO}_3$  inhibits mercury capture even at the lowest concentration tested (20 ppm). The mercury removal capacity decreases as the sulfur content of the used activated carbons increases from 1 to 10%. In one extreme case, an activated carbon with 10% sulfur, prepared by  $\text{H}_2\text{SO}_4$  impregnation, shows almost no mercury capacity. The results suggest that mercury and sulfur oxides are in competition for the same binding sites on the carbon surface.

### 1. Introduction

Activated carbon injection (ACI) has been widely studied as an effective means for mercury capture from flue gas. Both unpromoted (e.g., Norit Darco Hg) (1, 2) and halogen-promoted (e.g., Norit Darco Hg-LH) (1, 3, 4) activated carbons have been tested during full-scale field studies. Recent results indicate that brominated activated carbons are particularly effective and can capture 70–90% of the mercury from a sub-bituminous-derived flue gas at injection rates less than 2 lbs/MMacf (5). However, several studies also indicate that high concentrations of  $\text{SO}_x$  ( $\text{SO}_x = \text{SO}_2 + \text{SO}_3$ ) can interfere with the capture of mercury by activated carbon (1–4, 6). For example, at Mississippi Power's Plant Daniel, increasing the  $\text{SO}_3$  concentration in the flue gas from 0 to 6 ppm reduced native mercury capture by fly ash from 55% to 14% and reduced the effectiveness of ACI (Darco Hg at 10 lbs/MMacf) by 25–35% (2).

$\text{SO}_x$  enters flue gas from one of three channels: (1) During combustion, coal-S is converted to  $\text{SO}_2$ ; a small fraction of the sulfur is further oxidized to  $\text{SO}_3$  (7). During combustion of high-sulfur coals, as much as 1–2% of the sulfur is converted to  $\text{SO}_3$ , leading to flue gas concentrations in the range of 10–40 ppm (8, 9). High concentrations of  $\text{SO}_3$  in flue gas have long been considered a nuisance because  $\text{SO}_3$  can condense as sulfuric acid ( $\text{H}_2\text{SO}_4$ , the hydrated form of  $\text{SO}_3$ ) and lead to increased corrosion and fouling as well as decreased efficiency (9). (2)  $\text{SO}_3$  is sometimes added to flue gas upstream of an ESP as a conditioning agent and to improve ESP performance.  $\text{SO}_3$  (and  $\text{H}_2\text{SO}_4$ ) has a low vapor

pressure and can condense on fly ash; this reduces the resistivity of the ash and allows it to be removed more efficiently by the ESP (9). (3)  $\text{SO}_2$  can be oxidized to  $\text{SO}_3$  by SCR (Selective Catalytic Reduction) catalysts installed for  $\text{NO}_x$  reduction (7). SCR catalysts typically contain vanadium oxides, which are known catalysts for the oxidation of  $\text{SO}_2$  to  $\text{SO}_3$  (10).

The inhibiting effect of  $\text{SO}_x$  on Hg capture by ACI is a particularly vexing problem for power plants burning high-sulfur bituminous coals; the flue gas generated from this fuel has high concentrations of both  $\text{SO}_2$  (>1000 ppm) and  $\text{SO}_3$  (10–40 ppm). The poisoning effect upon activated carbons is also a concern for power plants injecting sulfur trioxide as a conditioning agent, with resulting flue gas  $\text{SO}_3$  levels sometimes greater than 10 ppm.

In addition to removing mercury, activated carbon can also be used as a catalyst for the oxidation of  $\text{SO}_2$  to sulfuric acid (11, 12) and as an  $\text{SO}_2$  sorbent (13–15). The oxygen source for  $\text{SO}_2$  conversion to sulfuric acid can be either the flue gas or oxygen bound to the activated carbon surface (12). Both mercury and  $\text{SO}_x$  bind to Lewis base (electron-donating) sites on the activated carbon surface (16). Mercury is known to chemically adsorb to activated carbon (16); Huggins et al. showed that mercury exists on carbon surfaces as  $\text{Hg}^{2+}$  bound to a soft atom such as chlorine or carbon (17).  $\text{SO}_2$  can form two different bonds with the carbon surface: a physical bond due to van der Waals forces with a heat of adsorption <50  $\text{kJ mol}^{-1}$  or a chemical bond with a heat of adsorption >80  $\text{kJ mol}^{-1}$  that is stable to temperatures above 200 °C (13, 18).  $\text{SO}_2$  and  $\text{SO}_3$  compete with mercury for adsorption sites on activated carbon; this competition might inhibit mercury capture and limit the effectiveness of ACI. In fact, some activated carbon catalysts for converting  $\text{SO}_2$  to  $\text{H}_2\text{SO}_4$  are self-poisoned by  $\text{SO}_3$  (19) or sulfate (10) buildup on the surface; a similar phenomenon might explain the inhibiting effect of  $\text{SO}_x$  on mercury capture. It has also been postulated that sulfuric acid that forms on the surface of activated carbon does not desorb and therefore inhibits mercury adsorption (16). Furthermore, activated carbon is a catalyst for the formation of sulfurlyl chloride; hence sulfur dioxide may deplete the surface chlorine with a concomitant reduction in mercury capture (20).

In this study we investigate the effect of  $\text{SO}_x$  concentration on the performance of several activated carbons. We also present surface analyses of the tested activated carbons and identify the form of the sulfur on the surface of the carbon. Experiments were conducted with both unpromoted and halogenated activated carbons as well as an unpromoted activated carbon treated with sulfuric acid. The sulfuric acid treated carbon was used to test the hypothesis that sulfuric acid blocks adsorption of mercury on the carbon surface. Potential mechanisms explaining the inhibiting effects of  $\text{SO}_x$  are presented.

### 2. Experimental Procedures

Sorbent samples are exposed to mercury in a bench-scale packed bed reactor that is a larger version of an apparatus described previously (21, 22). The assembly consists of a quartz tube reactor, 22 mm i.d. and 61 cm long, contained in a tube furnace. A 200 mg sorbent bed is placed in the reactor and is supported by approximately 1 g of glass wool. An additional 1 g plug of glass wool is placed above the sorbent bed. The sorbent is exposed to a simulated flue gas (SFG) containing  $\text{N}_2$ ,  $\text{O}_2$ ,  $\text{CO}_2$ ,  $\text{H}_2\text{O}$ ,  $\text{HCl}$ ,  $\text{NO}$ ,  $\text{SO}_2$ ,  $\text{SO}_3$ , and Hg for 6 h (360 min). In this study, we will use 'mercury content'

\* Corresponding author e-mail: evan.granite@netl.doe.gov.

**TABLE 1. Typical Simulated Flue Gas Concentrations for the Experiments Conducted in This Study**

species	concentration
O <sub>2</sub> (%)	5.25
SO <sub>2</sub> (ppm)	0, 500, 1000, 1500, or 1870
NO (ppm)	500
CO <sub>2</sub> (%)	12.5
HCl (ppm)	50
H <sub>2</sub> O (%)	0 or 1.0–1.5
SO <sub>3</sub> (ppm)	0, 20, 50, or 100
Hg (μg Nm <sup>-3</sup> )	9.3

to describe the amount of mercury (μg Hg/g sorbent) captured during the 6 h exposure.

Table 1 details the typical concentrations of the simulated flue gas components used in this study. Under typical experimental conditions, the flow rate of the simulated flue gas is 8 slpm, and the sorbent bed is held at 149 °C. Mercury is provided by a certified Dynacal permeation tube that is held at 90 °C in a water bath. The mercury concentration in the SFG is within the range typically observed in power plant flue gas. A total of 26.8 μg of mercury contacts the activated carbon bed during the 6 h experiment; the maximum mercury content for a 200 mg sample is therefore 134 μg g<sup>-1</sup>. N<sub>2</sub> and O<sub>2</sub> are provided by the plant air and nitrogen supplies; each stream passes through a desiccant trap and a carbon trap prior to entering the process. CO<sub>2</sub>, SO<sub>2</sub>, HCl (2% in N<sub>2</sub>), and NO (5% in N<sub>2</sub>) are supplied from certified gas cylinders. Water vapor is added to the SFG by bubbling N<sub>2</sub> through a water saturator held at 52 °C.

SO<sub>3</sub> is supplied to the system by passing N<sub>2</sub> through a cylindrical saturator containing SO<sub>3</sub>. The saturator is constructed of stainless steel and is cooled by a water/propylene glycol mixture maintained at subambient temperature (–15 to 6.4 °C) by a chiller/circulator. The SO<sub>3</sub> concentration in the SFG is calculated based on the vapor pressure of SO<sub>3</sub>, the exterior temperature of the saturator, and the flow rate of the N<sub>2</sub> carrier gas. When calculating the vapor pressure, we assume that the SO<sub>3</sub> in the saturator exists as the γ phase. Given the uncertainties associated with the SO<sub>3</sub> saturator, specifically the exact value and the stability of the temperature inside of the saturator, we assume that our estimate of the SO<sub>3</sub> concentration in the SFG is accurate within ±20%.

For all experiments, the concentrations of Hg, CO<sub>2</sub>, HCl, and NO are held constant at the values shown in Table 1. The H<sub>2</sub>O concentration is varied between 0% ('dry') and 1.0–1.5% ('wet'). Real flue gas contains higher concentrations of H<sub>2</sub>O than what is present in the SFG; we are limited by our ability to maintain H<sub>2</sub>O as a vapor, particularly in the room-temperature exhaust ductwork, and therefore could not explore typical H<sub>2</sub>O concentrations. Dry SFG is used because the addition of SO<sub>3</sub> significantly lowers the acid dew point and increases the likelihood of corrosion in the system; all experiments containing SO<sub>3</sub> use dry SFG. SO<sub>3</sub>-free experiments are also conducted with dry SFG because previous results indicate that the mercury capacity of activated carbons is dependent upon the moisture content of the SFG (23). The concentrations of the two sulfur species, SO<sub>2</sub> and SO<sub>3</sub>, are varied independently to investigate their impact on mercury capture.

Three different activated carbons were tested in this study: Norit Darco FGD, Norit Darco Hg-LH, and H<sub>2</sub>SO<sub>4</sub>-FGD. Both Darco FGD and Darco Hg-LH, a brominated activated carbon, were used as-received. H<sub>2</sub>SO<sub>4</sub>-FGD was prepared by adding 95% H<sub>2</sub>SO<sub>4</sub> to Darco FGD to incipient wetness. The impregnated carbon was then heated to dryness in an oven at 110 °C.

The mercury (μg g<sup>-1</sup>) and sulfur (%) contents of the activated carbon samples were determined by ICP-AES

(Inductively Coupled Plasma–Atomic Emission Spectroscopy). The activated carbons were first digested by adding a 0.1 g sample to 10 mL of nitric acid and 2 mL of 30% H<sub>2</sub>O<sub>2</sub>. When the effervescence subsided, 5 mL of DI water was added, and the mixture was digested in a microwave at 230 °C for 30 min. These samples were then brought to volume with water and analyzed. All solutions were dark-particulate free; a few did have minute amounts of light precipitate present, but since no HF was used, aluminosilicate materials were not digested. In some cases, the undigested activated carbon was also analyzed using a DMA-80 Direct Mercury Analyzer. The ICP-AES and DMA-80 results agreed to within ±10%. Surface compositions of several samples of both fresh and Hg-exposed activated carbon were also analyzed using XPS (X-ray Photoelectron Spectroscopy). During the experiments, the concentrations of gas-phase species were monitored by an online mass spectrometer.

Table 2 details the experiments conducted in this study. The experiment name is derived from the activated carbon used ('F' for FGD, 'LH' for Hg-LH, and 'SA' for H<sub>2</sub>SO<sub>4</sub>-FGD), the SO<sub>2</sub> concentration (0, 500, 1000, 1500, or 1870 ppm), the SO<sub>3</sub> concentration (0, 20, 50, or 100 ppm), and the moisture content ('d' for dry and 'w' for wet). For example, in experiment LH-500-0-w, 200 mg of Hg-LH was exposed to a wet SFG containing 500 ppm SO<sub>2</sub> and no SO<sub>3</sub>. Experiments were also conducted where the activated carbon sample was pre-exposed to SO<sub>3</sub> prior to mercury exposure. In experiment LH50-0-0-d, for example, the activated carbon sample was exposed to a mixture of 50 ppm SO<sub>3</sub> in N<sub>2</sub>, O<sub>2</sub>, and CO<sub>2</sub> (with HCl, SO<sub>2</sub>, and NO turned off) for 1 h prior to adding mercury and the other trace species to the SFG. Table 2 also lists the mercury (μg g<sup>-1</sup>) and sulfur (%) content of the exposed carbons as well as the mass fraction of the incident sulfur captured by the carbons. The mercury and sulfur contents of the unused activated carbons are included for reference.

All of the error bars plotted in this manuscript show the 1-σ level of precision, which is approximately ±25% for mercury content measurements and ±10% for sulfur content measurements. The large uncertainty in the mercury data arises from several sources. The uncertainty associated with the ICP-AES measurement is approximately ±10%. The mercury output from the permeation tube has an uncertainty of at least ±6%. The activated carbon samples are 200 mg of grab samples taken from a 5-lb bucket, which itself is taken from a much larger production batch of activated carbon. Thus, the possibility exists for using activated carbon samples that are not representative of the bulk material. When the activated carbon is placed into the packed bed, care is taken to produce a bed with uniform thickness. However, it is nearly impossible to produce a perfectly uniform bed. Several experiments were conducted with intentionally uneven packed beds; this resulted in significantly decreased mercury capture. Thus, we assume that the small, inherent variations in bed thickness can affect changes in the mercury content.

Results from full-scale field studies also indicate significant variability in mercury capture efficiency during ACI. Specifically, during long term injection tests, individual measurements of mercury capture efficiency (time scale of minutes – hours) can differ significantly from the long-term results (time scale of months) (4). When all of the potential sources of experimental uncertainty are considered, it is our opinion that the precision presented for the mercury capture data is appropriate for our experimental system and is consistent with previous work from this laboratory (21).

### 3. Results

**3.1. SO<sub>3</sub>-Free Experiments.** During SO<sub>3</sub>-free experiments, the SO<sub>2</sub> concentration was varied from 0 to 1870 ppm to investigate the effect of SO<sub>2</sub> on mercury capture. Figure 1

TABLE 2. Experiments Conducted in This Study

experiment	Hg content <sup>a</sup> ( $\mu\text{g g}^{-1}$ )	S content <sup>a</sup> (%)	fraction S captured <sup>b</sup> (%)	experiment	Hg content ( $\mu\text{g g}^{-1}$ )	S content (%)	fraction S captured (%)
F-1870-0-d	84.8	2.00	0.022	LH-0-20-d	12.2	3.00	5.2
F-1500-0-d	60.6	1.74	0.020	LH-0-50-d	6.13	7.04	6.0
F-1000-0-d	72.9	1.75	0.030	LH-0-100-d	4.59	8.56	3.7
F-500-0-d	81.0	1.54	0.038	LH50-0-0-d	9.26	2.36	8.8
F-0-0-d	71.3	1.28	N/A	LH50-0-50-d	4.70	5.69	4.0
F-1870-0-w	54.1	2.58	0.038	LH-1870-20-d	8.86	4.47	0.093
F-1500-0-w	45.3	2.45	0.042	LH-1870-50-d	7.55	5.19	0.11
F-500-0-w	39.3	2.82	0.16	LH-1870-100-d	4.17	8.50	0.19
F-0-0-w	54.8	1.19	N/A	LH50-1870-0-d	14.3	5.30	0.14
LH-1870-0-d	68.1	2.56	0.044	LH50-1870-50-d	4.61	7.35	0.16
LH-1500-0-d	42.7	2.25	0.044	F-0-20-d	16.5	1.83	1.7
LH-1000-0-d	50.0	2.04	0.058	F-0-50-d	20.0	2.11	0.95
LH-500-0-d	50.1	1.61	0.072	F-0-100-d	15.6	4.47	1.6
LH-0-0-d	58.4	0.69	N/A	F-1870-50-d	8.66	4.50	0.085
LH-1870-0-w	35.4	3.66	0.072	F-1870-100-d	4.52	6.00	0.12
LH-1500-0-w	33.2	3.34	0.080	SA-0-0-d	4.13	10.6	N/A
LH-1000-0-w	41.9	3.39	0.12	Raw FGD	3.04	0.92	N/A
LH-500-0-w	25.2	2.40	0.15	Raw Hg-LH	0.02	0.72	N/A
LH-0-0-w	41.3	1.16	N/A				

<sup>a</sup> The Hg and S contents were determined by ICP-AES. The maximum possible Hg content is  $134 \mu\text{g g}^{-1}$ . <sup>b</sup> The mass fraction of sulfur captured by the carbons assumes that the initial sulfur contents for Darco FGD and Hg-LH are 1.13% and 0.86%, respectively. These values represent the arithmetic mean of the sulfur content for the virgin material and the final sulfur content for the experiments that used neither  $\text{SO}_2$  nor  $\text{SO}_3$ . In the absence of  $\text{SO}_3$  a small fraction of the incident sulfur, typically less than 0.1%, was captured by the activated carbons. The maximum fractional capture of sulfur occurred in experiments that used  $\text{SO}_3$  but not  $\text{SO}_2$ . When  $\text{SO}_2$  and  $\text{SO}_3$  were both present,  $\text{SO}_3$  was captured preferentially, and the fractional sulfur capture was lowered relative to the  $\text{SO}_3$ -only case by the large concentration of  $\text{SO}_2$ .

shows the mercury capture results for Darco FGD and Hg-LH. A statistically significant relationship between  $\text{SO}_2$  concentration and mercury content is not apparent for either activated carbon under wet or dry conditions.

For both FGD and Hg-LH, the mercury content was ~50% higher in dry SFG than wet SFG. The decrease in mercury content in wet SFG is consistent with previous results presented by Yan et al. (23). Darco FGD captured approximately 40% more mercury than Hg-LH in both wet and dry SFG. This result contradicts results from several full-scale tests of ACI, where brominated carbons consistently outperform unpromoted activated carbons such as FGD (3, 5). These results suggest that, with excellent gas-solid contact provided by a packed-bed reactor, unpromoted carbons display good capacity for mercury and bromine promotion does not increase capacity. This is in contrast to the situation found during in-flight capture of mercury within the ductwork of a power plant; in this situation gas-solid contact is poor.

In addition to capturing mercury, the activated carbons also captured  $\text{SO}_2$ . Figure 2 shows the sulfur captured as a function of  $\text{SO}_2$  concentration in the SFG. Hg-LH typically captured more sulfur than FGD under similar (i.e., wet or dry) conditions, and more sulfur was captured in wet SFG than dry SFG.

XPS data indicated that the sulfur on the activated carbon surface was primarily sulfate. The sulfur present in a raw sample of Hg-LH was 87% sulfate, with the remainder present as elemental sulfur. Exposure of Hg-LH samples to SFG containing 500, 1000, and 1870 ppm of  $\text{SO}_2$  resulted in the surface sulfur being at least 97% sulfate. The large fraction of sulfate is consistent with the role of activated carbon as a catalyst for the oxidation of  $\text{SO}_2$  to sulfuric acid (11, 12). The larger amount of sulfur captured in the wet SFG may result from enhanced production of sulfuric acid in the presence of water.

**3.2. Experiments Containing  $\text{SO}_3$ .** We explored two routes of  $\text{SO}_3$  exposure for the activated carbon samples: varying the  $\text{SO}_3$  concentration in the SFG from 20 to 100 ppm and pre-exposing the activated carbon to 50 ppm  $\text{SO}_3$  for 1 h

prior to mercury exposure. Table 2 shows the mercury and sulfur contents for activated carbons exposed to  $\text{SO}_3$  and mercury.  $\text{SO}_3$  exposure led to higher final sulfur contents than were observed in  $\text{SO}_3$ -free SFG. Adding 20 ppm  $\text{SO}_3$  to dry SFG produced a final sulfur content of 3% for Darco Hg-LH; in contrast, the maximum sulfur content observed for Hg-LH in dry  $\text{SO}_3$ -free SFG was 2.5%. The higher sulfur content after exposure to  $\text{SO}_3$  is expected;  $\text{SO}_3$  has a significantly lower vapor pressure than  $\text{SO}_2$  and should be captured more efficiently by sorbents such as activated carbon.

Adding  $\text{SO}_3$  to the SFG significantly reduced the final mercury content of the activated carbon samples. The addition of 20 ppm  $\text{SO}_3$  to the SFG reduced mercury capture by nearly 80%, and higher  $\text{SO}_3$  concentrations led to further reductions in mercury capture. This observation is consistent with the effect of  $\text{SO}_3$  on ACI observed during full-scale field tests (2). Recent results also indicate that very low concentrations of  $\text{SO}_3$  (<2 ppm) adversely impact the performance of ACI for mercury control (24). The effect of  $\text{SO}_3$  on mercury capture presented here may be exaggerated relative to ACI because of the excellent gas-solid contact provided by the packed bed reactor.

As with the  $\text{SO}_3$ -free experiments, the  $\text{SO}_2$  concentration in the SFG does not have a strong effect on the final mercury content. For example, the final mercury content is nearly identical for experiments LH-0-100-d (no  $\text{SO}_2$  and 100 ppm  $\text{SO}_3$ ) and LH-1870-100-d (1870 ppm  $\text{SO}_2$  and 100 ppm  $\text{SO}_3$ ). It is evident from the data that  $\text{SO}_3$  has a stronger inhibiting effect on mercury capture than  $\text{SO}_2$ ; possible explanations for the effect of  $\text{SO}_3$  on mercury capture by activated carbon are discussed in the next section.

#### 4. Discussion

We consider two hypotheses to explain the inhibition of mercury capture by sulfur oxides: (1) depletion of surface chlorine through the formation of sulfonyl chloride (20) and (2) competitive adsorption between sulfur oxides, particularly  $\text{SO}_3$  and Hg (25, 26).

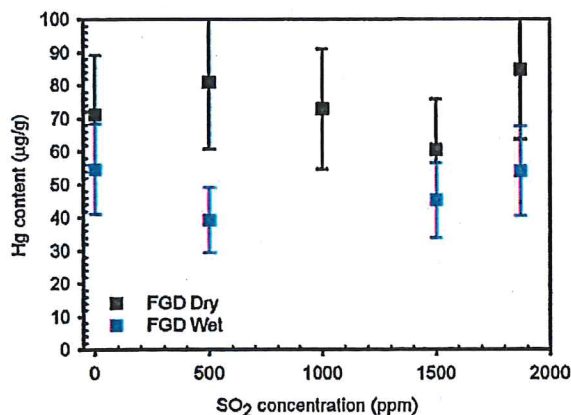
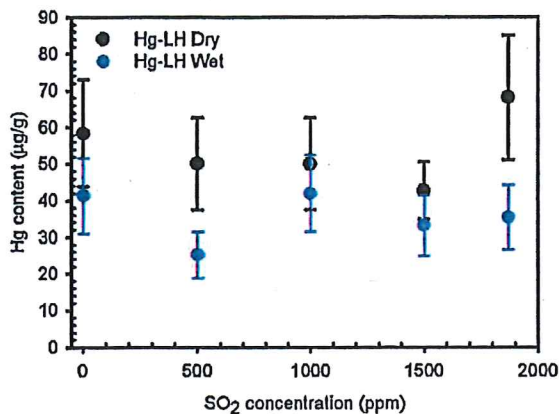


FIGURE 1. Mercury content ( $\mu\text{g g}^{-1}$ ) as a function of  $\text{SO}_2$  concentration for Darco FGD and Hg-LH under wet and dry SFG conditions. Error bars show the  $1\text{-}\sigma$  level of confidence. Hg content is independent of the  $\text{SO}_2$  concentration and reduced in the presence of water vapor.

The loss of surface chlorine via the formation of sulfuryl chloride could reduce mercury capture by altering the surface composition of the activated carbon. Halogenated (i.e., brominated or iodated) activated carbons are typically better mercury adsorbents than nonhalogenated activated carbons; (16) removing halogens from the surface could therefore negatively impact mercury capture. The presence of sulfuryl chloride or other flue gas halides, such as phosgene, in the SFG downstream of the packed bed would serve as a possible indication of mercury capture inhibition by this mechanism. Online mass spectrometer data show no presence of flue gas halides, but this does not rule out their formation. Flue gas halides are easily hydrolyzed and may be removed from the SFG via reaction with water prior to reaching the mass spectrometer (27).

Removal of surface halogens is unlikely to produce the profound drop in mercury capture efficiency observed during ACI testing. XPS analysis of both fresh and used Hg-LH shows no drop in surface chlorine or bromine concentrations due to exposure to SFG, and online mass spectrometer data do not indicate a change in  $\text{SO}_2$  concentration across the packed bed. Furthermore, the inhibiting effect of sulfur oxides on mercury capture by ACI has been observed for both halogenated and nonhalogenated activated carbons (1). While sulfuryl chloride formation may be catalyzed in the packed bed, the reaction is slow at the temperature used here (149 °C) (20). Thus, the extent of reaction, and therefore the impact on mercury capture, is low.

Inhibition of mercury capture because of competitive adsorption could occur because activated carbon is a catalyst

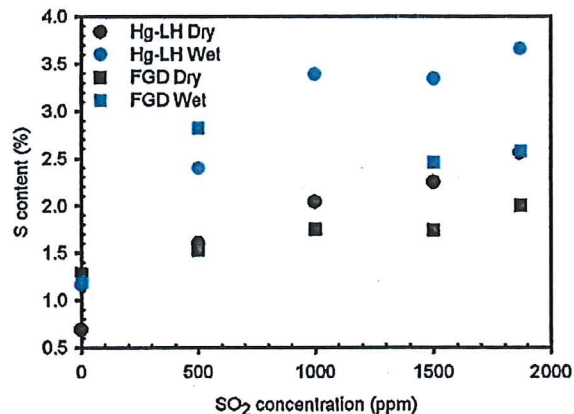


FIGURE 2. Sulfur content (%) as a function of  $\text{SO}_2$  concentration for Darco FGD and Hg-LH under wet and dry SFG conditions. The mass fraction of the sulfur captured by the carbon is less than 0.2% in all cases.

for the oxidation of  $\text{SO}_2$  to sulfuric acid or through adsorption of  $\text{SO}_3$  (which can hydrolyze to sulfuric acid).  $\text{SO}_2$  and  $\text{SO}_3$  compete with mercury for the same adsorption sites, specifically Lewis base sites, on the carbon surface. In flue gas, adsorption of  $\text{SO}_2$  or  $\text{SO}_3$  could be favored over mercury adsorption both kinetically and thermodynamically. Mercury concentrations in flue gas are typically  $\sim 1$  ppb; this is orders of magnitude smaller than typical concentrations of  $\text{SO}_2$  and  $\text{SO}_3$ , both of which are present at ppm levels. This concentration difference means that many more  $\text{SO}_x$  molecules collide with the surface of the activated carbon, thereby enhancing the adsorption of sulfur oxides versus mercury. Fast capture of  $\text{SO}_2$  or  $\text{SO}_3$  could exhaust the sites available for mercury capture and thereby inhibit mercury adsorption.

The XPS results presented earlier indicate that the sulfur on the activated carbon surface is present almost exclusively as sulfate. Sulfuric acid has a low vapor pressure, approximately 1 Torr at 150 °C (28), and is therefore unlikely to desorb from the activated carbon surface. Surface S(VI) can form from the direct adsorption of  $\text{SO}_3$  or from the oxidation of chemically bound  $\text{SO}_2$ .  $\text{SO}_2$  can form a strong bond with the carbon surface, with a heat of adsorption  $> 80$  kJ mol<sup>-1</sup> (13, 18). Miller et al. (29) observed that exposing mercury-laden activated carbon to  $\text{SO}_2$ , with  $\text{NO}_2$  present as an electron sink for  $\text{SO}_2$  oxidation, caused the mercury to desorb from the surface with a concomitant increase in surface S(VI) concentration (30). From this observation we can infer that the bond formed between S(VI) and the carbon surface is stronger than the bond formed between mercury and the surface. Thus, under conditions of either high  $\text{SO}_3$  concentration or oxidizing conditions for converting  $\text{SO}_2$  to sulfuric acid, mercury capture could be inhibited by competition with  $\text{SO}_3$  adsorption and/or  $\text{SO}_2$  oxidation.

According to the data presented in Figure 1, the  $\text{SO}_2$  concentration in the SFG does not appear to impact mercury capture by the activated carbons tested here. However, this fact alone does not disprove the hypothesis that sulfur oxides outcompete mercury for adsorption sites on the carbon surface. If mercury competes with S(VI) for binding sites on the activated carbon surface, then the S(VI) concentration of the activated carbon, and not the  $\text{SO}_2$  concentration in the SFG, is the important variable. We tested an extreme case of sulfur uptake with  $\text{H}_2\text{SO}_4$ -FGD, an activated carbon sample prepared by soaking FGD in 95%  $\text{H}_2\text{SO}_4$ . As shown in Table 2,  $\text{H}_2\text{SO}_4$ -FGD had a sulfur content of 10.6% and had a mercury content after exposure to SFG ( $4.13 \mu\text{g g}^{-1}$ ) similar to the raw FGD ( $3.04 \mu\text{g g}^{-1}$ ). This test suggested that high concentrations of surface-bound sulfur inhibit mercury capture, perhaps because of competition for binding sites.

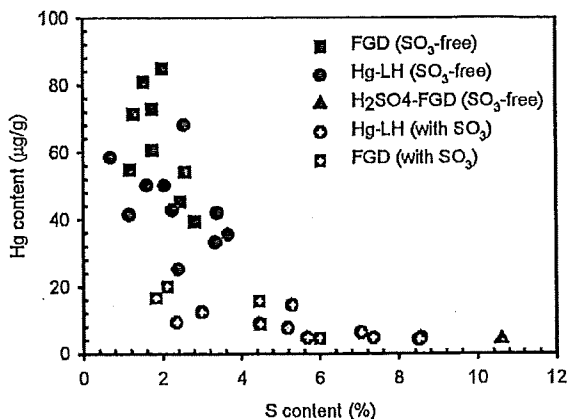


FIGURE 3. Mercury content ( $\mu\text{g g}^{-1}$ ) as a function of sulfur content (%) for all of the experiments presented in this study. Mercury content decreases with increasing sulfur content, and almost no mercury is captured at the highest sulfur content (10.6%) tested here.

Figure 3 shows that, for all of the experiments presented here, the mercury content decreases as sulfur content increases. It should be noted that Figure 3 convolves the effects of sulfur content and water vapor concentration; as shown in Figure 1, the mercury content is reduced in wet flue gas even when no sulfur is present in the SFG. Regardless, the data shown in Figure 3 are strong evidence for the direct competition between mercury and sulfur for binding sites on the carbon surface.

The data in Figure 3 suggest that  $\text{SO}_3$  has a stronger impact on mercury capture than  $\text{SO}_2$ . For example, at 3% S, approximately  $40 \mu\text{g g}^{-1}$  of Hg was captured in  $\text{SO}_3$ -free SFG, compared to  $\sim 10 \mu\text{g g}^{-1}$  in  $\text{SO}_3$ -laden SFG. A possible explanation for the enhanced effect of  $\text{SO}_3$  may be the form of sulfur present on the activated carbon surface. As noted previously,  $\text{SO}_2$  can form two different bonds with the carbon surface: a physical bond due to van der Waals forces with a heat of adsorption  $< 50 \text{ kJ mol}^{-1}$  or a chemical bond with a heat of adsorption  $> 80 \text{ kJ mol}^{-1}$  (13, 18). XPS results indicate that  $> 97\%$  of the sulfur captured in  $\text{SO}_3$ -free SFG is sulfate, suggesting the stronger, chemical bond. However, the surface concentration of sulfur measured by XPS is significantly lower than the bulk sulfur content determined by digesting the activated carbon in solution; the latter quantity is shown in Table 2 and Figure 3. One possible explanation for the discrepancy in sulfur concentration may be that a significant portion of the sulfur captured in the  $\text{SO}_3$ -free SFG is physically bound; the physically bound sulfur would be measured by the solution method but could desorb from the activated carbon surface under the vacuum conditions used for XPS. We assume that the  $\text{SO}_3$ , which is already oxidized to S(VI), exists on the activated carbon surface exclusively in the chemically bound form.

Previous research has suggested that sulfate competes with mercury for binding sites on the activated carbon surface (25, 26). Currently, it is not clear whether physically bound sulfur interferes with mercury capture by activated carbon, though it likely has a weaker effect than chemically bound sulfur, if there is any effect at all. Thus, the presence of physically bound sulfur from the  $\text{SO}_3$ -free SFG could explain the discrepancy between  $\text{SO}_3$ -free and  $\text{SO}_3$ -containing experiments in Figure 3. The current hypothesis is that all of the sulfur captured from the  $\text{SO}_3$ -laden SFG is chemically bound and therefore inhibits mercury capture, whereas a portion of the sulfur captured from  $\text{SO}_3$ -free SFG is physically bound and does not inhibit mercury capture.

It is important to note that both routes of exposing the activated carbon to  $\text{SO}_3$ , whether as a constituent of the SFG

or pre-exposing the sorbent, lead to significant reductions in mercury capture. This result further indicates that mercury and  $\text{SO}_3$  compete for the same adsorption sites on the activated carbon surface and suggests that  $\text{SO}_3$  adsorption is favored both kinetically and thermodynamically to mercury adsorption. Adding  $\text{SO}_3$  to the SFG, and placing it in direct competition with mercury for adsorption sites on the activated carbon surface, leads to reduced mercury capture. Similarly, the pre-exposure experiments as well as the experiment with the  $\text{H}_2\text{SO}_4$  treated activated carbon show that mercury cannot dislodge sulfur species from the activated carbon surface.

The competition between  $\text{SO}_x$ , particularly  $\text{SO}_3$ , and mercury for binding sites on the surface of activated carbon will likely limit the effectiveness of ACI for mercury removal in any high- $\text{SO}_x$  flue gas. Recent research has led to the development of chemical alterations, notably bromination, that enhances the mercury capture efficiency by increasing the reactivity of the activated carbon. However, as shown here and in previous studies (1),  $\text{SO}_3$  impedes mercury capture by brominated carbons as well as unpromoted activated carbons. This occurs because bromination increases the reactivity of the mercury-accepting sites; thus bromination also makes the activated carbons more reactive toward sulfur oxides, as shown in Figure 2.

Potential options for overcoming the impact of  $\text{SO}_x$  on ACI include removing sulfur species prior to carbon injection, removing  $\text{SO}_x$  and mercury concurrently by injecting basic sorbents (i.e., hydrated lime) along with activated carbon (24), or in cases where  $\text{SO}_3$  is used for flue gas conditioning, injecting the carbon upstream of the  $\text{SO}_3$ . Each of these approaches has advantages and disadvantages. Removing  $\text{SO}_x$ , specifically  $\text{SO}_3$ , prior to carbon injection should improve the efficiency of ACI. However, including flue gas desulfurization upstream of ACI poses potential logistical challenges and may increase the cost of an ACI retrofit. Injecting activated carbon upstream of  $\text{SO}_3$  has been shown to improve mercury capture in plants using  $\text{SO}_3$  flue gas conditioning (4), but the mercury capture efficiency in this configuration still lags behind the  $\text{SO}_3$ -free case. This is due in part to the higher temperature upstream of the  $\text{SO}_3$  injection point. The development of alternative fly ash conditioning agents may also merit further research.

#### Acknowledgments

The authors thank Robert Thompson of Parsons Project Services, Inc. for ICP-AES and DMA analyses of the carbon samples. John Baltrus of the Department of Energy provided XPS surface analysis of the carbons. Albert Presto acknowledges the support of a postdoctoral fellowship at the U.S. Department of Energy administered by the Oak Ridge Institute for Science and Education (ORISE). Funding support from the DOE Innovations for Existing Power Plants (IEP) Program is greatly appreciated. References in this paper to any specific commercial product, process, or service is to facilitate understanding and does not necessarily imply its endorsement by the U.S. Department of Energy.

#### Literature Cited

- (1) Sjostrom, S.; Wilson, C.; Bustard, J.; Spitznogle, G.; Toole, A.; O'Palko, A.; Chang, R. Full-scale evaluation of carbon injection for mercury control at a unit firing high sulfur coal. In *Proceedings of the U.S. Environmental Protection Agency - Department of Energy - EPRI Combined Power Plant Air Pollutant Control Symposium: The MEGA Symposium*; U.S. EPA - DOE - EPRI: 2006.
- (2) Berry, M.; Semmes, R.; Campbell, T.; Glesman, S.; Glesman, R. Impact of coal blending and  $\text{SO}_3$  flue gas conditions on mercury removal with activated carbon injection at Mississippi Power's Plant Daniel. In *Proceedings of the U.S. Environmental Protection Agency - Department of Energy - EPRI Combined Power Plant*

- Air Pollutant Control Symposium: The MEGA Symposium*; U.S. EPA - DOE - EPRI: 2006.
- (3) Nelson, S.; Landreth, R.; Zhou, Q.; Miller, J. Accumulated power-plant mercury-removal experience with brominated PAC injection. In *Proceedings of the U.S. Environmental Protection Agency - Department of Energy - EPRI Combined Power Plant Air Pollutant Control Symposium: The MEGA Symposium*; U.S. EPA - DOE - EPRI: 2004.
  - (4) Nelson, S. *Brominated sorbents for small cold-side ESPs, hot-side ESPs, and fly ash use in concrete*; Report to U.S. DOE/NETL, Cooperative Agreement No. DE-FC26-05NT42308; Sorbent Technologies Corporation: 2006.
  - (5) Sjostrom, S. *Evaluation of sorbent injection for mercury control. Topical Report for: Sunflower Electric's Holcomb Station*; Report to U.S. DOE/NETL, Cooperative Agreement No. DE-FC26-03NT41986; ADA-ES: 2005.
  - (6) Kang, S. *Field demonstration of enhanced sorbent injection for mercury control*; Report to U.S. DOE/NETL, Cooperative Agreement No. DE-FC26-04NT42306; Alstom Power, Inc.: 2006.
  - (7) Srivastava, R.; Miller, C.; Erickson, C.; Jambhekar, R. Emissions of sulfur trioxide from coal-fired power plants. *J. Air Waste Manage. Assoc.* 2004, 54, 750.
  - (8) Johnstone, H. Reactions of sulfur compounds in boiler furnaces. *Ind. Eng. Chem.* 1931, 23, 620.
  - (9) Moser, R. SO<sub>2</sub>'s impact on plant O&M: Part I. *Power* 2006, 150, 40.
  - (10) Halstead, J.; Armstrong, R.; Pohlman, B.; Sibley, S.; Maier, R. Nonaqueous heterogeneous oxidation of sulfur dioxide. *J. Phys. Chem.* 1990, 94, 3261.
  - (11) Lizzio, A.; DeBarr, J. Mechanism of SO<sub>2</sub> removal by carbon. *Energy Fuels* 1997, 11, 284.
  - (12) Yang, F.; Yang, R. Ab initio molecular orbital study of the mechanism of SO<sub>2</sub> oxidation catalyzed by carbon. *Carbon* 2003, 41, 2149.
  - (13) Raymundo-Pinero, E.; Cazorla-Amoros, D.; Salinas-Martinez de Lecea, C.; Linares-Solano, A. Factors controlling the SO<sub>2</sub> removal by porous carbons: Relevance of the SO<sub>2</sub> oxidation step. *Carbon* 2000, 38, 335.
  - (14) Davini, P. SO<sub>2</sub> adsorption by activated carbons with various burnoffs obtained from a bituminous coal. *Carbon* 2001, 39, 1387.
  - (15) Qiang, T.; Zhigang, Z.; Wenpei, Z.; Zidong, C. SO<sub>2</sub> and NO selective adsorption properties of coal-based activated carbons. *Fuel* 2005, 84, 461.
  - (16) Ralston, N.; Olson, E.; Wocken, C. *Mercury Information Clearinghouse Quarter 5 - Mercury Fundamentals*; Technical Report; Canadian Electric Association: 2005.
  - (17) Huggins, F.; Yap, N.; Huffman, G.; Senior, C. XAFS characterization of mercury captured from combustion gases on sorbents at low temperatures. *Fuel Proc. Technol.* 2003, 82, 167.
  - (18) Anurov, S. Physicochemical aspects of the adsorption of sulfur dioxide by carbon adsorbents. *Russ. Chem. Rev.* 1996, 65, 663.
  - (19) Siedlewski, J. The mechanism of catalytic oxidation on activated carbon. The influence of free carbon radicals on the adsorption of SO<sub>2</sub>. *Int. Chem. Eng.* 1965, 5, 297.
  - (20) Cicha, W.; Manzer, L. Process for producing oxochlorides of sulfur. U.S. Patent No. 5,879,652, 1999.
  - (21) Granite, E.; Pennline, H.; Hargis, R. Novel sorbents for mercury removal from flue gas. *Ind. Eng. Chem. Res.* 2000, 39, 1020.
  - (22) Presto, A.; Granite, E.; Karash, A.; Hargis, R.; O'Dowd, W.; Pennline, H. A kinetic approach to the catalytic oxidation of mercury in flue gas. *Energy Fuels* 2006, 20, 1941.
  - (23) Yan, R.; Ng, Y.; Liang, D.; Lim, C.; Tay, J. Bench-scale experimental study on the effect of flue gas composition on mercury removal by activated carbon adsorption. *Energy Fuels* 2003, 17, 1528.
  - (24) Dombrowski, K. Sorbent injection for small ESP mercury control. In *Proceedings of the 2006 Mercury Control Technology Conference*; 2006. www.netl.doe.gov (accessed March 2007).
  - (25) Dunham, G.; Olson, E.; Miller, S. Impact of flue gas constituents on carbon sorbents. In *Proceedings of the Air Quality II: Mercury, Trace Elements, and Particulate Matter Conference*; 2000.
  - (26) Olson, E.; Crocker, C.; Benson, S.; Pavlish, J.; Holmes, M. Surface compositions of carbon sorbents exposed to simulated low-rank coal flue gases. *J. Air Waste Manage. Assoc.* 2005, 55, 747.
  - (27) Hatakeyama, S.; Leu, M.-T. Rate constants for reactions between atmospheric reservoir species. 2. H<sub>2</sub>O. *J. Phys. Chem.* 1989, 93, 5784.
  - (28) Seinfeld, J. H.; Pandis, S. *Atmospheric Chemistry and Physics*; John Wiley & Sons, Inc.: 1998.
  - (29) Miller, S.; Dunham, G.; Olson, E.; Brown, T. Flue gas effects on a carbon-based mercury sorbent. *Fuel Proc. Technol.* 2000, 65-66, 343.
  - (30) Laumb, J.; Benson, S.; Olson, E. X-ray photoelectron spectroscopy analysis of mercury sorbent surface chemistry. *Fuel Proc. Technol.* 2004, 85, 577.

Received for review April 9, 2007. Revised manuscript received July 5, 2007. Accepted July 9, 2007.

ES0708316



PERGAMON

Carbon 40 (2002) 65–72

CARBON

## The effect of activated carbon surface moisture on low temperature mercury adsorption

Y.H. Li, C.W. Lee, B.K. Gullett\*

US Environmental Protection Agency, National Risk Management Research Laboratory (MD-65), Research Triangle Park, NC 27711, USA

Received 25 May 2000; accepted 2 March 2001

### Abstract

Experiments with elemental mercury ( $\text{Hg}^0$ ) adsorption by activated carbons were performed using a bench-scale fixed-bed reactor at room temperature ( $27^\circ\text{C}$ ) to determine the role of surface moisture in capturing  $\text{Hg}^0$ . A bituminous-coal-based activated carbon (BPL) and an activated carbon fiber (ACN) were tested for  $\text{Hg}^0$  adsorption capacity. About 75–85% reduction in  $\text{Hg}^0$  adsorption was observed when both carbon samples' moisture (~2 wt.% as received) was removed by heating at  $110^\circ\text{C}$  prior to the  $\text{Hg}^0$  adsorption experiments. These observations strongly suggest that the moisture contained in activated carbons plays a critical role in retaining  $\text{Hg}^0$  under these conditions. The common effect of moisture on  $\text{Hg}^0$  adsorption was observed for both carbons, despite extreme differences in their ash contents. Temperature programmed desorption (TPD) experiments performed on the two carbons after adsorption indicated that chemisorption of  $\text{Hg}^0$  is a dominant process over physisorption for the moisture-containing samples. The nature of the mercury bonding on carbon surface was examined by X-ray absorption fine structure (XAFS) spectroscopy. XAFS results provide evidence that mercury bonding on the carbon surface was associated with oxygen. The results of this study suggest that surface oxygen complexes provide the active sites for mercury bonding. The adsorbed  $\text{H}_2\text{O}$  is closely associated with surface oxygen complexes and the removal of the  $\text{H}_2\text{O}$  from the carbon surface by low-temperature heat treatment reduces the number of active sites that can chemically bond  $\text{Hg}^0$  or eliminates the reactive surface conditions that favor  $\text{Hg}^0$  adsorption. © 2002 Elsevier Science Ltd. All rights reserved.

**Keywords:** A. Activated carbon; C. Adsorption; Temperature programmed desorption (TPD); D. Adsorption properties; Surface oxygen complexes

### 1. Introduction

The emissions of mercury from coal combustion and waste incineration are a great environmental health concern. Coal combustion is considered the primary source of anthropogenic mercury emissions in the United States [1]. The control of mercury emissions is strongly dependent on the form of mercury emitted. Mercury in the flue gases emitted from municipal waste combustors (MWCs) has been found mainly in the form of mercuric chloride ( $\text{HgCl}_2$ ) due to the relatively high hydrogen chloride

(HCl) concentrations in MWC flue gases [2]. A major portion of the mercury emitted from many coal-fired power plants is in the elemental form ( $\text{Hg}^0$ ). Both  $\text{Hg}^0$  and  $\text{HgCl}_2$  exist as vapor at flue gas cleaning device operating temperatures. It is also known that  $\text{Hg}^0$  is more difficult to capture than its oxidized form, due to its higher volatility and insolubility in water [3].

Activated carbons are widely used in the removal of pollutants from water and gases. Direct injection of an activated carbon into the flue gas stream has been used as a relatively simple approach for controlling mercury emissions. Although research has been performed to study the adsorption of mercury by activated carbons, current knowledge on mercury adsorption by activated carbons is limited, presenting intriguing scientific questions related to the nature of the adsorption (physisorption or chemisorp-

\*Corresponding author. Tel.: +1-919-541-1534; fax: +1-919-541-0554.

E-mail address: gullett.brian@epa.gov (B.K. Gullett).

tion) and the effects of mercury species type in the gas and solid phases.

Adsorption of  $\text{Hg}^0$  by activated carbons at ambient temperatures (e.g. 23°C) has been suggested to be a combination of chemisorption and physisorption, whereas chemisorption is prevalent at higher temperatures; e.g. 140°C [4]. The  $\text{Hg}^0$  adsorption capacity of activated carbons decreases with increasing temperature and decreasing mercury concentration [4–6]. Many factors have been found to influence the efficiency of mercury removal, including carbon characteristics, flue gas composition, and the presence of active components (e.g. fly ash) [7]. The low concentrations of  $\text{Hg}^0$  in the flue gases ( $\sim 10 \mu\text{g}/\text{m}^3$ ) and short residence times ( $< 3 \text{ s}$ ) of the sorbent require injection of a large amount of activated carbon (high carbon/ $\text{Hg}^0$  ratio) in order to achieve adequate mercury removal [3,8].

Studies have shown that sulfur-impregnated activated carbons exhibit significantly greater  $\text{Hg}^0$  adsorption capacities compared to those of the thermally activated carbons [4–6,9–11]. However, heteroatoms such as sulfur (S) and chlorine (Cl), which are reactive for  $\text{Hg}^0$  capture, generally exist only as trace elements in activated carbons. On the other hand, appreciable amounts of oxygen (O) are almost invariably associated with activated carbons in the form of surface carbon–oxygen complexes produced from the activation process. Carbon–oxygen surface complexes are by far the most important structures influencing the surface characteristics and adsorption properties of activated carbons [12]. So far, no known research has been done to understand the role of carbon–oxygen surface complexes in  $\text{Hg}^0$  adsorption.

Krishnan et al. [4] showed that  $\text{Hg}^0$  capture capacities of the heat-treated (140°C, flowing nitrogen ( $\text{N}_2$ )) activated carbon samples were far less than those of unheated samples. In addition, the same heat treatment applied to a sulfur-impregnated carbon showed no significant reduction of  $\text{Hg}^0$  capture capacity. Based on these observations, they suggested that the active sites causing  $\text{Hg}^0$  adsorption in the activated carbons containing O, and the reduction of  $\text{Hg}^0$  capture capacity for the heat-treated carbons was due to the decomposition of certain surface functional groups. However, it is generally agreed that carbon–oxygen surface complexes are stable below 200°C [12], but decompose to produce  $\text{H}_2\text{O}$ , carbon dioxide ( $\text{CO}_2$ ), and carbon monoxide (CO) when heated to higher temperatures under an inert gas atmosphere. The major effect of heat treatment at low temperatures (e.g. 25–150°C) on carbon surfaces is the removal of adsorbed  $\text{H}_2\text{O}$  molecules [13]. Thus, the reduction of  $\text{Hg}^0$  capture from low temperature heat treatment, as observed by Krishnan et al. [4], could likely be caused by the removal of moisture from the carbon surfaces.

Oxygen complexes formed on the carbon surfaces may play an important role for  $\text{Hg}^0$  adsorption. Extensive studies on water adsorption by activated carbons found that

$\text{H}_2\text{O}$  is adsorbed on the carbon surfaces by means of hydrogen bonding [14–18]. Bansal et al. [18] showed that  $\text{H}_2\text{O}$  adsorption at lower relative pressures (e.g.  $P/P_0 < 0.4$ ) was correlated directly to the amounts of chemisorbed O on the carbon surfaces. The oxygen complexes on carbon surfaces form primary adsorption centers, which bind the  $\text{H}_2\text{O}$  molecules at low relative pressures. Adsorbed  $\text{H}_2\text{O}$  molecules can then become secondary adsorption centers as the  $\text{H}_2\text{O}$  vapor pressure increases. It has been shown that interactions between  $\text{H}_2\text{O}$  and carbon–oxygen complexes influence the reactivities of carbons for adsorption. One notable example is the catalytic oxidation of sulfur dioxide ( $\text{SO}_2$ ) by carbon in the presence of  $\text{O}_2$  and  $\text{H}_2\text{O}$ . In the absence of  $\text{H}_2\text{O}$  vapor, neither oxidized nor unoxidized carbon could catalyze the oxidation of  $\text{SO}_2$  [19,20]. In the presence of  $\text{O}_2$  and  $\text{H}_2\text{O}$ ,  $\text{SO}_2$  becomes adsorbed on carbon surfaces where it is catalytically converted to sulfuric acid in a consecutive process. The effect of  $\text{H}_2\text{O}$  on the heterogeneous oxidation of  $\text{SO}_2$  has been discussed in the literature [21]. During  $\text{H}_2\text{O}$  adsorption, a partial hydrolysis of anhydride groups and lactones occurs. The strongly adsorbed species, which could be assigned to sulfite ( $\text{SO}_3^{2-}$ ), are formed with the participation of acidic surface carbon–oxygen complexes. Infrared (IR) spectroscopic studies [20] have shown that the conversion of surface species occurred during the adsorption of  $\text{H}_2\text{O}$ .

The main objective of the work reported in this paper was to study the effect of adsorbed  $\text{H}_2\text{O}$  on  $\text{Hg}^0$  adsorption by activated carbons in order to understand the role of surface oxygen species in binding mercury. The thermal stability and the chemical characteristics of the adsorbed mercury were studied to determine the mechanism of  $\text{Hg}^0$  bonding on the carbon surface.

## 2. Experimental

Two activated carbons, a bituminous-coal-based activated carbon (BPL, Calgon Carbon Corporation) and an activated carbon fiber (ACN, American Kynol, Inc.) were tested for their  $\text{Hg}^0$  adsorption uptake capacity in this study. Selected characteristics of these carbons are shown in Table 1. BET (Brunauer–Emmett–Teller) and DR (Dubinin–Radushkevich) surface areas were measured by  $\text{N}_2$  adsorption at 77 K with  $P/P_0$  up to 0.99, and  $\text{CO}_2$  adsorption at 273 K with  $P/P_0$  up to about 0.03, respectively, using a volumetric adsorption apparatus (ASAP 2400, Micromeritics). All samples were degassed at 300°C under vacuum for 3 h prior to the measurements. The total pore volume was evaluated from the  $\text{N}_2$  adsorption isotherm at  $P/P_0 = 0.99$ , and the micropore volume was estimated from  $\text{CO}_2$  adsorption at 273 K using the DR equation. A  $\text{CO}_2$  molecular density of  $1.03 \text{ g}/\text{cm}^3$  and a cross-sectional area of  $0.187 \text{ nm}^2$  were assumed for estimating the DR surface area [22]. The particle size

Table 1  
Characteristics of activated carbon samples

	BPL	ACN
BET surface area (m <sup>2</sup> /g)	1136	1250
CO <sub>2</sub> surface area (m <sup>2</sup> /g)	976	1248
Total pore volume (cm <sup>3</sup> /g)	0.58	0.51
Micropore volume (cm <sup>3</sup> /g)	0.37	0.48
Particle size/fiber diameter (μm)	125–177	10
Moisture (% wt.)	2.2	2.0
Combustible (% wt.)	94.6	98.0
Ash (% wt.)	3.2	0.0

range of the BPL sample tested was 125–177 μm. The moisture and ash contents of the samples were measured by using a thermogravimetric analyzer (TGA-7, Perkin Elmer). The ACN sample is derived from a phenolic resin, in the form of needled felt with over 92% carbon and the remainder oxygen and hydrogen [23], with no ash. It is well known that the presence of metal oxides or inorganic impurities as ash in activated carbons could affect the chemical characteristics and adsorptive behavior [12]. By employing the ash-free ACN sample, the effect of ash associated with the BPL sample on Hg<sup>0</sup> adsorption, if it is significant, can be estimated.

Fig. 1 presents a schematic diagram of the experimental set-up. Industrial grade N<sub>2</sub> gas was used as a purge and Hg<sup>0</sup> carrier gas. A dryer and an O<sub>2</sub> trap were used to remove trace H<sub>2</sub>O vapor and O<sub>2</sub>, respectively, remaining

in the purge and carrier gas stream. A quartz fixed-bed reactor (1.27 cm ID) surrounded by a temperature-controlled electrical furnace was used for sample moisture removal, Hg<sup>0</sup> adsorption, and desorption experiments. To determine whether mercury is in the elemental (Hg<sup>0</sup>) or oxidized (Hg<sup>2+</sup>) forms in the reactor outlet, an additional electrical furnace operating at a temperature of 900°C was added downstream of the reactor to convert Hg<sup>2+</sup> to Hg<sup>0</sup> [24]. The Hg<sup>0</sup>-laden gas mixture was generated using a Hg<sup>0</sup>-containing permeation tube in a constant temperature system (Dynacalibrator Model 190, VICI Metronic). A Hg<sup>0</sup> concentration of 58 ± 2 ppb (476 μg/Nm<sup>3</sup>) in N<sub>2</sub> at a total flow rate of 340 ml/min was generated and used for the Hg<sup>0</sup> adsorption experiments. An ultraviolet (UV) mercury analyzer (Model 400A, BUCK Scientific) which has a detection limit of 2 ppb, was used to continuously measure the concentration of Hg<sup>0</sup> in the outlet stream. The experiments of carbon heat treatment for moisture removal, Hg<sup>0</sup> adsorption, and desorption can be performed consecutively in situ, using the experimental set-up shown in Fig. 1, so that moisture uptake due to exposure of the carbon sample to the atmosphere could be avoided.

To perform a Hg<sup>0</sup> adsorption experiment on an as-received carbon sample, the Hg<sup>0</sup>-laden gas mixture was first sent through the bypass to establish the baseline Hg<sup>0</sup> concentration prior to adsorption. After loading the pre-weighed carbon sample (about 20–40 mg, mixed with 2 g of sand) into the reactor, maintained at a temperature of 27°C (slightly above room temperature), the Hg<sup>0</sup>-laden N<sub>2</sub>

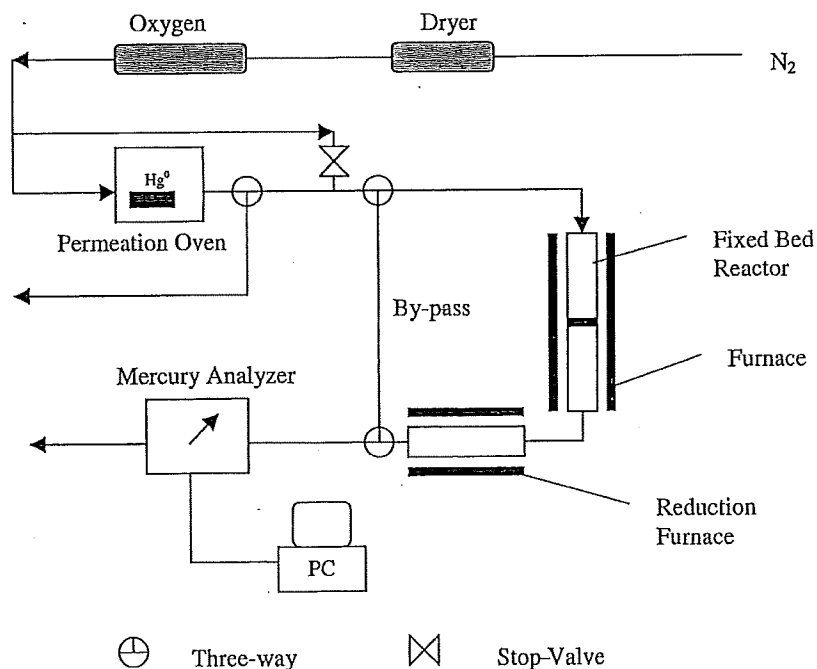


Fig. 1. Schematic diagram of fixed-bed reactor set-up.

flow was switched from the bypass to the reactor. The air-exposed, moisture-containing samples were then exposed to the  $\text{Hg}^0$ -laden  $\text{N}_2$  flow. The adsorption experiment was performed for 2 h, at which time the change in the outlet  $\text{Hg}^0$  concentration was insignificant. The  $\text{Hg}^0$  uptake for an adsorption experiment was calculated based on 100 min of adsorption time using the area between the inlet  $\text{Hg}^0$  concentration (baseline) and the breakthrough curve.  $\text{Hg}^0$  adsorption experiments were also performed on the moisture-free carbon samples after heat treatment. To remove moisture from the as-received carbon sample (loaded into the reactor prior to  $\text{Hg}^0$  adsorption), the sample was heated at a constant rate ( $8^\circ\text{C}/\text{min}$ ) to  $110^\circ\text{C}$  under an  $\text{N}_2$  atmosphere, then held for 30 min. The reactor was then cooled to the  $\text{Hg}^0$  adsorption temperature ( $27^\circ\text{C}$ ) under  $\text{N}_2$  flow, before the adsorption experiment, similar to that performed for the as-received samples, was started.

Temperature programmed desorption (TPD) experiments were performed to measure the thermal stability of the adsorbed mercury following the  $\text{Hg}^0$  adsorption experiment. The reactor, containing the  $\text{Hg}^0$ -exposed carbon sample, was purged with  $\text{N}_2$  gas at  $27^\circ\text{C}$  until the concentration of  $\text{Hg}^0$  measured by the UV analyzer fell to insignificant levels ( $<2$  ppb). The sample was then heated at a constant heating rate ( $8^\circ\text{C}/\text{min}$ ) to the final temperature of  $420^\circ\text{C}$ . Blank TPD experiments using carbon samples without mercury showed that there is no interference on the mercury analyzer with the loss of  $\text{CO}_2$  and  $\text{H}_2\text{O}$  from the carbon surfaces. The amount of  $\text{Hg}^0$  desorbed during the TPD run was estimated from the area under the outlet  $\text{Hg}^0$  concentration curve. Preliminary TPD experiments showed that more than 90% of the adsorbed  $\text{Hg}^0$  was desorbed when the temperature reached  $420^\circ\text{C}$ , so this was used as the final temperature.

XAFS spectroscopy analysis was conducted on both as-received and heat-treated carbon samples which had been exposed to  $\text{Hg}^0$  to provide information on the nature of mercury bonding on carbon surfaces. The difference in energy between two principal inflection points (IPD) on the mercury  $L_{\text{III}}$  absorption edge measured in XAFS spectra is a sensitive indicator of the structure and/or chemistry of the mercury adsorbed onto activated carbon and other sorbent materials [25]. Prior to the XAFS examination, the sample was transferred from a sealed sample container into a polypropylene sample holder and hung in the X-ray beam. The mercury  $L_{\text{III}}$  edge at  $12,284$  eV was used for the absorption experiments, and all measurements were carried out in fluorescence geometry. A 13-element germanium detector was used to record the spectra. A  $6 \mu\text{m}$  gallium filter was also used to maximize the signal/noise ratio. Details of the XAFS experimental procedures can be found elsewhere [25]. The XAFS spectrum was first divided into X-ray absorption near-edge structure (XANES) and extended X-ray absorption fine structure (EXAFS) spectral regions. The XANES spectrum was then smoothed and differentiated to obtain the  $d^2\text{Abs}/$

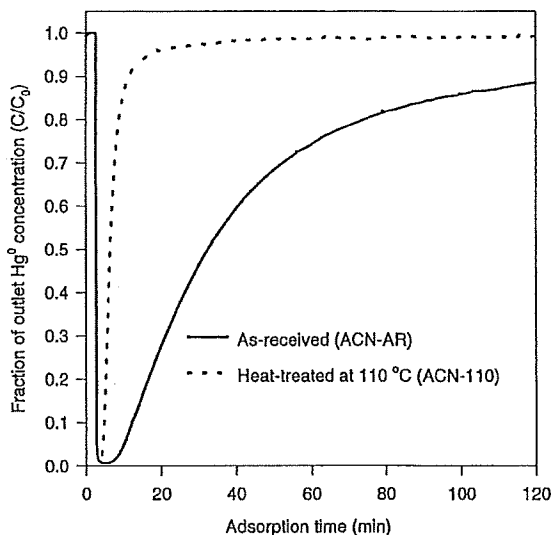


Fig. 2. Mercury adsorption breakthrough curves of ACN samples.

$(dE)^2$  spectrum, from which the inflection point difference (IPD) could be determined. The step-height was determined from the XAFS spectrum as the difference in background absorption above and below the edge.

### 3. Results and discussion

The  $\text{Hg}^0$  adsorption breakthrough curves for both the as-received (-AR) and the  $110^\circ\text{C}$  heat-treated (-110) ACN and BPL samples are shown in Figs. 2 and 3, respectively. The amounts of adsorbed  $\text{Hg}^0$  estimated from the break-

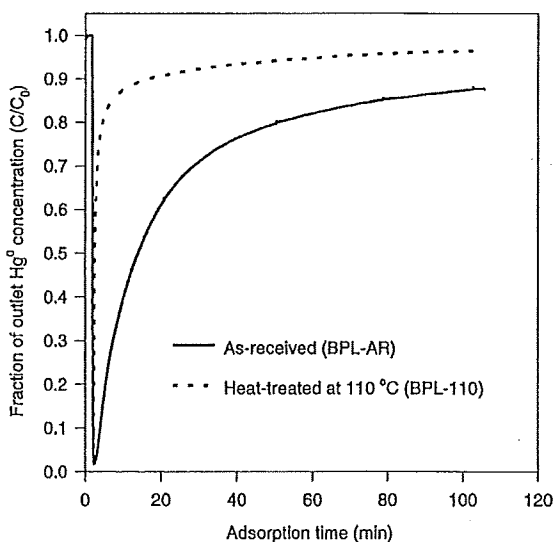


Fig. 3. Mercury adsorption breakthrough curves of BPL samples.

Table 2  
Mercury uptake from adsorption and recovery from desorption

Samples	Hg adsorption at 27°C	Hg desorption		Hg recovery (%)
	Hg captured ( $\mu\text{g/g}$ ) <sup>a</sup>	N <sub>2</sub> purge (%)	TPD (%)	
ACN-AR	236	12	86	98
ACN-110	34	42	54	96
BPL-AR	83	5	93	98
BPL-110	20	20	71	91

<sup>a</sup> Amount of mercury adsorbed for 100 min on dry carbon basis.

through curves are shown in Table 2. It can be seen that the Hg<sup>0</sup> uptake of the as-received carbon fiber sample (ACN-AR) is much larger (236  $\mu\text{g/g}$ ) than that (83  $\mu\text{g/g}$ ) of the coal-based carbon sample (BPL-AR), although the total surface area of BPL is only 10% less than that of ACN sample (see Table 1). The very similar values of BET and CO<sub>2</sub> surface areas for the carbon fiber sample (see Table 1) suggest that ACN is a microporous (<2 nm) carbon with homogeneous distribution of microporosity. The CO<sub>2</sub> surface area of sample BPL is lower than its BET surface area, suggesting that the sample contains some mesopores. The average micropore width evaluated from CO<sub>2</sub> adsorption with the DR method gives a similar value of about 1.5 nm for both carbon samples. The larger CO<sub>2</sub> surface area of the ACN sample compared to that of the BPL sample appears to suggest that the micropores of carbons may be effective for Hg<sup>0</sup> capture. However, the higher Hg<sup>0</sup> uptake of the ACN sample compared to that of the BPL sample could also be due to the influence of intraparticle diffusion. As shown in Table 1, the particle size of the BPL sample was much larger than the fiber diameter of ACN sample, suggesting that if there were any diffusion limitations associated with the micropores, the BPL sample would have a much longer internal diffusion length than that of the ACN sample.

As shown in Figs. 2, 3 and Table 2, the mercury Hg<sup>0</sup> uptake of both carbon samples was drastically reduced to the similar, low values (20–30  $\mu\text{g/g}$ ) after low temperature (110°C) heat treatment. Since heat treatment at such low temperatures does not change the pore structure [4], this suggests that the reduced Hg<sup>0</sup> capture after heat treatment is not caused by pore structure change. However, the adsorbed H<sub>2</sub>O molecules on carbon surfaces are removed when heated at low temperatures, e.g. 25–150°C [13], suggesting that the carbon surface moisture may play an important role in Hg<sup>0</sup> adsorption. The removal of surface moisture had a similar effect for both the ash-free ACN sample and the coal-based ash-containing BPL sample, indicating that the strong effect of moisture on Hg<sup>0</sup> adsorption may not be associated with the ash contained in coal-based carbons.

Figs. 4 and 5, respectively, show the ACN and BPL mercury concentration profiles as a function of run time

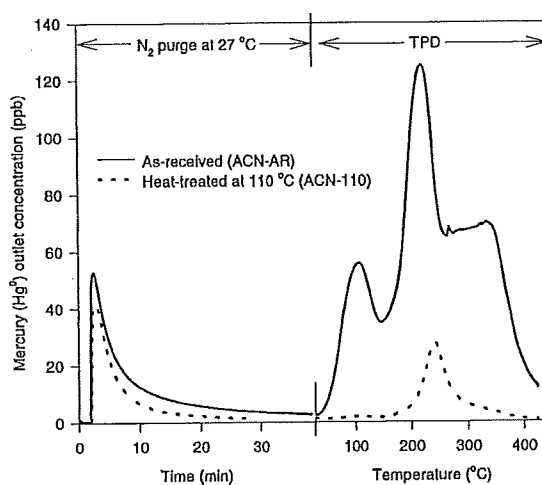


Fig. 4. Mercury concentration profiles of ACN samples during N<sub>2</sub> purge at 27°C and during TPD.

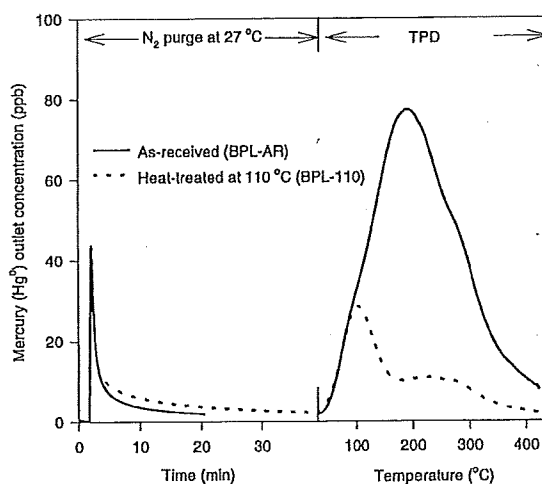


Fig. 5. Mercury concentration profiles of BPL samples during N<sub>2</sub> purge at 27°C and during TPD.

after adsorption at 27°C and as a function of temperature during the TPD. The chemisorbed  $\text{Hg}^0$  can be differentiated from the physisorbed  $\text{Hg}^0$  from these figures. The physisorbed  $\text{Hg}^0$  on the carbon surfaces is evolved when the reactor gas is switched from the  $\text{Hg}^0$ -laden  $\text{N}_2$  at the end of the adsorption experiment to pure  $\text{N}_2$  (27°C). The mercury evolved during the subsequent TPD run is referred to as chemisorbed  $\text{Hg}^0$ , since it is stable at the adsorption temperature (27°C) under the inert gas atmosphere ( $\text{N}_2$ ) and decomposes into gas species as the temperature rises. The amounts of  $\text{Hg}^0$  desorbed were calculated from the area under the outlet  $\text{Hg}^0$  concentration, and the results are presented in Table 2, expressed as a percentage of the  $\text{Hg}^0$  adsorbed that was measured during the adsorption experiment prior to the  $\text{N}_2$  purge. Similar amounts of  $\text{Hg}^0$  were measured between duplicate runs with and without operating the reduction furnace, which suggested that the mercury evolved during desorption was  $\text{Hg}^0$  and not an oxidized form. The mass balances between the adsorbed and desorbed  $\text{Hg}^0$  in all cases were greater than 90%, and most of the  $\text{Hg}^0$  adsorbed by the carbons was recovered by heating the samples to 420°C. Due to the system's response lag time ( $t_{\text{lag}}$ ), the true mercury desorption temperatures could be lower than those shown in Figs. 4 and 5. It was estimated that  $t_{\text{lag}}$  is about 30 s under the current experimental conditions, which would result in the true mercury desorption temperature of 4°C lower than those shown in Figs. 4 and 5. The possible influence of intraparticle diffusion and readsorption, which could affect the shape and position of the observed TPD profiles [26], was not assessed at the present time. The mercury concentration profile as a function of temperature obtained during the TPD run would provide information on the thermal stability of the adsorbed mercury.

For the two as-received samples (ACN-AR, BPL-AR), more than 86% of the adsorbed  $\text{Hg}^0$  was desorbed during the TPD runs at higher temperatures versus only 54 and 71% for their heat-treated counterparts.  $\text{Hg}^0$  evolved during the  $\text{N}_2$  purge accounts for only a small fraction of the total  $\text{Hg}^0$  adsorbed, especially with the BPL-AR. In the case of ACN-AR, two strong  $\text{Hg}^0$  desorption peaks can be seen (Fig. 4) at temperatures near 100 and 200°C. A plateau can also be observed when the temperature increases to 250–350°C. For the BPL-AR sample, only a broad desorption peak was observed (Fig. 5). A slow desorption process can also be observed at the end of  $\text{N}_2$  purge, which could make an additional contribution in the TPD profile, especially at low temperatures (<100°C). However, this contribution was estimated to be negligibly small.

Adsorption and desorption processes on the carbon surface are known to be governed by a distribution of adsorption energies [27]. Chemical bonds formed between the adsorbed molecules and the adsorption sites of an activated carbon are often quite strong. Since the TPD

experiments show that  $\text{Hg}^0$  is evolved over a wide temperature range,  $\text{Hg}^0$  bonds on the carbon surface probably involve different site types, which have varying bonding energies. The different  $\text{Hg}^0$  concentration profiles shown in Figs. 4 and 5 could imply that the nature of the carbon surface active sites for bonding  $\text{Hg}^0$  depends on the carbon characteristics. For the as-received samples, chemisorption of  $\text{Hg}^0$  appears to be the predominant process as indicated by Figs. 4 and 5. Since Figs. 4 and 5 show that the reduction of  $\text{Hg}^0$  capture for the heat-treated samples is related to reduction of chemisorbed  $\text{Hg}^0$ , it could be deduced that the removal of  $\text{H}_2\text{O}$  from the carbon surfaces by low-temperature heat treatment reduces the number of active sites that can chemically bond  $\text{Hg}^0$ . It is also possible that some moisture may still have remained bound to the micropore surface under the current mild heat treatment conditions [13]. The ACN-110 sample shows a narrow peak centered at about 250°C, and the BPL-110 sample shows a peak at about 100°C, both of which coincided with peaks observed from their as-received samples. These observations suggest that some of the active sites for bonding mercury chemically were not completely eliminated by low-temperature heat treatment, and at least one distinctive active site type is still remaining on each carbon surface for mercury bonding.

Table 3 shows the inflection point difference (IPD, eV) and the step-height of five samples determined by XAFS analysis. Sufficiently strong spectra measured from these samples have permitted the derivative analysis to be performed in order to obtain the IPD values, except for ACN-110, in which strong noise was encountered and the IPD value cannot be determined accurately. It has been shown that the mercury surface compounds with the smallest and most ionic anions ( $\text{O}^{2-}$ ,  $\text{O}^-$ ) have the largest values of IPD (e.g. >9.0), whereas those with the largest and more covalent anions have the smallest IPD values [25]. The XAFS spectral results represent a weighted average of all the mercury (physisorbed and chemisorbed) which remained bound on carbon surfaces. The effect of a mixture of physisorbed and chemisorbed mercury on the

Table 3  
Mercury  $L_{\text{III}}$ -edge XAFS analysis results

Sample	IPD (eV)	Step-height
ACN-AR <sup>a,b</sup>	9.0 <sup>a</sup> , 9.1 <sup>b</sup>	1.8 <sup>a</sup> , 1.6 <sup>b</sup>
ACN-110	n.d. <sup>c</sup>	0.17
BPL-AR	9.2	0.6
BPL-110	9.2	0.2

<sup>a</sup> Samples prepared from two different experiments under the same mercury adsorption conditions.

<sup>b</sup> Samples prepared from two different experiments under the same mercury adsorption conditions.

<sup>c</sup> n.d., not determined due to strong noise.

XAFS spectrum would lower the IPD value compared with that obtained from the reference mercury compounds [28]. As shown in Table 3, the IPD values derived from the XANES spectra are basically the same,  $9.1 \pm 0.1$  eV. These values are significantly higher than those for mercuric chlorides ( $8.4 \pm 0.2$  eV) [25], and since oxygen is the only anion in the system which is more ionic than chloride, there must be significant Hg–O bonding present. It has been suggested that the step-height value could be used as a semiquantitative measure of the relative concentration of the element in the sample [25]. As shown in Table 3, the step-heights obtained from the spectra are consistent with the values of the adsorbed mercury measured by the adsorption experiments (see Table 2). Furthermore, the XAFS results are consistent with the TPD results in that most of the adsorbed  $\text{Hg}^0$  was strongly bound and evolved at higher temperatures in all cases.

The above XANES results suggest that carbon-bound oxygen on the surface captures  $\text{Hg}^0$  during the adsorption experiments. Different types of oxygen surface groups are believed to exist on activated carbon surfaces. Depending on their history of formation and activation temperature, they could be carboxyl, lactone, phenolic, and carbonyl groups [29]. Electron transfer processes are likely to be involved during the chemisorption of  $\text{Hg}^0$ . Abundant evidence from the literature shows that different oxygen groups can participate in the electron transfer processes on carbon surfaces [30]. Extended  $\pi$  bonding in the extensive aromatic network of carbons permits electron clouds and charges to be highly delocalized. For example, the resonance-stabilized structures of the aromatic network in equilibration with the surface functional groups (e.g. quinonoid complexes) could take up electrons from  $\text{Hg}^0$  at specific conditions.

The desorbed mercury was found to be  $\text{Hg}^0$  from the TPD experiments. When thermal energy is applied to a chemisorbed  $\text{Hg}^0$ , it would be favorable for the electron(s) to return to the mercury rather than breaking the C–O bonds. Since certain oxygen complexes such as carboxyl and lactone groups would also decompose to produce  $\text{CO}_2$  and  $\text{H}_2\text{O}$  at low temperatures (e.g.  $< 420^\circ\text{C}$ ), it is not clear if  $\text{Hg}^0$  is bonded to these complexes. However, as described by Leon y Leon and Radovic [30], before the oxidation reactions can proceed they all have specific surface conditions that must be met such as pH, oxygen exposure, and the types of surface functional groups. The fact that the presence of surface moisture promotes  $\text{Hg}^0$  adsorption could imply that interactions between  $\text{H}_2\text{O}$  and carbon–oxygen complexes may create certain active sites or affect surface conditions which favor  $\text{Hg}^0$  adsorption. Based on the results from this study it is not known what particular surface functional groups are participating in  $\text{Hg}^0$  adsorption, and how the adsorbed surface  $\text{H}_2\text{O}$  could influence the reactivities of carbons. Further research is needed to characterize the carbon oxygen surface groups,

and to clarify the role of these functional groups and the specific conditions that favor  $\text{Hg}^0$  adsorption.

#### 4. Conclusions

The moisture on activated carbon surfaces has been found to have a significant effect on  $\text{Hg}^0$  adsorption at room temperature. The results from this study show that the  $\text{Hg}^0$  adsorption capacities of two activated carbon samples were drastically reduced after a low-temperature ( $110^\circ\text{C}$ ) treatment to remove the moisture. By comparing the results of an ash-free activated carbon sample (ACN) to those of a coal-based carbon (BPL), it is concluded that mineral matter or metal oxides in the coal-based carbon do not play a role in this effect. Results of the TPD experiments show that chemisorption of  $\text{Hg}^0$  is a dominant process during  $\text{Hg}^0$  adsorption for the moisture-containing carbon samples. At least two different active sites exist on the carbon surfaces. XAFS analysis provides evidence that  $\text{Hg}^0$  bonding on the carbon surfaces is associated with oxygen.

Results from both mercury desorption (TPD) and XAFS analyses suggest that surface oxygen complexes provide the active centers for mercury bonding. The mechanism of mercury bonding on the carbon surfaces likely involves electron transfer processes. The observation that the presence of surface moisture promotes mercury bonding suggested that interactions between  $\text{H}_2\text{O}$  and carbon–oxygen complexes might create certain active sites or surface conditions favoring  $\text{Hg}^0$  adsorption.

#### Acknowledgements

This research was supported in part by an appointment (Y.H. Li) to the Postdoctoral Research Program at the National Risk Management Research Laboratory administered by the Oak Ridge Institute for Science and Education through interagency agreement DW89938167 between the US Department of Energy and the US Environmental Protection Agency. The authors appreciate the assistance of Prof. Frank Huggins at University of Kentucky in providing the XAFS analysis. Appreciation is also extended to Dr. Carlos A. Leon y Leon for the discussions and suggestions on this subject through personal communication, and Joe Hayes of American Kynol, Inc. for providing the activated carbon fibers.

#### References

- [1] Keating MH, Mahaffey KR, Schoeny R, Rice GE, Bullock OR, Ambrose RB et al. In: Executive summary; EPA/452/R-97/003 (NTIS PB98-124738), Mercury study report to

- Congress, vol. I, Office of Air Quality Planning and Standards and Office of Research and Development, 1997, December.
- [2] Hall B, Lindqvist O, Ljungstrom E. *Environ Sci Technol* 1990;24:108–11.
- [3] Chang R, Offen GR. *Power Eng* 1995;99:51–7.
- [4] Krishnan SV, Gullett BK, Jozewicz W. *Environ Sci Technol* 1994;28:1506–12.
- [5] Huang HS, Wu JM, Livengood CD. *Hazard Waste Hazard Mater* 1996;13:107–19.
- [6] Korpziel JA, Vidic RD. *Environ Sci Technol* 1997;31:2319–25.
- [7] Carey TR, Hargrove Jr. OW, Richardson CF, Chang R, Meserole FB. *J Air Waste Manage Assoc* 1998;48:1166–74.
- [8] Rostam-Abadi M, Chen SG, Hsi HC, Rood M, Chang R, Carey T et al. In: Presented at the EPRI-DOE-EPA combined utility air pollutant control symposium, Washington, DC, 1997.
- [9] Sinha RK, Walker Jr. PL. *Carbon* 1972;10:754–6.
- [10] Otani Y, Emi H, Kanaoka C, Uchijima I, Nishino H. *Environ Sci Technol* 1988;22:708–11.
- [11] Vidic RD, McLaughlin JB. *J Air Waste Manage Assoc* 1996;46:241–50.
- [12] Bansal RC, Donnet JB, Stoeckli F. *Activated carbon*, New York: Marcel Dekker, 1988.
- [13] Bacon R, Tang MM. *Carbon* 1964;2:221.
- [14] Dubinin MM. In: Walker Jr. PL, editor, *Chemistry and physics of carbon*, vol. 2, New York: Marcel Dekker, 1966, pp. 51–120.
- [15] Puri BR. In: Walker Jr. PL, editor, *Chemistry and physics of carbon*, vol. 6, New York: Marcel Dekker, 1970, pp. 191–282.
- [16] Barton SS, Evans MJB, Holland J, Koresh LE. *Carbon* 1984;22:265.
- [17] Youssef AM, Ghazy TM, Nabarawy TE. *Carbon* 1982;20:113.
- [18] Bansal RC, Dhani TL, Parkash SS. *Carbon* 1978;16:389.
- [19] Stacy WO, Vastola FJ, Walker Jr. PL. *Carbon* 1968;6:917.
- [20] Zawadzki J. *Carbon* 1987;25(3):431–6; *Carbon* 1987;25(4):495–502.
- [21] Zawadzki J. In: Thrower PA, editor, *Chemistry and physics of carbon*, vol. 21, New York: Marcel Dekker, 1989, pp. 147–380.
- [22] Rodriguez-Reinoso F, Garrido J, Martin-Martinez JM, Molina-Sabio M, Torregrosa R. *Carbon* 1989;27:23–32.
- [23] Hayes Jr. JS. Novoloid fibers. In: 3rd ed, Kirk-Othmer: *encyclopedia of chemical technology*, vol. 16, 1981, pp. 125–38.
- [24] Krishnan SV, Gullett BK, Jozewicz W. In: Presented at the solid waste management thermal treatment and waste-to-energy technologies conference, USEPA/AEERL and AandWMA, Washington, DC, 1995.
- [25] Huggins FE, Huffman GP, Dunham GE, Senior CL. *Energy Fuels* 1999;13:114–21.
- [26] Gorte RJ. *J Catal* 1982;75:164–74.
- [27] Tremblay G, Vastola FJ, Walker Jr. PL. *Carbon* 1978;16:35–9.
- [28] Huggins FE, Yap N, Huffman GP, Senior CL. In: Presented at the Air and Waste Management Association's 92nd annual meeting and exhibition, June 20–24, St. Louis, MO, 1999.
- [29] Boehm HP. *Adv Catal* 1966;16:179–274.
- [30] Leon y Leon CA, Radovic LR. In: Thrower PA, editor, *Chemistry and physics of carbon*, vol. 24, New York: Marcel Dekker, 1994, pp. 213–310.

1  
2  
3  
4  
5  
6  
7  
8  
9  
10  
11  
12  
13  
14  
15  
16  
17  
18  
19  
20  
21  
22  
23  
24  
25  
26  
27  
28  
29  
30  
31  
32  
33  
34  
35  
36  
37  
38  
39  
40  
41  
42  
43  
44  
45  
46  
47  
48  
49  
50  
51  
52  
53  
54  
55  
56  
57  
58  
59  
60  
61  
62  
63  
64  
65  
66  
67  
68  
69  
70  
71  
72  
73  
74  
75  
76  
77  
78  
79  
80  
81  
82  
83  
84  
85  
86  
87  
88  
89  
90  
91  
92  
93  
94  
95  
96  
97  
98  
99  
100

# P<sub>4</sub> Production, LLC

Soda Springs Plant  
1853 Highway 34  
P.O. Box 816  
Soda Springs, Idaho 83276-0816  
Phone: (208) 547-4300  
Fax: (208) 547-3312

January 16, 2014

VIA CERTIFIED MAIL;  
RETURN RECEIPT REQUESTED – 7013 1090 0002 1009 1990

Mr. Daniel Pitman  
Air Quality Division  
State of Idaho Department of Environmental Quality  
1410 North Hilton  
Boise, ID 83706

RE: Facility ID 029-00001, P<sub>4</sub> Production, LLC (“P<sub>4</sub>”)  
Response to Public Comment

Mr. Pitman:

On December 2, 2013, the Idaho Conservation League (“ICL”) submitted written comments to the Idaho Department of Environmental Quality (“IDEQ”) regarding the proposed Tier II Operating Permit, T2-2012.0016, which establishes a Mercury Best Available Control Technology (“MBACT”) emission standard for P<sub>4</sub>’s Soda Springs facility. ICL’s comments inquired specifically about (1) the validity of the 746.4 lb/yr permit limit in relation to the variability of actual mercury emissions reported between the years 2000 and 2012, and (2) P<sub>4</sub>’s ability to segregate and/or pre-treat phosphate ore with high mercury content.

The 746.4 lb/yr permitted mercury emission limit is based on P<sub>4</sub>’s maximum potential to emit, estimated using stack test data generated in 2002 for gaseous and particulate mercury emitted from the kiln. The sum of the average of three data points was used for each of the four kiln hydrosonic stacks to generate an emission factor in lb/hr mercury emissions. The emission factor was then normalized for the actual quantity of kiln feed processed during the stack test period, which was then adjusted for the maximum kiln throughput to generate the maximum potential to emit. This permit limit is only 2.7% higher than the highest total annual mercury emissions reported by P<sub>4</sub> in the TRI records during the period from 2002 to 2012, which ranges between 489 and 725 lbs. The variability in P<sub>4</sub>’s annual emissions is primarily based on the amount of raw phosphate ore processed to meet production demand. Since the standard error in the stack test data used to calculate P<sub>4</sub>’s annual emissions estimates is significantly higher than the 2.7%

difference in question here, any effort to lower the permit limit based on TRI data would be trivial.

In addition, P4 may be required to limit the amount of ore processed to below historical levels in order to meet a more stringent limit. Although P4 has recently generated an extensive database regarding the mercury concentration of ore in the north pit of the new Blackfoot Bridge mine that suggests a consistently low concentration averaging approximately 0.5 ppm, P4 cannot predict the variability of mercury in that ore with any certainty; mercury concentration could vary as a result of a simple change in the ore resulting from a change in location, depth, pit, mine, mercury speciation in the rock, etc. A change as small as one tenth of a ppm could result in a significant increase in mercury emissions. Also, the consistently low concentration of mercury measured in the phosphate ore processed by P4 to date and estimated in ore from the new Blackfoot Bridge mine present little opportunity to selectively mine ore based on mercury concentration as a means to reduce emissions.

Finally, ore pretreatment was thoroughly evaluated as a technological option during the BACT review, and the lack of commercially available options precluded further consideration. Additional discussion of ore pretreatment is contained in sections 3.1.3, 3.1.5, 3.2.2, and 3.2.5 of the MBACT for Elemental Phosphorus Report dated March 2012, which was submitted to IDEQ along with P4's permit application.

In accordance with IDAPA 58.01.01.123 (*Rules for the Control of Air Pollution in Idaho*), I certify based on information and belief formed after reasonable inquiry, that the statements and information in this document are true, accurate, and complete. If you have any questions or would like more information, please contact Mr. Jim McCulloch at 547-1233.

Thank you for the opportunity to provide a response,



Sheldon D. Alver  
Vice President